Electronic Structure Theory and Multi-Structural Statistical Thermodynamics for Computational Chemical Kinetics

A DISSERTATION
SUBMITTED TO THE FACULTY OF THE GRADUATE SCHOOL
OF THE UNIVERSITY OF MINNESOTA
BY

Ewa Papajak

IN PARTIAL FULFILLMENT OF THE REQUIREMENTS
FOR THE DEGREE OF
DOCTOR OF PHILOSOPHY

Thesis adviser: Donald G. Truhlar

August 2012

ACKNOWLEDGEMENTS

To my parents Elżbieta and Andrzej and my sister Ula

Abstract

This thesis involves the development and application of methods for accurate computational thermochemistry. It consists of two parts. The first part focuses on the accuracy of the electronic structure methods. In particular, various augmentation schemes for one-electron basis sets are presented and tested for density functional theory (DFT) calculations and for wave function theory (WFT) calculations. The relationship between diffuse basis functions and basis set superposition error is discussed. For WFT, we also compare the efficiency of conventional one-electron basis-sets to that of newly developed explicitly correlated methods. Various ways of approaching the complete basis set limit of WFT calculations are explained, and recommendations are made for the best ways of achieving balance between the basis set size, higher-order correlation, and relativistic corrections. Applications of this work include computation of barrier heights, reaction and bond energies, electron affinities, ionization potentials, and noncovalent interactions.

The second part of this thesis focuses on the problem of incorporating multi-structural effects and anharmonicity effects in the torsional modes into partition function calculations, especially by using a new multi-structural torsion (MS-T) method. Applications of the MS-T method include partition functions of molecules and radicals important for combustion research. These partition functions are used to obtain thermodynamic functions that are the most reliable results available to date for these molecules. The multi-structural approach is also applied to two kinetics problems:

- the hydrogen abstraction from carbon-3 of 1-butanol by hydroperoxyl radical
- the 1,5-hydrogen shift isomerization of the 1-butoxyl radical

In both cases multi-structural effects play an important role in the final results.

Table of Contents

List of Tables

viii

ix

List of Figures

xvii

Part I.   Electronic Structure Theory

A primary goal of electronic structure theory is to provide high accuracy calculations of energetic and structural quantities that can be used to predict reliable molecular properties, thermodynamics, and kinetics of chemical reactions. Due to existing constraints on the computational cost that we can afford for increasingly large systems that we study and due to the high cost of the reliable electronic structure and dynamics methods that we use, the optimal choice of methods and approximations in the calculations is essential. This choice is a common theme of several projects on which I have been involved. Part I of this thesis presents five articles exploring the balance between the accuracy and cost of electronic structure methods. The success of practical applications often hinges on the choice of the basis set to be employed in the wave function theory (WFT) or density functional theory (DFT) calculations.

In the first article[1] (chapter 1) we show that significant improvement in the efficiency (accuracy vs. cost) can be achieved with an improved balance of saturation of the diffuse space, polarization functions, and degree of contraction of the basis set. In our further publications we proposed a minimal augmentation scheme for the commonly used basis sets for density functional theory[2] (chapter 2) and the "seasonal" augmentation scheme for wave function theory[3–4] (chapters 3–4) calculations.

Another interesting topic in the WFT calculations is the balance between the basis set completeness and the inclusion of higher-order correlation effects, spin–orbit coupling, and relativistic effects in the wave function theory. In the fifth article[5] (chapter 5) we evaluate several approaches to estimate the infinite basis set limit of explicitly correlated methods in order to be able to afford high accuracy in thermochemical data.

(1) E. Papajak, H.R. Leverentz, J. Zheng, and D.G. Truhlar, J. Chem. Theory Comput. **5**, 1197 (2009). E. Papajak, H.R. Leverentz, J. Zheng, and D.G. Truhlar, J. Chem. Theory Comput. **5**, 3330 (2009).

(2) E. Papajak and D.G. Truhlar, J. Chem. Theory Comput. **6**, 597 (2010)

(3) E. Papajak and D.G. Truhlar, J. Chem. Theory Comput. **7**, 10 (2011)

(4) E. Papajak, J. Zheng, X. Xu, H.R. Leverentz, and D.G. Truhlar, J. Chem. Theory
   Comput. **7**, 3027 (2011)

(5) E. Papajak and D.G. Truhlar, J. Chem. Phys. **137**, 064110 (2012)

Chapter 1.　Efficient Diffuse Basis Sets: cc-pVxZ+ and maug-cc-pVxZ

Ewa Papajak, Hannah R. Leverentz, Jingjing Zheng, and Donald G. Truhlar*

*Department of Chemistry and Supercomputing Institute,
University of Minnesota, Minneapolis, Minnesota 55455-0431*

We combine the diffuse basis functions from the 6-31+G basis set of Pople and coworkers with the correlation-consistent basis sets of Dunning and coworkers. In both wave function and density functional calculations, the resulting basis sets reduce the basis set superposition error almost as much as the augmented correlation-consistent basis sets, although they are much smaller. In addition, in density functional calculations the new basis sets, called cc-pVxZ+ where x = D, T, Q, …, or x = D+d, T+d, Q+d, ..., give very similar energetic predictions to the much larger aug-cc-pVxZ basis sets. However, energetics calculated from correlated wave function calculations are more slowly convergent with respect to the addition of diffuse functions. We also examined basis sets with the same number and type of functions as the cc-pVxZ+ sets but using the diffuse exponents of the aug-cc-pVxZ basis sets and found very similar performance to cc-pVxZ+; these basis sets are called minimally augmented cc-pVxZ, which we abbreviate as maug-cc-pVxZ.

1. Introduction

The choice of α basis set for electronic structure calculations is a key factor in determining both the reliability of a calculation and its cost.[1] In recent years, the correlation consistent (cc) basis sets of Dunning and coworkers[2-6] have become very popular. These are arranged in two series, in particular cc-pVxZ and aug-cc-pVxZ with xZ = DZ ("double zeta"), TZ ("triple zeta), QZ ("quadruple zeta"), etc. The prefix aug- (for "augmented") denotes the addition of diffuse basis functions, i.e., Gaussian functions with small exponential parameters times spherical harmonics. In the

aug-cc-pVxZ basis sets, one adds quite a few diffuse functions, e.g., in aug-cc-pVDZ one adds 4 diffuse functions on each H and 9 on each heavy (i.e., non-hydrogenic) atom, whereas in aug-cc-pVTZ one adds 9 diffuse functions on each H and 16 on each heavy atom. Another popular set of basis functions is 6-31+G(d)[7] and 6-311+G(2df,p) of Pople and coworkers[8] in which the single plus sign denotes the addition of no diffuse functions on hydrogens and 4 on each heavy atom. (The same Gaussian exponential parameters are used for the diffuse basis functions in these two bases.) We have recently had some success combining the plus strategy with the cc basis sets, yielding cc-pVDZ+, cc-pVTZ+, and cc-pVQZ+, and so we decided to make some systematic comparisons of the performance of these strategies when applied to the same test problems. Those systematic comparisons are the primary subject of this article. We also show that for density functional calculations very similar results can be obtained by drastically pruning the aug-cc-pVxZ basis sets; this latter strategy is called minimal aug-cc-pVxZ, abbreviated maug-cc-pVxZ.

The above considerations also extend to a sequence[6] of basis sets with xZ = (D+d)Z, (T+d)Z , etc. in which five extra d functions are added to each element from Al to Ar. Table 1 compares the number of basis functions in the various series of basis sets for one of our test cases, namely the complex of H_2SO_4 with NH_3 (similar trends would be observed for other sample molecules). The table shows that tremendous cost savings are attainable with the plus basis sets, if they are accurate enough. Are they?

2. Tests

Several issues were considered in choosing and designing our tests. First, diffuse functions are more important, in general, for energetics than for geometries and are more important for electron affinities, barrier heights, and noncovalent interactions than for ionization potentials and bond energies. Second, when simply examining the absolute accuracy of some computed properties, such as geometries or strengths of noncovalent interactions, the improvement in the basis set due to adding diffuse functions may be masked by other aspects of the calculations that lead to larger errors than basis set's incompleteness. Third, a special aspect of basis set incompleteness that demands

attention, especially in the computation of noncovalent interactions, is basis set superposition error (BSSE),[9,10] and if this is not small it is not even clear *how* to extract an estimate of the interaction energy from the calculations. For example, should one include a counterpoise correction (*CpC*) and how should that correction be defined? The *CpC* becomes not only ambiguous but also costly when one considers clusters containing more than two molecules,[11] and we therefore wish to keep it small and avoid it.

With these considerations in mind, we decided to carry out six sets of test calculations. In the first four we compare calculated ionization potentials, electron affinities, bond energies, and barrier heights to databases of accurate (or at least best available) estimates. In the fifth and sixth we examine the size of the basis set superposition error for a set of noncovalent complexes.

The databases used for the first four tests are as follows:

- ionization potentials: database IP13/3,[12,13] containing C, O, Si, P, Cl, OH, PH, SH, PH_2, O_2, S_2, and Cl_2;

- electron affinities: database EA13/3,[12,13] containing the same 13 species;

- atomization energies: database AE6,[14] containing SiH_4, SiO, S_2, propyne, glyoxal, and cyclobutane;

- barrier heights: database DBH24/08,[15] consisting of 4 subdatabases: HATBH6, NSBH6, UABH6 and HTBH6 containing 6 barrier heights each (forward and reverse barrier heights of three reactions) for heavy-atom transfer, nucleophilic substitution, unimolecular and association reactions, and hydrogen transfer, respectively.

As explained in previous work, all energetic data in these databases are zero point exclusive, and all calculations for comparison to these databases use standard (QCISD/MG3) geometries.[12–15] All the results presented here include spin-orbit contributions[16] for C, O, F, Si, S, Cl, OH, and HS species.

For the fifth and sixth test, we studied ten complexes, which are shown in Figure 1. For each complex we calculated the *BSSE* by the functional counterpoise method[9] of Boys and Bernardi and expressed it as a percentage $\%CpC = \dfrac{|CpC|}{BE} \times 100\%$ where *BE* is the *CpC*-corrected binding energy. To avoid comparing calculations at different

5

geometries (geometry can have a large effect on BSSE), all *CpC* and *BE* calculations were carried out at standard geometries. In particular, the geometries for $Cl_2(NH_3)$, $HCl(H_2S)$, $(C_2H_4)_2$, and $(CH_4)_2$ were taken from the NCCE31/05 database,[17–19] the geometry of oa-$H_2SO_4(NH_3)$ complex is a nonstationary point selected to show a particular interaction motif, and the others were optimized by the M06-2X[19] density functional with the MG3S[12] basis set. The geometries that are not published elsewhere are given in supporting information.

Because basis set requirements are different for density functional theory[20] (DFT) and wave function theory[21] (WFT), we made calculations with both. For density functionals we consider B3LYP, [22] M05-2X,[18] M06,[19] M06-2X,[19] M06-L,[23] and M06-HF.[24] Note that M06-L is a local density functional, and the others are all nonlocal (also called hybrid). For WFT, we consider Hartree-Fock[25] (HF), 2nd-order perturbation theory[26] (MP2), coupled cluster theory with single and double excitations[27] (CCSD), and CCSD with quasiperturbative connected triple excitations[28] (CCSD(T)).

All density functional calculations were performed using the *Gaussian 03*[29] program and the MN-GFM[30] functional module. CCSD(T) calculations were carried out by *Molpro-2006.1*.[31]

3. Diffuse functions

Since the exponential diffuse functions originally developed[7] for use with the 3-21G, 6-21G, and 6-31G basis sets were later found[8] to also be appropriate for use with the 6-311G basis set, we form the new "plus" basis sets by simply adding a diffuse *sp* shell to each non-hydrogenic atom, using the standard exponents that are used in both the 6-31+G and 6-311+G basis sets. To give the reader some idea of how these compare to the most diffuse exponents in the augmented correlation-consistent basis sets, Table 2 compares the exponents of the most diffuse *s, p,* and *d* functions in the triple zeta basis set series under consideration here. We see that the exponential parameters of *s* and *p* diffuse functions of the plus and aug basis sets are similar.

The question arises: what is a "diffuse" basis function. In practice the exponent of the most diffuse valence basis function in the cc-pVxZ series decreases as x increases. A similar trend is found in even-tempered basis sets.[32] Eventually, one might wonder, doesn't the most diffuse basis function become indistinguishable from a "diffuse" basis function? In principle, yes, but in practice, no. For example consider the most diffuse s on carbon in the cc-pVxZ bases. For $x = 2$–6, these are 0.1596, 0.1285, 0.1111, 0.1019, and 0.08635,[33] respectively, whereas the added diffuse s function in the plus set has exponent 0.0438, and the added diffuse s functions in the aug sets have exponents of 0.0469, 0.04402, 0.04145, 0.0394, and 0.0354. Thus there is a wide gap (0.086 to 0.044) between the most diffuse valence basis function and the added "diffuse" basis function, and one would have to go to unrealistically high x before there is any ambiguity; so the definition of "diffuse" is operationally clear.

One could imagine optimizing diffuse functions for various properties such as atomic or molecular Rydberg states, atomic or molecular electron affinities, atomic or molecular polarizabilities, atomic or molecular electron densities, and so forth. One would obtain different results by optimizing against different property databases, but the optimum diffuse functions by any of these approaches would be expected, based on experience, to be a factor of ~2–4 smaller than the exponent of the least diffuse valence basis function.

4. Results and discussion

Tables 3–6 give errors relative to the databases[12-15] explained in Section 2. Tables 3 and 4 show results for ionization potentials and electron affinities. The DFT errors are almost the same for the plus and aug basis sets, even for electron affinities. The coupled cluster calculations, however, are more slowly convergent with respect to the addition of diffuse functions. In order to illustrate this even more clearly, we added the heavy-atom diffuse d functions of the aug-cc-pVTZ basis to cc-pVDZ+. The CCSD(T) MUE dropped to only 2.73 kcal/mol for ionization potentials and 3.57 kcal/mol for electron affinities. Although diffuse functions are important for DFT,[12] it is apparently not necessary to exhaust the diffuse space as seems to be required in WFT.

Table 5 shows results for atomization energies. Here the diffuse functions have only a small effect. Table 6, however, shows a large effect for barrier heights, especially for nucleophilic substitution reactions (which is expected since these reactions involve anions). In all DFT cases (all four subdatabasis, two density functionals, and both double and triple zeta tests), the plus basis sets account quite well for the effect of diffuse functions seen with the larger aug basis sets. They are less successful for the WFT tests, but they often pick up a good fraction of the diffuse function increment at much less cost than is required for aug calculations.

A specific example of barrier height calculations is presented in Table 7. The forward and reverse barrier heights of one of the reactions in the DBH24/08 database were calculated using M06-2X density functional with cc-pVxZ, cc-pVxZ+, and aug-cc-pVxZ (x = T and Q) basis sets. Adding diffuse s and p functions to the heavy atoms changes the calculated barrier height by 4.64−9.46 kcal/mol. The additional effect of adding diffuse functions on hydrogens and higher angular momentum diffuse functions (d and f when x = T and d, f, and g when x = Q) provides a further change in barrier heights of only 0.70-0.85 kca/mol. The numbers of contracted Gaussian basis functions for this transition state are 146, 158, and 230 for the cc-pVTZ, cc-pVTZ+, and aug-cc-pVTZ basis sets, respectively; these numbers are 285, 297, and 424 for the cc-pVQZ, cc-pVQZ+, and aug-cc-pVQZ basis sets, respectively. The relative computational costs of the cc-pVxZ+ basis sets are 1.2 for x = T and 1.1 for x = Q. In the case of the aug-cc-pVxZ basis sets they are 4.4 for x = T and 5.5 for x = Q. These costs are calculated as ratio of the cost of a single-point energy calculation for the plus or aug basis set relative to the cost for the corresponding plain basis sets (cc-pVxZ); calculations were performed on a Linux cluster with two dual-core 2.6 GHz AMD Opteron processors. Therefore the plus basis sets take account of the main effect of diffuse functions for these barrier height calculations without significantly increasing computational costs.

Next we turn to BSSE. The first BSSE test is restricted to the two $H_2SO_4(NH_3)$ complexes. We averaged the *%CpC* over the two geometries, with five levels of DFT (M05-2X and all four members of the M06 functional family) and four levels of WFT

(HF, MP2, CCSD, and CCSD(T)) for a total of 18 cases for each basis set. The results are in Table 8, and they are dramatic; either the plus or the aug basis sets reduce *%CpC* by a factor of 2. With DFT, the computer time for the aug calculations in Table 8 is about 4 times larger than the cc-pVTZ calculations, whereas the time for the cc-pVTZ+ calculations only 1.5 times larger than that for cc-pVTZ with the four hybrid density functionals and almost the same as cc-pVTZ with M06-L.

The cc-pV(T+d)Z+ basis is very similar in quality to the MG3S basis set[12] that our group has used successfully in many applications. For example, MG3S has 269 contracted functions vs. 259 (Table 1) for cc-pV(T+d)Z+, and they have identical diffuse *s* and *p* exponents (Table 2). However MG3S gives 13.5% for the test in Table 8, so cc-pVTZ+ should be considered as a possible improvement for calculating noncovalent interactions.

The final test involves averaging *%CpC* over all ten complexes with the M06-2X density functional and the HF, MP2, CCSD, and CCSD(T) levels of WFT, for a total of 50 cases for each basis set. The results are in Table 9. Here the cc-pV(T+d)Z+ basis set reduces *%CpC* by 36% whereas aug-cc-pV(T+d)Z reduces it by 49%, averaged over the 50 cases.

So far these tests have been applied to the plus basis sets. Next we consider whether similar performance would be obtained with the maug-cc sets. (One can anticipate, especially from the discussion in Section 3, that the performance *will* be similar, but it may be useful to quantitatively validate this.) Table 10 shows some results, similar to Table 6, for maug-cc basis sets; the results for maug-cc-pVDZ are similar to those in Table 6 for the plus basis sets. The results for maug-cc-pVDZ and maug-cc-pVTZ are very similar for reactions in the DBH24/08 database to those for cc-pVDZ+ and cc-pVTZ+ basis sets. For %*CpC* we tested the maug-cc-pV(T+d)Z basis set; a comparison of the cc-pV(T+d)Z+ basis set with the maug-cc-pV(T+d)Z basis set for the binding energies and basis set superposition errors of the dimers shown in Figure 1 is given in Table 11. Again, we see very similar performance for cc+ and maug-cc basis sets, as expected.

A strategy similar to the plus and maug strategies is to delete all diffuse functions of the aug-cc-pVxZ basis sets on hydrogenic atoms and keep all the diffuse functions on nonhydrogenic atoms.[34–36] Another strategy is to delete the highest-angular-momentum diffuse functions on both hydrogenic atoms and nonhydrogenic atoms. Both these strategies have been employed more widely than the plus or maug strategy, although they both lead to much larger basis sets (for a given x) than plus or maug. Note that reducing the number of basis functions for a given x either decreases computation time for that x or allows the use of higher x and therefore increases accuracy.

The effect of diffuse functions on CpC has also been examined previously.[35–37] It is beyond the scope of the present study to review the interesting theoretical issues underlying the applicability (or not) of DFT to electron affinities, but the interested reader can consult a review[40] for this. Jensen,[41] in a more recent study, examined the importance of diffuse s, p, and d functions for computing electron affinities, multipole moments, and polarizabilities by DFT and found that diffuse s and p functions are more important than diffuse d functions, but diffuse d functions are sometimes important. He also pointed out the difficulty or impossibility of optimizing the diffuse functions in certain cases.

Selective pruning of unaugmented cc-pVxZ basis sets has also been examined. Wilson and coworkers examined such truncations[38,39] and showed, for example, that h and g functions can often be deleted from the cc-pV5Z basis set with only a small loss of accuracy for energies or geometries.

5. Concluding remarks

While the addition of diffuse functions is necessary, in many cases only diffuse functions of low angular momentum (i.e. diffuse s and p functions) are needed, and furthermore they are often needed only on heavy atoms. The cc-pVxZ+ basis sets are designed to take advantage of this, and as a consequence their basis set size and cost are much smaller than those of the aug-cc-pVxZ basis sets, which include diffuse functions of both low and high angular momentum on all atoms. However, the quality of DFT results obtained by using cc-pVTZ+ is much closer to that of aug-cc-pVTZ than to that of

cc-pVTZ. Similarly, results for cc-pVDZ+ are closer to those of aug-cc-pVDZ than to those of cc-pVDZ. In fact, in many cases the plus basis sets perform equally well as the aug ones. The benefits of using cc-pVxZ+ basis sets with WFT are less dramatic than in the case of DFT. However, they can serve as a good intermediate step between cc-pVTZ and aug-cc-pVTZ and in fact they are often affordable where the full aug basis is not.

Supporting Information Available. Five geometries of complexes optimized by M06-2X/MG3S and one [oa-H_2SO_4 (NH_3)] contrived geometry for the dimers shown in Figure 1 and geometries of the corresponding individual gas-phase monomers with which the binding energies of those dimers were calculated. This material is available free of charge via the Internet at http://pubs.acs.org/.

Table 1. Number of contracted basis functions for $H_2SO_4(NH_3)$

	$x = D$	$x = T$	$x = T+d$	$x = Q$
cc-pVxZ	113	254	259	484
cc-pVxZ+	137	278	283	508
aug-cc-pVxZ	187	395	400	714
maug-cc-pVxZ	137	278	283	508
cc-pV(x+d)Z	118	254	264	489
cc-pV(x+d)Z	142	283	288	513
aug-cc-pV(x+d)Z	192	400	405	719
maug-cc-pV(x+d)Z	142	283	288	513

Table 2. Most diffuse exponents of various symmetries

l	Basis Set	H	C	N	O	S	Cl
s	cc-pVTZ	0.1027	0.1285	0.1787	0.2384	0.1322	0.1625
	cc-pVTZ+	0.1027	0.0438	0.0639	0.0845	0.0405	0.0483
	aug-cc-pVTZ	0.02526	0.04402	0.0576	0.07376	0.0497	0.0591
	maug-cc-pVTZ	0.1027	0.04402	0.0576	0.07376	0.0497	0.0591
p	cc-pVTZ	0.388	0.1209	0.1725	0.214	0.1098	0.1301
	cc-pVTZ+	0.388	0.0438	0.0638	0.0845	0. 0405	0.0483
	aug-cc-pVTZ	0.102	0.03569	0.0491	0.05974	0.0351	0.0419
	maug-cc-pVTZ	0.388	0.03569	0.0491	0.05974	0.0351	0.0419
d	cc-pVTZ	1.057	0.318	0.469	0.645	0.269	0.344
	cc-pVTZ+	1.057	0.318	0.469	0.645	0.269	0.344
	aug-cc-pVTZ	0.247	0.1	0.151	0.214	0.101	0.135
	maug-cc-pVTZ	1.057	0.318	0.469	0.645	0.269	0.344

Table 3. Mean unsigned errors (MUEs) (in kcal/mol) in ionization potentials

	B3LYP	M06-2X	CCSD(T)
cc-pVDZ	3.14	2.98	10.23
cc-pVDZ+	4.63	2.87	8.85
aug-cc-pVDZ	4.77	2.96	5.68
cc-pVTZ	4.15	2.39	3.44
cc-pVTZ+	4.59	2.63	3.15
aug-cc-pVTZ	4.67	3.45	1.93

Table 4. Mean unsigned errors (MUEs) (in kcal/mol) in electron affinities

	B3LYP	M06-2X	CCSD(T)
cc-pVDZ	20.84	18.77	30.98
cc-pVDZ+	3.05	4.05	10.49
aug-cc-pVDZ	3.03	3.69	5.27
cc-pVTZ	10.14	8.35	15.05
cc-pVTZ+	2.34	3.06	5.34
aug-cc-pVTZ	2.51	2.98	2.01

Table 5. Mean unsigned errors per bond (MUEPBs) (in kcal/mol) in atomization energies[a]

	B3LYP	M06-2X	CCSD(T)
cc-pVDZ	2.80	2.07	8.87
cc-pVDZ+	3.16	2.38	8.87
aug-cc-pVDZ	2.81	2.13	8.07
cc-pVTZ	0.85	0.40	3.12
cc-pVTZ+	0.94	0.44	3.11
aug-cc-pVTZ	0.94	0.42	2.62

[a]The MUE in atomization energies is divided by the average number (4.83) of bonds per molecule in the AE6 database.

Table 6. Mean unsigned errors (MUEs) (in kcal/mol) in the barrier heights of the DBH24/08 database

	HATBH6	NSBH6	UABH6	HTBH6	DBH24
B3LYP/cc-pVDZ	8.63	12.89	2.21	6.48	7.55
B3LYP/cc-pVDZ+	7.45	3.91	2.02	5.98	4.84
B3LYP/aug-cc-pVDZ	7.53	4.15	2.17	5.71	4.89
B3LYP/cc-pVTZ	6.86	9.59	1.65	4.88	5.75
B3LYP/cc-pVTZ+	6.69	4.23	1.71	4.68	4.33
B3LYP/aug-cc-pVTZ	6.81	3.32	1.70	4.71	4.13
M06-2X/cc-pVDZ	2.78	9.64	1.29	1.94	3.91
M06-2X/cc-pVDZ+	1.90	1.34	1.24	1.53	1.50
M06-2X/aug-cc-pVDZ	1.46	1.25	1.35	1.27	1.33
M06-2X/cc-pVTZ	1.08	5.21	1.02	1.43	2.18
M06-2X/cc-pVTZ+	0.77	0.76	1.13	1.30	0.99
M06-2X/aug-cc-pVTZ	0.67	0.66	1.10	1.30	0.93
CCSD(T)/cc-pVDZ	3.94	7.94	1.40	3.03	4.08
CCSD(T)/cc-pVDZ+	4.35	1.08	1.44	1.76	2.16
CCSD(T)/aug-cc-pVDZ	2.27	1.99	0.68	0.76	1.42
CCSD(T)/cc-pVTZ	1.90	5.27	0.47	1.41	2.26
CCSD(T)/cc-pVTZ+	1.65	0.81	0.55	0.99	1.00
CCSD(T)/aug-cc-pVTZ	0.95	0.78	0.33	0.70	0.69

Table 7. Barrier heights (kcal/mol) of the reaction $OH^- + CH_3F \leftrightarrow HOCH_3 + F^-$ calculated using cc-pVxZ, cc-pVxZ+, and aug-cc-pVxZ (x = T and Q) basis sets with the M06-2X density functional[a]

Basis set	V_f	V_r
cc-pVTZ	-12.71	8.67
cc-pVTZ+	-3.25	17.52
aug-cc-pVTZ	-2.40	18.28
cc-pVQZ	-8.38	12.91
cc-pVQZ+	-2.37	17.85
aug-cc-pVQZ	-1.60	18.55

[a] V_f is the forward barrier height and V_r is the reverse barrier height.

Table 8. *%CpC* values averaged over results from five levels of DFT, four levels of WFT, and two geometries of $H_2SO_4(NH_3)$

Basis Set	Average *%CpC*
cc-pVTz	17.0
cc-pV(T+d)Z	17.0
cc-pVTZ+	8.1
cc-pV(T+d)Z+	8.2
aug-cc-pVTZ	8.9
aug-cc-pV(T+d)Z	8.7

Table 9. Average *%CpC* values over four levels of WFT and one level of DFT for all ten complexes

Basis Set	Average
cc-pV(T+d)Z	39.4
cc-pV(T+d)Z+	25.3
aug-cc-pV(T+d)Z	20.2

Table 10. Mean unsigned errors (MUEs) (in kcal/mol) in the barrier heights of the DBH24/08 database using cc-pVDZ+ and maug-cc-pVTZ basis sets[a]

	HATBH6	NSBH6	UABH6	HTBH6	DBH24
B3LYP/maug-cc-pVDZ	7.66	3.31	2.02	5.83	4.71
M06-2X/maug-cc-pVDZ	1.95	1.25	1.23	1.39	1.46
CCSD(T)/maug-cc-pVDZ	4.15	0.99	1.44	1.85	2.11
B3LYP/maug-cc-pVTZ	6.71	3.28	1.71	4.68	4.09
M06-2X/maug-cc-pVTZ	0.73	0.73	1.14	1.29	0.97
CCSD(T)/maug-cc-pVTZ	1.70	0.30	0.55	1.00	0.89

[a]The maug-cc-pV*x*Z basis set is the aug-cc-pV*x*Z with all diffuse functions removed except for the *s* and *p* diffuse functions on nonhydrogenic atoms.

Table 11. Counterpoise correction (*CpC*, kcal/mol) from M06-2X calculations for various dimers using the cc-pV(T+d)Z+ and maug-cc-pV(T+d)Z basis sets

Dimer	cc-pV(T+d)Z+	maug-cc-pV(T+d)Z[a]	ΔCpC[b]
chb-$(H_2O)_2$	0.16	0.12	-0.03
bhb-$(H_2O)_2$	0.25	0.24	-0.02
na-$H_2SO_4(NH_3)$	0.38	0.35	-0.02
oa-$H_2SO_4(NH_3)$	0.11	0.11	0.00
sp-$(CO_2)_2$	0.09	0.06	-0.03
ts-$(CO_2)_2$	0.08	0.06	-0.02
ct-$NH_3(Cl_2)$	0.21	0.23	0.02
dd-$H_2S(HCl)$	0.13	0.10	-0.02
pp-$(C_2H_4)_2$	0.06	0.06	0.00
wi-$(CH_4)_2$	0.03	0.03	0.00
MSD[c]			-0.01

[a]The maug-cc-pV(T+d)Z basis set is the aug-cc-pV(T+d)Z with all diffuse functions removed except for the *s* and *p* diffuse functions on nonhydrogenic atoms.
[b]This column gives the energy difference (in kcal/mol) between the two previous columns; the cc-pV(T+d)Z+ *CpC* result is subtracted from the maug-cc-pV(T+d)Z *CpC* one.
[c]MSD stands for "mean signed difference" and is the average of the ΔCpC values (in kcal/mol).

Hydrogen Bonded
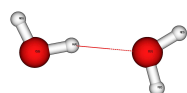
chb-$(H_2O)_2{}^a$
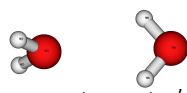
bhb-$(H_2O)_2{}^b$
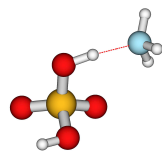
na-$H_2SO_4(NH_3)^c$
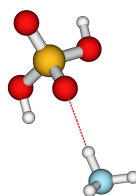
oa-$H_2SO_4(NH_3)^d$

Quadrupole-Quadrupole
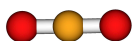
sp-$(CO_2)_2{}^e$
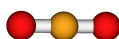
ts-$(CO_2)_2{}^f$

Other
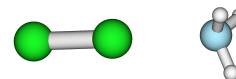
ct-$NH_3(Cl_2)^g$

dd-$H_2S(HCl)^h$
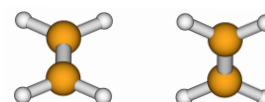
pp-$(C_2H_4)_2{}^i$
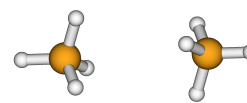
wi-$(CH_4)_2{}^j$

Figure 1 Ten complexes used for the BSSE tests: (a) conventionally hydrogen-bonded (chb) water dimer, (b) bifurcated hydrogen-bonded (bhb) water dimer, (c) hydrogen-bonded dimer of sulfuric acid and ammonia where nitrogen is a hydrogen acceptor (na), (d) hydrogen-bonded dimer of sulphuric acid and ammonia where oxygen is a hydrogen acceptor (oa), (e) slipped parallel (sp) carbon dioxide dimer, (f) T-shaped (ts) carbon dioxide dimer, (g) charge trasfer (ct) dimer of chlorine and ammonia, (h) dipole-dipole (dd) hydrogen chloride and sulfur hydride dimer, (i) π–π stacking (pp) ethane dimer, and (j) weak interaction (wi) methane dimer.

19

References

[1]Davidson, E. R.; Feller, D. *Chem. Rev.* **1986**, *86*, 681.

[2]Dunning, T. H. *J. Chem. Phys.* **1989**, *90*, 1007.

[3]Kendall, R. A.; Dunning, T. H.; Harrision, R. J. *J. Chem. Phys.* **1992**, *96*, 6796; Kendall, R. A.; Dunning T. H.; Harrison, R. J. *J. Chem. Phys.* **1992**, *96*, 6796.

[4]Woon, D. E.; Dunning, T. H. *J. Chem. Phys.* **1993**, *98*, 1358.

[5]Woon, D. E.; Dunning, T. H. *J. Chem. Phys.* **1994**, *100*, 2975.

[6]Dunning, T. H., Jr.; Peterson, K. A.; Wilson, A. K. *J. Chem. Phys.* **2001**, *114*, 9244.

[7]Clark, T.; Chandresekhar, J.; Schleyer, P. v. R. *J. Comput. Chem.* **1983**, *4,* 294.

[8]Frisch, M. J.; Pople, J. A.; Binkley, J. S. *J. Chem. Phys.* **1984**, *80*, 3265.

[9]Boys, S. F.; Bernardi, F. *Mol. Phys.* **1970**, *19*, 553.

[10]Schwenke, D. W.; Truhlar, D. G. *J. Chem. Phys.* **1985**, *82*, 2418. Simon, S.; Duran, M.; Dannenberg, J. J. *J. Chem. Phys.* **1996**, *105*, 11024. Errata: **1987**, *86*, 3760.

[11]Valiron, P.; Mayer, I. *Chem. Phys. Lett.* **1997**, *275*, 46.

[12]Lynch, B. J.; Zhao, Y.; Truhlar, D. G. *J. Phys. Chem. A* **2003**, *107*, 1384.

[13]Lynch, B. J.; Truhlar, D. G. *J. Phys. Chem. A* **2003**, *107*, 3898.

[14]Lynch, B. J.; Truhlar, D. G. *J. Phys. Chem. A* **2004**, *107*, 8996. Erratum: *J. Phys. Chem. A* **2004**, *108*, 1460.

[15]Zheng, J.; Zhao, Y.; Truhlar, D. G. *J. Chem. Theory Comput.* **2007**, *3*, 569; Zheng, J.; Zhao, Y.; Truhlar, D. G. *J. Chem. Theory Comput.*, submitted.

[16]Lynch, B. J.; Zhao, Y.; Truhlar, D. G. J. *Phys. Chem. A* **2005**, *109*, 1643.

[17]Zhao, Y.; Truhlar, D. G. *J. Phys. Chem.* A **2005**, *109*, 5656.

[18]Zhao, Y.; Schultz, N. E.; Truhlar, D. G. *J. Chem. Theory Comput.* **2006**, *2*, 364.

[19]Zhao, Y.; Truhlar, D. G. *Theor. Chem. Acc.* **2008**, *120*, 215.

[20]Kohn, W.; Becke, A. D.; Parr, R. G. *J. Phys. Chem.* **1996**, *100,* 12974.

[21]Raghavachari, K.; Anderson, J. B. *J. Phys. Chem.* **1996**, *100,* 12960.

[22]Stephens, P. J.; Devlin, F. J.; Chabalowski, C. F.; Frisch, M. J. *J. Phys. Chem.* **1994**, *98*, 11623.

[23]Zhao, Y.; Truhlar, D. G. *J. Chem. Phys.* **2006**, *125*, 194101/1.

[24] Zhao, Y.; Truhlar, D. G. *J. Phys. Chem. A* **2006**, *110*, 13126.

[25] Roothaan, C. C. J. *Rev. Mod. Phys*. **1951**, *23*, 69.

[26] Møller, C.; Plesset, M. S. *Phys. Rev*. **1934**, *46*, 618.

[27] Purvis, G. D.; Bartlett, R. J. *J. Chem. Phys*. **1982**, *76*, 1910.

[28] Raghavachari, K.; Trucks, G. W.; Pople, J. A.; Head-Gordon, M. *Chem. Phys. Lett*. **1989**, *157*, 479.

[29] Frisch, M. J.; Trucks, G. W.; Schlegel, H. B.; Scuseria, G. E.; Robb, M. A.; Cheeseman, J. R.; Montgomery, Jr., J. A.; Vreven, T.; Kudin, K. N.; Burant, J. C.; Millam, J. M.; Iyengar, S. S.; Tomasi, J.; Barone, V.; Mennucci, B.; Cossi, M.; Scalmani, G.; Rega, N.; Petersson, G. A.; Nakatsuji, H.; Hada, M.; Ehara, M.; Toyota, K.; Fukuda, R.; Hasegawa, J.; Ishida, M.; Nakajima, T.; Honda, Y.; Kitao, O.; Nakai, H.; Klene, M.; Li, X.; Knox, J. E.; Hratchian, H. P.; Cross, J. B.; Bakken, V.; Adamo, C.; Jaramillo, J.; Gomperts, R.; Stratmann, R. E.; Yazyev, O.; Austin, A. J.; Cammi, R.; Pomelli, C.; Ochterski, J. W.; Ayala, P. Y.; Morokuma, K.; Voth, G. A.; Salvador, P.; Dannenberg, J. J.; Zakrzewski, V. G.; Dapprich, S.; Daniels, A. D.; Strain, M. C.; Farkas, O.; Malick, D. K.; Rabuck, A. D.; Raghavachari, K.; Foresman, J. B.; Ortiz, J. V.; Cui, Q.; Baboul, A. G.; Clifford, S.; Cioslowski, J.; Stefanov, B. B.; Liu, G.; Liashenko, A.; Piskorz, P.; Komaromi, I.; Martin, R. L.; Fox, D. J.; Keith, T.; Al-Laham, M. A.; Peng, C. Y.; Nanayakkara, A.; Challacombe, M.; Gill, P. M. W.; Johnson, B.; Chen, W.; Wong, M. W.; Gonzalez, C.; and Pople, J. A. *Gaussian03*, *Revision C.02*, Gaussian, Inc.: Wallingford, CT, 2004.

[29] Frisch, M. J.; Trucks, G. W.; Schlegel, H. B.; Scuseria, G. E.; Robb, M. A.; Cheeseman, J. R.; Montgomery, Jr., J. A.; Vreven, T.; Kudin, K. N.; Burant, J. C.; Millam, J. M.; Iyengar, S. S.; Tomasi, J.; Barone, V.; Mennucci, B.; Cossi, M.; Scalmani, G.; Rega, N.; Petersson, G. A.; Nakatsuji, H.; Hada, M.; Ehara, M.; Toyota, K.; Fukuda, R.; Hasegawa, J.; Ishida, M.; Nakajima, T.; Honda, Y.; Kitao, O.; Nakai, H.; Klene, M.; Li, X.; Knox, J. E.; Hratchian, H. P.; Cross, J. B.; Bakken, V.; Adamo, C.; Jaramillo, J.; Gomperts, R.; Stratmann, R. E.; Yazyev, O.; Austin, A. J.; Cammi, R.; Pomelli, C.; Ochterski, J. W.; Ayala, P. Y.; Morokuma, K.; Voth, G. A.; Salvador, P.; Dannenberg, J. J.; Zakrzewski, V. G.; Dapprich, S.; Daniels, A. D.; Strain, M. C.;

Farkas, O.; Malick, D. K.; Rabuck, A. D.; Raghavachari, K.; Foresman, J. B.; Ortiz, J. V.; Cui, Q.; Baboul, A. G.; Clifford, S.; Cioslowski, J.; Stefanov, B. B.; Liu, G.; Liashenko, A.; Piskorz, P.; Komaromi, I.; Martin, R. L.; Fox, D. J.; Keith, T.; Al-Laham, M. A.; Peng, C. Y.; Nanayakkara, A.; Challacombe, M.; Gill, P. M. W.; Johnson, B.; Chen, W.; Wong, M. W.; Gonzalez, C.; and Pople, J. A. *Gaussian03, Revision C.02*, Gaussian, Inc.: Wallingford, CT, 2004.

[30] Zhao, Y.; Truhlar, D. G. *MN-GFM: Minnesota Gaussian Functional Module–version 3.0*; University of Minnesota: Minneapolis, MN, 2007.

[31] Werner, H.; Knowles, P. J.; Scheutz, M.; Lindh, R.; Celani, P.; Korona, T.; Rauhut, G.; Manby, F. R.; Amos, R. D.; Bernhardsson, A.; Berning, A.; Cooper, D. L.; Deegan, M. J. O.; Dobbyn, A. J.; Ecker, F. H. C.; Hertzer, A.; Lloyd, W.; McNicholas, S. J.; Meyer, W.; Mura, M. E.; Nicklass, A.; Palmieri, P.; Pitzer, R.; Schumann, U.; Stoll, H.; Stone, A. J.; Torroni, R.; Thorsteinsson, T. 1997, *MOLPRO 2006.1*; University College Consultants Ltd.: Cardiff, Wales, UK, 2006.

[32] Bardo, R. D.; Ruedenberg, K. *J. Chem. Phys.* **1973**, *59*, 5956.

[33] Wilson, A. K.; van Mourik, T.; Dunning, T. H. Jr. *Theochem*. **1997**, *388*, 339.

[34] Sinnokrot, M. O.; Sherill, C. D. *J. Phys. Chem. A* **2003**, *107*, 8377.

[35] Hwang, R.; Muh, S. B.; Lee, J. S. *Mol. Phys.* **2003**, *101*, 1429.

[36] Elsohly, A. M.; Tschumpter, G. S. *Int. J. Quantum Chem.* **2009**, *109*, 91.

[37] Halkier, A.; Koch, H.; Jorgensen, P.; Christiansen, O.; Nielsen, I. M. B.; Helgaker, T. *Theor. Chem. Acc.* **1997**, *97*, 150.

[38] Prascher, B. P.; Wilson, B. R.; Wilson, A. K. *J. Chem. Phys.* **2007**, *127*, 124110.

[39] Mintz, B.; Friskell, S.; Shah, A.; Wilson, A. K. *Int. J. Quantum Chem.* **2007**, *107* 3077.

[40] Rienstra-Kiracofe, J. C.; Tsuchumper, G. S., Schaefer, H. F. III; Nanadi, S.; Ellison, G. B. *Chem. Rev.* **2002**, *102*, 1231.

[41] Jensen, F. *J. Chem. Phys.* **2002**, *117*, 9234.

Errata and Addendum: Efficient Diffuse Basis Sets: cc-pV*x*Z+ and maug-cc-pV*x*Z
(for Journal of Chemical Theory and Computation 5, 1197–1202 (2009). DOI:
10.1021/ct800575z).

Ewa Papajak, Hannah R. Leverentz, Jingjing Zheng, and Donald G. Truhlar*

*Department of Chemistry and Supercomputing Institute,
University of Minnesota, Minneapolis, Minnesota 55455-0431*

Errata.

Some data in Tables 3–6 are corrected. These corrections do not change any of our
discussion or conclusions in the paper. In the second paragraph of Section 4, "cc-
pVDZ+" should be "cc-pVTZ+".

Addendum.

We also present here some further calculations that do not correct an error in the original
article but that provide further relevant information. In particular, we note that the article
tested the new plus basis sets for ionization potentials, electron affinities, atomization
energies, barrier heights, and basis set superposition errors. We then presented tests of
another set of basis sets, called maug basis sets, obtained by truncating the aug basis sets
to the same size as the plus basis sets. The maug basis sets were tested only for barrier
heights and basis set superposition errors, and we found very similar performance to the
plus basis sets. As an example of the differences in the basis sets, diffuse functions on O
in maug-cc-pVTZ have exponential parameters of 0.07376 for s functions and 0.05974
for p; these exponential parameters are smaller than those in the plus basis set, where
both parameters are 0.0854. The most difficult tests of the adequacy of a scheme for
diffuse basis functions are provided by electron affinities. We have now tested maug-cc-
pV*x*Z against cc-pV*x*Z+ with both $x = D$ and $x = T$ for electron affinities, and we found
better performance with the maug basis sets for M06-2X (better on average) and
CCSD(T) (always better), especially for systems containing oxygen atoms (and to a
lesser extent for Si$^-$ and C$^-$), but better performance (on average) with the plus basis set
for B3LYP. However, in all 78 cases the anion energies are lower for the maug basis set
than the corresponding plus one, so the improvement of the plus basis sets for B3LYP

23

electron affinities is presumably due to cancellation of basis set error with a large error in the opposite direction from the functional itself. Table A1 gives two additional rows for the original Table 4 that show the mean unsigned errors in electron affinities with two maug basis sets. The conclusion is that anion energies and electron affinities are more sensitive than barrier heights and basis set superposition errors to the precise values of the diffuse exponents, and the maug basis sets are more accurate for such calculations, probably because the exponents were optimized for atomic anions.[1]

Table 3. Mean unsigned errors (MUEs) (in kcal/mol) in ionization potentials

	B3LYP	M06-2X	CCSD(T)
cc-pVDZ+	4.88	3.09	8.57
aug-cc-pVTZ		2.70	

Table 4. Mean unsigned errors (MUEs) (in kcal/mol) in electron affinities

	B3LYP	M06-2X	CCSD(T)
cc-pVDZ		20.10	
cc-pVDZ+	3.17	2.66	9.77
aug-cc-pVDZ		2.37	
cc-pVTZ		9.85	
cc-pVTZ+		1.92	
aug-cc-pVTZ		1.55	

Table 5. Mean unsigned errors per bond (MUEPBs) in (kcal/mol) in atomization energies

	B3LYP	M06-2X	CCSD(T)
cc-pVDZ+	3.15	2.38	8.88

Table 6. Mean unsigned errors (MUEs) (in kcal/mol) in the barrier heights of the DBH24/08 database

	HATBH6	NSBH6	UABH6	HTBH6	DBH24
B3LYP/cc-pVDZ+	7.57	3.79	5.81	4.80	
M06-2X/cc-pVDZ+	2.02	1.17	1.37	1.45	
CCSD(T)/cc-pVDZ+	4.15	0.82	1.79	2.05	

Table A1. Mean unsigned errors (MUEs) (in kcal/mol) in electron affinities

	B3LYP	M06-2X	CCSD(T)
maug-cc-pVDZ	3.19	2.46	9.41
maug-cc-pVTZ	2.49	1.57	4.88

References

(1) Kendall, R. A.; Dunning, Jr., T. H. Jr.; Harrison, R. J. *J. Chem. Phys.* **1992**, *96*, 6796.

Chapter 2.   Efficient Diffuse Basis Sets for Density Functional Theory

Ewa Papajak and Donald G. Truhlar

Department of Chemistry and Supercomputing Institute,
University of Minnesota, 207 Pleasant Street S.E.,
Minneapolis, MN 55455-0431, USA

Eliminating all but the *s* and *p* diffuse functions on the non-hydrogenic atoms and all diffuse functions on the hydrogen atoms from the aug-cc-pV(x+d)Z basis sets of Dunning and coworkers, where (where x = D, T, Q, …), yields the previously proposed "minimally augmented" basis sets, called maug-cc-pV(x+d)Z. Here we present extensive and systematic tests of these basis sets for density functional calculations of chemical reaction barrier heights, hydrogen bond energies, electron affinities, ionization potentials, and atomization energies; the tests show that the maug-cc-pV(x+d)Z basis sets are as accurate as the aug-cc-pV(x+d)Z ones for density functional calculations, but the computational cost savings are a factor of about two to six.

1. Introduction

For many quantum mechanical electronic structure calculations on molecules and chemical reactions, the results are sensitive to the inclusion of diffuse basis functions. Diffuse basis functions are spherical harmonics (or powers of Cartesian coordinates) times Gaussian functions with small exponents. These functions have long tails that allow the electrons to be farther from the nuclei. This is especially important for calculations on systems that require a good description of electrons in weakly bound orbitals or the outer parts of orbitals, such as many anions, transition states, and noncovalently bound systems.

Two systematic approaches to adding diffuse functions have emerged. The first is to add standard diffuse *s* and *p* functions (4 functions altogether) to nonhydrogenic

atoms—this is called a "plus" or "+" basis set—or to add diffuse s and p basis functions to nonhydrogenic atoms and diffuse s basis functions to H—this is called a "double +" or "++" basis set.[1] The second approach is to add a diffuse function to every atom for every symmetry already present in the original basis; this is called the augmented ("aug") approach.[2] For example, if a given basis set for sulfur atom has $s, p, d,$ and f basis functions, one adds $s, p, d,$ and f diffuse functions to that atom (a total of 16 functions, where all basis functions in this article use the spherical harmonic option–not the Cartesian one). Thus, as the underlying basis set becomes more complete, the number of diffuse functions increases. This makes the aug basis sets both larger and more rapidly convergent than the plus basis sets as the highest angular momentum of nondiffuse basis functions increases. However, in our previous paper[3] we have shown that in density functional calculations, the more expensive aug approach is not necessary, that is, the fixed number of diffuse functions of the plus sets is sufficient for results of double-, triple- and quadruple-zeta quality. In particular, we showed that augmentation of the cc-pVxZ (where x = D, T, Q, …) basis sets with the diffuse functions from the basis sets of Pople and coworkers, which yields cc-pVxZ+ basis sets, accounts for most of the effect that the full, much more expensive aug- basis set provide. We also mentioned that the aug-cc-pVxZ basis sets can be truncated to contain only s and p diffuse functions on the non-hydrogenic atoms. We called this series of basis sets minimally augmented and abbreviated them as maug-cc-pVxZ, and we presented some calculations with this kind of basis set; however the primary focus of the previous paper was on the plus strategy.

We have now carried out systematic tests of the performance of the maug-cc-pVxZ basis sets (where x stands for (D+d), (T+d), or (Q+d)) for density functional calculations, using both the popular B3LYP[4–7] density functional and also the recent, highly accurate M06-2X[8] density functional. We present the results of these tests here as a letter. Our tests involve computation of several commonly calculated and challenging molecular energetic properties. Barrier heights are the most important reaction parameters used for mechanism evaluation and kinetics calculations. Moreover they are a good challenge for our purposes, since the accuracy of the description of transition states sometimes depends strongly on the presence and quality of the diffuse

28

functions in a basis set. Since diffuse functions are often crucial in the description of noncovalent interactions such as hydrogen bonding, we also present tests on hydrogen bonding. Perhaps the most difficult test of the adequacy of the diffuse part of the basis set is the prediction of electron affinity values, because it involves anion calculations. Ionization potentials and atomization energy are also considered, because they are key thermochemical quantities.

In order to more specifically investigate the need for the diffuse basis functions on hydrogen atoms, we calculated electron affinity values for metal hydride.

To warn readers that all conclusions about the need for diffuse functions in density functional theory (DFT) calculations cannot be extended with equal success to wave function theory (WFT) calculations, we also present results of the electron affinity calculations at the second-order perturbation theory (MP2)[9] level.

Similar truncations as in maug-cc-pV(x+d)Z basis sets were performed for the maug-cc-pVxZ basis sets. The conclusions about the diffuse functions are the same as for the (x+d) series, which contains tight d functions on the elements in the $3p$ block of the periodic table. However, the use of (x+d) basis sets is recommended as they provide better quality results, especially at the DZ level and for hypervalent moelcules. The results for aug-cc-pVxZ, maug-cc-pVxZ, and cc-pVxZ basis sets are available in the supporting information, and main body of this letter will discuss only aug-cc-pV(x+d)Z, maug-cc-pV(x+d)Z, and cc-pV(x+d)Z basis sets.

2. Methods and databases

The databases employed for the present study are for barrier heights, hydrogen-bond interaction energies, electron affinities, ionization potentials, and bond energies. All energetic results presented in this communication were obtained using the *Gaussian 03*[10] program and the MN-GFM[11] functional module. The cost estimates listed in table 1 were calculated using the *Gaussian 09* program. All results are based on single-point calculations run at geometries[12] optimized with the QCISD/MG3 method (for the BH24, EA13/3, IP13/3, and AE6 databases) and the MC-QCISD/3[13] method (for the HB6 database) levels, and vibrational contributions are excluded (that is, we are testing the

methods for Born-Oppenheimer electronic energies (including nuclear repulsion), not for enthalpies). QCISD denotes quadratic configuration interaction with single and double excitations.[14] The geometries for all the species in the five databases considered are available in the databases' respective references given below.

The results provided by the two density functionals B3LYP and M06-2X with the fully augmented aug-cc-pV(x+d)Z basis sets, minimally augmented maug-cc-pV(x+d)Z basis sets, and unaugmented cc-pV(x+d)Z basis sets containing no diffuse functions were compared to the best estimates in the following databases:

- DBH24/08[15,16] database of diverse barrier heights, consisting of the best estimates for 24 barrier heights for the heavy-atom transfer reaction, nucleophilic substitution, hydrogen transfer, and unimolecular and association reactions;

- HB6[17] database, consisting of hydrogen bond energies for $(NH_3)_2$, $(HF)_2$, $(H_2O)_2$, NH_3-H_2O, $(HCONH_2)_2$, and $(HCOOH)_2$;

- EA13/3[18,19] database, consisting of electron affinities for C, S, O, Si, P, Cl, OH, PH, SH, PH_2, O_2, S_2, and Cl_2;

- IP13/3[18,19] database, consisting of contains ionization potentials for the same 13 species as in EA13/3 database;

- AE6[20] representative atomization energy database, consisting of atomization energies of SiH_4, SiO, S_2, propyne, glyoxal, and cyclobutane.

Since the computed values are compared here with experimental or well converged theoretical values in the databases, all the computed energetic data had the spin-orbit contributions added on for F, C, O, Cl, Si, S, OH, and HS,[21] and the experimental data had the zero-point contributions subtracted from them.

In table 1, we define the diffuse space in the fully augmented, minimally augmented, and unaugmented basis sets. In order to compare the approximate cost of the calculations involving the basis sets used in the tests, we report the sum N of the number of basis functions used in the calculations, summed over all the test cases in all five databases used, and the sum raised to the fourth power (N^4) which is how the cost of the hybrid DFT calculations in popular computer programs scale in the limit of large systems when linear-scaling algorithms are not used. For clarity the N^4 values were normalized

(denoted by subscript Nor) to the N^4 value for the least expensive basis set cc-pV(D+d)Z. In order to quantify the cost savings for a given x (x = D, T, Q) achieved by using maug basis sets instead of aug ones, we show in the $(N^4)_{Rel}$ column values normalized to the aug-cc-pV(x+d)Z N^4 values for each x. Since the limit of asymptotic scaling is never fully reached in practice, we also illustrate the timings with a real example; in particular we list single-point timings calculations on the medium-size molecule 1,4-butanedithiol $(C_4H_{10}S_2)$.

3. Results

Tables 2-7 provide the mean signed errors (MSEs) and the mean unsigned errors (MUEs, which can also be called mean absolute errors) for a given level of theory in the calculations involving species in a given database. We define MSE and MUE as follows:

$$MSE = \frac{1}{n} \sum_{i=1}^{n} e_i \tag{1}$$

$$MUE = \frac{1}{n} \sum_{i=1}^{n} |e_i| \tag{2}$$

In equations $1 - 2$, e_i is an error in a single property value (for example an ionization potential value for one molecule) in the database, which contains a total of n such values for different species. The mean error values for the atomization energies of the molecules in AE6 are divided by 4.83, which is the average number of bonds per molecule in this database, so that the results may be interpreted on a per bond basis.

It may be useful to comment on the meaning of the electron affinities. It is well know that density functional calculations with certain kinds of approximate density functionals predict unbound negative in the limit of a large basis set.[22] Nevertheless calculations with standard basis sets have been shown to often give stable and useful results.[23] The results presented here are a test of the stability of such standard calculations to the size of the diffuse subspace of the basis set.

4. Discussion

The tables show that there is essentially complete agreement between predictions of the fully (aug) and minimally (maug) augmented basis sets for density functional calculations in the triple zeta and quadruple zeta cases. For quadruple zeta, the MUE of the maug results is actually lower than the MUE of the aug results in six of the ten cases, and in the other four cases, the maug MUE is never higher than the aug MUE by more than 3%. And yet, the diffuse functions have a very important effect. For example, in table 4 for electron affinities, the MUE for the unaugmented basis is a factor of 2 or 4 times higher than the error in the maug basis, but no significant increase in accuracy is attained by proceeding from the maug basis to the fully augmented basis. At the triple zeta level, the effects of diffuse functions are larger, for example, decreasing the MUE by factors of 4 and 7 for the electron affinities, but again the maug MUE is almost the same as the aug MUE. For triple zeta, maug has a lower MUE for four of the six cases and never has an MUE higher than the aug one by more than 9%.

The effect of diffuse functions is largest for double zeta basis sets, with the MUE for electron affinities in unaugmented calculations being 7 or 9 times larger than that for the maug basis. We believe it is due to the fact that the unaugmented cc-pVDZ basis set is the least diffuse basis set considered in the present article. Therefore the effect of pruning of some of the diffuse functions on the quality of the results is the most significant at the double-zeta level. On average though, the ratio of the maug MUE to the aug one is greater than unity by only 13%, and it is only 2% greater than unity if we omit hydrogen bonding. The full aug set of the diffuse functions decreases the double zeta MUE for hydrogen bonding by a factor of 7–8, whereas the maug diffuse functions decrease it by only a factor of 5.

The cost savings that come from using the maug series of basis sets instead of aug are very large. Using the N^4 asymptotic scaling factors of table 1 shows that the minimally augmented diffuse basis sets maug-cc-pV(x+d)Z offer the same quality results as their aug analogs at a cost reduced by 73%, 73%, and 67% for x = Q, T, and D respectively. Alternatively if we use actual costs for specific calculations on 1,4-butanedithiol, the time savings using maug vs. aug basis sets are 82%, 68%, and 68% for

quadruple, triple, and double zeta basis sets, respectively, and for the B3LYP functional (these timings not shown in the table) they are 69%, 76%, and 52%.

One caveat on the conclusions drawn here is that the databases used for the tests presented here include no metal atoms, so the conclusions have been established only for nonmetals, although it would not be surprising if they were also found to hold for compounds containing metal atoms.

Another noteworthy point is that maug triple zeta is usually very close to the basis set limit for DFT, at least for the nonmetal systems in the present study.

To show that the diffuse functions on hydrogen are practically redundant, we present the dependence of the electron affinity of lithium hydride (LiH) in table 7. A metal hydride would be the case where H would be most likely to need diffuse functions, and electron affinities provide the toughest test of the need for diffuse functions, so the particular choice of an electron affinity of a metal hydride is a serious challenge. Deleting the diffuse functions on hydrogenic atoms from an "aug-" basis sets yields what we call a "jul-" basis set. From the data shown in Table 7 one can see that even for the electron affinity of metal hydride the diffuse functions on hydrogen are unnecessary for DFT calculations of energetic molecular properties. In particular, the difference in performance of aug and jul basis sets is practically non-existent. Results for two other metal hydrides (BeH and MgH) are available in supporting information; the error encountered by using jul instead of aug varies from 0.2% to 3.2% and from 1.4% to 9.4% for MgH and BeH, respectively, and so the results for these systems confirm the unimportance of diffuse functions on hydrides. For completeness we note that the monatomic hydrogen anion is an exception; for this one-center, two-electron system, it is essential to include diffuse functions for an accurate description (however, since the energy of this system has already been calculated accurately to several significant figures with explicitly correlated basis functions, its basis set requirements are a not a major concern here).

Table 8 shows that WFT is more slowly convergent than DFT with respect to the number of the diffuse functions on heavy atoms in the basis set used. However, the effect of diffuse functions on H has previously been shown to negligible for energetic

calculations even in WFT. In particular, an extensive study of basis set effects on the calculated bond energy and electron affinity of LiH showed that "diffuse functions on hydrogen have little importance for thermochemical calculations."[25]

The present study adds to previous work showing that conclusions about basis sets derived from many years of experience with WFT calculations do not necessarily hold for DFT.[18,26–31]

Although it is not the main point of this paper, we note that tables 2-6 contain 45 direct comparisons of mean unsigned errors for B3LYP to those for M06-2X for a given basis set and database. In one case the mean unsigned errors are the same, and in all other cases, M06-2X has the better performance.

5. Conclusions

The only case in tables 2-6 where the augmentation of the cc-pV(x+d)Z basis sets with the full aug set of the diffuse functions performs significantly better in the density functional theory calculations than the maug basis set is for two studied cases of hydrogen bonding at the double zeta level. In the other 28 cases considered here, the maug basis actually has a lower mean unsigned error (MUE) than the aug one in 12 of the cases, and the average ratio of the maug MUE to the aug one is only 1% greater than unity.

The present tests have been restricted to the main group. We recommend that for energetic molecular properties, including barrier heights, the aug basis sets be truncated to the maug level for density functional calculations on systems composed of main-group atoms.

Supporting Information Available: Additional tables showing root-mean-square errors and results for basis sets without tight d functions plus calculations on MgH and BeH.. This information is available free of charge via the Internet at http://pubs.acs.org.

Table 1. Definitions of the diffuse spaces in the various basis sets, numbers of basis functions in the databases, normalized and relative numbers of basis functions raised to the fourth power, and the normalized and relative computational time of a single-point energy calculation on $C_4H_{10}S_2$ using M06-2X.

basis set	Li–Ar	H	N	$(N^4)_{Nor}$	$(N^4)_{Rel}$	$(C_4H_{10}S_2)_{Nor}$	$(C_4H_{10}S_2)_{Rel}$
aug-cc-pV(Q+d)Z	spdfg	spdf	17597	934	1.00	411	1.00
maug-cc-pV(Q+d)Z	sp	-	12665	251	0.27	74	0.18
cc-pV(Q+d)Z	-	-	12073	207	0.22	53	0.13
aug-cc-pV(T+d)Z	spdf	spd	10035	99	1.00	36	1.00
maug-cc-pV(T+d)Z	sp	-	7209	26	0.27	11.5	0.32
cc-pV(T+d)Z	-	-	6609	19	0.19	8.6	0.24
aug-cc-pV(D+d)Z	spd	sp	4989	6	1.00	4.5	1.00
maug-cc-pV(D+d)Z	sp	-	3783	2	0.33	1.5	0.32
cc-pV(D+d)Z	-	-	3183	1	0.17	1.0	0.22

Table 2. Errors in predictions of the barrier heights (kcal/mol) in the BH24/08 database

basis set	B3LYP		M06-2X	
	MSE	MUE	MSE	MUE
aug-cc-pV(Q+d)Z	-3.99	4.06	0.03	0.93
maug-cc-pV(Q+d)Z	-3.97	4.06	0.09	0.92
cc-pV(Q+d)Z	-4.79	4.85	-0.50	1.38
aug-cc-pV(T+d)Z	-4.08	4.14	-0.06	0.88
maug-cc-pV(T+d)Z	-4.02	4.10	0.08	0.91
cc-pV(T+d)Z	-5.26	5.42	-0.87	2.06
aug-cc-pV(D+d)Z	-4.83	4.90	-0.60	1.20
maug-cc-pV(D+d)Z	-4.69	4.72	-0.39	1.33
cc-pV(D+d)Z	-7.01	7.54	-2.32	3.75

Table 3. Errors in predictions of the hydrogen bonding energies (kcal/mol) in the HB6 database

basis set	B3LYP		M06-2X	
	MSE	MUE	MSE	MUE
aug-cc-pV(Q+d)Z	-0.76	0.76	0.11	0.29
maug-cc-pV(Q+d)Z	-0.73	0.73	0.10	0.28
cc-pV(Q+d)Z	-0.23	0.55	0.42	0.46
aug-cc-pV(T+d)Z	-0.73	0.73	0.17	0.31
maug-cc-pV(T+d)Z	-0.67	0.67	0.17	0.34
cc-pV(T+d)Z	0.51	0.74	1.02	1.02
aug-cc-pV(D+d)Z	-0.39	0.40	0.37	0.37
maug-cc-pV(D+d)Z	-0.27	0.64	0.43	0.61
cc-pV(D+d)Z	2.97	2.97	2.91	2.91

Table 4. Errors in predictions of the electron affinities (kcal/mol) in the EA13/3 database

EA13/3	B3LYP		M06-2X	
basis set	MSE	MUE	MSE	MUE
aug-cc-pV(Q+d)Z	-1.99	2.33	0.78	1.47
maug-cc-pV(Q+d)Z	-1.96	2.31	0.82	1.49
cc-pV(Q+d)Z	4.35	5.30	5.30	5.30
aug-cc-pV(T+d)Z	-2.07	2.37	0.67	1.46
maug-cc-pV(T+d)Z	-2.04	2.36	0.70	1.49
cc-pV(T+d)Z	9.49	10.13	9.99	9.99
aug-cc-pV(D+d)Z	-2.45	2.75	0.87	2.21
maug-cc-pV(D+d)Z	-2.53	2.92	0.71	2.28
cc-pV(D+d)Z	20.59	20.85	20.37	20.37

Table 5. Errors in predictions of the ionization potentials (kcal/mol) in the IP13/3 database

	B3LYP		M06-2X	
basis set	MSE	MUE	MSE	MUE
aug-cc-pV(Q+d)Z	3.42	4.62	0.66	2.26
maug-cc-pV(Q+d)Z	3.41	4.61	0.64	2.25
cc-pV(Q+d)Z	3.19	4.42	0.51	2.14
aug-cc-pV(T+d)Z	3.54	4.65	0.99	2.63
maug-cc-pV(T+d)Z	3.53	4.63	0.96	2.62
cc-pV(T+d)Z	2.94	4.14	0.57	2.31
aug-cc-pV(D+d)Z	4.01	4.72	1.08	2.81
maug-cc-pV(D+d)Z	4.14	4.67	1.26	2.99
cc-pV(D+d)Z	1.67	3.15	-0.67	2.84

Table 6. Errors in predictions of the atomization energies (kcal/mol per bond) in the AE6 database

| | B3LYP | | M06-2X | |
basis set	MSE	MUE	MSE	MUE
aug-cc-pV(Q+d)Z	-0.42	0.59	0.01	0.22
maug-cc-pV(Q+d)Z	-0.43	0.61	0.01	0.22
cc-pV(Q+d)Z	-0.38	0.56	0.03	0.22
aug-cc-pV(T+d)Z	-0.68	0.76	-0.19	0.33
maug-cc-pV(T+d)Z	-0.70	0.79	-0.23	0.36
cc-pV(T+d)Z	-0.59	0.69	-0.16	0.29
aug-cc-pV(D+d)Z	-2.31	2.31	-1.65	1.73
maug-cc-pV(D+d)Z	-2.67	2.67	-1.94	1.94
cc-pV(D+d)Z	-2.29	2.29	-1.59	1.65

Table 7. Electron affinity (kcal/mol) of lithium hydride LiH.

basis set	B3LYP	M06-2X
aug-cc-pV(Q+d)Z	10.12	6.55
jul-cc-pV(Q+d)Z	10.14	6.52
maug-cc-pV(Q+d)Z	10.05	6.42
cc-pV(Q+d)Z	7.82	3.71
aug-cc-pV(T+d)Z	9.97	6.28
jul-cc-pV(T+d)Z	9.96	6.20
maug-cc-pV(T+d)Z	9.84	6.09
cc-pV(T+d)Z	6.24	1.96
aug-cc-pV(D+d)Z	10.33	6.51
jul-cc-pV(D+d)Z	10.20	6.18
maug-cc-pV(D+d)Z	10.05	6.18
cc-pV(D+d)Z	5.75	1.15

Table 8. Errors in predictions of the electron affinity (kcal/mol) in the EA13/3 database in MP2 calculations

basis set	MSE	MUE
aug-cc-pV(T+d)Z	1.44	2.26
maug-cc-pV(T+d)Z	4.01	4.31
cc-pV(T+d)Z	14.36	14.36

References

[1] Clark, T.; Chandrasekhar, J.; Spitznagel, G. W.; Schleyer, P. v. R. *J. Comp. Chem.* 1983, *4*, 294.

[2] Kendall, R. A.; Dunning, T. H. Jr.; Harrison, R. J. *J. Chem. Phys.* 1992, *96*, 6796.

[3] Papajak, E.; Leverentz, H. R.; Zheng, J.; Truhlar, D. G. *J. Chem. Theory Comput.* 2009, *5,* 1197. Erratum and addendum: Papajak, E.; Leverentz, H. R.; Zheng, J.; Truhlar, D. G. *J. Chem. Theory Comput.* 2009, *5*, 3330.

[4] Lee, C.; Yang, W.; Parr, R. G. *Phys Rev. B* 1988, 37, 785.

[5] Becke, A. D. *Phys. Rev. A* 1988, 38,3098.

[6] Becke, A. D. *J. Chem. Phys.* 1993, 98, 5848.

[7] Stephens, P. J.; Devlin, F. J.; Chabalowski, C. F.; Frisch, M. J. *J. Phys. Chem.* 1994, *98,* 11623.

[8] Zhao, Y.; Truhlar, D. G. *Theor. Chem. Acc.* 2008, *120*, 215; Zhao, Y.; Truhlar, D. G. *Acc. Chem. Res.* 2008, *41*, 157.

[9] Møller, C.; Plesset, M. S. *Phys. Rev.* 1934, *46*, 618.

[10] Frisch, M. J.; Trucks, G. W.; Schlegel, H. B.; Scuseria, G. E.; Robb, M. A.; Cheeseman, J. R.; Montgomery, J. A., Jr.; Vreven, T.; Kudin, K. N.; Burant, J. C.; Millam, J. M.; Iyengar, S. S.; Tomasi, J.; Barone, V.; Mennucci, B.; Cossi, M.; Scalmani, G.; Rega, N.; Petersson, G. A.; Nakatsuji, H.; Hada, M.; Ehara, M.; Toyota, K.; Fukuda, R.; Hasegawa, J.; Ishida, M.; Nakajima, T.; Honda, Y.; Kitao, O.; Nakai, H.; Klene, M.; Li, X.; Knox, J. E.; Hratchian, H. P.; Cross, J. B.; Bakken, V.; Adamo, C.; Jaramillo, J.; Gomperts, R.; Stratmann, R. E.; Yazyev, O.; Austin, A. J.; Cammi, R.; Pomelli, C.; Ochterski, J. W.; Ayala, P. Y.; Morokuma, K.; Voth, G. A.; Salvador, P.; Dannenberg, J. J.; Zakrzewski, V. G.; Dapprich, S.; Daniels, A. D.; Strain, M. C.; Farkas, O.; Malick, D. K.; Rabuck, A. D.; Raghavachari, K.; Foresman, J. B.; Ortiz, J. V.; Cui, Q.; Baboul, A. G.; Clifford, S.; Cioslowski, J.; Stefanov, B. B.; Liu, G.; Liashenko, A.; Piskorz, P.; Komaromi, I.; Martin, R. L.; Fox, D. J.; Keith, T.; Al-Laham, M. A.; Peng, C. Y.; Nanayakkara, A.; Challacombe, M.; Gill, P. M. W.; Johnson, B.; Chen, W.; Wong, M. W.; Gonzalez, C.; Pople, J. A. *Gaussian 03 – revision C.02*; Gaussian, Inc.: Wallingford, CT, 2004.

[11] Zhao, Y.; Truhlar, D. G. *MN-GFM: Minnesota Gaussian Functional Module – version 3.0*; University of Minnesota: Minneapolis, MN, 2007.

[12] Lynch, B. J.; Zhao, Y.; Truhlar, D. G. *J. Phys. Chem. A* 2003, 107, 1384.

[13] Lynch, B. J.; Truhlar, D. G. *J. Phys. Chem. A* 2003, 107, 3898.

[14] Pople, J. A.; Head-Gordon, M.; Raghavachari, K. *J. Chem. Phys.* 1987, *87*, 5968.

[15] Zheng, J.; Zhao, Y.; Truhlar, D. G. *J. Chem. Theory Comput.* 2007, *3*, 569.

[16] Zheng, J.; Zhao, Y.; Truhlar, D. G. *J. Chem. Theory Comput.* 2009, *5*, 808.

[17] Zhao, Y., Truhlar, D. G. *J. Chem. Theory Comput.* 2005, 1, 415.

[18] Lynch, B. J.; Zhao, Y.; Truhlar, D. G. *J. Phys. Chem. A* 2003, *107*, 1384.

[19] Lynch, B. J.; Truhlar, D. G. *J. Phys. Chem. A* 2003, *107*, 3898.

[20] Lynch, B. J.; Truhlar, D. G. *J. Phys. Chem. A* 2004, *107*, 8996. Erratum: *J. Phys. Chem. A* 2004, *108*, 1460.

[21] Lynch, B. J.; Zhao, Y.; Truhlar, D. G. *J. Phys. Chem. A* 2005, *109*, 1643.

[22] Jarecki, A. A.; Davidson, E. R. *Chem.Phys. Lett.* 1999, *300*, 44.

[23] Galbraith, J. M.; Schaefer, H. F. III *J. Chem. Phys.* 1996, *105*, 862.

[24] Horny, L.; Petraco, N. D. K.; Schaefer, H. F. III *J. Am. Chem. Soc.* 2002, *124,* 14716.

[25] Lynch, B. J.; Zhao, Y.; Truhlar, D. G. *ACS Symp. Ser.* 2007, *958*, 153.

[26] Jensen, F. *J. Chem. Phys.* **2002**, *116*, 7372. Jensen, F. *J. Chem. Phys.* **2002**, *117*, 9234.

[27] Prascher, B. P.; Wilson, A. K. *Mol. Phys.* **2007**, *105*, 2899.

[28] Schneider, A. C.; Andzelm, J. W. *J. Comp. Chem.* **1997**, *18*, 775.

[29] Halls, M. D.; Schlegela, H. B. *J. Chem. Phys.* **1998**, *109*, 10587.

[30] Florian, J.; Johnson, B. G. *J. Phys. Chem.* **1995**, 99, 5899.

[31] Bauschlicher, C. W.; Partridge, H. Jr. *Chem.Phys. Lett* **1995**, 240, 533.

Chapter 3. Convergent Partially Augmented Basis Sets for Post-Hartree–Fock Calculations of Molecular Properties and Reaction Barrier Heights

Ewa Papajak* and Donald G. Truhlar
*Department of Chemistry and Supercomputing Institute,
University of Minnesota, 207 Pleasant Street S.E.,
Minneapolis, MN 55455-0431, USA*

We present sets of convergent, partially augmented basis set levels corresponding to subsets of the augmented "aug-cc-pV(n+d)Z" basis sets of Dunning and coworkers. We show that for many molecular properties a basis set fully augmented with diffuse functions is computationally expensive and almost always unnecessary. On the other hand unaugmented cc-pV(n+d)Z basis sets are insufficient for many properties that require diffuse functions. Therefore, we propose using intermediate basis sets. We developed an efficient strategy for partial augmentation, and in this article we test it and validate it. Sequentially deleting diffuse basis functions from the "aug" basis sets yields the "jul", "jun", "may", "apr", … etc. basis sets. Tests of these basis sets for Møller–Plesset second order perturbation theory (MP2) show the advantages of using these partially augmented basis sets and allow us to recommend which basis sets offer the best accuracy for a given number of basis functions for calculations on large systems. Similar truncations in the diffuse space can be performed for the aug-cc-pVxZ, aug-cc-pCVxZ, etc. basis sets.

1. Introduction

In quantum mechanical electronic structure calculations the orbitals in configuration state functions may be represented as linear combinations of contracted functions, which in turn are linear combinations of spherical harmonics times radial functions with pre-optimized exponential parameters. The radial functions can be Gaussian or Slater-type functions. Slater-type functions are more physical, but for ease of

computation of the two-electron integrals, Slater-type functions are usually replaced by linear combinations of Gaussian-type functions.[1,2] The so called zeta-level reflects the degree of decontraction of the primitive Gaussian functions used to represent valence orbitals. For example for carbon, valence double-zeta denotes two contracted functions designed to represent $2s$ orbitals and two contracted subshells to represent $2p$ orbitals, whereas valence triple-zeta denotes three, etc. Since the core is single-zeta quality in most modern basis sets, one often says "double zeta" instead of "valence double zeta", and so forth for triple, quadruple, etc. Double-, triple- and quadruple-zeta are usually abbreviated DZ, TZ, and QZ respectively. The contraction coefficients and exponential parameters for standard basis sets are available as lists called basis sets. Standard basis sets usually include polarization functions (e. g., d functions for carbon, p functions for hydrogen) and sometimes include diffuse functions.

The choice of the basis set for a given problem is critical, because it greatly affects the quality of the results as well as the cost of acquiring them. A basis set that is too large can make higher-level methods unaffordable for a given system or a given level unaffordable for larger systems. On the other hand, too small a basis set can prevent taking full advantage of the potential accuracy of an otherwise very accurate electronic structure level. We have been especially interested in the requirements for diffuse basis functions as they play an important role in calculations of such commonly computed molecular properties as electron affinities, noncovalent interaction energies, and barrier heights for chemical reactions. Diffuse functions are characterized by very small exponential parameters, which allow the electrons to be further away from the nuclei, so they are crucial for many systems and properties involving anions, transition states, excited states, and polarizability. However, if an unnecessarily large set of diffuse functions is used, the calculations may become unfeasible or unnecessarily expensive.

Three approaches to supplying basis sets with diffuse functions have emerged and have been widely used. In basis sets developed by Pople, Schleyer, and coworkers[3,4] (sometimes called Pople-type basis sets), s and p diffuse functions are added on atoms heavier than He, which is indicated by "+" in the name of the basis set. A second "+" in the name indicates that in addition to the diffuse functions on the non-hydrogenic atoms, diffuse s functions are added on the hydrogen atoms. Correlation consistent basis sets by Dunning and coworkers (including cc-pVnZ,[5–9] and cc-

pV(n+d)Z,[10]) are augmented with gradually increasing sets of diffuse functions for increasing decontraction of the valence space (aug-cc-pVnZ[5–9,11,12] and aug-cc-pV(n+d)Z[10]). The angular momentum quantum numbers included in the diffuse spaces of aug-cc-pVnZ and aug-cc-pV(n+d)Z basis sets for n = D, T, and Q are listed in table 1. The other rows of this table (other than "aug-") will be explained below. In a third approach, Jensen recommended including sets of diffuse functions (on all atoms) such that the number of diffuse functions increases with increasing n.[13] The Pople strategy is not convergent in the diffuse space, in that the number of diffuse functions is not systematically increased when the zeta level is increased, whereas the Dunning and Jensen approaches are convergent.

We will use the term "augmentation" to denote adding diffuse functions to a basis (whereas "extension" means raising the zeta level or adding polarization functions); and we will use "full augmentation" to denote adding a diffuse function for every angular momentum present in the unaugmented basis set. The aug- basis sets are fully augmented. It has been known for a long time that augmentation on hydrogen atoms is less important than augmentation on nonhydrogenic atoms (e.g., Schleyer and coworkers defined the "+" basis sets that omit augmentation on hydrogen atoms;[3] del Bene and Shavitt[14] showed that they could converge proton affinities and hydrogen bonding energies with respect to basis set without diffuse functions on H; and Lynch and one of the authors[15] showed that diffuse functions are not needed on H even in molecules where H has a partial negative charge), and the present article is mainly concerned with the level of augmentation on nonhydrogenic atoms. We have previously shown that the full augmentation of nonhydrogenic atoms in the basis sets defined by Dunning and coworkers often leads to unnecessary expense in calculations by density functional theory (DFT).[16,17] In particular, we showed that the non-convergent "+" approach is often sufficient for DFT calculations, and a basis set obtained by deleting all diffuse functions in aug- basis sets except the diffuse s and p functions on non-hydrogenic atoms has been called minimally augmented, denoted by the prefix maug-.[16] However, we have also seen that wave function theory (WFT) calculations are more sensitive than DFT calculations to the saturation of the diffuse space in the nonhydrogenic basis space as well as to the size

44

of the basis set in general.[16,17] This is because correlation energy in WFT converges very slowly with respect to the number of one-electron basis functions, and this slow convergence occurs because products of one-electron functions in a Slater-determinant poorly describe the cusps in the two-electron densities as the interelectronic distance approaches zero. The most slowly convergent part of the electron correlation energy is the part covered by second-order Møller–Plesset perturbation theory[18] (MP2); the reason for this is that although higher-order corrections are important, the contributions of the weakly coupled virtual orbitals at second order are quantitatively larger,[19,20] and it is important to understand how to include them efficiently. In practical work, in order to obtain as accurate results as one can afford using WFT for a given system, it is a common practice[21–26] to calculate the MP2 energy part at the complete basis set limit and to add higher-order corrections (e. g., the difference between an MP2 calculation and a calculation by the coupled cluster method with single and double excitations and a quasiperturbative treatment of connected triple excitations[27] CCSD(T) and MP2) calculated with a smaller basis set. Therefore achieving the MP2 CBS limit is of a great practical interest.

One popular way to determine the MP2 CBS limit is extrapolation.[28–30] Recently, Møller-Plesset perturbation calculations employing basis functions that depend explicitly on electron–electron distances (MP2-R12 or MP2-F12[31–44]) have provided a powerful, alternative way to approach the MP2 basis set limit in a very efficient way, by explicitly improving the description of the cusp. MP2-F12 is very rapidly convergent with respect to the size of the one-electron basis set. In some key studies, the rapid convergence of the MP2-F12 method has often been established based on heats of formation,[45] absolute correlation energy,[48] and energies of reaction,[48] but we note that, for neutral molecules and cations, heats of formation and energies of reaction are typically insensitive to the inclusion of the diffuse basis functions; thus a more recent study by Werner et al.[46] that examined not only reaction energies and atomization energies but also electron affinities, ionization potentials, equilibrium structures, vibrational frequencies, and intermolecular interaction energies and study by Kjaergaard et al.[47] on hydrogen bonded systems are more relevant to the question of how many diffuse functions one should use for a diverse

45

set of molecular properties (Werner et al. also cite earlier diverse benchmarking studies). Recently, basis sets have been prepared specifically for use in F12 calculations.[48] Those basis sets are specifically limited to minimal augmentation, but the reader was informed that "the inclusion of just *s* and *p* diffuse functions may not be sufficient" in all cases, and "further extension of the higher angular momentum functions might then be considered." Werner et al.[46] employed these minimally augmented basis sets and fully augmented ones in their F12 benchmarking, but did not consider intermediate augmentation. In the present article we will consider this, in particular we systematically explore various levels of partial augmentation in both MP2 and MP2-F12 calculations with databases for atomization energies, barrier heights, hydrogen bond energies, ionization potentials, and electron affinities.

It is an oversimplification to assume that "the more diffuse functions the better." The size of the diffuse space of a basis set is just one of the parameters of a basis set, and it must be considered in conjunction with the space spanned by primitive valence functions, the level of contraction, and the number of polarization functions. Full augmentation with many diffuse functions that make only a small difference in the property to be calculated increases the size (and, one hopes, the accuracy) of the basis set a given zeta level, but the gain may be small relative to other ways to increase the accuracy such as increasing the zeta level. In practice, when attempting to improve a basis set one should ask which aspect of the basis set is most limiting at any given level, and then one should improve that specific part of the basis set first. We have found that this is not always the way calculations are done. Very often basis sets are fully augmented or fully augmented on nonhydrogenic atoms while staying at given zeta level when it would be more efficient to do only a partial augmentation on nonhydrogenic atoms and spend the saved resources by going to a higher zeta level or adding more polarization functions.

The questions we are attempting to answer are the following:

- Which molecular properties are most sensitive to the augmentation of the diffuse space? What level of augmentation is advisable for these properties?

- At what point is saturation of the diffuse space reached for key properties such as barrier heights, electron affinities, ionization potentials, noncovalent interaction energies, atomization energies, and bond energies?
- What is the right order of steps in improving the basis set for a given problem? At a given zeta-level and for a given property, is it more beneficial to add more diffuse functions or to attempt to go to the higher zeta sooner with a minimal or intermediate number of diffuse functions?

A variety of *ad hoc* partially augmented basis sets have been used for specific calculations in various publications. Here we put forward a systematic partial augmentation scheme and test it carefully for MP2 and MP2-F12 calculations. The naming convention for the systematically partially augmented basis sets is based on the months and involves successively truncating the "aug" basis sets of Dunning and coworkers to well defined levels called "jul," "jun," "may," etc.

A second objective of the present article is that it allows us to compare the accuracy of MP2-F12 to MP2.

2. Definition of the new basis sets

In our calculations we use the correlation consistent cc-pV(n+d)Z basis sets of Dunning and coworkers with spherical harmonic d, f, and g subshells. Notice that a cc-pV(n+d)Z basis set for an atom lighter than Al is defined to be same as cc-pV(n+d)Z.[10] Table 1 defines the diffuse spaces of the fully and partially augmented basis sets. As seen in the table, deleting all diffuse basis functions on hydrogen and helium atoms from "aug" basis sets yields the "jul" basis set, which has already been defined.[17] The "jun", "may", …, etc. basis sets are obtained by sequentially removing the diffuse subshells on the heavy atoms, where "heavy atoms" is used here as a synonym for atoms heavier than He. The new basis sets are systematically convergent in that, just as aug-cc-pV(n+d)Z converges to a fully augmented complete-valence basis set as n increases, jun-cc-pV(n+d)Z converges to a fully-heavy-atom-augmented complete-valence basis set as n increases, and so does may- or apr-. As discussed in the introduction, it has been known

47

for a long time that augmentation on heavy atoms is less important than augmentation on hydrogen atoms.

3. Methods and databases

All of the MP2 calculations for this paper (except when timing MP2-F12 vs. MP2) were carried out using the *Gaussian 03*[49] and *Gaussian 09*[50] program packages. All of the MP2-F12/3C calculations were performed using the *MolPro 2009*[51] program.

In order to test performance of the partially augmented basis sets, we have used previously-optimized geometries of the species contained in the DBH24/08,[52,53] HB6/04,[54] EA13/3,[55,56] IP13/3,[55,56] AE06[57] databases.

These databases contain, respectively, 24 diverse barrier heights, 6 hydrogen bond energies (4 of which were used for the present tests), 13 electron affinities, 13 ionization potentials, and 6 atomization energies.

We carried out restricted single-point-energy MP2 and MP2-F12 calculations for both open- and closed-shell species. Results of these MP2 and MP2-F12 single-point calculations using basis sets ranging from aug-cc-pV(n+d)Z through partially augmented basis sets to non-diffuse cc-pV(n+d)Z were then compared to MP2-F12/aug-cc-pV(Q+d)Z values that should be close to the complete basis set limit and that serve as a reference. MP2-F12/aug-cc-pV(Q+d)Z data was generated for the following properties:

- 24 (forward and backward) barrier heights using quadratic configuration interaction with single and double excitations QCISD/MG3S geometries (listed in DBH24/08 database[52,53]) for the species (reactants, transition states, and products) involved in the following 12 reactions:

$$H + N_2O \leftrightarrow OH + N_2 \qquad (1)$$

$$H + HCl \leftrightarrow HCl + H \qquad (2)$$

$$CH_3 + FCl \leftrightarrow CH_3F + Cl \qquad (3)$$

$$Cl^- + CH_3Cl \leftrightarrow ClCH_3 + Cl^- \qquad (4)$$

$$F^- + CH_3Cl \leftrightarrow FCH_3 + Cl^- \qquad (5)$$

$$OH^- + CH_3F \leftrightarrow CH_3OH + F^- \qquad (6)$$

$$H + N_2 \leftrightarrow HN_2 \tag{7}$$

$$H + C_2H_4 \leftrightarrow CH_3CH_2 \tag{8}$$

$$HCN \leftrightarrow HNC \tag{9}$$

$$CH_4 + OH \leftrightarrow CH_3 + H_2O \tag{10}$$

$$H + OH \leftrightarrow O + H_2 \tag{11}$$

$$H + H_2S \leftrightarrow H_2 + HS \tag{12}$$
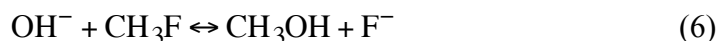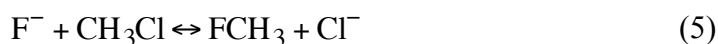
- the hydrogen bonding energy calculations for the $NH_3 - NH_3$, $HF - HF$, $H_2O - H_2O$, $NH_3 - H_2O$ dimers for the MC-QCISD/3 geometries. This subset of the HB6/04 database[54] will be called HB4.

- the electron affinities for the C, S, O, Si, P, Cl, OH, SH, PH, PH_2, O_2, S_2, and Cl_2 using QCISD/MG3S geometries listed in EA13/3 database.[55,56]

- the ionization potentials of the same 13 atoms and molecules as for electron affinities for the QCISD/MG3S geometries listed in IP13/3 database.[55,56]

- the atomization energies per bond for the SiH_4, SiO, S_2, propyne (C_3H_4), glyoxal ($C_2H_2O_2$), and cyclobutane (C_4H_8) were calculated using the QCISD/MG3S geometries in AE06 database.[57]

In all our calculations the Born-Oppenheimer electronic energies including nuclear repulsion were considered; vibrational contributions were not included. Spin-orbit energies were added (when nonzero) as in previous work.[16,17]

For this article, all the MP2-F12/aug-cc-pV(n+d)Z calculations were carried out using the aug-cc-pVnZ/JKFIT[58] and aug-cc-pVnZ/MP2FIT[59,60] density-fitting basis sets. For all the calculations involving non-diffuse (cc-pV(n+d)Z) orbital basis sets cc-pVnZ/JKFIT[58] and cc-pVnZ/MP2FIT[59,60] density fitting basis sets were used. In order to reduce cost of the calculations and at the same time pose a bigger challenge for the partially augmented (month-cc-pV(n+d)Z) we used the density fitting basis sets recommended for the cc-pVnZ basis sets. The density fitting basis sets might not be completely converged for all basis sets, but they should be close enough to convergence that their small extent of incompleteness does not affect our conclusions. All the MP2-

F12 calculations use 3C ansatz with orbital invariant amplitudes and were carried out with full non-linear fit of the geminal expansion.

4. **Results**

In order to allow the assessment of computational costs (computer time and storage) of the various basis sets, table 2 lists total numbers of contracted basis functions for all the calculations carried out for this article. This provides representative relative numbers for typical applications. Table 3 summarizes relative computer timings normalized to the least expensive basis set used (cc-pV(D+d)Z). For the ease of estimating computational savings by using partially instead of fully augmented basis sets at the same zeta level, we also list timings normalized to the unaugmented basis set for the same n.

Basis sets in the first column of all tables are listed in the order of decreasing size. In each case the basis set listed above the unaugmented basis set is the minimally augmented (maug) basis set containing s and p functions on heavy atoms (which means heavier than He) and no diffuse functions on H and He atoms. Subminimal augmentation (diffuse s functions on heavy atoms) gives results at best slightly better than no augmentation and is not recommended. Therefore, in this article except for unaugmented results, no results are presented for subminimal augmentation.

Both MP2 and MP2-F12 results are compared with MP2-F12/aug-cc-pVQZ values. Tables 4-8 list mean signed deviation (MSD) and mean unsigned deviation (MUD) from this reference. Except for atomization energies, we define MSD and MUD as

$$MSD = \frac{1}{N}\sum_{i=1}^{N} d_i \ , \tag{13}$$

$$MUD = \frac{1}{N}\sum_{i=1}^{N} |d_i| \ , \tag{14}$$

where N is the number of energetic data computed (24 for barrier heights, 6 for hydrogen bonding energies, 13 for electron affinities and ionization potentials), and d_i is the deviation (in kcal/mol) of the i-th value from the reference value.

50

In order to report MSD and MUE for atomization energies on the per-bond basis, mean deviations, computed using equations 13 and 14, were divided by the average number of bonds in the AE06 database as in equations 15 and 16.

$$MSD = \frac{1}{4.83N} \sum_{i=1}^{N} d_i \qquad (15)$$

$$MUD = \frac{1}{4.83N} \sum_{i=1}^{N} |d_i| \qquad (16)$$

Root mean square deviation values (RMSD) for all the properties are available in the supporting information. In tables 4–8 we provide mean deviations of MP2 (tables 4-6) and MP2-F12 (tables 6-8) results from the reference values. We have also listed maximum unsigned deviations (MaxUD) for completeness.

Counterpoise corrections[61] are sometimes used to estimate corrections for basis set superposition error, but such corrections are problematic in terms of accuracy[62] and become increasing complex as one considers systems with more components[63] and hence are often omitted. In table 5 we present an analog of the triple-zeta results in table 4 for the HB04 database. In comparison with the results given in table 4, the counterpoise-corrected results do not show different trends or lead to different conclusions on augmentation, and the errors are increased upon making the "correction". Therefore, to make the rest of the convergence tests as straightforward as possible, no counterpoise corrections are applied in tables 4 or 6–8.

5. Discussion

In the discussion (as in Table 3) we abbreviate cc-pV(D+d)Z, cc-pV(T+d)Z, and cc-pV(Q+d)Z as DZ, TZ, and QZ, respectively. Similarly, month-cc-pV(n+d)Z is abbreviated in the text as month-nZ.

Tables 4-6 show the mean deviations of MP2 energies computed with augmented, partially augmented, and not augmented basis sets from the near-CBS reference values. In all cases, for triple and quadruple zeta basis sets the difference in MUD for jul- and

jun- basis sets compared to aug- is usually small compared to the absolute value of the deviations, and in most cases they are negligibly small. The same holds true for jul-DZ.

The tables show many outstanding successes for partial augmentation, especially for barrier heights and hydrogen bond energies. For example, for barrier heights, aug-QZ, apr-QZ, and QZ differ from the near-CBS reference value by 0.2, 0.3, and 1.2 kcal/mol, respectively, but Table 2 shows that aug-QZ has about 40% more basis functions than apr-QZ. A similar observation can be made for may-TZ. For hydrogen bond energies, apr-QZ, may-TZ, and jul-DZ are all more accurate than aug-QZ. *The key point is not that they are more accurate, which (obviously) arises mainly from cancellation of errors, but that they are not significantly less accurate.*

Comparison of tables 4 and 6 to tables 7 and 8 shows that MP2 results converge more slowly with respect to the saturation of the diffuse space of the basis set than do MP2-F12 calculations, as expected from the discussion in section 1. Tables 7 and 8 show that in MP2-F12 calculations only triple- and quadruple-zeta atomization energy calculations seem to be insensitive to addition of diffuse basis functions. This is probably due to the fact that the underlying cc-pV(n+d)Z basis set is sufficiently diffuse for n = {T or Q} and not diffuse enough for n = D for calculation of bond energies. However, inclusion of diffuse functions seems to be crucial for all other properties, including (perhaps surprisingly) ionization potentials.

It is interesting that for the tested properties the aug basis sets never offer any significant improvement at either the MP2 or MP2-F12 level over jul- basis sets. On the other hand, the unaugmented basis sets usually have much higher MUDs than partially augmented basis sets. Therefore partially augmented basis sets provide intermediate options that are more balanced than either fully augmented or unaugmented basis sets with respect to the computational cost and the quality of the results.

At any given zeta level (n) and augmentation level (month-), if one can afford additional cost and wishes to improve the quality of the calculations by increasing the size of the basis set, one would only be interested in doing so, if the larger basis set offered significantly lower mean deviations. Mean deviations in electron affinity listed in table 7 show that only partially augmented basis sets offer such an advantage. To see this

for MP2-F12 calculations, recall that in the tables each basis set is larger than all those below it (as shown quantitatively in Table 2). Then consider starting with DZ and moving up. The error in table 7 decreases significantly as we increase the basis set only through jun- and jul-, but not for aug-. The higher, triple-zeta unaugmented basis set also does not offer decrease in error relative to that of jul-DZ. Therefore aug-DZ and TZ should be skipped. The next basis set to offer an improvement in the quality of the results is jun-TZ as that will be the first next more expensive basis set that offers a lower MUD. The jul-TZ basis set offers further improvement. Then aug-TZ and QZ can be skipped until improvement is again found with apr-QZ. Similar conclusions are drawn from other tables, for both MP2 and MP2-F12, except for atomization energies at the triple and quadruple zeta levels (tables 6 and 8), which do not seem to require diffuse functions.

The trend is even more striking for calculations without F12. Consider, for example, the barrier height calculations in table 4. One achieves higher accuracy with apr-QZ than with aug-TZ, jul-TZ, jun-TZ, or may-TZ, but simply going to QZ without any diffuse functions is less accurate than any of these triple-zeta levels. Table 3 shows that the cost savings in using apr-QZ rather than aug-QZ to include the diffuse space is more than a factor of 5. This is one of the main lessons of the present study and is more important than the small deviations from one another of MUDs in the 0.5–0.8 kcal/mol range or the small deviations from one another of the MUDs in the 0.15–0.3 kcal/mol range. Similarly, now considering barrier heights in table 4, TZ is inaccurate, but may-TZ is more accurate than aug-DZ and is less expensive than aug-TZ by about a factor of 4. Thus, in calculations where one cannot afford to go all the way to aug-TZ, the errors may be decreased considerably compared to TZ by using intermediate augmentation. As a third example, consider hydrogen bonding in table 4. The main point is not the small differences from one another of the MUDs in the range 0.01–0.17 kcal/mol but rather the fact that even apr-QZ accounts well for the effect of diffuse functions at the quadruple-zeta level, even may-TZ accounts well for them at the TZ level, and even jun-DZ accounts well for them at the DZ level. Usually, when diffuse functions are important we find that $(n+1)Z$ is not more accurate than jul-nZ or jun-nZ. In other words the fully augmented and unaugmented basis sets hardly ever seem to be good choices as compared

to the new intermediate basis set levels, and in many cases truncation to a basis set intermediate between unaugmented or fully augmented on only heavy atoms is the best choice.

An excessive number of diffuse functions not only increases the cost, but also it often leads to difficult SCF convergence and, as shown in figure 1, it can increase the basis set superposition error.

The fact that the aug-nZ basis sets approach the CBS limit in a systematic way is often correctly considered to be one of their chief advantages. However, if one accepts that diffuse functions are not needed on hydrogenic atoms, a basis set sequence such as jun-nZ (X = D, T, Q, ...) also approaches the CBS limit systematically (i. e., is "convergent") and it does so in a more efficient manner. Thus partially augmented basis sets would appear to be very useful for focal point[23,64] analysis.

We have not examined reduction in the number of polarization functions, but previous work[65] shows that savings are possible in that area as well.

Another possible use of the partially augmented basis sets is in dual-basis calculations where Hartree-Fock calculations are performed in a small basis set and the post-Hartree-Fock calculation is performed in a large set.[66,67]

The second objective of this article is to compare MP2-F12 to MP2. Both kinds of calculations converge to the same MP2 CBS limit, but at different rates. Comparing table 4 to table 7 shows that for barrier heights MP2-F12/jul-DZ is more accurate than MP2/aug-TZ or MP2/aug-QZ. Furthermore MP2-F12/may-TZ is as accurate as MP2/jul-QZ. For ionization potentials (tables 6 and 8) MP2-F12/jul-DZ is more accurate than MP2/jun-QZ. For atomization energies (tables 6 and 8), we find that MP2-F12/DZ is more accurate than MP2/aug-QZ. However, MP2-F12 is not more accurate than MP2 for hydrogen bonding.

6. Conclusions

Of all the energetic molecular properties considered here, unaugmented basis sets are adequate only for atomization energies at the triple and quadruple zeta levels.

Both MP2 and MP2-F12 theory are sensitive to the saturation of the diffuse space; however in most cases presented here the full augmentation is unnecessary. Instead of using fully augmented (aug) or unaugmented basis sets, we recommend using the new partially augmented basis sets.

For MP2 calculations of properties requiring diffuse basis functions, we recommend jun-QZ, jul-TZ, and jul-DZ for especially reliable results, but the tables show that except for electron affinities (and therefore probably for most properties involving anions) one can usually cut back to may-QZ or jun-TZ.

In MP2-F12 calculations of properties sensitive to the number of diffuse functions, we recommend using may-QZ, jun-TZ, and jul-DZ, which offer considerable savings compared to aug- basis sets and significant improvement over unaugmented cc-pV(n+d)Z basis sets.

Supporting Information Available: Root mean square errors for all the properties in this article are listed in Supporting Information available via the Internet at http://pubs.acs.org.
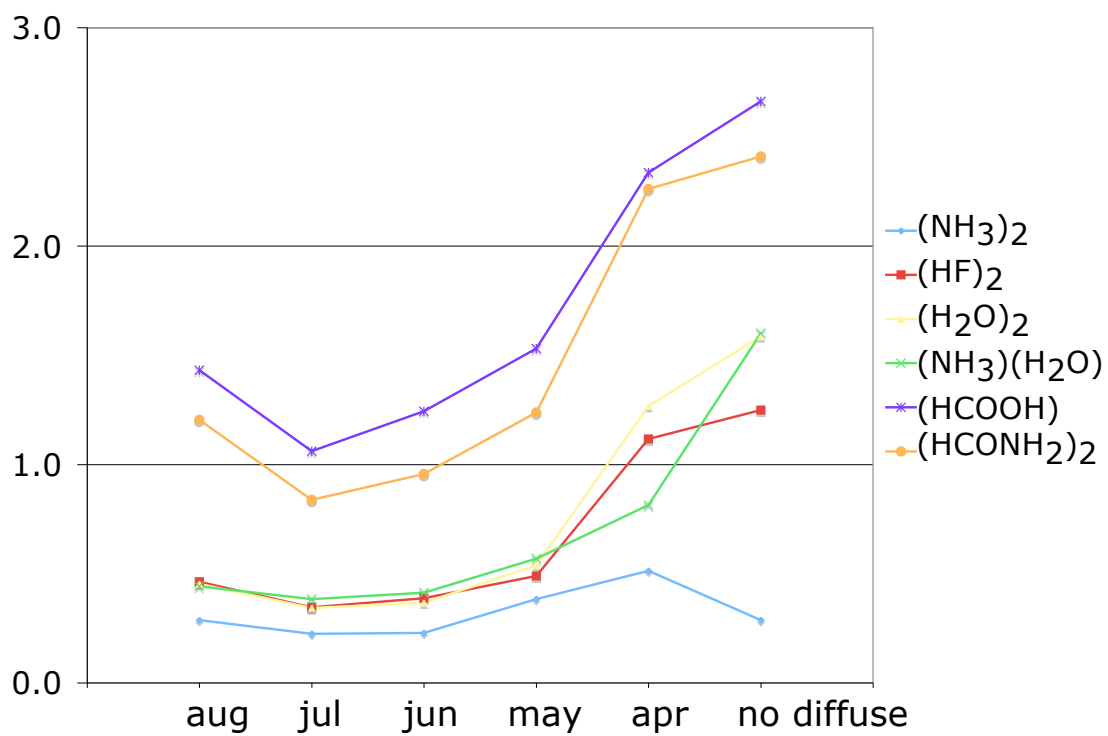
Figure 1. Counterpoise corrections [kcal/mol] for hydrogen bonded dimers for triple-zeta basis sets.

Table 1. Angular Momenta Included in the Diffuse Space in Tested Basis Sets

Basis set[a]	Li through Ca	H and He
aug-cc-pV(Q+d)Z	s p d f g	s p d f
jul-cc-pV(Q+d)Z	s p d f g	-
jun-cc-pV(Q+d)Z	s p d f	-
may-cc-pV(Q+d)Z	s p d	-
apr-cc-pV(Q+d)Z[b]	s p	-
cc-pV(Q+d)Z	-	-
aug-cc-pV(T+d)Z	s p d f	s p d
jul-cc-pV(T+d)Z	s p d f	-
jun-cc-pV(T+d)Z	s p d	-
may-cc-pV(T+d)Z[c]	s p	-
cc-pV(T+d)Z	-	-
aug-cc-pV(D+d)Z	s p d	s p
jul-cc-pV(D+d)Z	s p d	-
jun-cc-pV(D+d)Z[d]	s p	-
cc-pV(D+d)Z	-	-

[a] The same diffuse functions can be employed for month-cc-pV(n+d)Z or cc-pV(n+d)Z and for month-cc-pVnZ or cc-pVnZ

[b] Same as maug-cc-pV(Q+d)Z

[c] Same as maug-cc-pV(T+d)Z

[d] Same as maug-cc-pV(D+d)Z

Table 2. Number of Basis Functions Used in MP2 Calculations

	N_{bf}[a]					sum		
	DBH24/08	HB4	EA13/3	IP13/3	AE06	total[b]	norm.[c]	rel.[d]
aug-cc-pV(Q+d)Z	9129	4068	3218	3218	2528	22161	5.7	1.5
jul-cc-pV(Q+d)Z	7865	3460	3058	3058	2224	19665	5.1	1.3
jun-cc-pV(Q+d)Z	7262	3199	2770	2770	2044	18045	4.6	1.2
may-cc-pV(Q+d)Z	6793	2996	2546	2546	1904	16785	4.3	1.1
apr-cc-pV(Q+d)Z	6458	2851	2386	2386	1804	15885	4.1	1.0
cc-pV(Q+d)Z	6190	2735	2258	2258	1724	15165	3.9	1.0
aug-cc-pV(T+d)Z	5034	2208	1900	1900	1411	12453	3.2	1.5
jul-cc-pV(T+d)Z	4323	1866	1810	1810	1240	11049	2.8	1.4
jun-cc-pV(T+d)Z	3854	1663	1586	1586	1100	9789	2.5	1.2
may-cc-pV(T+d)Z	3519	1518	1426	1426	1000	8889	2.3	1.1
cc-pV(T+d)Z	3251	1402	1298	1298	920	8169	2.1	1.0
aug-cc-pV(D+d)Z	2387	1009	1024	1024	685	6129	1.6	1.6
jul-cc-pV(D+d)Z	2071	857	984	984	609	5505	1.4	1.4
jun-cc-pV(D+d)Z	1736	712	824	824	509	4605	1.2	1.2
cc-pV(D+d)Z	1468	596	696	696	429	3885	1.0	1.0

[a] Number of contracted basis functions used for all the calculations in the database.
[b] Sum of N_{bf} over all five databases
[c] Sum normalized to cc-pV(D+d)Z
[d] Sum relative to cc-pV(n+d)Z for the same n

Table 3. Timing Summary for the MP2 and MP2-F12 for All Species in the Databases.

Basis set[a]	MP2		MP2-F12		
	norm.[b]	rel.[c]	norm.(MP2) [b]	norm. [d]	rel.[e]
aug-QZ	388.9	6.3	942.6	46.9	3.4
jul-QZ	154.4	2.5	492.4	24.5	1.8
jun-QZ	112.9	1.8	402.7	20.0	1.4
may-QZ	88.3	1.4	337.9	16.8	1.2
apr-QZ	72.3	1.2	303.0	15.1	1.1
QZ	62.1	1.0	278.4	13.9	1.0
aug-TZ	30.1	5.0	144.2	7.2	2.8
jul-TZ	15.6	2.6	80.3	4.0	1.5
jun-TZ	10.4	1.7	65.7	3.3	1.3
may-TZ	7.8	1.3	57.8	2.9	1.1
TZ	6.0	1.0	51.9	2.6	1.0
aug-DZ	2.4	2.4	38.1	1.9	1.9
jul-DZ	1.8	1.8	24.8	1.2	1.2
jun- DZ	1.3	1.3	22.1	1.1	1.1
DZ	1.0	1.0	20.1	1.0	1.0

[a] Labels month-nZ or nZ denote month-cc-pV(n+d)Z or cc-pV(n+d)Z

[b] Sum normalized to MP2 with the same program on the same machine with the smallest basis set used (cc-pV(D+d)Z)

[c] Sum relative to MP2 with the same program on the same machine with the smallest basis set with the same n

[d] Sum relative to MP2-F12 with the same program on the same machine with the smallest basis set used

[e] Sum relative to MP2-F12 with the same program on the same machine with the smallest basis set with the same n

Table 4. Mean and Maximum Deviations of MP2 Barrier Height (kcal/mol), Hydrogen Bonding Energy (kcal/mol), and Electron Affinity (kcal/mol) from Reference Value.

	Barrier Height			Hydrogen Bonding			Electron Affinity		
	MSD	MUD	MaxUD	MSD	MUD	MaxUD	MSD	MUD	MaxUD
aug-cc-pV(Q+d)Z	-0.03	0.15	0.43	0.09	0.09	0.13	0.64	1.36	2.64
jul-cc-pV(Q+d)Z	0.06	0.19	0.57	0.01	0.01	0.02	0.68	1.41	2.64
jun-cc-pV(Q+d)Z	0.13	0.20	0.61	-0.01	0.02	0.03	1.14	1.70	3.18
may-cc-pV(Q+d)Z	0.20	0.25	0.78	-0.03	0.03	0.04	1.50	1.93	3.49
apr-cc-pV(Q+d)Z	0.20	0.29	0.89	0.01	0.02	0.04	1.97	2.28	3.93
cc-pV(Q+d)Z	-0.40	1.18	8.27	0.38	0.38	0.49	7.18	7.18	3.18
aug-cc-pV(T+d)Z	0.01	0.49	1.05	0.17	0.17	0.21	1.90	2.28	4.29
jul-cc-pV(T+d)Z	0.19	0.58	1.39	0.04	0.04	0.08	2.01	2.38	4.29
jun-cc-pV(T+d)Z	0.49	0.66	2.14	-0.03	0.04	0.07	3.04	3.10	5.60
may-cc-pV(T+d)Z	0.65	0.79	3.05	0.05	0.09	0.10	4.47	4.47	6.96
cc-pV(T+d)Z	-0.18	2.15	11.10	0.88	0.88	1.05	14.83	14.83	32.17
aug-cc-pV(D+d)Z	-0.28	1.21	3.25	0.34	0.34	0.48	4.09	4.64	8.95
jul-cc-pV(D+d)Z	0.20	1.44	4.41	0.10	0.10	0.19	4.36	4.91	8.95
jun-cc-pV(D+d)Z	1.27	2.16	5.50	0.31	0.31	0.45	8.94	8.94	13.36
cc-pV(D+d)Z	0.08	3.92	15.81	1.93	1.93	2.44	30.26	30.26	61.09

Table 5. Mean and Maximum Deviations of MP2 Counterpoise-Corrected Hydrogen Bonding Energy (kcal/mol) from the Reference Value.

	Hydrogen Bonding		
	MSD	MUD	MaxUD
aug-cc-pV(T+d)Z	-0.24	0.24	0.28
jul-cc-pV(T+d)Z	-0.29	0.29	0.36
jun-cc-pV(T+d)Z	-0.38	0.38	0.45
may-cc-pV(T+d)Z	-0.45	0.45	0.56
cc-pV(T+d)Z	-0.51	0.51	0.81

Table 6. Mean and Maximum Deviations of MP2 Ionization Potentials (kcal/mol) and Atomization Energies per Bond (kcal/mol) from Reference Value.

	Ionization Potential			Atomization Energy		
	MSD	MUD	MaxUD	MSD	MUD	MaxUD
aug-cc-pV(Q+d)Z	-2.00	2.26	7.52	-1.03	1.03	1.82
jul-cc-pV(Q+d)Z	-2.02	2.27	7.52	-1.09	1.09	1.97
jun-cc-pV(Q+d)Z	-2.27	2.47	7.86	-1.21	1.21	2.12
may-cc-pV(Q+d)Z	-2.38	2.55	8.09	-1.26	1.26	2.18
apr-cc-pV(Q+d)Z	-2.43	2.60	8.19	-1.28	1.28	2.19
cc-pV(Q+d)Z	-2.55	2.70	7.86	-1.28	1.28	2.17
aug-cc-pV(T+d)Z	-3.26	3.28	7.80	-2.44	2.44	4.28
jul-cc-pV(T+d)Z	-3.28	3.30	7.80	-2.60	2.60	4.68
jun-cc-pV(T+d)Z	-3.89	3.89	8.67	-2.86	2.86	5.08
may-cc-pV(T+d)Z	-4.20	4.20	9.17	-2.98	2.98	5.19
cc-pV(T+d)Z	-4.55	4.55	10.40	-3.01	3.01	5.09
aug-cc-pV(D+d)Z	-6.25	6.25	10.99	-7.38	7.38	13.87
jul-cc-pV(D+d)Z	-6.31	6.31	10.99	-7.69	7.69	14.68
jun-cc-pV(D+d)Z	-8.65	8.65	13.81	-8.51	8.51	15.87
cc-pV(D+d)Z	-10.23	10.23	19.13	-8.62	8.62	15.57

Table 7. Mean and Maximum Deviations of MP2-F12 Barrier Height (kcal/mol), Hydrogen Bonding Energy (kcal/mol), and Electron Affinity from Reference Value.

| | Barrier Height | | | | | Hydrogen Bonding | | | Electron Affinity | | |
| | MSE | | MUD | | MaxUD | MSE | MUD | MaxUD | MSD | MUD | MaxUD |
	DBH24	(DBH06[a] DBH18[b])	DBH24	(DBH06[a] DBH18[b])							
aug-cc-pV(Q+d)Z	0.00[c]	(0.00[c] 0.00[c])	0.00[c]	(0.00[c] 0.00[c])	0.00[c]	0.00[c]	0.00[c]	0.00[c]	0.00[c]	0.00[c]	0.00[c]
jul-cc-pV(Q+d)Z	0.02	(0.00 0.02)	0.03	(0.02 0.03)	0.08	0.02	0.02	0.03	0.03	0.04	0.13
jun-cc-pV(Q+d)Z	0.02	(0.00 0.03)	0.03	(0.01 0.03)	0.08	0.02	0.02	0.02	0.10	0.10	0.14
may-cc-pV(Q+d)Z	0.03	(0.01 0.04)	0.04	(0.04 0.04)	0.10	0.02	0.02	0.03	0.27	0.27	0.42
apr-cc-pV(Q+d)Z	0.00	(-0.12 0.05)	0.08	(0.12 0.06)	0.40	0.08	0.08	0.10	0.71	0.71	0.91
cc-pV(Q+d)Z	-0.51	(-2.07 0.00)	0.87	(3.04 0.15)	7.09	0.46	0.46	0.57	4.88	4.88	13.63
aug-cc-pV(T+d)Z	0.06	(-0.06 0.10)	0.11	(0.07 0.12)	0.77	0.04	0.04	0.04	0.23	0.23	0.36
jul-cc-pV(T+d)Z	0.09	(-0.04 0.14)	0.16	(0.09 0.18)	0.69	0.14	0.14	0.15	0.33	0.33	0.56
jun-cc-pV(T+d)Z	0.13	(0.03 0.16)	0.18	(0.14 0.20)	0.75	0.14	0.14	0.15	0.62	0.62	1.07
may-cc-pV(T+d)Z	0.16	(0.00 0.21)	0.25	(0.22 0.26)	1.12	0.24	0.24	0.28	1.86	1.86	2.47
cc-pV(T+d)Z	-0.56	(-2.53 0.10)	1.44	(4.37 0.46)	9.24	1.09	1.09	1.27	9.79	9.79	22.66
aug-cc-pV(D+d)Z	0.03	(0.13 0.00)	0.26	(0.32 0.25)	0.69	0.08	0.08	0.10	1.02	1.02	1.83
jul-cc-pV(D+d)Z	0.15	(0.21 0.13)	0.39	(0.40 0.39)	1.32	0.38	0.38	0.46	1.18	1.18	1.78
jun-cc-pV(D+d)Z	0.54	(1.31 0.28)	0.84	(1.37 0.66)	2.19	0.56	0.56	0.70	4.27	4.27	5.71
cc-pV(D+d)Z	-0.54	(-2.14 0.00)	2.66	(6.76 1.29)	12.38	2.31	2.31	2.86	19.64	19.64	39.98

[a] Reactions containing anions ($Cl^- \cdots CH_3Cl$, $F^- \cdots CH_3Cl$, $F^- \cdots CH_3F$, $OH^- \cdots CH_3F$).

[b] The rest of the reactions in DBH24/08 (not listed in a).

[c] Zero by definition.

Table 8. Mean and Maximum Deviations of MP2-F12 Ionization Potentials (kcal/mol) and Atomization Energies per Bond (kcal/mol) from Reference Value.

	Ionization Potential			Atomization Energy		
	MSD	MUD	MaxUD	MSD	MUD	MaxUD
aug-cc-pV(Q+d)Z	0.00[a]	0.00[a]	0.00[a]	0.00[a]	0.00[a]	0.00[a]
jul-cc-pV(Q+d)Z	-0.01	0.02	0.04	0.01	0.01	0.02
jun-cc-pV(Q+d)Z	-0.04	0.04	0.06	0.00	0.01	0.01
may-cc-pV(Q+d)Z	-0.09	0.09	0.13	-0.01	0.01	0.02
apr-cc-pV(Q+d)Z	-0.15	0.15	0.23	-0.01	0.01	0.03
cc-pV(Q+d)Z	-0.31	0.31	0.90	0.01	0.02	0.05
aug-cc-pV(T+d)Z	-0.13	0.14	0.26	-0.03	0.04	0.06
jul-cc-pV(T+d)Z	-0.17	0.17	0.25	-0.01	0.03	0.06
jun-cc-pV(T+d)Z	-0.35	0.35	0.58	-0.03	0.04	0.08
may-cc-pV(T+d)Z	-0.68	0.68	1.02	-0.04	0.04	0.11
cc-pV(T+d)Z	-1.28	1.28	2.77	0.06	0.07	0.18
aug-cc-pV(D+d)Z	-0.74	0.80	1.50	-0.19	0.22	0.46
jul-cc-pV(D+d)Z	-0.99	1.01	1.62	-0.10	0.19	0.33
jun-cc-pV(D+d)Z	-2.86	2.86	5.36	-0.06	0.23	0.35
cc-pV(D+d)Z	-4.91	4.91	9.08	0.24	0.34	0.87

[a]Zero by definition.

64

References

[1] Hehre, W. J.; Stewart, R. F.; Pople, J. A. *J. Chem. Phys*. **1969**, *51*, 2657.

[2] Davidson, E. R.; Feller, D. *Chem. Rev*. **1986**, *86*, 681.

[3] Clark, T.; Chandresekhar, J.; Schleyer, P. v. R. *J. Comput. Chem.* **1983**, *4*, 294.

[4] Frisch, M. J.; Pople, J. A.; Binkley, J. S. *J. Chem. Phys.* **1984**, *80*, 3265.

[5] Woon, D. E; Dunning, T. H. Jr. *J. Chem. Phys*. **1994**, *100*, 2975.

[6] Woon, D. E.; Dunning, T. H. Jr. *J. Chem. Phys.* **1993**, 98, 1358.

[7] Koput, J.; Peterson, K. A. *J. Phys. Chem. A*, **2002**, *106*, 9595.

[8] Balabanov, N. B.; Peterson, K. A *J. Chem. Phys*., **2005**, *123*, 064107.

[9] Wilson, A. K.; Woon, D.E.; Peterson, K.A.; Dunning, T.H. Jr. *J. Chem. Phys.* **1999**, *110*, 7667.

[10] Dunning, T.H. Jr., Peterson, K.A.; Wilson, A. K. *J. Chem. Phys.* **2001**, *114*, 9244.

[11] Dunning, T. H. Jr. *J. Chem. Phys.* **1989**, 90, 1007.

[12] Kendall, R. A.; Dunning, T. H. Jr.; Harrison, R.J. *J. Chem. Phys.* **1992**, *96*, 6796.

[13] Jensen, F., *J. Chem. Phys.* **2002**, *117*, 9234.

[14] Del Bene, J. E.; Shavitt, I. *J. Mol. Struct. Theochem* **1994**, *307*, 27.

[15] Lynch, B. J. Truhlar, D. G. In *Electron Correlation Methodology*; Wilson, A.K., Peterson, K. A., Eds.; ACS Symposium Series 958; American Chemical Society: Washington, DC, 2007.

[16] Papajak, E.; Leverentz, H. R.; Zheng, J.; Truhlar, D. G. *J. Chem. Theory Comput.* **2009**, *5*, 1197; erratum: Papajak, E.; Leverentz, H. R.; Zheng, J.; Truhlar, D. G. *J. Chem. Theory Comput.* **2009**, *5*, 3330.

[17] Papajak, E.; Truhlar, G.D. *J. Chem. Theor. Comput.* **2010**, *6,* 597-601.

[18] Møller, C.; Plesset, M. S. *Phys. Rev.* **1934**, *46*, 618.

[19] Petersson, G. A.; Braunstein, M. *J. Chem. Phys* **1985**, *83*, 5129.

[20] East, A. L. L.; Allen, W. D. *J. Chem. Phys*. **1993**, *99*, 4638.

[21] Hobza, P.; Sponer, J. *J. Am. Chem. Soc.* **2002**, *124*, 11802.

[22] Jurecka, P.; Sponer, J.; Cerny, J.; Hobza, P. *Phys. Chem. Chem. Phys.*, **2006**, *8*, 1985 – 1993.

[23] Schuurmann, M. S.; Muir, S. R.; Allen, W. D.; Schaefer, H. F. *J. Chem. Phys.* **2004**, *120*, 11586.

[24] Soteras, I.; Orozco, M.; Luque, F. J. *J. Comput. Aided Mol. Des* **2010**, *24*, 281.

[25] N. J. DeYonker, T. R. Cundari, and A. K. Wilson, J. Chem. Phys. **2006**, *124*, 114104.

[26] Y. Zhao; D. G. Truhlar, J. Phys. Chem. A **2006**, *110*, 10478.

[27] Raghavachari, K.; Trucks, G. W.; Pople, J. A.; Head-Gordon, M. *Chem. Phys. Lett.* **1989**, *157*, 479.

[28] Fast, P. L.; Corchado, J. C.; Sanchez, M. L.; Truhlar, D. G. *J. Phys. Chem. A* **1999**, *103*, 5129.

[29] Peterson, K. A.; Dunning, T. H. *J. Phys. Chem.* **1995**, *99*, 3898.

[30] Schwenke, D. *J. Chem. Phys.* **2005**, *122*, 014107.

[31] Kutzelnigg, W. *Theor Chim Acta* **1985**, *68*, 445.

[32] Kutzelnigg, W.; Klopper, W. *J. Chem. Phys.* **1991**, *94*, 1985.

[33] Klopper, W.; Kutzelnigg, W. *Chem. Phys. Lett.* **1987**, *134*, 17.

[34] Klopper, W.; Samson, C. C. M. *J. Chem. Phys.* **2002**, *116*, 6397.

[35] Manby, F. R. *J. Chem. Phys.* **2003**, *119*, 4607.

[36] Ten-no, S.; Manby, F. R. *J. Chem. Phys.* **2003**, *119*, 5358.

[37] Ten-no, S. *J. Chem. Phys.* **2004**, *121*, 117.

[38] Valeev, E. F. *Chem. Phys. Lett.* **2004**, *395*, 190.

[39] Valeev, E. F.; Jansen, C. L. *Chem. Phys. Lett.* **2004**, *121*, 1214.

[40] Ten-no, S. Chem. Phys. Lett. **2004**, *121*, 117**.**

[41] Werner, H. –J.; Adler, T. B.; Manby, F. R. *J. Chem. Phys.* **2007**, *126*, 164102.

[42] Crawford, T. D.; Sherrill, C. D.; Valeev, E. F.; Fermann, J. T.; King, R. A.; Leininger,

M. L.; Brown, S. T.; Janssen, C. L.; Seidl, E. T.; Kenny, J. P.; Allen, W. D. *J. Comp. Chem.* **2007**, *28*, 1610.

43 Knizia, G.; Werner, H. –J. *J. Chem. Phys.* **2008**, *128*, 154103.

44 Marchetti, O. Werner, H. –J. *J. Phys. Chem. A* **2009**, *113*, 11580.

45 Bischoff, F. A.; Wolfsegger, S.; Tew, D. P.; Klopper, W. *Mol. Phys.* **2009**, *107*, 963.

46 Werner, H.-J.; Knizia, G.; Adler, T. B.; Marchetti, O. *Z. Phys. Chem.* **2010**, *224*, 493.

47 Lane, J. R.; Kjaergaard, H. G. *J. Chem. Phys.* **2009**, *131*, 034307.

48 Peterson, K. A.; Adler, T. B.; Werner, H.-J. *J. Chem Phys.* **2008**, *128*, 084102.

49 Frisch, M. J.; Trucks, G. W.; Schlegel, H. B.; Scuseria, G. E.; Robb, M. A.; Cheeseman, J. R.; Montgomery, J. A., Jr.; Vreven, T.; Kudin, K. N.; Burant, J. C.; Millam, J. M.; Iyengar, S. S.; Tomasi, J.; Barone, V.; Mennucci, B.; Cossi, M.; Scalmani, G.; Rega, N.; Petersson, G. A.; Nakatsuji, H.; Hada, M.; Ehara, M.; Toyota, K.; Fukuda, R.; Hasegawa, J.; Ishida, M.; Nakajima, T.; Honda, Y.; Kitao, O.; Nakai, H.; Klene, M.; Li, X.; Knox, J. E.; Hratchian, H. P.; Cross, J. B.; Bakken, V.; Adamo, C.; Jaramillo, J.; Gomperts, R.; Stratmann, R. E.; Yazyev, O.; Austin, A. J.; Cammi, R.; Pomelli, C.; Ochterski, J. W.; Ayala, P. Y.; Morokuma, K.; Voth, G. A.; Salvador, P.; Dannenberg, J. J.; Zakrzewski, V. G.; Dapprich, S.; Daniels, A. D.; Strain, M. C.; Farkas, O.; Malick, D. K.; Rabuck, A. D.; Raghavachari, K.; Foresman, J. B.; Ortiz, J. V.; Cui, Q.; Baboul, A. G.; Clifford, S.; Cioslowski, J.; Stefanov, B. B.; Liu, G.; Liashenko, A.; Piskorz, P.; Komaromi, I.; Martin, R. L.; Fox, D. J.; Keith, T.; Al-Laham, M. A.; Peng, C. Y.; Nanayakkara, A.; Challacombe, M.; Gill, P. M. W.; Johnson, B.; Chen, W.; Wong, M. W.; Gonzalez, C.; Pople, J. A. *Gaussian 03*, revision C.02; Gaussian, Inc.: Wallingford, CT, 2004;

50 Frisch, M. J.; Trucks, G. W.; Schlegel, H. B.; Scuseria, G. E.; Robb, M. A.; Cheeseman, J. R.; Scalmani, G.; Barone, V.; Mennucci, B.; Petersson, G. A.; Nakatsuji, H.; Caricato, M.; Li, X.; Hratchian, H. P.; Izmaylov, A. F.; Bloino, J.; Zheng, G.; Sonnenberg, J. L.; Hada, M.; Ehara, M.; Toyota, K.; Fukuda, R.; Hasegawa, J.; Ishida, M.; Nakajima, T.; Honda, Y.; Kitao, O.; Nakai, H.; Vreven, T.; Montgomery, Jr., J. A.; Peralta, J. E.; Ogliaro, F.; Bearpark, M.;

Heyd, J. J.; Brothers, E.; Kudin, K. N.; Staroverov, V. N.; Kobayashi, R.; Normand, J.; Raghavachari, K.; Rendell, A.; Burant, J. C.; Iyengar, S. S.; Tomasi, J.; Cossi, M.; Rega, N.; Millam, N. J.; Klene, M.; Knox, J. E.; Cross, J. B.; Bakken, V.; Adamo, C.; Jaramillo, J.; Gomperts, R.; Stratmann, R. E.; Yazyev, O.; Austin, A. J.; Cammi, R.; Pomelli, C.; Ochterski, J. W.; Martin, R. L.; Morokuma, K.; Zakrzewski, V. G.; Voth, G. A.; Salvador, P.; Dannenberg, J. J.; Dapprich, S.; Daniels, A. D.; Farkas, Ö.; Foresman, J. B.; Ortiz, J. V.; Cioslowski, J.; Fox, D. J. *Gaussian 09*, revision A.1, Gaussian, Inc., Wallingford CT, 2009.

[51] MOLPRO, version 2009.1, a package of ab initio programs, H.-J. Werner, P. J. Knowles, R. Lindh, F. R. Manby, M. Schutz, P. Celani, T. Korona, A. Mitrushenkov, G. Rauhut, T. B. Adler, R. D. Amos, A. Bernhardsson, A. Berning, D. L. Cooper, M. J. O. Deegan, A. J. Dobbyn, F. Eckert, E. Goll, C. Hampel, G. Hetzer, T. Hrenar, G. Knizia, C. Koppl, Y. Liu, A. W. Lloyd, R. A. Mata, A. J. May, S. J. McNicholas, W. Meyer, M. E. Mura, A. Nicklass, P. Palmieri, K. Pfluger, R. Pitzer, M. Reiher, U. Schumann, H. Stoll, A. J. Stone, R. Tarroni, T. Thorsteinsson, M. Wang, and A. Wolf.

[52] Zheng, J.; Zhao, Y.; Truhlar, D. G. J. Chem. Theory Comput. **2007**, *3*, 569.

[53] Zheng, J.; Zhao, Y.; Truhlar, D. G. J. Chem. Theory Comput. **2009**, *5*, 808.

[54] Zhao, Y.; Truhlar, D. G. J. Chem. Theory Comput. **2005**, *1*, 415.

[55] Lynch, B. J.; Zhao, Y.; Truhlar, D. G. J. Phys. Chem. A **2003**, *107*, 1384.

[56] Lynch, B. J.; Truhlar, D. G. J. Phys. Chem. A **2003**, *107*, 3898.

[57] Lynch, B. J.; Truhlar, D. G. J. Phys. Chem. A **2004**, 107, 8996.

[58] Weigend, F. *Phys. Chem. Chem. Phys.* **2002**, *4*, 4285.

[59] Hättig, C. *Phys. Chem. Chem. Phys.* **2005**, *7*, 59

[60] Weigend, F.; Kohn, A.; Hattig, C. *J. Chem. Phys.* **2002**, *116*, 3175.

[61] Boys, S. F.; Bernardi, F. *Mol. Phys.* **1970**, *19*, 553.

[62] Alvarez-Idaboy, J. R.; Galano, A. *Theor. Chem. Acc.* **2010,** *126*, 75.

[63] Skwara, B.; Bartkowiak, W.; Da Silva, D. L. *Theor. Chem. Acc.* **2009,** *122*, 127.

[64] King, R. A.; Allen, W. D.; Ma, B.; Schaefer, H. F. III *Faraday Discuss.* **1998**, *110*, 23.

[65] Mintz, B.; Lennox, K. P.; Wilson, A. K. *J. Chem. Phys.* **2004**, *121*, 5629.

[66] Jurgens-Lutovsky, R.; Almlof, J. *J. Chem. Phys. Lett.* **1991**, 178, 431.

[67] Wolinski, K.; Pulay, P. *J. Chem. Phys.* **2003***, 118*, 9497.

Chapter 4.   Perspectives on Basis Sets Beautiful: Seasonal Plantings of Diffuse Basis Functions

Ewa Papajak, Jingjing Zheng, Xuefei Xu, Hannah R. Leverentz, and Donald G. Truhlar

Department of Chemistry, University of Minnesota, Minneapolis, MN 55455-0431 USA

We present a perspective on the use of diffuse basis functions for electronic structure calculations by density functional theory and wave function theory. We especially emphasize minimally augmented basis sets and calendar basis sets. We base our conclusions on our previous experience with commonly computed quantities, such as bond energies, barrier heights, electron affinities, noncovalent (van der Waals and hydrogen bond) interaction energies, and ionization potentials, on Stephens et al.'s results for optical rotation, and on our own new calculations (presented here) of polarizabilities and of potential energy curves of van der Waals complexes. We emphasize the benefits of partial augmentation of the higher-zeta basis sets in preference to full augmentation at a lower zeta level. Benefits and limitations of the use of fully, partially, and minimally augmented basis sets are reviewed for different electronic structure methods and molecular properties. We have found that minimal augmentation is almost always enough for density functional theory (DFT) when applied to ionization potentials, electron affinities, atomization energies, barrier heights, and hydrogen-bond energies. For electric dipole polarizabilities, we find that augmentation beyond minimal has an average effect of 8% at the polarized triple zeta level and 5% at the polarized quadruple zeta level. The effects are larger for potential energy curves of van der Waals complexes. The effects are also larger for wave function theory (WFT); even for WFT though, full augmentation is not needed for most purposes and a level of augmentation between minimal and full is optimum for most problems. The calendar basis sets named after the months provide a convergent sequence of partially augmented basis sets that can be used for such

calcuations. For example, the jun-cc-pV(T+d)Z basis set is very useful for MP2-F12 calcuations of barrier heights and hydrogen bond strengths.

Introduction

It has been realized for a long time[1,2] that basis sets for electronic structure calculations of many molecular properties must contain diffuse basis functions for quantitative accuracy. It has also been shown many times that diffuse functions have a relatively small effect for a number of molecular properties (for example for ionization potentials and stationary point geometries of many molecules). It is best to avoid using diffuse basis functions when they are unnecessary or to avoid using more than the required number when they are necessary because adding diffuse functions to a basis set not only increases the cost of the calculation but can cause problems with SCF convergence and can increase basis set superposition error (BSSE). However, systematic studies of how to include the diffuse space efficiently that are based on large sets of data for various molecular properties and barrier heights are few and far between.

We have recently conducted a series of such studies including barrier heights, electron affinities, ionization potentials, atomization energies, and hydrogen bond energies.[3–6] We conclude that much current practice includes more diffuse functions than are needed. Often better accuracy could be achieved if the additional cost were invested in higher-zeta basis set or more polarization functions. Our conclusions on how to achieve higher accuracy on a per-cost basis can be widely useful for practical electronic structure calculations, and so we summarize them in this article. In addition to considering our own results, we comment briefly on optical rotation studies of Stephens, Sadlej, and coworkers.[7–9]

In addition to reviewing and integrating previously published work, this paper presents new calculations of polarizability and potential energy curves, which provide interesting challenges for efficient basis set selection.

Minimally Augmented Basis Sets

In the correlation consistent basis sets, Dunning and coworkers[10] defined "aug-" (which denotes "augmented") to mean adding one diffuse basis function to every atom for every angular momentum of basis functions already present on that atom. We call such basis sets fully augmented. For example, the cc-pVTZ basis set for methane has s, p, d, and f functions on C and s, p, and d functions on H, so aug-cc-pVTZ adds diffuse s, p, d, and f subshells to C and diffuse s, p, and d subshells to H. Dunning and coworkers individually optimized the exponential parameters for each aug- basis set.

In contrast, the earlier "plus" basis sets originally systematized by Pople and coworkers[11] added only diffuse s and p subshells to nonhydrogenic functions and no diffuse functions to hydrogen atoms. We call this minimal augmentation. In Pople-type basis sets one uses the same exponential parameters for diffuse functions in any basis set for a given atom. For example 6-31+G(d,p) and 6-311+G(2df,2p) use the same exponential parameters for diffuse functions on C.

We have defined three kinds of minimal augmentation, denoted by "+", "maug-", and "ma-". We next explain these in turn.

The "+" kind of minimal augmentation can be applied to any basis set for any atom for which exponential parameters have been defined for adding diffuse functions to the 6-31G or 6-311G basis sets. We then add a plus suffix. For example cc-pVTZ+ denotes a minimally augmented cc-pVTZ basis set with the exponential parameters for diffuse functions from Ref. 11. Some basis sets of the + type have other names; for example, the MG3S basis set[12] is minimally augmented, and in fact is the same as 6-311+G(3d2f,2df,2p) for H through Si, but it is improved[13] for S, P and Cl. The generalization of the + approach to basis sets other than 6-31+G and 6-311+G was introduced in Ref. 3.

The maug- kind of minimal augmentation can be applied to any aug- type correlation consistent basis set. One simply truncates the diffuse space to the minimal augmentation level. For example maug-cc-pVTZ retains the diffuse s and p functions on carbon with the exponential parameters optimized for the aug- case, but deletes all other diffuse functions. This approach was introduced in Refs. 3 and 4. We note that other

levels of augmentation between minimal (maug-) and full (aug-) have also been defined for correlation-consistent basis sets, and these are discussed in Ref. 6 and below.

The maug- kind of minimal augmentation[5] may be used with any nondiffuse basis set. One simply creates diffuse functions for atoms heavier than He by dividing the smallest s and p exponential parameters already present by a factor of three. The ma- type of minimal augmentation was originally proposed for the def2- basis sets,[14] which are the second-generation default basis sets of the TURBOMOLE program, as developed in Karlsruhe. For example the ma-TZVP basis set is obtained from the def2-TZVP basis set for carbon by adding diffuse functions obtained this way.[5] For basis sets other than the Karlsruhe def2- series, one simply adds ma- as a prefix, e.g., ma-LANL2DZ.

Examples of applications of the efficient "+" and "maug-" basis sets to problems involving large molecules are available both in work by our group[15–17] and in work by other research groups.[18,19]

It is sometimes assumed that adding extra basis functions is a useful cautionary step so it does not hurt to use aug- when a smaller basis set would be sufficient. However, using full augmentation raises the cost, and if it is done at the expense of not increasing the size of the valence space, it can be harmful. For example, it is often more beneficial to increase a basis set from maug-cc-pVDZ to maug-cc-pVTZ rather than increase it to aug-cc-pVDZ, even for properties that are sensitive to including diffuse functions, for example, barrier heights, hydrogen bond energies, and electron affinities. When applying density functional theory, the only exceptions to this general finding in our tests were B3LYP calculations of hydrogen bonding energies, which also showed no improvement in accuracy from augmentation of the quadruple zeta basis set, and which showed higher accuracy of maug than aug at the triple zeta level; these findings indicate that the error is dominated for B3LYP by the intrinsic error in the density functional, not by the lack of completeness of the basis set.

There are also other ways that adding extra diffuse basis functions could be harmful. For example it can increase basis set superposition error. It is sometimes speculated that adding more functions to the basis set increases its completeness and should therefore reduce the basis set superposition error; however, it is especially the

functions that overlap other centers that cause BSSE, so it is also possible to increase BSSE by adding diffuse functions. We have studied this and have shown[3] that the increased diffuse space of the fully augmented basis sets does not necessarily decrease the counterpoise correction for basis set superposition error, and in fact it can increase it. One could hypothesize that this is an indication of the limitations of counterpoise corrections, not necessarily increased BSSE. In any case, one can conclude from this that an expensive full augmentation followed by an also expensive counterpoise correction calculation is not necessarily accurate, besides being uneconomical.

Density Functional Theory

We have found[3–5] that minimal augmentation is almost always enough for density functional theory (DFT) when applied to ionization potentials, electron affinities, atomization energies, barrier heights, and hydrogen-bond energies. Indeed it has advantages over full augmentation not only in cost but also in sometimes reducing slow SCF convergence and basis set superposition error. We also note that minimal augmentation (relative to no augmentation) is often more advantageous in DFT than in wave function theory (WFT).[20] Minimal augmentation is especially important for barrier heights, hydrogen bonding, and electron affinities, but less important for bond energies and ionization potentials.[3]

In DFT calculations, the savings from using minimal augmentation instead of full augmentation can be significant since DFT is often applied to challenging problems such as large systems or direct dynamics calculations that require a large number of electronic structure calculations on the fly. In such cases it is very undesirable to increase the cost of the calculations by using more than the minimum number of basis functions required for chemical accuracy. Raising the cost by overaugmentation may make it necessary to adopt compromises such as a reduced number of steps in dynamics calculations, using a smaller than necessary grid, using a lower-zeta basis set, etc. The other extreme is the omission of all diffuse functions because of the cost. *Our default recommendation for DFT is to use minimally augmented basis sets instead of full augmentation for properties such as*

barrier heights, electron affinities, polarizabilities, and noncovalent interactions;
however, no augmentation is needed for ionization potentials and atomization energies.

Wave Function Theory and Calendar Basis Sets

Correlated wave function calculations are more sensitive to diffuse basis set expansion beyond minimal than are density functional calculations, and therefore we recommend higher than minimal saturation of the diffuse space, but we still recommend less than full augmentation in most cases.

The reason for the slower convergence of correlated wave function calculations, when compared to density functional calculations, is easily understood. When including dynamic electron correlation in WFT, one uses the basis functions not only to represent the single-particle density, but also to build the cusps into the many-electron wave function in the region where two electrons come together. The cusp is built up from a large number of configurations, extending to fairly high angular momentum for individual orbitals, but with each configuration having a small coefficient, and hence second-order perturbation theory (MP2) already provides realistic predictions of these coefficients[21,22] (the higher-order correlations are important, but are less dominant in the description of the cusps). As a consequence the basis set requirements may be examined at the MP2 level. We therefore recently studied the effect of diffuse functions on basis set convergence of MP2 calculations, and we developed a convergent sequence of partially augmented convergent correlation-consistent basis sets named after the months.[6]

In these studies we found that even in WFT, just as in DFT, for all practical purposes one does not need diffuse functions on hydrogen atoms. Thus our first recommendation is to delete these on all hydrogen and helium atoms; this yields basis sets we label as jul-, a naming convention that we actually introduced in a previous paper.[3] (This is sometimes called[23] aug′, but aug′ has been used to denote more than one possible modification to the aug- basis sets, so we believe that a unique notation is useful.)

The other calendar basis sets are obtained by successively deleting diffuse subshells on heavier atoms.[6] Consider carbon. The aug- and jul- triple zeta basis sets have

diffuse *s*, *p*, *d*, and *f* subshells. We delete the *f* subshell to get jun-, then the *d* subshell to get may-, which is equivalent to maug- for triple zeta. But at the quadruple zeta level, carbon has diffuse *s*, *p*, *d*, *f*, and *g* diffuse subshells. We delete the *g* subshell to get jun-, the *f* subshell to get may-, and the *d* subset to get apr-, which is equivalent to maug- for quadruple zeta. Thus when one increases the basis from jun-cc-pVTZ to jun-cc-pVQZ, one not only increases the valence basis but also one adds a diffuse *f* subshell; in this sense the diffuse space is convergent when one increases the zeta level but keeps the month constant (unlike the case in going from 6-31+G(d,p) to 6-311+G(2df,2p). Thus, for some problems the calendar basis sets can provide a more efficient sequence of basis sets (than unaugmented, minimally augmented, or fully augmented sets) for basis set extrapolation to the complete basis set limit.

The lowest exponents in the unaugmented cc-pV*x*Z basis sets decrease as *x* increases. Therefore, even though unaugmented, the underlying cc-pV*x*Z basis sets become more and more diffuse. This is one of the reasons why–for the previously published data on barrier heights, electron affinities, and hydrogen bonding interactions–the need for the diffuse functions decreases as the valence space increases. For DZ we recommended jul-, while for QZ we can reduce the basis set to jun- or even may- without significant loss in accuracy.

In general, the goal of most electronic structure calculations is not to achieve an accuracy on the order of, for example, 0.1 kcal/mol at any cost but rather to achieve as high accuracy possible at a reasonable cost. The actual accuracy objective is dictated by the system's size and character and by the electronic structure method itself. For example, it is unreasonable to invest additional ~30% of computational time to improve accuracy by about 0.1 kcal/mol when the expected accuracy of the method is ~1 kcal/mol and the additional cost would have been better invested into increasing other features of the basis set or using a different level of theory. The need for this kind of approach is evidenced by the enormous number of calculations in the literature that employ double-zeta and triple-zeta basis sets, even though these calculations are clearly not at the basis set limit.

Jun- basis sets are a much better default option than aug- basis sets for correlated WFT calculations. Based on our tests,[6] it is always more beneficial for the accuracy of barrier heights, hydrogen bonding, electron affinities, ionization potentials, and atomization energies to invest additional computational resources into increasing a basis set from cc-pVDZ to jun-cc-pVTZ rather than to aug-cc-pVDZ or cc-pVTZ. The analogous statement is true for the jun-cc-pVTZ to may-cc-pVQZ transition (skipping the aug-cc-pVTZ and cc-pVQZ). We note that, averaged over a large database, aug- triple zeta calculations involve about 27% more basis functions than jun- triple zeta.[6]

An alternative way to converge correlated WFT calculations with respect to the basis set is the F12 method[24,25] in which basis functions depending explicitly on interelectronic distances are added to the basis. This is a powerful method because it eliminates much of the need to build up the electron–electron cusps by a succession of higher-angular-momentum basis functions. This method is expected to revolutionize quantum chemistry over the next several years by allowing nearly complete-basis-set calculations with much less effort than was previously required. For F12 calculations we recommend may- quadruple-zeta, jun- triple-zeta, and jul- double-zeta.[6]

The next section considers wave function calculations on properties not included in our previous systematic tests, and we will examine whether some of these properties are in greater need of diffuse functions than the properties considered so far.

Wave Function Calculations of van der Waals Potential Curves, Polarizabilities, Raman Intensities, and Optical Rotation

Accurate calcuations of electrical properties of molecules often require large basis sets, including multiple polarization functions and diffuse functions.[26–36] It is therefore interesting to study the need for higher-angular-momentum diffuse functions, and we present some calcuations exploring this need in this section.

The long-range portions of the long-range of van der Waals potential curves between nonpolar molecules depend on induced low-order electric multipole moments, and therefore they provide a challenging test of the need for diffuse basis functions; here we report new calcuations designed to examine this issue. Potential energy curves were

calculated for Ne_2, $(CH_4)_2$, $(H_2O)_2$, and $(C_2H_4)_2$ by using coupled cluster theory with single and double excitations and a quasiperturbative treatment of connected triple excitations[37] [CCSD(T)] using the *Gaussian 09*[38] program package; the results are presented in tabular form in Supporting Information and are plotted in figures 1 – 6. The geometries of methane dimer, two orientations of water dimer (non-planar C_s and cyclic C_{2h}) and two orientations of ethylene dimer (T-shaped and stacked) are shown in the figures. The potential energy curves show that diffuse functions play a larger role for van der Waals potentials than they do for the properties examined earlier in this perspective. Nevertheless some savings are possible. For example, jun-QZ and jun-TZ agree reasonably well with aug-QZ and aug-TZ respectively.

Figure 3 shows particularly rapid convergence with respect to increasing the number of diffuse functions with all curves from maug- to aug- being closely grouped at all three zeta levels, although they are far from the unaugmented curves. The curves in Fig. 4 also converge rapidly.

Another problem for which full augmentation is sometimes recommended is the calculation of electric dipole polarizabilities. First, we used the analytic polarizability algorithm in *MolPro 2009*[39] to calculate HF and and MP2 spherically averged polarizabilities for four molecules: methane (CH_4), water (H_2O), 3-mercaptopropan-1-ol ($HO(CH_2)_3SH$), and pyridine (C_5H_5N). These results are in Table 1. Then we used the finite field approximation with a field strength of 0.005 atomic units to calculate the zz element of the polarizability tensor for water and methane by the HF, MP2, and MP2-F12 methods. These results are in Tables 2 and 3.

Table 1 shows that diffuse functions on the H atoms have a significant effect on the results (more than a couple of percent) in the case of double zeta basis sets. However, for TZ and QZ the average difference between aug- and jul- is only 0.05 and 0.02 $Å^3$, respectively. For nonhydrogenic atoms, as in the case of properties considered in earlier sections of this perspective, we find that, at the lower-zeta levels the higher angular momentum functions affect the results significantly. However, the lower angular momentum functions in jun-TZ and jul-DZ provide of most of the difference between augmented and non-augmented basis sets. At higher zeta levels full augmentation only

adds additional cost and does not affect the accuracy at all. For example the results obtained with the jun-QZ basis set agree well with those obtained with aug-QZ with the largest percentage error being 2% for H_2O.

Tables 2 and 3 allow us to compare MP2-F12 covergence to MP2 convergence for polarizability elements. For the MP2-F12 calcuations of electric dipole polarizabilities, one finds that may-, jun-, and jul- quadruple zeta basis sets all have mean unsigned percentage errors (with respect to the largest fully augmented basis set) of about 2.7 % and less, jul- and jun- triple zeta basis sets have mean unsigned percentage errors less than 5.7%, and jul- double zeta has a mean unsigned percentage error of 11%.

We conclude that diffuse functions are especially important in the polarizability calculations employing double-zeta basis sets and partially augmented basis sets of higher-zeta levels can be useful for polarizabilities.

This is consistent with findings of Sadlej et al. who introduced one diffuse function for each shell in their single contracted basis sets for electric properties, while their large basis sets are augmented only with a single s on hydrogenic atoms and a single s and a single p on other elements.[40,41] These basis sets have been found to perform well for the Raman intensities by Schlegel,[42] which is also consistent with our results since Raman intensities depend on the derivatives of polarizabilities with respect to nuclear coordinates. However, Zuber et. al.[43] find that full augmentation on heavy atoms and additional p functions on the hydrogen atoms are necessary for the accurate description of Raman and Raman optical activity (ROA) scattering.

Optical rotation is an example of a property, like van der Waals potential curves, that is especially sensitive to the diffuse space of the basis set. Diffuse functions are necessary for good results; however the most thorough studies suggest that some savings can be made. For example, in Refs. 7 and 9 the authors state that their HF and DFT 6-311++G(2d,2p) results, which are augmented but much less than fully augmented, agree well with results obtained by aug-cc-pVTZ.

Summary

Diffuse functions are an important component of basis sets, but in most cases we

recommend less than full augmentation with diffuse functions. For density functional theory we usually recommend minimal augmentation, and for correlated wave function theory we usually recommend a jun- level of augmentation.

References

[1] Clark, T.; Chandresekhar, J.; Spitznagel, G. W.; Schleyer, P. v. R. *J. Comp. Chem.* **1983**, *4*, 264.

[2] Davidson, E. R.; Feller, D. *Chem. Rev.* **1986**, *86*, 681.

[3] Papajak, E.; Leverentz, H. R.; Zheng, J.; Truhlar, D. G. J. *Chem. Theory Comput.* **2009**, *5*, 1197; **2009**, *5*, 3330(E).

[4] Papajak, E.; Truhlar, D. G. J. *Chem. Theory Comput.* **2010**, *6*, 597.

[5] Zheng, J.; Xu, X.; Truhlar, D. G. *Theor. Chem. Acc.* **2011**, *128*, 295.

[6] Papajak, E.; Truhlar, D. G. *J. Chem. Theory Comput.* **2011**, *7*, 10.

[7] Stephens, P. J.; Devlin, F. J., Cheeseman, J. R.; Frisch, M. J. *J. Phys. Chem. A* **2001,** *105,* 5356.

[8] Baranowska, A.; Laczkowski, K. Z.; Sadlej, A. J. *J. Comput. Chem.* **2010**, *31*, 1176.

[9] Cheeseman, J. R., Frisch, M. J., Devlin, F. J., Stephens, P. J. *J. Phys. Chem. A* **2000**, *104*, 1039.

[10] Kendall, R. A.; Dunning Jr., T. H.; Harrison, R. J. *J. Chem. Phys.* **1992**, *96*, 6769.

[11] Frisch, M. J.; Pople, J. A.; Binkley, J. S. *J. Chem. Phys.* **1984,** *80*, 3265.

[12] Fast, P. L.; Sanchez, M. L.; Truhlar, D. G. *Chem. Phys. Lett.* **1999**, *306*, 407.

[13] Curtiss, L. A.; Raghavachari, K.; Redfern C.; Rassolov, V.; Pople, J. A. *J. Chem. Phys.* **1998**, 109, 7764.

[14] F. Weigend, F.; Ahlrichs, R. *Phys. Chem. Chem. Phys.* **2005**, *7*, 3297.

[15] Zheng, J.; Truhlar, D. G. *J. Phys. Chem. A* **2009**, *113*, 11919.

[16] Zheng, J.; Truhlar, D. G. *Phys. Chem. Chem. Phys.* **2010**, *12*, 7782.

[17] Yang, K.; Zheng, J.; Zhao, Y.; Truhlar, D. G. *J. Chem. Phys.* **2010**, *132*, 164117.

[18] Meyer, M. M.; Kass, S. R. *J. Org. Chem.* **2010**, *75*, 4274.

[19] Hermosilla, L.; Catak, S.; Van Speybroeck, V.; Waroquier, M.; Vandenbergh, J.; Motmans, F;, Adriaensens, P.; Lutsen, L.; Cleij, T.; Vanderzande, D. *Macromolecules* **2010**, *43*, 7424.

[20] Lynch, B. J.; Zhao, Y.; Truhlar, D. G. *J. Phys. Chem. A* **2003**, *107*, 1384.

[21] Petersson, G. A.; Braunstein, M. *J. Chem. Phys.* **1985**, *83*, 5129.

[22] East, A. L. L.; Allen W. D. *J. Chem. Phys.* 1993, *99*, 4638.

[23] Sullivan M. B.; Iron, M. A.; Redfern, P. C.; Martin, J. M. L.; Curtiss, L. A.; Radom, L. *J. Phys. Chem. A* **2003**, *107*, 5617.

[24] Ten-no, S. *Chem. Phys. Lett.* **2004**, *398*, 56.

[25] Werner, H.-J.; Adler, T. B.; Manby, F. R. *J. Chem. Phys.* **2007**, *126*. 164102.

[26] Werner, H.J.; Meyer, W. *Mol. Phys.* **1976**, *31*, 855.

[27] Werner, H.J.; Meyer, W. *Phys. Rev. A* **1976**, *13*, 13.

[28] Morrison, M. A.; Hay, P. J. *J. Phys. B* **1977**, *10*, L647.

[29] Eades, R. A.; Truhlar, D. G.; Dixon, D. A. *Phys. Rev. A* **1979**, *20*, 867.

[30] Douglass, C. H. Jr.; Weil, D. A.; Eades, R. A.; Truhlar, D. G.; Dixon, D. A. In *Chemical applications of Atomic and Molecular Electrostatic Potentials*; Politzer, P., Truhlar, D. G., Eds.; Plenum:New York, 1981; p. 173.

[31] Darling, C. L.; Schlegel, H. B. *J. Phys. Chem.* **1994**, *98*, 5855.

[32] Peterson, K.A.; Dunning Jr., T.H. *J. Mol. Struct. Theochem* **1997**, *400*, 93.

[33] Cybulski, A. M. *J. Chem. Phys.* **1999**, *111*, 10520.

[34] Oliveira, L.N.; Amaral, O.A.V.; Castro, M.A.; Fonseca, T.L. *Chem. Phys.* **2003**, *289*, 221.

[35] Arruda, P.M.; Neto, A.C.; Jorge, F.E. *Int. J. Quantum Chem* **2009**, *109*, 1189.

[36] Camiletti, G.G.; Canal Neto, A.; Jorge, F.E.; Machado, S.F. J. *Mol. Struct. Theochem* **2009**, *910*, 122.

[37] Raghavachari, K.; Trucks, G. W.; Pople, J. A.; Head-Gordon, M. *Chem. Phys. Lett.* **1989**, *157*, 479.

[38] Frisch, M. J.; Trucks, G. W.; Schlegel, H. B.; Scuseria, G. E.; Robb, M. A.; Cheeseman, J. R.; Scalmani, G.; Barone, V.; Mennucci, B.; Petersson, G. A.; Nakatsuji, H.; Caricato, M.; Li, X.; Hratchian, H. P.; Izmaylov, A. F.; Bloino, J.; Zheng, G.; Sonnenberg, J. L.; Hada, M.; Ehara, M.; Toyota, K.; Fukuda, R.; Hasegawa, J.; Ishida, M.; Nakajima, T.; Honda, Y.; Kitao, O.; Nakai, H.; Vreven, T.; Montgomery, Jr., J. A.; Peralta, J. E.; Ogliaro, F.; Bearpark, M.; Heyd, J. J.; Brothers, E.; Kudin, K. N.; Staroverov, V. N.; Kobayashi, R.; Normand, J.; Raghavachari, K.; Rendell, A.; Burant, J. C.; Iyengar, S. S.; Tomasi, J.; Cossi, M.; Rega, N.; Millam, N. J.; Klene, M.; Knox, J. E.; Cross, J. B.; Bakken, V.; Adamo, C.; Jaramillo, J.; Gomperts, R.; Stratmann, R. E.; Yazyev, O.; Austin, A. J.; Cammi, R.; Pomelli, C.; Ochterski, J. W.; Martin, R. L.; Morokuma, K.; Zakrzewski, V. G.; Voth, G. A.; Salvador, P.; Dannenberg, J. J.; Dapprich, S.; Daniels, A. D.; Farkas, Ö.; Foresman, J. B.; Ortiz, J. V.; Cioslowski, J.; Fox, D. J. *Gaussian 09, Revision A.1,* Gaussian, Inc., Wallingford CT, 2009.

[39] Werner, H.-J.; Knowles, P. J.; Lindh, R.; Manby, F. R.; Schutz, M.; Celani, P.; Korona, T.; Mitrushenkov, A.; Rauhut, G.; Adler, T. B.; Amos, R. D.; Bernhardsson, A.; Berning, A.; Cooper, D. L.; Deegan, M. J. O.; Dobbyn, A. J.; Eckert, F.; Goll, E.; Hampel, C.; Hetzer, G.; Hrenar, T.; Knizia, G.; Koppl, C.; Liu, Y.; Lloyd, A. W.; Mata, R. A.; May, A. J.; McNicholas, S. J.; Meyer, W.; Mura, M. E.; Nicklass, A.; Palmieri, P.; Pfluger, K.; Pitzer, R.; Reiher, M.; Schumann, U.; Stoll, H.; Stone, A. J.; Tarroni, R.; Thorsteinsson, T.; Wang, M.; Wolf, A. *MOLPRO version 2009.1,* University College Consultants Ltd., Cardiff, Wales, UK, 2009.

[40] Benkova, Z.; Sadlej, A. J.; Oakes, R. E.; Bell, S. E. J. *J. Comput. Chem.* **2005**, *26*, 145.

[41] Baranowska, A.; Sadlej, A. J. *J. Comput. Chem.* **2010**, *31*, 552.

[42] Halls, M. D.; Schlegel, H. B. *J. Chem. Phys.* **1999**, *111*, 8819.

[43] Zuber, G., Hug, W. *J. Phys. Chem.* **2004**, *108*, 2108.

Table 1. HF and MP2 polarizability [$Å^3$] values, average unsigned errors [$Å^3$], and percentage errors [%] for basis sets of different degrees of augmentation.[a]

	H_2O		CH_4		C_5H_5N		$HO(CH_2)_3SH$		Mean Unsigned Error		MU Percentage Error	
	HF	MP2	HF	MP2	HF	MP2	HF	MP2	HF	MP2	HF	MP2
aug-cc-pV(Q+d)Z	1.26	1.43	2.37	2.45	9.43	9.61	9.27	9.71	0.00	0.00	0.0	0.0
jul-cc-pV(Q+d)Z	1.24	1.40	2.36	2.43	9.43	9.61	9.26	9.74	0.01	0.02	0.4	0.7
jun-cc-pV(Q+d)Z	1.24	1.40	2.36	2.43	9.43	9.61	9.26	9.73	0.01	0.02	0.4	0.7
may-cc-pV(Q+d)Z	1.24	1.39	2.36	2.43	9.43	9.59	9.26	9.71	0.01	0.02	0.5	0.9
apr-cc-pV(Q+d)Z[b]	1.16	1.28	2.27	2.32	9.31	9.46	9.10	9.52	0.12	0.15	3.8	4.7
cc-pV(Q+d)Z	1.09	1.17	2.27	2.31	9.01	9.13	8.85	9.19	0.28	0.35	6.7	8.4
aug-cc-pV(T+d)Z	1.25	1.41	2.37	2.45	9.43	9.63	9.25	9.76	0.01	0.02	0.3	0.5
jul-cc-pV(T+d)Z	1.20	1.33	2.35	2.42	9.42	9.61	9.22	9.69	0.04	0.03	1.6	1.9
jun-cc-pV(T+d)Z	1.20	1.33	2.35	2.41	9.42	9.60	9.21	9.67	0.04	0.05	1.6	2.2
may-cc-pV(T+d)Z[b]	1.09	1.19	2.19	2.23	9.19	9.34	8.88	9.26	0.24	0.29	7.0	8.2
cc-pV(T+d)Z	0.98	1.03	2.18	2.20	8.59	8.63	8.41	8.66	0.54	0.65	12.2	14.6
aug-cc-pV(D+d)Z	1.20	1.36	2.36	2.44	9.40	9.63	9.17	9.67	0.05	0.03	1.5	1.4
jul-cc-pV(D+d)Z	1.09	1.20	2.28	2.33	9.36	9.57	9.02	9.44	0.15	0.17	5.2	6.1
jun-cc-pV(D+d)Z[b]	0.92	1.02	1.99	2.01	8.91	9.08	8.36	8.67	0.54	0.60	14.6	15.7
cc-pV(D+d)Z	0.74	0.76	1.91	1.91	7.77	7.83	7.53	7.63	1.09	1.27	24.2	27.2

[a]The methane (CH_4) and water (H_2O) geometries were optimized at the QCISD/MG3S level, while 3-mercaptopropan-1-ol ($HO(CH_2)_3SH$) and pyridine (C_5H_5N) geometries were optimized at the MP2-F12/aug-cc-pV(Q+d)Z level with frozen core electrons. Note that for elements up through Mg, cc-pV(X+d)Z is the same as cc-pVXZ.
[b]same as maug-

84

Table 2. HF, MP2, and MP2-F12 finite-field approximation to zz element of the polarizability tensor [A^3] of H$_2$O for basis sets of different degrees of augmentation.

	H$_2$O		
	HF	MP2	MP2-F12
jul-cc-pV(5+d)Z	1.25	1.40	1.41
aug-cc-pV(Q+d)Z	1.26	1.42	1.42
jul-cc-pV(Q+d)Z	1.24	1.38	1.38
jun-cc-pV(Q+d)Z	1.24	1.38	1.38
may-cc-pV(Q+d)Z	1.24	1.37	1.38
apr-cc-pV(Q+d)Z	1.14	1.24	1.29
cc-pV(Q+d)Z	1.11	1.19	1.25
aug-cc-pV(T+d)Z	1.24	1.40	1.41
jul-cc-pV(T+d)Z	1.19	1.31	1.33
jun-cc-pV(T+d)Z	1.18	1.30	1.33
may-cc-pV(T+d)Z	1.06	1.15	1.23
cc-pV(T+d)Z	1.00	1.05	1.16
aug-cc-pV(D+d)Z	1.19	1.34	1.38
jul-cc-pV(D+d)Z	1.06	1.15	1.22
jun-cc-pV(D+d)Z	0.88	0.95	1.13
cc-pV(D+d)Z	0.75	0.78	1.01

Table 3. HF, MP2, and MP2-F12 finite-field approximation to zz element of the polarizability tensor [A^3] of CH$_4$ for basis sets of different degrees of augmentation.

	CH$_4$		
	HF	MP2	MP2-F12
aug-cc-pV(T+d)Z	2.37	2.45	2.44
jul-cc-pV(T+d)Z	2.35	2.42	2.42
jun-cc-pV(T+d)Z	2.35	2.42	2.42
may-cc-pV(T+d)Z	2.19	2.23	2.33
cc-pV(T+d)Z	2.18	2.21	2.31
aug-cc-pV(D+d)Z	2.36	2.44	2.44
jul-cc-pV(D+d)Z	2.28	2.33	2.37
jun-cc-pV(D+d)Z	1.99	2.01	2.24
cc-pV(D+d)Z	1.91	1.91	2.18
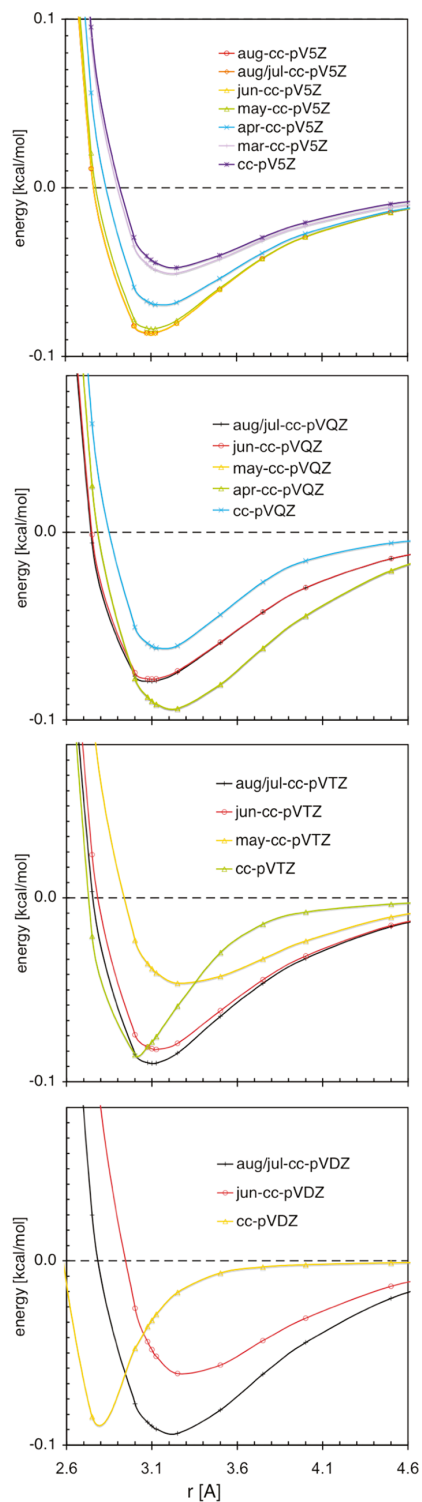
Figure 1. CCSD(T) interaction energy (in kcal/mol) for Ne_2 relative to the energy of Ne atoms at infinite separation for quintuple-, quadruple-, triple-, and double-zeta basis sets. The abscissa r is the distance between the Ne atoms. No counterpoise corrections are applied in Figures 1 – 6.
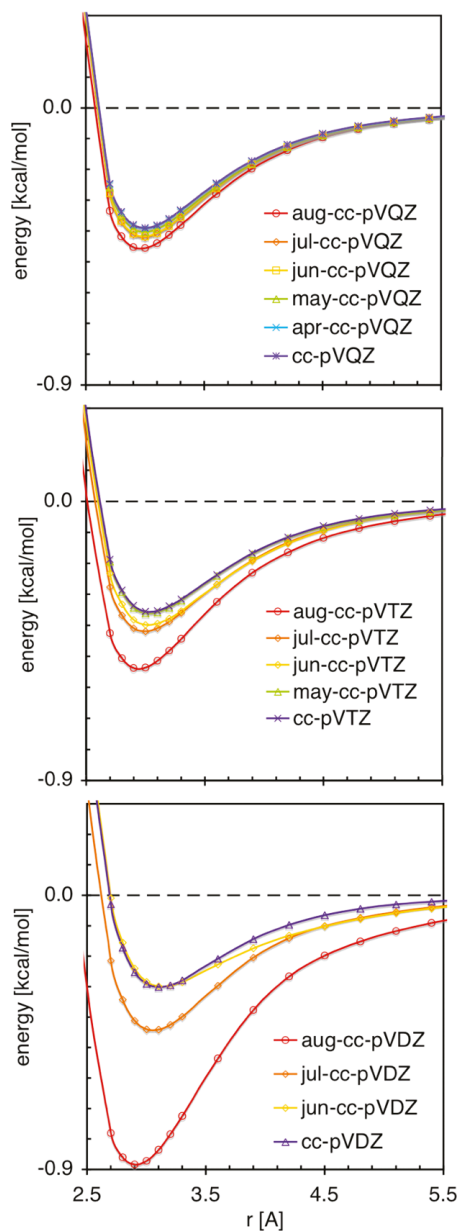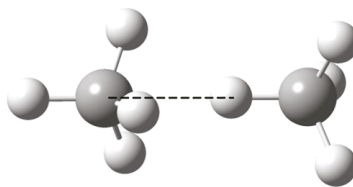
Figure 2. CCSD(T) interaction energy (in kcal/mol) for CH_4 dimer relative to the energy of two CH_4 molecules at infinite separation for quadruple-, triple-, and double-zeta basis sets. The abscissa r is the distance between the C and H atoms as indicated by dashed line (---) in the figure. The structures have C_{3v} symmetry.
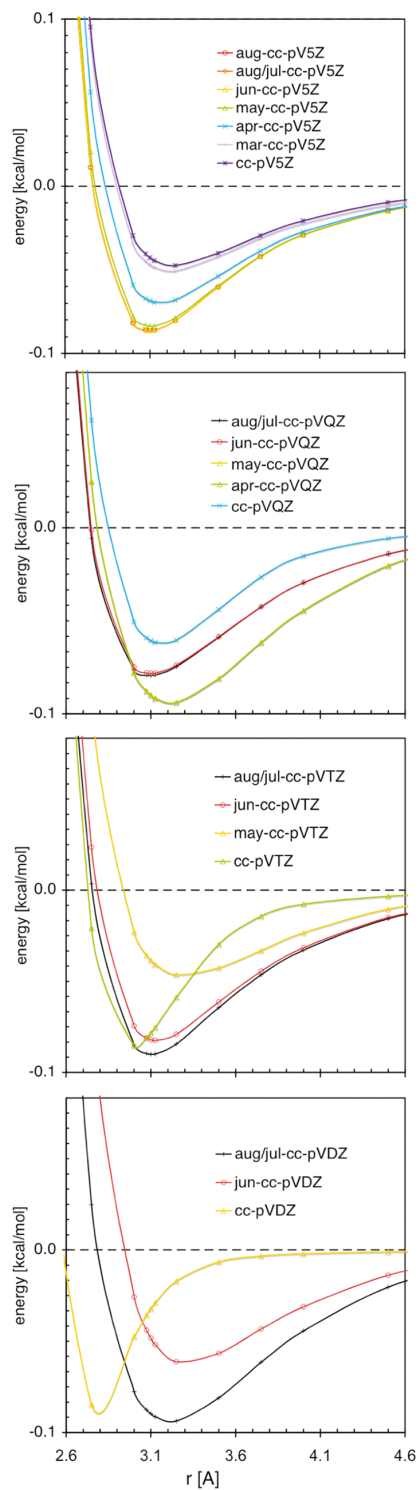
Figure 3. CCSD(T) interaction energy (in kcal/mol) for $(H_2O)_2$ relative to the energy of H_2O molecules at infinite separation for quadruple-, triple-, and double-zeta basis sets. The abscissa r is the distance between the O atoms as indicated by dashed line (---) in the figure.
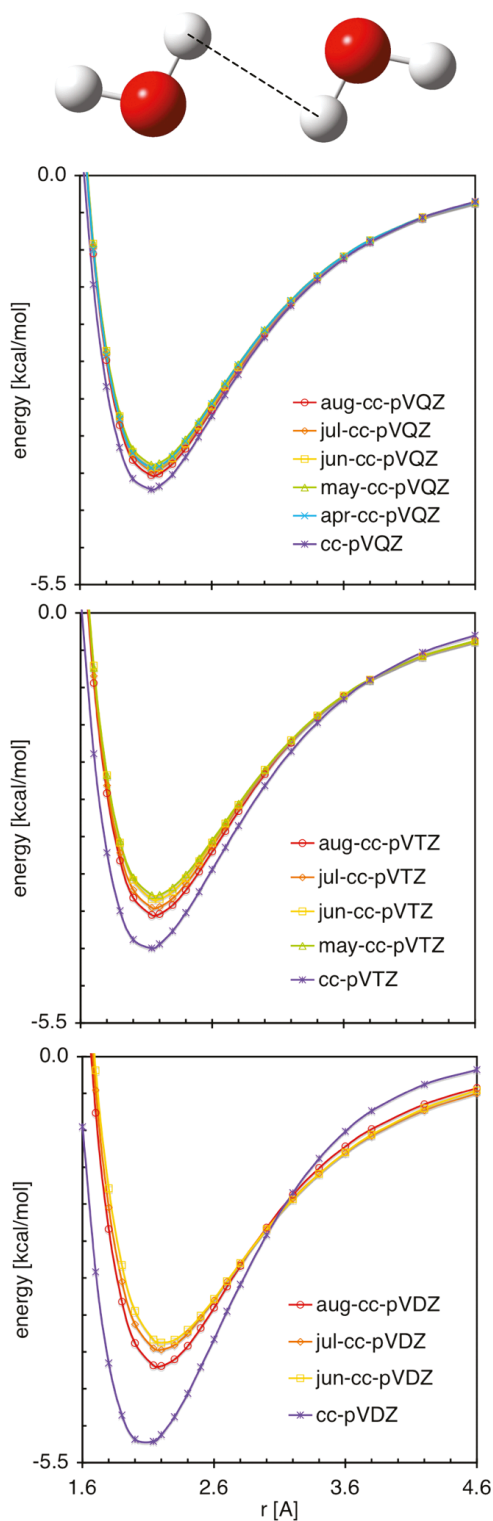
Figure 4. CCSD(T) interaction energy (in kcal/mol) for $(H_2O)_2$ relative to the energy of $(H_2O)_2$ molecules at infinite separation for triple-zeta basis sets. The abscissa r is the distance between two H atoms as indicated by dashed line (---) in the figure.
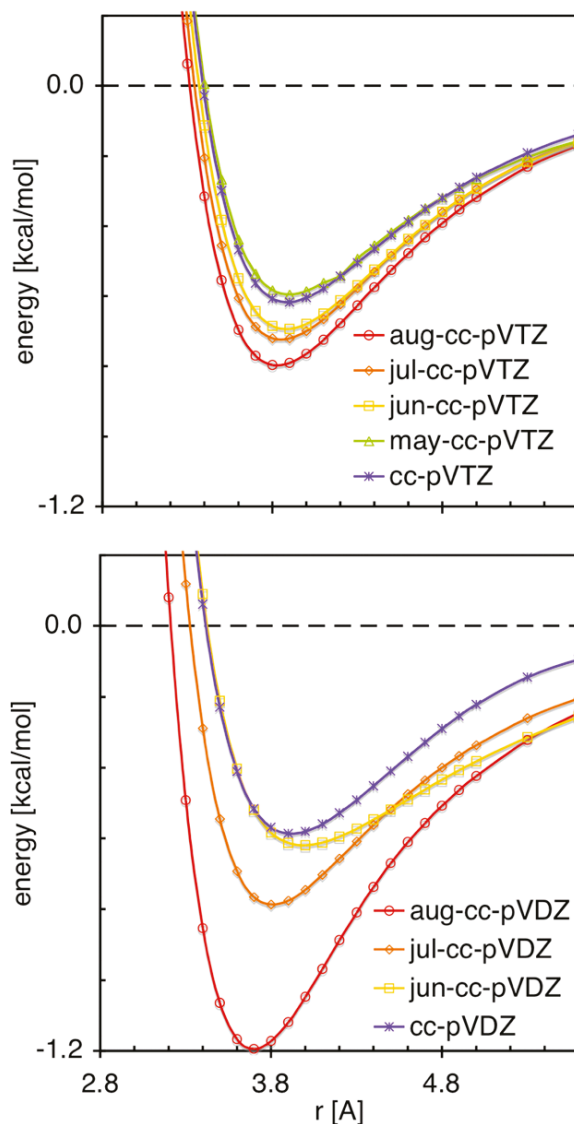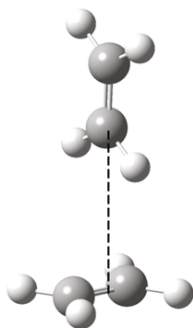
Figure 5. CCSD(T) interaction energy (in kcal/mol) for $(C_2H_4)_2$ relative to the energy of C_2H_4 molecules at infinite separation. The abscissa *r* is the distance indicated by dashed line (---) in the figure.
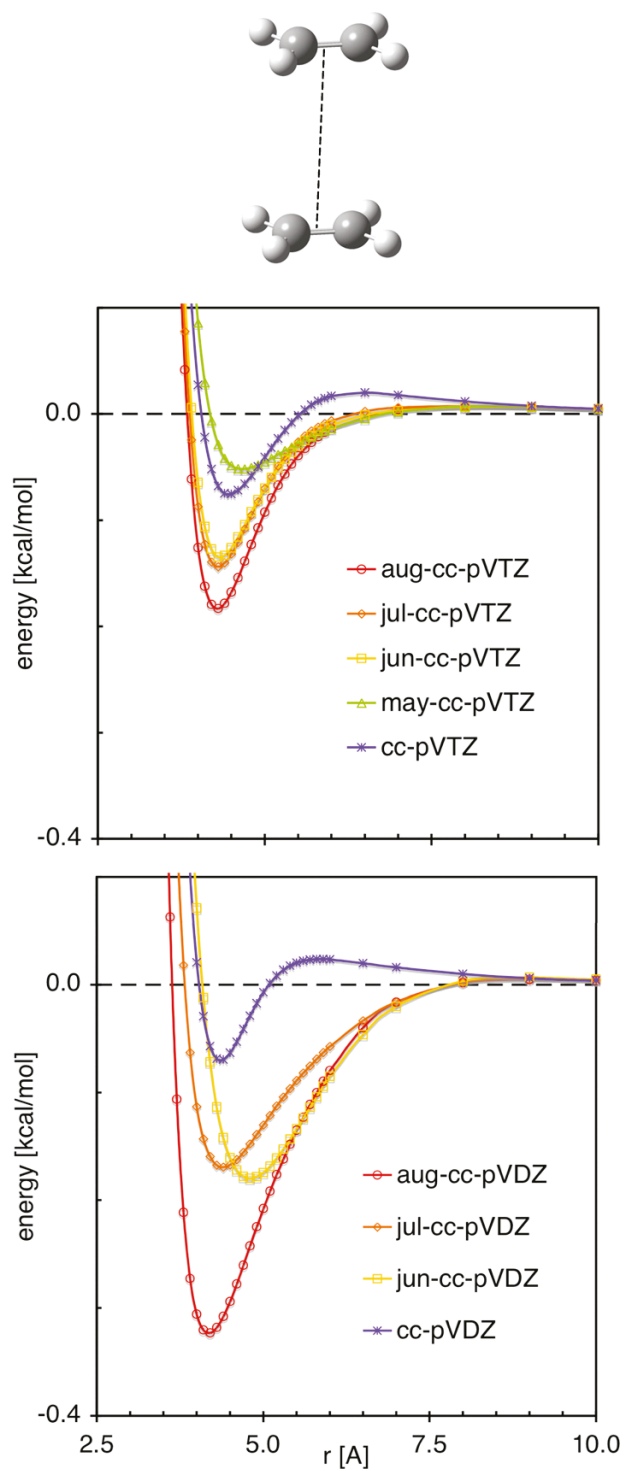
Figure 6. CCSD(T) interaction energy (in kcal/mol) for $(C_2H_4)_2$ relative to the energy of C_2H_4 molecules at infinite separation. The abscissa *r* is the distance indicated by dashed line (---) in the figure.

Chapter 5. What is the Most Efficient Way of Approaching the Complete Basis Set Limit of Wave Function Methods for Thermochemistry

Ewa Papajak and Donald G. Truhlar*
*Department of Chemistry and Minnesota Supercomputing Institute, University of Minnesota,
Minneapolis, MN 55455-0431 USA*

As electronic structure methods are being used to obtain quantitatively accurate thermochemical data and barrier heights for increasingly larger molecules, the choice of an efficient basis set is becoming more critical. However, the optimum strategy for achieving basis set convergence can depend on the way that electron correlation is treated and can take advantage of flexibility in the order in which basis functions are added. Here we study several approaches for estimating accurate thermodynamic data from electronic structure calculations. First and second, we evaluate methods of estimating the basis set limit of explicitly correlated second order Møller-Plesset theory and of explicitly correlated coupled cluster theory with single and double excitations and a quasiperturbative treatment of connected triple excitations by using explicitly correlated basis functions (in the F12a implementation) along with valence, polarization, and diffuse one-electron basis functions. Third, we test the scheme of adding a higher-order correction to MP2 results (sometimes called MP2/CBS + ΔCCSD(T)). Finally, we re-evaluate the basis set requirements of these methods in light of a comparison to Weizmann-3.2 and Weizmann-4 results.

I. INTRODUCTION

Accurate evaluation of energies of reaction and chemical reaction barrier heights is important for calculating the thermodynamics and kinetics of chemical processes. Coupled cluster calculations of these quantities based on increasingly larger basis sets are

widely used in the literature, where they are used both for comparison with the experimental results and as benchmark values for evaluation or parametrization of less computationally demanding methods. In particular, the coupled cluster method with singles, doubles, and quasiperturbative connected triples, CCSD(T),[1] is often said to be "the gold standard of quantum chemistry" and is often accurate to 1 kcal/mol or better when a complete enough basis set is used. However it is also computationally demanding for moderate-sized and large systems. For this reason it has become popular to *estimate* the complete-basis-set (CBS) limit of CCSD(T) calculations rather than calculate it directly.

There are several methods in common use for obtaining CCSD(T)/CBS limits. The first method, which will be called the straight method, involves carrying out CCSD(T) results with larger and larger basis sets until the results converge. The efficiency of this approach can be greatly improved by the use of basis functions that depend explicitly on the interelectronic distances (R12, F12, F12a, and F12b methods).[2–21]

The second method, which will be called extrapolation, is similar to the straight method, but one does not actually carry out a calculation with a nearly complete basis set; instead one extrapolates to the limit from two or three calculations with smaller but systematically increasing basis sets. In the light of recent developments and the impressive efficiency of the explicitly correlated methods, extrapolation without explicit correlation is becoming of only historical interest, since similar accuracy can be achieved with R12,[22–24] and F12a[11,12,25] or F12b[11,12,25] methods in a single step.[26]

The third method will be called the dual-level method. In it one first writes the CCSD(T)/CBS energy as

$$E_{CCSD(T)}^{CBS} = E_{MP2}^{CBS} + \Delta E^{CBS} \tag{1}$$

where E_{MP2}^{CBS} is the CBS limit of the energy calculated by second-order Møller–Plesset perturbation theory (MP2),[27] and

$$\Delta E_{CCSD(T)}^{CBS} = E_{CCSD(T)}^{CBS} - E_{MP2}^{CBS} \tag{2}$$

is the coupled cluster correction. Then we recognize, that, as has been pointed out and explained in various contexts,[28–31,43] E_{MP2} converges much more slowly with respect to basis set size than does ΔE. The first step in using eq 1 is to estimate E_{MP2}^{CBS}. The second step is to estimate the CCSD(T) correction by calculating it with larger and larger basis set until ΔE converges. One can use smaller basis sets for step 2 than for step 1.

$$\Delta E_{CCSD(T)}^{CBS} \approx E_{CCSD(T)}^{FBS} - E_{MP2}^{FBS} \tag{3}$$

where FBS denotes the finite basis set used to calculate ΔE. One could also use extrapolation for one or both terms of eq. 1.

Approaches similar to eqs 1–3 have been used in a variety of additive schemes of greater complexity, where multiple correction terms are involved. The Gaussian-n approach by Pople, Curtiss, Raghavachari, and coworkers[32–35] was the first popular example of such a scheme. Works of Hobza use similar strategy, but without following the precise scheme of G-n methods. Focal point analysis of Allen and coworkers[36,37] and multicoefficient correlation methods (MCCMs)[38–40] by our group are based on a similar idea and may also be considered to be elaborations of the older SEC[41] and SAC[42] schemes. Employing sequences of basis sets and extending them until convergence is attained may be also viewed as special cases of the focal point method.[43,44] The complete basis set (CBS) methods[45,46] of Petersson and coworkers involve more detailed analyses of the asymptotic convergence of the correlation energy but may be considered to be foundational papers supporting all the future developments.

In employing the straight and dual-level methods, one usually employs a sequence of correlation-consistent (cc) basis sets (although MCCMs have been shown to be often more efficient with other basis sets[47]). Correlation consistent basis sets by Dunning and coworkers (including cc-pVnZ,[48–52] and cc-pV(n+d)Z,[53]) have the advantage that they have been designed to converge to the complete basis set limit systematically, thereby in principle allowing extrapolation to the limit from much smaller basis sets. Originally, they have been augmented with large and gradually increasing sets of diffuse functions to accompany increasing degrees of decontraction of the valence space n (aug-cc-pVnZ,[32–36,54,55] and aug-cc-pV(n+d)Z[37]). It has been shown previously that in cases where diffuse functions are needed, partial augmentation of Dunning's basis sets is a more efficient

approach than the originally suggested fully augmented approach.[56–61] It also leads to fewer SCF convergence problems. Partial augmentation of cc-pVnZ basis sets leads to jul-cc-pVnZ, jun-cc-pVnZ, may-cc-pVnZ, …, etc. basis sets, where "jul-" indicates a full "aug" set of diffuse functions on heavy atoms, but no augmentation on hydrogen atoms, and the "jun", "may", "apr", … etc. basis sets (so called seasonal basis sets) are the same as "jul" minus successive subshells of higher-angular-momentum diffuse functions on heavy atoms.[43,45]

Rather than actually employing a sequence of basis sets, it is also very common to use only one basis set that, based on experience, is expected to be nearly complete. Clearly this is more convenient. Based on experience accumulated to date, many workers choose the aug-cc-pVTZ, cc-pVQZ, or aug-cc-pVQZ basis sets or extrapolation schemes involving these sets without further testing. *However, to provide guidance it is useful to have available systematic studies of which basis sets are large enough to yield results within given tolerances of the CBS limit. This is a key goal of the present study.*

Great efficiency in approaching the complete basis set limit can be attained by using explicitly correlated basis function, as in the R12, F12, F12a, and F12b schemes. The combination of F12 explicitly correlated basis functions with, e. g., jun-cc one-electron basis functions is expected to be a powerful approach to reach the CBS limit of MP2, and the analogous F12a scheme is known to be a powerful approach to reach the CCSD(T)/CBS limit.

At this point, we insert a note on nomenclature. The basis sets considered here do not include core correlation or core polarization functions, thus they converge to what might best be called the valence CBS limit. But it is very common in practical applications in the literature (almost universal) to call this the CBS limit, so we will use the shorter "CBS limit", but the reader should keep this in mind. Core correlation contributions can be estimated,[62,63] but that is beyond our present scope. Although core correlation and core polarization effects will be included in our best estimates (see below), our goal here is to test the widely employed methods that do not include core correlation or core polarization.

In the present article we therefore address the following questions:

(1) *What is the most efficient one-electron basis set from among the cc, aug-cc, and seasonal sequences for using the F12 scheme to reach the MP2-F12/CBS limit within various tolerances by the straight approach?*

In order to answer this question, we use MP2-F12/CBS results as our benchmark values. It is understood that, even with an infinite basis set, MP2 theory results carry large errors and so the purpose of this first query is to establish which basis sets efficiently approximate MP2-F12/CBS barrier height and reaction energy values, not how to calculate the most accurate values of these properties. As illustrated by eqs 1–3, MP2-F12/CBS results near to the CBS limit can then be used together with higher-order corrections in order to obtain accurate data.

(2) *What is the most efficient one-electron basis set from among the cc, aug-cc, and seasonal sequences for using the F12a scheme to reach the CCSD(T)/CBS limit within various tolerances by the straight approach?*

(3) *What are the most efficient one-electron basis set pairs to employ in MP2-F12 and CCSD(T)-F12a calculations to for dual-level calculations employing eq 3?*

In order to address questions (2) and (3), we use CCSD(T)/CBS results as our benchmark values. We should keep in mind though that CCSD(T) is not an exact theory. It is widely appreciated that decreasing a source of error in a computational method reaches a point of diminishing returns when that source of error is reduced to the point where it is no longer dominant. For example, if CCSD(T)/CBS has a typical error of 0.4 kcal/mol, one expects to get more accurate results with a basis set with a typical incompleteness error of 0.5 kcal/mol than with a basis set with a typical incompleteness error of 1.0 kcal/mol. However, increasing the basis set to reduce basis set errors from 0.3 kcal/mol to 0.15 kcal/mol is hardly warranted since the error can only decrease below ~0.4 kcal/mol by cancellation of errors. This brings us to the fourth question:

(4) *At what basis set size do CCSD(T) and dual-level calculations stop becoming more accurate on average?*

To answer question (4) we compare CCSD(T) and dual-level calculations with various sizes of basis sets to the most accurate data available for the quantities studied here – Weizmann-4 (W4)[64], Weizmann-3.2 (W3.2), and CCSDT(2)$_Q$/CBS+CV+R

calculations (where CV denotes core-valence correlation and R denotes relativistic corrections) – rather than to CCSD(T)/CBS calculations, which are relevant to questions (2) and (3). We note that W4 calculations have 95% confidence interval of 0.16 kcal/mol for thermochemical data.[48] Thus it is seldom called for to get closer than 0.16 kcal/mol to the CBS limit. Note also that W4 corresponds approximately to CCSDTQ5/CBSD+CV+R+DBOC, where DBOC denotes the diagonal Born-Oppenheimer correction, and W3.2 corresponds approximately to CCSDT(Q)/CBS+CV+R+DBOC.

II. COMPUTATIONAL DETAILS

In this article, we evaluate methods based on their predictions of the forward and reverse barrier heights and the energy of reaction for the following 16 reactions:

• *radical hydrogen transfer:*

$$HO_2 \cdot + CH_3OH \rightarrow H_2O_2 + \cdot CH_2OH \tag{R1}$$

$$HO_2 \cdot + CH_3OH \rightarrow H_2O_2 + CH_3O \cdot \tag{R2}$$

$$\cdot CH_3 + CH_3OH \rightarrow CH_4 + \cdot CH_2OH \tag{R3}$$

$$\cdot CH_3 + CH_3OH \rightarrow CH_4 + CH_3O \cdot \tag{R4}$$

$$\cdot OH + CH_4 \rightarrow \cdot CH_3 + H_2O \tag{R5}$$

$$H \cdot + OH \rightarrow O \, (^3P) + H_2 \tag{R6}$$

$$H \cdot + H_2S \rightarrow H_2 + HS \tag{R7}$$

-heavy atom transfer:

$$H \cdot + N_2O \rightarrow \cdot OH + N_2 \tag{R8}$$

$$H \cdot + HCl \rightarrow H \cdot + HCl \tag{R9}$$

$$\cdot CH_3 + FCl \rightarrow CH_3F + Cl \cdot \tag{R10}$$

-nucleophilic substitution:

$$Cl^- + CH_3Cl \rightarrow Cl^- + CH_3Cl \tag{R11}$$

$$F^- + CH_3Cl \rightarrow Cl^- + CH_3F \tag{R12}$$

$$OH^- + CH_3F \rightarrow F^- + CH_3OH \tag{R13}$$

-unimolecular and association reactions:

$$H \cdot + N_2 \rightarrow HN_2 \cdot \tag{R14}$$

$$H \cdot + C_2H_4 \rightarrow \cdot CH_2CH_3 \qquad\qquad (R15)$$

$$HCN \rightarrow HNC \qquad\qquad (R16)$$

Reactions R5 – R16 constitute DBH24/08 database that has been developed as a statistically representative set of reactions for barrier height calculations and has been used before for evaluation computational methods for calculation of barrier heights.[65] To that set we add hydrogen abstraction reactions from methanol (reactions R1 – R4) since they can be representative of larger and more complicated organic systems.[66]

Our goal is to draw general conclusions about basis set strategy, and we believe that the best way to do this is to average the results of basis set convergence tests over multiple data. The full set of 48 data is called the thermochemical kinetics 48 (TK48) database; it contains the energy of reaction and the forward and reverse barrier heights of the sixteen reactions listed above.

In order to test sensitivity of the basis set errors to the diffuse basis sets, TK48 is divided into ATK9 and NTK39. ATK9 includes barriers and reaction energies of the reactions that involve anions (R11–R13), which are expected to be more sensitive to the saturation of the diffuse space. NTK39 consists of analogous data for the neutral reactions (R1–R10 and R14–R16), which should be less sensitive to augmentation.

III. METHODS

Barrier height and reaction energy calculations were performed using the *MolPro 2009*[67] program. All calculations in the present tests are single-point energy calculations at pre-optimized geometries. For the stationary points of the reactions R5 through R16, we used QCISD/MG3 geometries from previous studies.[68,69] Geometries for the methanol reactions (R1 – R4) were M06-2X/MG3S calculations taken from reference 50. In all cases we include spin-orbit contributions for all open-shell systems by the same procedure as used previously.[70] For the single-point calculations of the open-shell systems we used the restricted formalism for all levels; in particular, we used RHF, RMP2-F12,[71] and RRCCSD(T)-F12a in this study.

IV. COST ESTIMATES

One cannot adequately judge the relative success of various computational methods without considering cost, which we express here in units of CPU time. Unfortunately, precise comparisons of CPU times are impossible, because such times depend on the software, the computer, the load on that computer, the way that the method is coded, the number of processors used, and many other variables. Nevertheless the trends in computer time are meaningful if one does not interpret them too finely; for example, it is usually meaningful if two computer times (on the same computer with the same number of processors) vary by more than a factor of two on the same computer.

In order to quantify the relative cost of the methods that we test in this study, we have calculated single-point energies of the same molecule, on the same machine (Chinook at the Pacific Northwest National Laboratory), using the same number (8) of processors, same amount of memory (437 MW), and same software (MolPro 2009) for all the combinations of levels and basis sets. For this purpose phosphinomethanol was chosen, because it has a reasonable ratio of first period : second period : third period atoms (6 : 2 : 1), and it is affordable even for very complete calculations. Unfortunately, it is rather small so the times for expensive methods have not reached their asymptotic scaling regime.

We report CPU time of these single-point calculations as relative to the most inexpensive (HF/cc-pV(D+d)Z) calculation in Table I.

V. RESULTS AND DISCUSSION

Tables II–V summarize mean unsigned basis-set errors of all the single- and dual-level methods for barrier heights and reaction energies using various basis sets. First, we examine convergence of MP2-F12 with respect to the basis set in order to address *question 1*. Table II lists mean unsigned errors for the barrier heights and reaction energies in TK48. As benchmark values we used MP2-F12/jul-cc-pV(5+d)Z results. Since the sensitivity of the neutral and anionic reactions to diffuse functions is different, we list separately the errors on the reactions containing anions (in ATK9 column) and neutral reactants only (NTK39 column). The table shows that triple-ζ basis sets provide

results already converged to within ~0.1 kcal/mol to the quintuple-ζ values. For very highly-converged MP2/CBS estimates, may-cc-pV(Q+d)Z can be employed; however jun-cc-pV(T+d)Z already converges all three columns to better than the 0.16 kcal/mol limit mentioned earlier. Notice that may-cc-pV(T+d)Z is about a factor of two more accurate than the only slightly less expensive (see MPW2-F12 column of Table I) aug-cc-pV(D+d)Z basis set.

In order to address ***question 2***, in table III we list deviations of the CCSD(T) theory with various basis sets from the near-CBS values (CCSD(T)-F12/apr-cc-pV(5+d)Z). As in MP2, triple- and quadruple-ζ results are within 0.2 and 0.1 kcal/mol of the quintuple zeta results. Beyond the jun-cc-pV(T+d)Z basis set, improvement is very slow compared to the rapid increase in the costs (which can be seen in the last column of table I). For example, consecutive basis sets, despite nearly doubling the cost, improve the average errors by hundredths of kcal/mol or not at all. The jul-cc-pV(T+d)Z basis set achieve better than 0.16 kcal/mol for all three columns of Table III with a cost lower than aug-cc-pV(T+d)Z by a factor of 2.0, and jun-cc-pV(T+d)Z does about as well with a cost lowering of a factor of 2.9. The may-cc-pV(T+d)Z basis set raises the basis set errors to only 0.19 – 0.24 kcal/mol with a cost lowering (again relative to aug-) of a factor of 3.7, whereas the error is very large when diffuse basis functions are totally omitted. These comparisons provide a dramatic illustration of the efficiency of seasonal basis sets.

In order to answer ***question (3)***, we need to balance errors introduced by the two terms of eqn. 1. We denote the basis used for the first term as X and that for the second step as Y. When choosing X, the demand on the accuracy should depend on the uncertainty introduced by the level of theory (and the basis set used) at which higher order corrections are going to be calculated. However, as mentioned above, triple-ζ basis sets provide results already converged to within ~0.1 kcal/mol of CBS values, which, as we will show below, is more than an order of magnitude lower than the error of the MP2/CBS result itself. For the very accurate dual-level schemes, may-cc-pV(Q+d)Z would be recommended, but as discussed in conjunction with question 1, that will usually be overkill. To find the best strategy we will explicitly consider combinations of X and Y.

The suitable choice of balanced pairs of basis sets X and Y can be made using tables II and IV. By comparing these tables pair X = may-cc-pV(Q+d)Z, Y = jun-cc-pV(T+d)Z is well balanced for very high accuracy (0.10 kcal/mol) since with the basis set combination the MP2-F12 and ΔCCSD(T) terms would be introducing comparable cost and error. For the somewhat more realistic goal of better than 0.16 kcal/mol, Tables II and IV show that Y = may-cc-pV(T+d)Z is a good candidate to match with X = jun-cc-pV(T+d)Z, and Y = jul-cc-pV(D+d)Z or even jun-cc-pV(D+d)Z appear to be good candidates to match with X = may-cc-pV(T+d)Z.

A more direct evaluation of the combinations may be based on table V which lists basis set errors of results obtained using eq 3 as determined by comparing to the near-CCSD(T) limit. For example, in order to evaluate the combination of X = jun-T with Y = jun-D (where we have now introduced an obvious shorthand notation), consider that CCSD(T)/jun-DZ by itself has an error of 0.68 kcal/mol (table III). However, when we combine it with additional MP2-F12/jun-T calculation, the error goes down to 0.27 kcal/mol (table V). In this case, the dual method is twice as expensive as the CCSD(T) component calculation. If we wanted to use only CCSD(T) (straight approach), similar improvement could only be achieved if the basis set was increased to may-T, which is roughly 8 times more expensive than the CCSD(T)/jun-D calculation.

To put the orders of errors discussed here in perspective and address *question (4)*, one should consider the error of the CCSD(T)/CBS and dual-level approaches. Therefore, we have compared the CCSD(T) results to the best available estimates. For the reactions R6–R16 we used Weizmann 3.2 and 4 results of Martin and coworkers as the best available estimates[72]. Since our calculations do include spin-orbit corrections, but do not include DBOC corrections, the analogous Weizmann values were used from reference 72. In the case of reactions R1–R4, CCSDT(2)$_Q$/CBS[73] benchmarks[66] were used. These CBS values were obtained[66] by extrapolation from cc-pVTZ and cc-pVQZ basis sets and have been shown to agree well with experiment. They also include spin-orbit and relativistic corrections. The errors of MP2-F12 and CCSD(T)-F12a are summarized in table IV. We see that on average CCSD(T)/5Z results differ from these benchmarks by 0.44 kcal/mol, which is much higher than the hundredths of kcal/mol in table VI. This

means that in the search for the most accurate results, beyond the CCSD(T) with triple-ζ basis sets, additional computational resources should be invested in higher-order correlation and relativistic effects rather than increasing basis set.

Similarly, when we evaluate the dual-level results using the errors with respect to the best available estimates in table VII, we see that the improvement achieved by going from X =jun-D and Y = jun-T (within 0.27 kcal/mol of CCSD(T)/CBS) to X = may-Q and Y = jun-T (0.09 kcal/mol) is very insignificant in comparison with the total errors.

In fact, there seems to be no statistically significant advantage in going beyond X : Y = jun-T : may-T or X : Y = jun-T : aug-D, each of which has a mean basis set error of only 0.47 kcal/mol. In fact X : Y = aug-D : jun-D has a mean basis set error only slightly larger at 0.52 kcal/mol.

In order to compare the efficiency of the single and dual methods on a quality vs. cost basis, tables VIII–X list selected methods (MP2, CCSD(T), and dual-level) in order of increasing cost. Table VIII is based on the full database (TK48), and tables IX and X correspond respectively to the subsets of reactions involving anions (ATK9) and those involving only neutral species (NK39). To avoid clutter with basis sets that do not offer significant improvement, the tables list only methods that offer improvement, with respect to less expensive methods, both in deviations relative to the CCSD(T)/CBS limit (second last column) and in deviations with respect to the best estimate.[74] In other words, some rows were deleted so that *both* of the final two columns are monotonically decreasing functions as the cost goes up — the idea being that only if both criteria improve is it worth increasing the cost. Methods that do not appear in at least on of tables VIII–X can hardly be recommended in the final analysis.

The most astonishing conclusion concerning the errors with respect to the best estimate (these errors are listed in the last columns of tables VIII–X) is that beyond CCSD(T)-F12a with aug-D basis set the errors on the barrier heights and reaction energies are dominated by the limitations of the method, not the basis set. For example increasing the basis set from aug-D to may-Q decreases the CCSD(T)/CBS error of 0.32 kcal/mol to 0.04 kcal/mol, but the BE error remains exactly the same (0.45 kcal/mol), so this method is not included in Table VIII. Based on such considerations, we recommend

103

that further improvements should involve full triple excitations, perturbative quadruple excitations, core correlation, and relativistic effects before increasing the basis set to or beyond quadruple-ζ basis set.

VI. CONCLUSIONS

- MP2 results for barrier height and reaction energy should only be used with higher-order correlation corrections. MP2-F12 converges much faster with respect to the basis set than do calculations without explicitly correlated functions. Augmentation is necessary to get good results, but this can be done efficiently with partial augmentation (seasonal basis sets) without needing full augmentation (aug-).

- CCSD(T)-F12a convergence with respect to the best estimates is nonexistent beyond partially augmented triple zeta basis sets, because the error is dominated by other effects. Therefore core correlations, relativistic effects, and higher-order electron correlation are recommended before proceeding to quadruple-ζ basis sets.

- For the dual level approach we found two reasonably efficient basis set combinations X = may-Q : jun-T and jun-T : jun-D. If we consider reliability vs. cost these combinations of MP2-F12 and CCSD(T)-F12 with two different basis sets perform better as compared to just CCSD(T), but the difference in error at a similar cost is not remarkable.

- In order to achieve chemical accuracy (< 1 kcal/mol) it is important that all contributions to the error be converged with respect to the basis set.[75] However, the present results show that although estimating CBS limit values is interesting from the theoretical point of view, it often does not reduce errors with respect to the best estimates. Therefore when the highest accuracy of the results is a goal, improving the largest source of error would be a more efficient approach. In the case of WFT methods it means including more effects (higher-order correlation corrections, correlation of the outer core electrons, and relativistic effects) at a reasonable size of the basis set as opposed to including CBS-level contributions at the CCSD(T) valence correlation level.

TABLE I. The cost of HF, MP2-F12, and CCSD(T)-F12a single point calculation (CPU time) of $CH_2(OH)PH_2$ molecule normalized to the smallest calculation (HF/cc-pVDZ).

	HF[a]	MP2-F12	CCSD(T)-F12a
aug-cc-pV(Q+d)Z	1090	4300	68900
jul-cc-pV(Q+d)Z	491	2250	34900
jun-cc-pV(Q+d)Z	386	2010	27000
may-cc-pV(Q+d)Z	278	1840	21500
apr-cc-pV(Q+d)Z	237	1740	18600
cc-pV(Q+d)Z	205	1660	16000
aug-cc-pV(T+d)Z	90	1070	7740
jul-cc-pV(T+d)Z	45	532	3840
jun-cc-pV(T+d)Z	27	469	2710
may-cc-pV(T+d)Z	21	430	2110
cc-pV(T+d)Z	16	400	1710
aug-cc-pV(D+d)Z	4.8	322	775
jul-cc-pV(D+d)Z	2.7	180	396
jun-cc-pV(D+d)Z	1.5	160	285
cc-pV(D+d)Z	1.0	146	223

[a] an average of two HF runs: for the MP2-F12 and CCSD(T)-F12a calculation.

TABLE II. Mean unsigned errors (in kcal/mol) on MP2 barrier heights and reaction energies using MP2-F12/jul-cc-pV(5+d)Z values as a benchmark.

	TK48	ATK9	NTK39
apr-cc-pV(5+d)Z	0.01	0.02	0.01
aug-cc-pV(Q+d)Z	0.03	0.03	0.03
jul-cc-pV(Q+d)Z	0.04	0.05	0.04
jun-cc-pV(Q+d)Z	0.03	0.04	0.03
may-cc-pV(Q+d)Z	0.04	0.04	0.04
apr-cc-pV(Q+d)Z	0.07	0.14	0.05
cc-pV(Q+d)Z	0.69	2.74	0.22
aug-cc-pV(T+d)Z	0.07	0.09	0.07
jul-cc-pV(T+d)Z	0.12	0.11	0.13
jun-cc-pV(T+d)Z	0.13	0.15	0.12
may-cc-pV(T+d)Z	0.18	0.26	0.16
cc-pV(T+d)Z	1.19	3.92	0.56
aug-cc-pV(D+d)Z	0.32	0.36	0.31
jul-cc-pV(D+d)Z	0.46	0.37	0.48
jun-cc-pV(D+d)Z	0.70	1.30	0.56
cc-pV(D+d)Z	2.45	6.25	1.58

TABLE III. Mean unsigned errors (in kcal/mol) on CCSD(T)-F12a barrier heights and reaction energies as compared to the CCSD(T)-F12a/apr-cc-pV(5+d)Z results.

	TK48	ATK9	NTK39
aug-cc-pV(Q+d)Z	0.05	0.05	0.05
jul-cc-pV(Q+d)Z	0.05	0.07	0.05
jun-cc-pV(Q+d)Z	0.04	0.03	0.04
may-cc-pV(Q+d)Z	0.04	0.02	0.04
apr-cc-pV(Q+d)Z	0.09	0.18	0.07
cc-pV(Q+d)Z	0.63	2.46	0.21
aug-cc-pV(T+d)Z	0.14	0.20	0.12
jul-cc-pV(T+d)Z	0.15	0.15	0.15
jun-cc-pV(T+d)Z	0.14	0.18	0.14
may-cc-pV(T+d)Z	0.20	0.24	0.19
cc-pV(T+d)Z	1.09	3.50	0.54
aug-cc-pV(D+d)Z	0.32	0.45	0.29
jul-cc-pV(D+d)Z	0.45	0.42	0.46
jun-cc-pV(D+d)Z	0.68	1.37	0.52
cc-pV(D+d)Z	2.23	5.79	1.40

TABLE IV. Mean unsigned errors (in kcal/mol) of ΔCCSD(T)-F12a corrections to barrier heights and reaction energies as compared to the CCSD(T)-F12a/apr-cc-pV(5+d)Z values of the corrections.

	TK48	TK9	TK39
aug-cc-pV(Q+d)Z	0.03	0.03	0.03
jul-cc-pV(Q+d)Z	0.03	0.02	0.03
jun-cc-pV(Q+d)Z	0.03	0.03	0.03
may-cc-pV(Q+d)Z	0.03	0.02	0.03
apr-cc-pV(Q+d)Z	0.05	0.06	0.04
cc-pV(Q+d)Z	0.11	0.28	0.07
aug-cc-pV(T+d)Z	0.11	0.15	0.10
jul-cc-pV(T+d)Z	0.10	0.12	0.09
jun-cc-pV(T+d)Z	0.09	0.10	0.09
may-cc-pV(T+d)Z	0.11	0.10	0.12
cc-pV(T+d)Z	0.22	0.47	0.16
aug-cc-pV(D+d)Z	0.23	0.22	0.23
jul-cc-pV(D+d)Z	0.25	0.22	0.25
jun-cc-pV(D+d)Z	0.28	0.24	0.28
cc-pV(D+d)Z	0.44	0.68	0.38

TABLE V. Mean unsigned errors[a] on data in NK48 database calculated by the dual-level method using eq 3.

X	jun-Q	may-Q	apr-Q	aug-T	jul-T	jun-T	may-T	T	aug-D
Y									
jun-Q	—	—	—	—	—	—	—	—	—
may-Q	0.04	—	—	—	—	—	—	—	—
apr-Q	0.06	0.06	—	—	—	—	—	—	—
Q	0.11	0.11	0.10	—	—	—	—	—	—
aug-T	0.11	0.11	0.13	—	—	—	—	—	—
jul-T	0.10	0.10	0.12	0.12	—	—	—	—	—
jun-T	0.09	0.09	0.12	0.11	0.13	—	—	—	—
may-T	0.11	0.11	0.13	0.11	0.13	0.14	—	—	—
T	0.21	0.21	0.20	0.20	0.20	0.22	0.25	—	—
aug-D	0.22	0.23	0.25	0.24	0.24	0.25	0.29	1.18	—
jul-D	0.24	0.25	0.26	0.25	0.26	0.28	0.30	1.17	0.34
jun-D	0.27	0.27	0.28	0.28	0.27	0.27	0.29	1.16	0.31
D	0.42	0.43	0.41	0.42	0.41	0.41	0.40	1.01	0.49

a Mean unsigned errors (kcal/mol) as compared to the CCSD(T)/apr-5 values.

TABLE VI. Mean unsigned errors (in kcal/mol) on MP2-F12 and CCSD(T)-F12a barrier heights and reaction energies as compared to the best available estimates: W3.2, W4, and CCSDT(2)$_Q$/CBS.

	MP2-F12			CCSD(T)-F12a		
	TK48	ATK9	NTK39	TK48	ATK9	NTK39
apr-5	2.85	0.89	3.30	0.44	0.11	0.52
aug-Q	2.84	0.87	3.30	0.43	0.16	0.49
jul-Q	2.84	0.84	3.31	0.44	0.18	0.50
jun-Q	2.85	0.87	3.30	0.44	0.14	0.51
may-Q	2.85	0.88	3.30	0.45	0.13	0.53
apr-Q	2.83	0.76	3.31	0.50	0.29	0.55
Q	3.12	2.32	3.30	0.89	2.57	0.50
aug-T	2.83	0.87	3.28	0.41	0.18	0.46
jul-T	2.84	0.81	3.30	0.41	0.14	0.48
jun-T	2.86	0.92	3.31	0.44	0.12	0.51
may-T	2.88	0.98	3.32	0.50	0.18	0.58
T	3.36	3.56	3.31	1.14	3.62	0.57
aug-D	2.88	0.98	3.32	0.45	0.39	0.47
jul-D	2.92	0.94	3.38	0.52	0.38	0.56
jun-D	3.23	2.15	3.48	0.79	1.26	0.68
D	3.99	6.03	3.52	2.19	5.90	1.33

TABLE VII. Mean unsigned errors[a] on data in NK48 database calculated by the dual-level method using eq 3.

X	jun-Q	may-Q	apr-Q	aug-T	jul-T	jun-T	may-T	T	aug-D
Y:									
jun-Q	–	–	–	–	–	–	–	–	–
may-Q	0.45	–	–	–	–	–	–	–	–
apr-Q	0.47	0.47	–	–	–	–	–	–	–
Q	0.49	0.50	0.49	–	–	–	–	–	–
aug-T	0.43	0.43	0.45	–	–	–	–	–	–
jul-T	0.44	0.45	0.47	0.42	–	–	–	–	–
jun-T	0.46	0.46	0.48	0.43	0.43	–	–	–	–
may-T	0.50	0.50	0.52	0.47	0.46	0.47	–	–	–
T	0.57	0.58	0.57	0.55	0.53	0.55	0.57	–	–
aug-D	0.49	0.49	0.51	0.47	0.46	0.47	0.51	1.21	–
jul-D	0.52	0.53	0.54	0.51	0.50	0.53	0.56	1.20	0.53
jun-D	0.54	0.54	0.55	0.53	0.50	0.52	0.54	1.18	0.52
D	0.70	0.70	0.69	0.69	0.66	0.67	0.67	1.12	0.69

[a] Mean unsigned errors (kcal/mol) as compared to the Weizmann and CCSDT(2)Q/CBS limit values.

110

TABLE VIII. Mean unsigned errors on 48 data (TK48) in kcal/mol with respect to coupled cluster limit benchmarks and the best available estimates in the order of the increasing cost.

Method[a]				cost	CC/CBS Error[b]	BE Error[c]
MP2-F12		CCSD(T)-F12a				
diffuse	ζ	diffuse	ζ			
–	D	–	–	38	3.84	3.99
jun	D	–	–	42	3.07	3.23
jul	D	–	–	47	2.77	2.92
–	–	–	D	58	2.23	2.19
–	–	jun	D	74	0.68	0.79
–	–	jul	D	104	0.45	0.52
		aug	D	203	0.32	0.45
–	–	jun	T	711	0.14	0.44
jul	T	jun	T	860	0.13	0.43
aug	T	jul	T	1309	0.12	0.42

[a] for single-level calculations only one basis set is listed; for dual-level calculations using eq 3, first two columns (MP2-F12 basis set) list X bases, while third and fourth (CCSD(T)-F12a basis set) list Y bases used. In all cases basis sets with tight d functions on third row atoms (+d) were used.

[b] error with respect to the CCSD(T)-F12a/apr-cc-pV(5+d)Z values.

[c] error with respect to the Best Estimate: W3.2 and W4 values from reference 72 for DBH24 data and CCSDT(2)$_Q$/CBS (T,Q-extrapolation) values[66] for the methanol reactions.

TABLE IX. Mean unsigned errors on ATK9 data in kcal/mol with respect to coupled cluster limit and the best available estimates in the order of the increasing cost.

Method[a]				cost	CC/CBS Error[b]	BE Error[c]
MP2-F12		CCSD(T)-F12a				
diffuse	ζ	diffuse	ζ			
–	D	–	–	38	5.92	6.03
jun	D	–	–	42	2.26	2.15
jul	D	–	–	47	1.05	0.94
–	–	jul	D	104	0.42	0.38
may	T	jun	D	191	0.35	0.30
jun	T	jun	D	203	0.26	0.21
–	–	may	T	553	0.24	0.18
jun	T	may	T	682	0.16	0.12
may	Q	may	T	1103	0.08	0.10

[a] for single-level calculations only one basis set is listed; for dual-level calculations using eq 3, first two columns (MP2-F12 basis set) list X bases, while third and fourth (CCSD(T)-F12a basis set) list Y bases used. In all cases basis sets with tight d functions on third row atoms (+d) were used.

[b] error with respect to the CCSD(T)-F12/apr-cc-pV(5+d)Z values.

[c] error with respect to the Best Estimate: W3.2 and W4 values from reference 72 for DBH24 data and CCSDT(2)$_Q$/CBS (T,Q-extrapolation) values[66] for the methanol reactions.

TABLE X. Mean unsigned errors on NTK39 data in kcal/mol with respect to coupled cluster limit and Weizmann results in order of increasing cost.

Method[a]				cost	CC/CBS Error[b]	BE Error[c]
MP2-F12		CCSD(T)-F12a				
diffuse	ζ	diffuse	ζ			
–	D	–	–	38	3.36	3.52
jun	D	–	–	42	3.26	3.48
jul	D	–	–	47	3.17	3.38
–	–	–	D	58	1.40	1.33
–	–	jun	D	74	0.52	0.68
–	–	jul	D	104	0.46	0.56
aug	D	jun	D	159	0.29	0.55
jun	T	aug	D	332	0.24	0.53
jun	T	may	T	682	0.14	0.51
–	–	aug	T	2036	0.12	0.46
may	Q	aug	T	2586	0.10	0.50
–	–	aug	Q	18190	0.05	0.49

[a] for single-level calculations only one basis set is listed; for dual-level calculations using eq 3, first two columns (MP2-F12 basis set) list X bases, while third and fourth (CCSD(T)-F12 basis set) list Y bases used. In all cases basis sets with tight d functions on third row atoms (+d) were used.

[b] error with respect to the CCSD(T)-F12a/apr-cc-pV(5+d)Z values.

[c] error with respect to the Best Estimate: W3.2 and W4 values from reference 72 for DBH24 data and CCSDT(2)$_Q$/CBS (T,Q-extrapolation) values[66] for the methanol reactions.

[1] K. Raghavachari, G. W. Trucks, J. A. Pople, and M. Head-Gordon, Chem. Phys. Lett. **157**, 479 (1989).

[2] W. Kutzelnigg, Theor Chim Acta **68**, 445 (1985).

[3] W. Klopper and W. Kutzelnigg, Chem. Phys. Lett. **134**, 17 (1987).

[4] W. Kutzelnigg and W. Klopper, J. Chem. Phys. **1991**, *94*, (1985).

[5] W. Klopper and C. C. M. Samson, J. Chem. Phys. **116**, 6397 (2002).

[6] F. R. Manby, J. Chem. Phys. **119**, 4607 (2003).

[7] S. Ten-no and F. R. Manby, J. Chem. Phys. **119**, 5358 (2003).

[8] S. Ten-no, Chem. Phys. Lett. **398**, 56 (2004).

[9] W. Klopper J. Chem. Phys. **120**, 10890 (2004).

[10] S. Ten-no, J. Chem. Phys. **121**, 117 (2004).

[11] A. J. May and F. R. Manby, J. Chem. Phys. **121**, 4479 (2004).

[12] E. F. Valeev, Chem. Phys. Lett. **395**, 190 (2004).

[13] E. F. Valeev and C. L. Jansen, Chem. Phys. Lett. **121**, 1214 (2004).

[14] D. P. Tew and W. Klopper, J. Chem. Phys. **123**, 074101 (2005).

[15] E. F. Valeev, Chem. Phys. Lett. **418**, 333 (2006).

[16] F. R. Manby, H.-J. Werner, T. B. Adler, and A. J. May, J. Chem. Phys. **124**, 094103 (2006).

[17] H. -J. Werner, T. B. Adler and F. R. Manby, J. Chem. Phys. **126**, 164102 (2007).

[18] J. Noga, S. Kedžuch, and J. Šimunek, J. Chem. Phys. **127**, 034106 (2007).

[19] T. B. Adler, G. Knizia, and H. -J. Werner, J. Chem. Phys. **127**, 221106 (2007).

[20] G. Knizia, T. B. Adler, and H. –J. Werner, J. Chem. Phys. **130**, 054104 (2009).

[21] T. D. Crawford, C. D. Sherrill, E. F. Valeev, J. T. Fermann, R. A. King, M. L. Leininger, S. T. Brown, C. L. Janssen, E. T. Seidl, J. P. Kenny, and W. D. Allen, J. Comp. Chem. **28**, 1610 (2007).

[22] H. Fliegl, W. Klopper, and C. Hättig, J. Chem. Phys. **122**, 084107 (2005).

[23] H. Fliegl, C. Hättig, W. Klopper, Int. J. Quantum Chem. **106**, 2306 (2006).

[24] D. P. Tew and W. Klopper, J. Phys. Chem. A, **111**, 11242 (2007).

[25] S. Kedžuch, M. Milko, and J. Noga, Int. J. Quantum Chem. **105**, 929 (2005).

[26] J. Noga, P. Valiron, and W. Klopper, J. Chem. Phys. **115**, 2022 (2001).

[27] C. Møller and M. S. Plesset, Phys. Rev. **46**, 618 (1934).

[28] P. Hobza and J. Sponer, J. Am. Chem. Soc. **124**, 11802 (2002).

[29] P. Jurecka, J. Sponer, J. Cerny, and P. Hobza, Phys. Chem. Chem. Phys. **8**, 1985 (2006).

[30] G. A. Petersson and M. Braunstein, J. Chem. Phys. **83**, 5129 (1985).

[31] A. L. L. East and W. D. Allen, J. Chem. Phys. **99**, 4638 (1993).

[32] L. A. Curtiss, K. Raghavachari, G. W. Trucks, and J. A. Pople, J. Chem. Phys. **94**, 7221 (1991).

[33] L. A. Curtiss, K. Raghavachari, P. C. Redfern, V. Rassolov, and J. A. Pople, J. Chem. Phys. **109**, 7764 (1998).

[34] L. A. Curtiss, P. C. Redfern, K. Raghavachari, and J. A. Pople, J. Chem. Phys. **114**, 108 (2001).

[35] L. A. Curtiss and K. Raghavachari, ACS Symp. Ser **677**, 176 (1998)

[36] A. L. L. East and W. D. Allen, J. Chem. Phys. **99**, 4638 (1993).

[37] A. G. Császár, W. D. Allen, and H. F. Schaefer, J. Chem. Phys. **108**, 9751 (1998).

[38] P. L. Fast, J. C. Corchado, M. L. Sanchez, and D. G. Truhlar, J. Phys. Chem. A **103**, 5129 (1999).

[39] B. J. Lynch and D. G. Truhlar, J. Phys. Chem. A **107**, 3898 (2003).

[40] T.-H. Li, H.-R. Chen, and W. -P. Hu Chem. Phys. Lett. **412**, 430 (2005).

[41] F. B. Brown and D. G. Truhlar, Chem. Phys. Lett. **117**, 307 (1985).

[42] M. S. Gordon and D. G. Truhlar, J. Amer. Chem. Soc. **108**, 5412 (1986).

[43] M. S. Schuurman, S. R. Muir, W. D. Allen, and H. F. Schaefer J. Chem. Phys. **120**, 11586 (2004).

[44] R. A. King, W. D. Allen, B. Ma, and H. F. Schaefer III, Faraday Discuss. **110**, 23 (1998).

[45] M. R. Nyden and G. A. Petersson, J. Chem. Phys. **75**, 1843 (1981).

[46] G. A. Petersson, ACS Symp. Ser. **677**, 237 (1998).

[47] B. J. Lynch and D. G. Truhlar, J. Phys. Chem A **107**, 3898 (2003).

[48] D. E. Woon and T. H. Dunning Jr., J. Chem. Phys. **100**, 2975 (1994).

[49] D. E. Woon, T. H. Dunning Jr., J. Chem. Phys. **98**, 1358 (1993).

[50] J. Koput, K. A. Peterson, J. Phys. Chem. A **106**, 9595 (2002).

[51] N. B. Balabanov, K. A. Peterson, J. Chem. Phys. **2005**, 123, 064107.

[52] Wilson, A. K.; Woon, D.E.; Peterson, K.A.; Dunning, T.H. Jr. J. Chem. Phys. **110**, 7667 (1999).

[53] T. H. Dunning Jr., K. A. Peterson, and A. K. Wilson, J. Chem. Phys. **114**, 9244 (2001).

[54] T. H. Dunning Jr., J. Chem. Phys. **90**, 1007 (1989).

[55] R. A. Kendall, T. H. Dunning, Jr.; Harrison, R.J. J. Chem. Phys. **96**, 6796 (1992).

[56] E. Papajak, H. R. Leverentz, J. Zheng, and D. G. Truhlar, J. Chem. Theory Comput. **5**, 1197 (2009); **5**, 3330 (2009).

[57] E. Papajak and D. G. Truhlar, J. Chem. Theory Comput. **6**, 597 (2010).

[58] J. Zheng, X. Xu, and D. G. Truhlar, Theor. Chem. Acc. **128**, 295 (2011).

[59] E. Papajak and D. G. Truhlar, J. Chem. Theory Comput. **7**, 10 (2011).

[60] J. R. Cheeseman and M. J. Frisch, J. Chem. Theory Comput. **7**, 3323 (2011).

[61] E. Papajak, J. Zheng, X. Xu, H. R. Leverentz, and D. G. Truhlar, J. Chem. Theory Comput. **7**, 3027 (2011).

[62] J. M. L. Martin, A. Sundermann, P. L. Fast, and D. G. Truhlar, Journal of Chemical Physics **113**, 1348 (2000).

[63] K. A. Peterson and T. H. Dunning Jr., 2002 J. Chem. Phys. **117**, 10548 (2002).

[64] A. Karton, E. Rabinovitch, J. M. L. Martin, and B. Ruscic, J. Chem. Phys. **125**, 144108 (2006).

[65] J. Zheng, Y. Zhao, and D. G. Truhlar, J. Chem. Theory Comput. **5**, 808 (2009).

[66] J. Alecu and D. G. Truhlar, J. Phys. Chem. A **115**, 2811 (2011).

[67] H.-J. Werner, P. J. Knowles, F. R. Manby, M. Schütz, P. Celani, G. Knizia, T. Korona, R. Lindh, A. Mitrushenkov, G. Rauhut, T. B. Adler, R. D. Amos, A. Bernhardsson, A. Berning, D. L. Cooper, M. J. O. Deegan, A. J. Dobbyn, F. Eckert, E. Goll, C. Hampel, A. Hesselmann, G. Hetzer, T. Hrenar, G. Jansen, C. Köppl, Y. Liu, A. W. Lloyd, R. A. Mata, A. J. May, S. J. McNicholas, W. Meyer, M. E. Mura, A. Nicklaß, P. Palmieri, K. Pflüger, R. Pitzer, M. Reiher, T. Shiozaki, H. Stoll, A. J. Stone, R. Tarroni, T.

Thorsteinsson, M. Wang, and A. Wolf, *Molpro* computer program, version 2010.1 (University of Birmingham, Birmingham, 2010).

[68] Y. Zhao, N. González-García, and D. G. Truhlar, J. Phys. Chem. A **109**, 2012 (2005).

[69] B. J. Lynch, Y. Zhao, and D. G. Truhlar, J. Phys. Chem. A **107**, 1384 (2003).

[70] B. J. Lynch, Y. Zhao, and D. G. Truhlar, J. Phys. Chem. A **109**, 1643 (2005).

[71] P. J. Knowles, J. S. Andrews, R. D. Amos, N. C. Handy, and J. A. Pople, Chem. Phys. Lett. **186**, 130 (1991).

[72] A. Karton, A. Tarnopolsky, J.-, F. Lamere, G. C. Schatz, and J. M. L. Martin, J. Phys. Chem. A **112**, 12868 (2008).

[73] S. Hirata, P.-D. Fan, A. A. Auer, M. Nooijen, and P. Piecuch, J. Chem. Phys. **121**, 12197 (2004).

[74] See Supplementary Material Document for the full versions of tables VIII–X, including all single- and dual-level methods tested in this study.

[75] K. A. Peterson, D. Feller, and D. A. Dixon, Theor. Chem. Acc. **131**, 1079 (2012).

Part II.   Multi-Structural Statistical Thermodynamics and Kinetics

We[1] have recently proposed an efficient method (MS-T) for accounting for anharmonicity effects, nonseparability of rotational, vibrational, and torsional motions, and conformational complexity in calculations of the partition functions of large molecules. Part II of this thesis consists of five articles. The first of them[1] (chapter 6) presents the theory behind the MS-T method. The articles that follow describe applications of this method to thermodynamics of molecules[2] (chapter 7) and radicals[3] (chapter 8) important in combustion research. They show how critical the statistical model employed for computation of the partition function is to the accuracy of the thermodynamical data. In further research on kinetics[4,5] (chapters 9 and 10) we have also found that multi-structural and anharmonicity effects appreciably affect the accuracy of calculations of thermodynamics of molecules and radicals, and they significantly change the reaction rate coefficients predicted by variational transition state theory.

(1) J. Zheng, T. Yu, E. Papajak, I.M. Alecu, S.L. Mielke, and D.G. Truhlar, Phys. Chem. Chem. Phys. **13**, 10885 (2011).

(2) P. Seal, E. Papajak, T. Yu, and D.G. Truhlar, J. Chem. Phys.**136**, 034306 (2012).

(3) E. Papajak, P. Seal, and D.G. Truhlar, accepted for publication in J. Chem. Phys. on July 8, 2012.

(4) P. Seal, E. Papajak, and D.G. Truhlar, J. Phys. Chem. Lett. **3**, 264 (2012).

(5) X. Xu, E. Papajak, J. Zheng, and D.G. Truhlar, Phys. Chem. Chem. Phys. **14**, 4204 (2012).

Chapter 6.   Practical Methods for Including Torsional Anharmonicity in Thermochemical Calculations on Complex Molecules: The Internal-Coordinate Multi-Structural Approximation

Jingjing Zheng, Tao Yu, Ewa Papajak, I. M. Alecu, Steven L. Mielke, and Donald G. Truhlar

Department of Chemistry and Supercomputing Institute, University of Minnesota, Minneapolis, MN 55455-0431

Many methods for correcting harmonic partition functions for the presence of torsional motions employ some form of one-dimensional torsional treatment to replace the harmonic contribution of a specific normal mode. However, torsions are often strongly coupled to other degrees of freedom, especially other torsions and low-frequency bending motions, and this coupling can make assigning torsions to specific normal modes problematic. Here, we present a new class of methods, called multi-structural (MS) methods, that circumvents the need for such assignments by instead adjusting the harmonic results by torsional correction factors that are determined using internal coordinates. We present three versions of the MS method: (i) MS-AS based on including all structures (AS), i.e., all conformers generated by internal rotations; (ii) MS-ASCB based on all structures augmented with explicit conformational barrier (CB) information, i.e., including explicit calculations of all barrier heights for internal-rotation barriers between the conformers; and (iii) MS-RS based on including all conformers generated from a reference structure (RS) by independent torsions. In the MS-AS scheme, one has two options for obtaining the local periodicity parameters, one based on consideration of the nearly separable limit and one based on strongly coupled torsions. The latter involves assigning the local periodicities on the basis of Voronoi volumes. The methods are illustrated with calculations for ethanol, 1-butanol, and 1-pentyl radical as well as two one-dimensional torsional potentials. The MS-AS method is particularly interesting

119

because it does not require any information about conformational barrier or about the paths that connect the various structures.

I. Introduction

Torsional motion constitutes an especially challenging form of vibrational anharmonicity for which the harmonic approximation is often highly inaccurate. Furthermore, the presence of multiple torsional degrees of freedom often results in many low-energy conformers that contribute significantly to the partition function. Feynman path integral methods[1,2] provide an accurate and straightforward way to include torsional effects in quantum mechanical partition functions, and while they have already provided important benchmark results for small systems,[3-5] more affordable methods are needed for many applications involving complex molecules.

A variety of separable approximations are available[6-20] that replace the harmonic contribution of specific normal modes by solutions of one-dimensional (1-D) torsional treatments, and nonseparable treatments have also been advanced.[9, 14, 16, 21-25] In many instances torsions are strongly mixed with other torsions and/or with other low-frequency motions such as bending, and in such cases one cannot identify them with specific normal modes. We divide the nonseparable treatments into two classes, those that do not assume a one-to-one correspondence between torsions and individual normal modes, and those that do; we call these mixed torsion models and normal mode substitution models. The only widely discussed model that allows mixed torsions is the Pitzer–Gwinn approximation.[21] This requires evaluating the full-dimensional classical configuration integral,[26] which—although less expensive than a path integral—is still too expensive for routine use on large molecules because it requires either extensive Monte Carlo sampling by direct dynamics (electronic structure calculations on the fly) or the careful fitting of an analytic nonseparable potential function. Reduced-dimensional path integrals[23, 27-29] and classical configuration integrals covering only torsional degrees of freedom[9, 16] have also been considered but are more expensive than the methods to be proposed here. On the other hand, methods employing normal mode substitution[7-10, 12-14, 22] are not general enough for our purpose.

In this article we will consider a family of new torsional approximations that employ internal coordinate correction factors to the harmonic treatment that avoid not only the separability assumption but also the restriction associated with assigning torsions to specific normal modes.

In many cases, the thermochemical properties of a chemical substance can be reasonably estimated by using the group additivity method — the assumption that the thermodynamic properties of a given species can be obtained by summing the contributions from each group comprising that species. The most widely employed version of group additivity was formulated by Benson,[30] and established general group additivity values through a two-step process involving first compartmentalizing similar molecules with known thermodynamic properties into their constituent groups — where a group is defined as a polyvalent atom and all of its ligands — and then deriving the contribution to various thermodynamic properties due to each group through multivariable linear regression fits to the available experimental data.[30] The original group additivity values established by Benson for stable molecules were later adapted to several classes of free radical species by O'Neal and Benson,[31, 32] and were subsequently updated by Cohen[33] to account for new experimental and theoretical findings. More recently, Lay et al.[34] developed an alternative technique for estimating bulk thermodynamic properties, often with improved accuracy, from a single group called the H atom bond increment (HBI) group. We used these various group additivity techniques to estimate the entropies of the species studied in this work and compare them to our methods.

For the convenience of the reader, we use a consistent set of acronyms for frequently repeated phrases and methods. A glossary of these acronyms is provided in Appendix A.

II. Theory
II. A. Overview

The most direct consequence of internal rotation is the occurrence of multiple conformational minima. A conventional approach[35, 36] to calculating partition functions in

such cases is to use the harmonic approximation for the minimum-energy structure and to replace contributions from certain normal modes with a hindered rotor treatment by using the tables of Pitzer and Gwinn[21] or an analytic hindered rotor[7, 10], or free rotor approximation. A somewhat more complicated case occurs when a torsion is unsymmetrical (or isotopically substituted) so that the minima encountered along the torsion are distinguishable. Then, if one assumes that the vibrational modes are separable, the partition function for each of the unsymmetrical torsional motions has contributions from each distinguishable conformer. However the treatment of torsions as separable can be very unrealistic.[12, 37-41] A better approach is to start with a list of distinguishable structures (i.e., distinguishable conformers) and to sum their contributions, including at least torsional anharmonicity. We call such methods multi-structural (MS) approximations, and these are the subjects of the present paper.

II. B. MS-AS method with nearly separable torsions

II. B. 1. *Theory*. Let Q denote a multidimensional partition function and q denote the partition function for a single degree of freedom. In the convention used in this article, all partition functions have their zero of energy at their local minimum (rather than being normalized to unity at 0 K). We will consider J distinguishable structures, i.e., conformational minima, $j = 1, 2, \ldots, J$, and we will include anharmonicity in several torsions labeled $\tau = 1, 2, \ldots, t$; we note that t has the same value for all structures. Let the energies of the minima be U_j where U_1 has a value of zero, and all other U_j are positive. We divide the t torsions into two types: nearly separable (NS) and strong coupled (SC). For NS torsions, we may define a parameter $M_{j,\tau}$ to be the total number of minima, whether distinguishable or not, along torsional coordinate τ of structure j (each of these minima correspond to another structure).

In our initial presentation we shall restrict attention to the special case that all the torsions are nearly separable and we will further assume that the $M_{j,\tau}$ minima may be reasonably approximated as being evenly distributed along the torsional coordinate τ. In Section II.B.2 we will present an alternative derivation of the MS-AS approximation based on a different rationale for assigning the $M_{j,\tau}$ parameters and that may be useful

in more general contexts, including some cases of strong coupling between the torsions. The alternative derivation explicitly accounts for cases where the minima are not approximately evenly distributed along a given torsional coordinate. In section II.C we will present a variation of the multi-structural method that utilizes explicit barrier information instead of the $M_{j,\tau}$ parameters, and in section II.D we will consider a variation of the method designed to treat the most challenging cases of strong coupling wherein parameters are obtained by Voronoi tessellation.[42-44] In general we can use a hybrid scheme for obtaining $M_{j,\tau}$; for example, we use the notation $NS:SC = n:m$ to denote that n torsions are treated as nearly separable and m torsions are treated as strong coupled. In this language, the present section (II.B.1) is devoted to the case $t:0$.

We will denote the torsional symmetry numbers as σ_τ and the number of distinguishable minima for torsional coordinate τ of structure j as $P_{j,\tau}$ where

$$P_{j,\tau} = M_{j,\tau}/\sigma_\tau. \tag{1}$$

The symmetry numbers σ_τ can be determined by treating the least symmetric of the two rotating fragments as a fixed frame and counting the number of identical structures obtained when the more symmetrical top is rotated from 0 to 360 degrees and relaxed (for example, the symmetry numbers for methanol, nitromethane, and 1,2 dichloroethane are 3, 3, and 1, respectively). Once all the structures are found, the number, $P_{j,\tau}$, of unique structures connected to structure j (including itself) by internal rotation τ may often be identified by counting the structures that have similar torsion angles for all other internal rotations; when strong torsional coupling exists additional considerations may be necessary as will be discussed further below. Attempts have been made[12, 45] to fully automate the assignment of the $P_{j,\tau}$ (or equivalently the $M_{j,\tau}$), but such approaches are beyond the scope of the present study.

In general, the internal moment of inertia, $I_{j,\tau}$, associated with rotation about a specific axis τ is a continuous function of geometry, but we will approximate it as a constant within the domain of each specific structure and will assign values $I_{j,\tau}$ that are calculated for rotation about the bond axis associated with torsion τ at the minimum-energy geometry of structure j using the method of Pitzer.[46] (In previous articles,[13, 14] we

denoted Pitzer's method for calculating the internal moment of inertia for an internal rotation as the curvilinear method, abbreviated C.) Pitzer[46] has pointed out that the geometry dependence of the moments of inertia approximately compensates for the change in the product of the vibrational frequencies as a function of the internal rotation angle. This justifies holding the internal moments of inertia fixed at their values at the minimum-energy geometry when the vibrational motions are approximated by a classical harmonic treatment; however, we include quantum effects, and we use this approximation even when the classical harmonic approximation is not valid.

Pitzer's method[46] for calculating internal moments of inertia assumes that all molecular fragments that undergo internal rotation are attached to a unique fixed frame; for cases with more than one torsion the scheme is approximate unless a determinant-based approach is used to fully account for intermode coupling. A more-general treatment is available in the work of Kilpatrick and Pitzer[47] that accounts for the coupling between torsional motions and removes the requirement of a unique fixed frame. In the following, when we refer to Pitzer moments we are referring to moments calculated in the absence of intermode coupling; approaches that include intermode coupling have only rarely been employed in earlier work, but here, in addition to the uncoupled Pitzer moments, we also employ the general treatment of Kilpatrick and Pitzer.[47] The Kilpatrick and Pitzer[47] treatment leads to the calculation of a kinetic energy matrix for internal rotation denoted as $\mathbf{D}$ (alternatively one may work with the kinetic energy matrix $\mathbf{S}$ associated with overall rotation and internal rotation) which may be diagonalized to yield moments associated with linear combinations of coupled torsions. The moments of Pitzer[46] are the diagonal elements of the $\mathbf{D}$ matrix and in the limit of weak torsional coupling (where $\mathbf{D}$ is strongly diagonally dominant) torsional motion is well represented by rotation about a single bond. Our torsional approximation scheme begins by approximating torsional motions as being uncoupled within the domain of a specific structure so we begin by employing the approximate Pitzer moments. However, in the high-temperature limit the partition function scales as the square root of the determinant of $\mathbf{D}$, and we gradually switch to the Kilpatrick–Pitzer coupled moments as the temperature is increased.

The torsional coordinate associated with the Pitzer internal moments of inertia describes the rotation of a rigid top against a fixed frame, and various considerations have been used to define physical torsion coordinates for flexible systems.[48-50] In our internal-coordinate treatment, we approximate the torsional coordinate by a single dihedral angle. Thus, our torsional force constants and other results have a small dependence on the choice of coordinate system, i.e., on which dihedral angle we choose. One consequence of using internal coordinate torsion angles is that subtle deviations from expected symmetries may be observed; for example, methyl groups may deviate very slightly from the expected three-fold symmetry. In such cases we use values of $M_{j,\tau}$, $P_{j,\tau}$, and σ_τ that would have been obtained from the more symmetrical structures. All of the methods presented here assume that the domains of different conformers do not significantly overlap; in cases where slight symmetry lowering leads to strongly overlapping structures it may be best to include only one of the strongly overlapping structures and treat this conformer using a symmetry number that would have been appropriate in the absence of symmetry lowering.

If there is only one conformer and we neglect coupling between electronic, vibrational, and rotational degrees of freedom, the total partition function of a system can be written as

$$Q_{\text{total}} = Q_{\text{trans}}Q_{\text{elec}}Q_{\text{rot}} \prod_{m=1}^{F} q_{\text{vib},m} \qquad (2a)$$

where Q_{trans} is the translational partition function, Q_{elec} is the electronic partition function, Q_{rot} is the rotational partition function, $F = 3N - 6$ for a nonlinear molecule (where N is number of atoms in the system), and $q_{\text{vib},m}$ is the vibrational partition function of mode m. However, we do not use that simplification; instead, we write

$$Q_{\text{total}} = Q_{\text{trans}}Q_{\text{elec}}Q_{\text{con-rovib}} \qquad (2b)$$

where $Q_{\text{con-rovib}}$ is the conformational-rovibrational partition function. In this article, the translational and electronic partition functions are not discussed. We mainly focus on the vibrational partition function, but eqn (2b) also allows for a conformational average and for the change of rotational partition function from structure to structure. Thus, we do not

assume that rotation is separable in an overall sense because the rotational partition function depends on the structure.

Special consideration is needed with considering symmetry numbers for systems with internal rotations. The overall torsional symmetry number associated with the torsion-only degrees of freedom is

$$\sigma_{\text{torsion}} = \prod_{\tau=1}^{t} \sigma_\tau \tag{3}$$

and is the same for all structures. However, the structures can include cases both with and without rotational symmetry so that rotational symmetry number $\sigma_{\text{rot},j}$ depends on j. It should be realized that the rotational symmetry elements that transform symmetrical structures into themselves transform unsymmetrical structures into *other* unsymmetrical structures that appear in the list of the J structures that are distinguishable when only considering torsional symmetry, and therefore $\sigma_{\text{rot},j}$ depends on how these structures are treated. We can make this clear by an example. Consider pentane,[51] which has 11 torsional conformers if we do not consider the two methyl groups; eight of these structures have no rotational symmetry and thus have $\sigma_{\text{rot},j}$ equal to 1, whereas three of them have $\sigma_{\text{rot},j}=2$. Of the eight structures with $\sigma_{\text{rot},j}=1$, only four are distinguishable when rotation is considered because each structure may be transformed into one other structure by an overall rotation. Thus, if all eleven structures are included in the MS-AS partition function calculations each of the rotational partition functions should use a symmetry number of 2. Alternatively, one could include only the seven structures that are distinguishable after considering both rotational and torsional symmetries, in which case the rotational partition functions would use the structure-dependent $\sigma_{\text{rot},j}$ values.

We propose a new family of approximations to be called multi-structural methods. The first member of the family is the MS-AS method in which we include all structures. The conformational-rovibrational partition function is given in the MS-AS method by

$$Q_{\text{con-rovib}}^{\text{MS-AS}} = \sum_{j=1}^{J} Q_{\text{rot},j} \exp\left(-\beta U_j\right) Q_j^{\text{HO}} Z_j \prod_{\tau=1}^{t} f_{j,\tau} \tag{4}$$

126

where $Q_{\text{rot},j}$ is the rotational partition function of structure j (here we use the classical approximation for rotational partition functions, see eqn (B4)), β is $1/k_BT$ where k_B is Boltzmann's constant and T is temperature, Q_j^{HO} is the usual normal-mode harmonic oscillator vibrational partition function calculated at structure j, Z_j is a factor (specified below) designed to ensure that the MS-AS scheme reaches the correct high-T limit (within the parameters of the model), and $f_{j,\tau}$ is an internal-coordinate torsional anharmonicity function that, in conjunction with Z_j, adjusts the harmonic result of structure j for the presence of the torsional motion associated with coordinate τ.

We use MS-HO to denote the partition function calculated without Z_j and $f_{j,\tau}$, that is, with all Z_j and all $f_{j,\tau}$ equal to unity. One can use normal-mode analysis to obtain frequencies to calculate Q_j^{HO}. A key advantage of eqn (4) over the MS-HO approximation is that it includes torsional anharmonicity, but it is not necessary to assign each torsional motion to a specific normal mode. The MS-HO approximation is already an improvement over treatments that include only the lowest-energy conformation, and the importance of including a conformational average when computing enthalpies has recently been emphasized.[36, 52]

We define the torsional correction functions $f_{j,\tau}$ as the ratio of a partition function for some accurate method to treat a given torsion divided by a harmonic partition function for a frequency $\overline{\omega}_{j,\tau}$, where the frequency $\overline{\omega}_{j,\tau}$ is defined as the harmonic frequency obtained using internal coordinates rather than a normal-coordinate frequency. This scheme avoids identifying each torsional mode with a specific normal mode. The internal-coordinate torsional frequency is obtained by

$$\overline{\omega}_{j,\tau} = \sqrt{\frac{k_{j,\tau}}{I_{j,\tau}}} \tag{5}$$

$$k_{j,\tau} \equiv \left.\frac{\partial^2 V}{\partial \phi_\tau^2}\right|_{\phi_\tau = \phi_{\tau,\text{eq.j}}} \tag{6}$$

where $k_{j,\tau}$ is the force constant of a specific torsion τ at structure j, V is the potential energy, and the torsion τ is represented by a dihedral angle ϕ_τ whose equilibrium value is $\phi_{\tau,\mathrm{eq}.j}$.

The internal-coordinate force constants can be calculated either by numerical finite differences or by transforming force constant matrices expressed in Cartesian coordinates into force constant matrices in non-redundant internal coordinates.[53-58] In the numerical finite difference method, one rotates one of the two tops with respect to the other by a small amount and uses central differences to calculate the second derivative from the equilibrium energy and single-point energies of the two slightly distorted geometries. In the transformation method, one has to be careful to select an appropriate set of $3N - 6$ independent internal coordinates. The strategy we employ to select the $3N - 6$ independent internal coordinates is that (i) all bond stretching coordinates are included, (ii) only one dihedral angle is selected for each torsional mode, and (iii) the rest of the coordinates are bond angles and other dihedral angles not related to torsions (e.g., dihedral angles for out-of-plane motion in a ring structure) that are selected while avoiding redundant choices. By using such a set of $3N - 6$ independent internal coordinates, the second partial derivative of V with respect to the dihedral angle is the force constant for this torsion. In this paper, all the torsional force constants are calculated by the transformation method.

The reference Pitzer–Gwinn (RPG) method[14, 21] denotes the use of a one-dimensional Pitzer–Gwinn approximation applied to a reference potential (rather than the true potential as in the Pitzer–Gwinn method) where the reference potential is obtained from limited information. The reference potential was previously taken as[7, 14, 21, 46]

$$V_m = \frac{W_m}{2}\left[1 - \cos(M_m \phi_m)\right] \tag{7}$$

where V_m is the potential of normal mode m, ϕ_m is a torsion coordinate, M_m is the number of minima in mode m, and W_m is a torsional barrier height. If all the torsional barriers do not have the same height, W_m would be an effective or average height. Here we instead use

$$V_{j,\tau} = U_j + \frac{W_{j,\tau}}{2}\left[1 - \cos M_{j,\tau}(\phi_\tau - \phi_{\tau,\text{eq}.j})\right]; \quad \frac{-\pi}{M_{j,\tau}} \le \phi_\tau - \phi_{\tau,\text{eq}.j} \le \frac{\pi}{M_{j,\tau}} \tag{8}$$

where $W_{j,\tau}$ is an effective barrier height associated with structure j. When the RPG method is applied to eqn (8), $f_{j,\tau}$ can be written as

$$f_{j,\tau} = \sigma_\tau \left[\frac{q_{j,\tau}^{\text{RC}}}{q_{j,\tau}^{\text{CHO}}}\right] \tag{9}$$

where $q_{j,\tau}^{\text{CHO}}$ and $q_{j,\tau}^{\text{RC}}$ are the classical harmonic oscillator and reference classical partition functions of the torsion τ for structure j, respectively, given by

$$q_{j,\tau}^{\text{CHO}} = \frac{1}{\hbar\beta\overline{\omega}_{j,\tau}} \tag{10}$$

and[14]

$$q_{j,\tau}^{\text{RC}} = \frac{1}{M_{j,\tau}} q_{j,\tau}^{\text{FR}} \exp(-\beta W_{j,\tau}/2)I_0(\beta W_{j,\tau}/2) \tag{11}$$

where $\hbar$ is Planck's constant divided by 2π, I_0 is a modified Bessel function, and the free rotor (FR) partition function is given by

$$q_{j,\tau}^{\text{FR}} = \frac{\sqrt{2\pi I_{j,\tau}/\beta}}{\hbar\sigma_\tau} \tag{12}$$

Equation (7) assumes that all barriers along a torsional coordinate have the same height W_m or at least may be represented by a single average barrier, and that all of the minima have the same energy, whereas eqn (8) provides the flexibility for each structure to have an independent minimum and barrier height. The $W_{j,\tau}$ can be chosen as the average of the barrier heights on either side of this minimum. However, we next make a simplification so that we do not need to know these barriers. The simplification takes advantage of the fact that for a potential of the form of eqn (8) and a geometry-independent internal moment of inertia, the barrier heights, internal moment of inertia, and the torsional frequency are interrelated by[7, 14]

$$W_{j,\tau} = \frac{2I_{j,\tau}\overline{\omega}_{j,\tau}^2}{M_{j,\tau}^2} \tag{13}$$

Using this relation, eqns (11) and (9) are rewritten as

$$q_{j,\tau}^{\mathrm{RC}} = \frac{1}{M_{j,\tau}} q_{j,\tau}^{\mathrm{FR}} \exp(-\beta I_{j,\tau} \overline{\omega}_{j,\tau}^2 / M_{j,\tau}^2) I_0(\beta I_{j,\tau} \overline{\omega}_{j,\tau}^2 / M_{j,\tau}^2)$$

(14)

and

$$f_{j,\tau} = \frac{\overline{\omega}_{j,\tau} \sqrt{2\pi\beta I_{j,\tau}}}{M_{j,\tau}} \exp(-\beta I_{j,\tau} \overline{\omega}_{j,\tau}^2 / M_{j,\tau}^2) I_0(\beta I_{j,\tau} \overline{\omega}_{j,\tau}^2 / M_{j,\tau}^2)$$

(15a)

Notice that eqn (15a) can be rearranged to

$$f_{j,\tau} = \frac{\sqrt{2\pi\beta k_{j,\tau}}}{M_{j,\tau}} \exp(-\beta k_{j,\tau} / M_{j,\tau}^2) I_0(\beta k_{j,\tau} / M_{j,\tau}^2)$$

(15b)

which shows that $f_{j,\tau}$ is independent of $I_{j,\tau}$. This situation results because both the numerator and denominator of eqn (9) have the same functional dependence on $I_{j,\tau}$. The inclusion of the Z_j factor (discussed next) restores the expected dependence of the partition function on the moments of inertia as the high-T limit is approached. Note also that the modified Bessel function $I_0(x)$ approaches $\dfrac{\exp(x)}{\sqrt{2\pi x}}$ as x approaches infinity; therefore, when the temperature approaches zero, i.e., β approaches infinity, all the $f_{j,\tau}$ become 1, and the MS-AS partition function reduces to the MS-HO partition function. Consequently, the MS-AS and MS-HO methods yield the same zero-point energy (ZPE).

Next we consider two corrections, both introduced via the factor Z_j, which ensure that we reach a correct high-temperature limit. One is to replace the normal-mode partition function in the high-T limit by an internal-coordinate (local-mode[59, 60]) one, and the other is to correct for kinetic energy coupling of the torsions to one another. The factor Z_j is written for this purpose as

$$Z_j = \frac{g_j Q_{\mathrm{rot},j} Q_j^{\mathrm{HO}} + (1 - g_j) Q_j^{\mathrm{imp}}}{Q_{\mathrm{rot},j} Q_j^{\mathrm{HO}}}$$

(16)

where Q_j^{imp} is an improved approximation, $g_j \to 1$ at low T where the effects of rotational-vibrational coupling are minimal, and $g_j \to 0$ at high T. We will approximate Q_j^{imp} as

$$Q_j^{\text{imp}} = Q_{\text{rot},j} Q_j^{\text{HO}} Z_j^{\text{int}} Z_j^{\text{coup}} \tag{17}$$

where the Z_j^{int} replace the normal-mode vibrational partition functions in the high-T

limit by internal-coordinate ones, and Z_j^{coup} replaces the uncoupled moments of inertia

for individual torsions by values that account for their coupling.

Before considering the approximations used for g_j, Z_j^{int}, and Z_j^{coup} we need to

consider the high-T limit of the denominator of eqn (16):

$$\lim_{T \to \infty} Q_{\text{rot},j} Q_j^{\text{HO}} = \frac{\sqrt{\pi}}{\sigma_{\text{rot},j}} \left(\frac{2}{\hbar^2 \beta} \right)^{3/2} \left| \det \mathbf{I}_j^{\text{rot}} \right|^{1/2} \left(\frac{1}{\hbar \beta} \right)^F \prod_{m=1}^{F} \omega_{j,m}^{-1} \tag{18}$$

where $\mathbf{I}_j^{\text{rot}}$ is the 3×3 moment of inertia matrix for overall rotation of structure j and

$\omega_{m,j}$ is a normal-mode frequency. We do not factor the vibrational part of eqn (18) into

a stretch-bend factor and a torsion factor because we avoid assigning torsions to specific

normal modes.

At high-temperature the torsions become more separable from the other vibrations

and it is reasonable to replace the product of normal-mode frequencies in eqn (18) by the

product of the $\overline{\omega}_{j,\tau}$ torsional frequencies and $F - t$ stretch-bend frequencies $\overline{\overline{\omega}}_{j,\overline{m}}$ in the

space orthogonal to the torsions. Note that $\overline{\overline{m}}$ is a generalized normal-mode label that is

not based on normal modes. In particular we take

$$Z_j^{\text{int}} = \frac{\displaystyle\prod_{\overline{\overline{m}}=1}^{F-t} \overline{\overline{\omega}}_{j,\overline{\overline{m}}}^{-1} \prod_{\tau=1}^{t} \overline{\omega}_{j,\tau}^{-1}}{\displaystyle\prod_{m=1}^{F} \omega_{j,m}^{-1}} \tag{19}$$

where the $\overline{\overline{\omega}}_{j,\overline{\overline{m}}}$ are obtained from the Wilson GF matrix method[53-58]

$$\mathbf{GFL} = \mathbf{L\Lambda} \tag{20}$$

where the dimensions of the $\mathbf{G}$ and $\mathbf{F}$ matrices are reduced to $(F - t) \times (F - t)$, $\mathbf{L}$ is the

matrix of the generalized normal mode eigenvectors, $\mathbf{\Lambda}$ is the eigenvalue matrix and its

diagonal elements are the square of the vibrational frequencies. The $\mathbf{F}$ matrix in internal

coordinates is obtained by

$$\mathbf{F} = \mathbf{A}^{\mathsf{T}}\mathbf{F}^{\mathrm{Cart}}\mathbf{A} \tag{21}$$

where $\mathbf{A}$ is the generalized inverse of the Wilson $\mathbf{B}$ matrix, $\mathbf{F}^{\mathrm{Cart}}$ is the force constant matrix in Cartesian coordinates, and T denotes a transpose. The Wilson $\mathbf{B}$ matrix constructed here only contains the non-torsional internal coordinates and the rows for torsional internal coordinates are removed; therefore its dimension is $(F - t) \times 3N$. The G matrix is given by

$$\mathbf{G} = \mathbf{B}\mathbf{u}\mathbf{B}^{\mathsf{T}} \tag{22}$$

where $\mathbf{u}$ is a diagonal matrix with the reciprocals of the atomic masses on the diagonal. We note that whereas the $f_{j,\tau}$ do not depend on the moments of inertia, as shown in eqn (15b), the product $Q_j^{\mathrm{HO}} Z_j^{\mathrm{int}} \prod_{\tau=1}^{t} f_{j,\tau}$ approaches the uncoupled-torsion high-T limit given

by $\prod_{\bar{\bar{m}}=1}^{F-t} \hbar\beta\bar{\bar{\omega}}_{j,\bar{\bar{m}}}^{-1} \prod_{\tau=1}^{t} q_{j,\tau}^{\mathrm{FR}} / P_{j,\tau}$.

Next, we consider Z_j^{coup}. In eqns (5) and (12)–(15), we employ the torsional moment-of-inertia approximation of Pitzer,[46] which is the best one can do for a torsion uncoupled to other torsions; however, we can obtain a more accurate result by allowing the torsions to be coupled to one another. To account for this coupling in the free-rotor high-T limit we need a correction factor equal to

$$Z_j^{\mathrm{coup}} = \left(\frac{\left| \det \mathbf{D}_j \right|}{\prod_{\tau=1}^{t} I_{j,\tau}} \right)^{1/2} \tag{23}$$

where $\mathbf{D}$ is the kinetic energy matrix for internal rotation of Kilpatrick and Pitzer.[47]

Finally we consider g_j. A simple expression having the correct limits and the approximately correct functional form[7] is

$$g_j = \left(\prod_{\tau=1}^{t} \tanh \frac{q_{j,\tau}^{\mathrm{FR}}}{P_{j,\tau} q_{j,\tau}^{\mathrm{CHO}}} \right)^{1/t} \tag{24a}$$

and eqn (24a) can be rearranged to

$$g_j = \left(\prod_{\tau=1}^{t} \tanh \frac{\sqrt{2\pi k_{j,\tau}\beta}}{M_{j,\tau}} \right)^{1/t}$$

(24b)

From a computational point of view we note that the partition function is independent of $\left| \det \mathbf{D}_j \right|$ and $\overline{\omega}_{j,\tau}$ when $g_j \rightarrow 1$.

Equations (4), (15b), (16), and (24b) constitute our final result for the MS-AS method. Therefore, the MS-AS method does not require any saddle point optimization or scanning to determine torsional barriers, and one only needs information for each minimum.

The thermodynamic functions for the free energy, average energy, and entropy using the MS-AS method are given in Appendix B. Alternative variants of the MS-AS method are given in Appendix C.

II.B.2 *Alternative derivation.* In Sect. II.B.1 the MS-AS method was introduced via an ansatz in which we assumed that the spacing between structures along a particular torsional coordinate τ was approximately uniform. We now present a derivation of the MS-AS approximation from an alternative point of view.

If we assume that the torsional motion is uncoupled to the remaining degrees of freedom the partition function would factor as

$$Q \approx Q_\perp Q^{\text{torsions}}$$

(25)

where $Q_\perp$ denotes the contribution to the total partition function from all non-torsional degrees of freedom. The quantum mechanical torsional partition function could be approximated by a classical mechanical (CM) configuration integral scaled by a Pitzer–Gwinn quantum mechanical (QM) correction factor, F^{PG},

$$Q^{\text{torsions}} \approx F^{\text{PG}} Q^{\text{torsions,CM}}$$

(26)

and the classical mechanical torsional partition function could be approximated as[47]

$$Q^{\text{torsions, CM}} = \left(\frac{1}{2\pi\beta\hbar^2} \right)^{t/2} \left(\det\{\mathbf{D}\} \right)^{1/2} \int_0^{2\pi/\sigma_1} \cdots \int_0^{2\pi/\sigma_t} d\phi_1 \cdots d\phi_t \exp\left[-\beta V(\phi_1,\ldots,\phi_t) \right] \quad (27)$$

where the torsional kinetic energy matrix, **D**, is evaluated at the global minimum and its coordinate dependence has been neglected. We now assume that the topography of the torsional subspace is characterized by J distinct basins each characterized by a (local-)minimum-energy structure. We further assume that we can subdivide the torsional space into a set of disjoint subdomains Ω_j. If we relax the requirement of eqn (25) so that the torsional motion is only uncoupled from the remaining degrees of freedom within a particular subdomain we obtain the approximation

$$Q = \sum_{j=1}^{J} Q_{j\perp} \left(\frac{1}{2\pi\beta\hbar^2} \right)^{t/2} \left(\det\{\mathbf{D}_j\} \right)^{1/2} F_j^{PG} \int_{\Omega_j} d\phi_1 \cdots d\phi_t \exp\left[-\beta V(\phi_1,\ldots,\phi_t) \right]. \quad (28)$$

We proceed by approximating the subdomains Ω_j as

$$\frac{-\pi}{\overline{M}_{j,\tau}} \leq \phi_\tau - \overline{\phi}_{j,\tau} \leq \frac{\pi}{\overline{M}_{j,\tau}}; \tau = 1,\ldots,t \quad (29)$$

where $\overline{M}_j$ can be integer or non-integer, and $\overline{\phi}_{j,\tau}$ denotes the center of the subdomain j. The requirement that the subdomains span the entire torsional subspace leads to the result that

$$\sum_{j=1}^{J} \prod_{\tau=1}^{t} \frac{\sigma_\tau}{\overline{M}_{\tau,j}} = 1 \quad (30)$$

We further assume that the potential is separable in the torsional coordinates within a subdomain, i.e., that

$$V(\phi_1,\ldots,\phi_t) \approx \sum_{\tau=1}^{t} V_{j,\tau}(\phi_\tau) \quad (31)$$

and that the separable 1-D potentials may be approximated as

$$V_{j,\tau} = U_j + \frac{W_{j,\tau}}{2} \left[1 - \cos \tilde{M}_{j,\tau}(\phi_\tau - \phi_{\tau,\text{eq.}j}) \right] \quad (32)$$

where the $\phi_{\tau,\text{eq.}j}$ denote, as before, the equilibrium torsion angles of structure j, the $\tilde{M}$ are periodicity parameters, and the remaining parameters are the same as discussed in Sect. II B.1. We define

$$\overline{P}_j = \frac{\overline{M}_j}{\sigma_\tau} \quad (33)$$

134

and

$$\tilde{P}_{j,\tau} = \frac{\tilde{M}_{j,\tau}}{\sigma_\tau}. \tag{34}$$

The expression in eqn (28) reduces to the MS-AS approximation if we take

$$Q_{j\perp} = Q_{\mathrm{rot},j}\exp\!\left(-\beta U_j\right)Q_j^{\mathrm{HO}}\,\frac{Z_j}{Z_j^{\mathrm{coup}}}\prod_{\tau=1}^{t}\frac{1}{q^{\mathrm{QHO}}(\overline{\omega}_{j,\tau})}, \tag{35}$$

where $q^{\mathrm{QHO}}(\overline{\omega}_{j,\tau})$ is a quantum mechanical harmonic oscillator partition function for an oscillator with a frequency $\overline{\omega}_{j,\tau}$ given by eqn (5), the Pitzer–Gwinn correction factors are calculated via

$$F_j^{\mathrm{PG}} = \prod_{\tau=1}^{t}\frac{q^{\mathrm{QHO}}(\overline{\omega}_{j,\tau})}{q^{\mathrm{CHO}}(\overline{\omega}_{j,\tau})}, \tag{36}$$

and if we take

$$\overline{M}_{j,\tau} = \tilde{M}_{j,\tau} = M_{j,\tau}, \tag{36}$$

From the above derivation we can see that the parameter $M_{j,\tau}$ plays three roles in the MS-AS method. Firstly, it controls the local periodicity by means of eqns (8) and (32). Secondly, it determines the implicit barrier height by eqn (13). Thirdly, it determines the volume of the torsional subspace spanned by a particular structure.

II.C. MS-ASCB method

In this section we present a higher-level MS method that explicitly includes the conformational barrier (CB) heights and barrier positions in the $f_{j,\tau}$ by using the segmented reference Pitzer–Gwinn[14, 61] (SRPG) approximation; this is called the MS-ASCB method, where ASCB denotes "based on all structures and conformational barriers". In the SRPG approximation, a more realistic reference potential is obtained by interpolating the region between each barrier and well with its own reference potential. This yields a continuous torsional potential given by

$$
V_{j,\tau} = \begin{cases} U_j + \dfrac{W_{j,\tau}^L}{2}\left[1 - \cos\left(\dfrac{(\phi_\tau - \phi_{\tau,\mathrm{eq}.j})\pi}{(\phi_{\tau,\mathrm{eq}.j} - \phi_{j,\tau}^L)}\right)\right]; & \phi_{j,\tau}^L \le \phi_\tau \le \phi_{\tau,\mathrm{eq}.j} \\[2em] U_j + \dfrac{W_{j,\tau}^R}{2}\left[1 - \cos\left(\dfrac{(\phi_\tau - \phi_{\tau,\mathrm{eq}.j})\pi}{(\phi_{j,\tau}^R - \phi_{\tau,\mathrm{eq}.j})}\right)\right]; & \phi_{\tau,\mathrm{eq}.j} \le \phi_\tau \le \phi_{j,\tau}^R \end{cases} \tag{37}
$$

This scheme yields

$$
f_{j,\tau}^{\mathrm{MS\text{-}ASCB}} = \sigma_\tau \left[\frac{q_{j,\tau}^{\mathrm{SRC}}}{q_{j,\tau}^{\mathrm{CHO}}}\right] \tag{39}
$$

where

$$
\begin{aligned}
q_{j,\tau}^{\mathrm{SRC}} = q_{j,\tau}^{\mathrm{FR}} \Bigg[& \frac{(\phi_{\tau,\mathrm{eq}.j} - \phi_{j,\tau}^L)}{2\pi}\exp(-\beta W_{j,\tau}^L/2)I_0(\beta W_{j,\tau}^L/2) \\
& + \frac{(\phi_{j,\tau}^R - \phi_{\tau,\mathrm{eq}.j})}{2\pi}\exp(-\beta W_{j,\tau}^R/2)I_0(\beta W_{j,\tau}^R/2)\Bigg]
\end{aligned} \tag{40}
$$

the zero of energy is taken as $U_j, W_{j,\tau}^L$ and $W_{j,\tau}^R$ are the left and right barrier heights, respectively, for torsion mode τ of structure j, and $\phi_{j,\tau}^L$ and $\phi_{j,\tau}^R$ are the locations of these barriers. In contrast to the MS-AS scheme, the barrier heights in the SRPG method have to be calculated by scans or by optimizing all saddle points connecting all the structures, which adds significant computational cost and human effort.

II.D. MS-AS method for strongly coupled torsions

Occasionally a subset of the torsional coordinates may be so strongly coupled that it is difficult or impossible to assign a set of $M_{j,\tau}$ parameters in the MS-AS method, even when allowing for non-integer values as suggested in II.B.2. For such cases we present a strongly coupled option for the MS-AS method that is parameterized by Voronoi tessellation.[42-44]

In the strongly coupled MS-AS scheme we partition the torsional space into a set of nearly separable (NS) coordinates and a set of strongly coupled (SC) coordinates. In general, the strongly coupled coordinates may be further partitioned into two or more subspaces, with each subspace involving only those coordinates that are strongly coupled

to each other. However, for simplicity in the following discussion, we will outline only the case for a single subspace of SC coordinates; the generalization to treat multiple subspaces of SC coordinates is straightforward. We will denote the number of NS coordinates as t_{NS} and the number of SC coordinates as t_{SC}, where $t_{NS} + t_{SC} = t$, and we will label particular coordinates in these subspaces by subscripts τ_{NS} and τ_{SC}, respectively.

Voronoi tessellation divides a space into cells around a discrete set of points. In our application, the space to be tessellated is described by the dihedral angles $\phi_1, \phi_2, ..., \phi_{t_{SC}}$ and the points correspond to structures. Each cell corresponds to a specific structure and consists of all torsional configurations closer to this structure than to any other structure when only the t_{SC} strongly coupled degrees of freedom are considered. We used the Euclidean norm for our distance metric. In principle, we could work with only the symmetry unique portion of the torsional space; however, because we choose to work with ordinary dihedral angles rather than symmetrized coordinates, and (as discussed earlier) these coordinates can display slight deviations from the true symmetry of the system, we do not exploit symmetry in this portion of the calculation. Thus, in order to tessellate the space we include two kinds of points. The first kind is the coordinates (sets of t_{SC} dihedral angles) of the distinguishable structures; the second kind is the coordinates of minima of the potential energy function that correspond to indistinguishable structures but where the angles are determined by adding $2\pi / \sigma_{\tau_{SC}}$ to selected angles of the associated distinguishable structure. We label the points $\tilde{j} = 1, 2, ..., \tilde{J}$, where $\tilde{J}$ is greater than or equal to J. For example, if we were treat the torsions of propane as strongly coupled (actually they are nearly separable), we would have $J = 1$ and $\tilde{J} = 9$. We label the points as $\tilde{j} = 1, 2, ..., J$ for distinguishable structures and $\tilde{j} = J + 1, J + 2, ..., \tilde{J}$ for indistinguishable structures. One may then calculate the volume $\Omega_{\tilde{j}}^{SC}$ of each cell and associate that volume with that point. We calculate the cell volumes using the convex hull code *hull* of Clarkson.[62, 63] In order to properly handle the periodic nature of the coordinates, we include periodic replicas in the tessellation calculation.

137

By definition, the volume of the SC torsional subspace neglecting indistinguishability of identical particles is

$$\Omega^{\text{SC,tot}} = \sum_{\tilde{j}=1}^{\tilde{J}} \Omega_{\tilde{j}}^{\text{SC}} = (2\pi)^{t_{\text{SC}}} \tag{41}$$

After accounting for indistinguishability, the total volume of the SC torsional subspace may be calculated by

$$\Omega^{\text{SC}} = \sum_{\tilde{j}=1}^{J} \Omega_{\tilde{j}}^{\text{SC}} \tag{42}$$

we should find that

$$\frac{\Omega^{\text{SC}}}{\Omega^{\text{SC,tot}}} = \frac{1}{\sigma_1 \sigma_2 .. \sigma_{t_{\text{SC}}}} \tag{43}$$

but slight deviations may occur due to symmetry distortions resulting from the limitations of working in a coordinate system of ordinary dihedral angles. In such cases it may be desirable to rescale the distinguishable volumes so that this equality holds exactly or to work with volumes that are averages of selected distinguishable and indistinguishable structures that are related by additional symmetries (see the later discussion of mirror image structures of pentyl radical for an example).

When the torsional subspace is so strongly coupled that we cannot assign $M_{j,\tau_{\text{SC}}}$ by considerations based on considering each torsion separately, then we replace all $M_{j,\tau_{\text{SC}}}$ for strongly coupled torsions of a given j by a single M_j^{SC} equal to

$$M_j^{\text{SC}} = \frac{2\pi}{\left(\Omega_j^{\text{SC}}\right)^{1/t_{\text{SC}}}} \tag{44}$$

When this is done, eqn (30) with $\overline{M}_{j,\tau}$ replaced by $M_{j,\tau}$ is automatically satisfied if eqn (43) holds.

When the SC method is used, the intrinsically separable effective potentials of eqn (8) are no longer defined. The strongly coupled MS-AS scheme is not a classical partition function, augmented by a Pitzer–Gwinn quantum correction, for a particular effective torsional potential. Instead, it is an interpolation scheme that yields correct

138

values in the low- and high-temperature limits and gives reasonable values between these limits.

If one treats all the coordinates as if they constitute a single set of strongly coupled coordinates, then the Voronoi tessellation, together with the equations above, provides a fully automatable way of assigning the M parameters. However, grouping nearly separable degrees of freedom together with strongly coupled ones results in an approximation in which the contribution to the partition function of the nearly separable torsions is not expected to be as accurate as when one uses the method of Section II.B.1 for these torsions. Thus, we recommend keeping the dimensions of the SC subspaces as small as is feasible. That is, we recommend assigning torsions to SC subspaces only when they are coupled so strongly that we cannot assign $M_{j,\tau_{SC}}$ values based on considering each torsion separately.

II.E. MS-RS method

Although wherever feasible we strongly recommend the inclusion of all structures in the partition function calculation, as is done in the MS-AS scheme, we recognize that a lower level of treatment is needed in some circumstances where the harmonic approximation is qualitatively incorrect and where finding and optimizing all structures requires too much work. In such instances, we propose a reference-structure treatment involving the generation of structures by independent torsions. To apply this method, one chooses one structure as a reference structure, and one considers only the other structures that can be generated by independently rotating the torsions, one at a time. One can start from any reasonable reference structure. If any structure among the generated structures is found to have a lower energy than the starting structure, one can optionally start over taking this lower-energy structure as the new reference structure. The number of structures that needs to be optimized for this approach scales linearly with the number of torsions, t, so for large molecules it can be much more affordable than the MS-AS scheme where the number of structures scales exponentially with t.

Label the reference structure as $j = 1$, and number the distinguishable structures, which are denoted $j[\tau, i(\tau)]$, generated by rotating about torsional coordinate τ in the

139

reference structure as $i(\tau) = 1, \cdots, P_{1,\tau}$. We adopt the convention that $i(\tau) = 1$ corresponds to a null rotation, which leads to the reference structure for every τ. We define the multi-structure reference-structure (MS-RS) approximation to the conformational-rovibrational partition function as

$$Q_{\text{con-rovib}}^{\text{MS-RS}} = Q^{\text{ref}} \prod_{\tau=1}^{t} \sum_{i(\tau)=1}^{P_{1,\tau}} \frac{Q_{j[\tau,i(\tau)]}^{\text{IT}}}{Q_{j=1}^{\text{IT}}} \tag{45}$$

where

$$Q^{\text{ref}} = Q_{\text{rot},1} \exp(-\beta U_1) Q_1^{\text{HO}} Z_1 \prod_{\tau'=1}^{t} f_{1,\tau'} \tag{46}$$

$$Q_j^{\text{IT}} = Q_{\text{rot},j} \exp(-\beta U_j) Q_j^{\text{HO}} Z_j \prod_{\tau'=1}^{t} P_{j,\tau'} f_{j,\tau'} \tag{47}$$

and the remaining quantities are the same as those discussed for the MS-AS method. Notice that in eqn (46) we set $j = 1$, which denotes the reference structure. If the reference structure is not the lowest-energy structure included, then U_1 need not be zero (as it was in the MS-AS and MS-ASCB methods); in general, U_j is 0 for the lowest-energy structure included in eqn (45), and for all the other structures, U_j is the equilibrium potential energy relative to the lowest-energy structure included. The inclusion of the $P_{j,\tau'}$ factor in eqn (47) results in the Q_j^{IT} being scaled by a quantity proportional to the volume of the torsional subspace spanned by this structure; thus, the ratio of factors in eqn (45) properly accounts for the differences in the domain sizes of the various structures. Notice $P_{j,\tau}$ used in MS-RS method is obtained from $M_{j,\tau}$ and σ_τ by eqn (1).

Notice that the $P_{j,\tau}$ and σ_τ are not directly needed for the MS-AS method (unlike $M_{j,\tau}$, they cancel out in the final equations, although their knowledge is useful for ascertaining whether or not all the structures are accounted for); however, the MS-RS method explicitly requires the $P_{j,\tau}$ (or the σ_τ from which they may be calculated by eqn (1)) as well as $M_{j,\tau}$. Except for the $P_{j,\tau}$, the MS-RS method requires no information that is not needed for MS-AS calculations, and it requires information for

only a subset of the structures. In cases where a subset of torsional motions are strongly coupled the MS-RS scheme may not perform as well as when the coupling is small; in such instances one may seek extensions of the MS-RS scheme that, for instance, treat the NS torsions independently but which include additional structures obtained by modifying the reference structure by two or more simultaneous rotations from within the SC torsional subspace. Such extensions may provide additional accuracy while retaining the desirable computational scaling of the MS-RS approach, but they are beyond the scope of the present study.

III. Calculations and Results

To illustrate the MS methods, we apply the MS-HO, MS-AS, and MS-ASCB methods to two one-dimensional (1-D) model potentials and to ethanol. Note that the MS-AS and MS-RS methods are identical for some simple cases such as ethanol and 1-D potentials. However, we will compare the MS-HO, MS-AS, and MS-RS methods for 1-butanol and 1-pentyl radical in the present study.

The M06-2X[64] density functional was used for calculating the geometries and energetics of ethanol and the 1-pentyl radical, and the MPW1K[65] density functional was used for 1-butanol. The 6-311+G(2df,2p) basis set[66, 67] was used for all the calculations. All density functional calculations were performed using the *Gaussian 09* program.[68]

Because meta-GGA density functionals are sensitive to integration grids, we performed a grid-convergence analysis on the frequencies of ethanol and 1-pentyl radical using the M06-2X/6-311+G(2df,2p) method. As shown in Table 1, the frequencies calculated by M06-2X/6-311+G(2df,2p) are well converged when one uses the density functional integration grid that has 99 radial shells around each atom and 974 angular points in each shell. Therefore this grid (99, 974) was used for all M06-2X calculations in this article. The pruned (99, 590) grid, which is called *ultrafine* in *Gaussian09*, was used for calculations with the MPW1K functional, which are less sensitive to the fineness of the integration grids.

All the minima of ethanol, 1-pentyl radical, and 1-butanol are fully optimized and confirmed by normal-mode analysis. The saddle points of ethanol that connect the minima are also optimized and are confirmed to have one imaginary frequency.

Table 2 shows the notation that is used for torsion angles in this paper. This notation is based on standard notation but is also specialized to the needs of the present study.

Partition functions are calculated from 100 K to 50000 K. The 50000 K result is tabulated not because this is an accessible temperature, but rather to illustrate the high-temperature limit for formal purposes.

The frequencies ($\omega_{j,m}$, $\overline{\omega}_{j,\tau}$, and $\overline{\overline{\omega}}_{j,\overline{m}}$) used in the calculations are all scaled and the scaling factors designed to give accurate ZPEs are used.[69]

We also employed Benson's group additivity (GA) method[30, 31, 70] to calculate entropies of ethanol, 1-pentyl radical, and 1-butanol for comparison. For this purpose we use not only Benson's[30] group parameters but also those of Cohen[31] and Lay et al.[34]

III.A. 1-D models

In order to better understand the proposed methods, we first apply them to two 1-D torsion models. One is an artificial 1-D model potential designed to show the effect of a shallow minimum, and the other is the 1-D torsion potential of H_2O_2 from the work of Koput et al.[71] that has been used in a prior study[14] of torsional methods.

The first 1-D model potential is given by

$$V /\text{cm}^{-1} = 121.352549 + 90.0\cos(2\phi) + 60.0\cos(3\phi) \qquad (48)$$

where ϕ is the torsion angle. This potential has three minima in the range of [0, 2π) and we assume they are all distinguishable, i.e., $M = P = 3$. This potential is plotted in Fig. 1, and the rotational barrier heights and the locations of minima are also given in the figure. The internal moment of inertia is assumed to be 1.53618 amu Å^2 and to be independent of ϕ. The harmonic frequencies calculated using eqn (5) are 126.41 and 62.85 cm^{-1} for the deep and shallow minima, respectively.

The small barriers and the presence of a very shallow minimum for this potential make it an interesting model to test the proposed methods. The accurate partition

functions were calculated by the torsional eigenvalue summation (TES) method.[14] The calculated partition functions and the percentage errors of the approximate schemes relative to the TES values are listed in Table 3.

Table 4 shows the errors of the multi-structural methods when the shallow minimum is ignored (because the MS-ASCB method requires information for all the barriers, it is not included in Table 4.). When ignoring this shallow well, we set $M = P = 2$ which alters the effective barrier heights of the reference potential.

The 1-D torsional potential for H_2O_2 is given by[71]

$$V/cm^{-1} = 811.3053546 + 1037.4\cos(\phi) + 674.2\cos(2\phi) + 46.9\cos(3\phi) + 2.7\cos(4\phi) \quad (49)$$

This potential energy curve is plotted together with the heights and locations of the barriers in Fig. 2. The minima are mirror-image structures and are therefore distinguishable ($J = P = M = 2$). The internal moment of inertia is 0.423202 amu $Å^2$ and the harmonic frequency of each minimum is 382.6 cm^{-1}. This 1-D potential has been studied in a previous paper[14] in which the effective barrier height used in the RPG scheme was chosen as the average of the two barrier heights. In the MS-AS method (which also uses the RPG scheme for torsions), the effective barrier height is calculated by eqn (13).

Table 5 lists the calculated partition functions and the percentage errors of the approximate schemes relative to the TES values for the 1-D potential of H_2O_2.

III.B. Ethanol

The ethanol molecule has two torsions. One involves internal rotation about the C–C bond, and the other involves internal rotation about the C–O bond. If the torsions are considered separately, they each have 3 minima along their torsion coordinates. The torsion around the C–C bond only has one distinguishable minimum because the three hydrogen atoms of the methyl group are identical whereas the torsion around the C–O bond leads to 3 distinguishable minima. Although two of these structures are isoenergetic, they are mirror images and thus distinguishable. Therefore, as shown in Fig. 3, the ethanol molecule, with two torsions, has three distinguishable structures that contribute to the total partition function.

Table 6 lists the information used in the MS-AS and MS-ASCB calculations for ethanol. Table 7 lists the partition function calculated using the MS-HO, MS-AS, and MS-ASCB methods.

Fig. 4 shows the percentage difference of the partition functions of structure E-t from that of E-g$^+$ or E-g$^-$ using the harmonic approximation. Note that the each harmonic partition function used here takes its own minimum as the zero of energy.

Fig. 5 shows the ratio of the partition function of ethanol calculated by the multi-structural method to that calculated by the single-structure HO (SS-HO) approximation (J, Z_j, and $f_{j,\tau}$ are equal to 1) at the global minimum (E–t).

III.C. 1-pentyl radical

The 1-pentyl radical has four torsions that are associated with internal rotation about each of the four C–C bonds. We label the five carbon atoms as: $H_2C^{(1)}$–$H_2C^{(2)}$–$H_2C^{(3)}$–$H_2C^{(4)}$–$H_3C^{(5)}$, and the four torsions are around the 1–2, 2–3, 3–4, and 4–5 C–C bonds, respectively. The 1-pentyl radical constitutes an example of a system displaying significant torsional coupling, in particular involving the $\tau = 1$ ($C^{(1)}$–$C^{(2)}$) and $\tau = 2$ ($C^{(2)}$–$C^{(3)}$) internal rotations; assigning $M_{j,\tau}$ parameters in such circumstances merits special care. In the absence of steric hindrance effects,[37-39] torsion involving a –CH$_2$ radical group is expected to have 6-fold periodicity and low barrier heights yielding three distinguishable minima. The 4–5 torsion is expected to have three total minima, only one of which is a distinguishable minimum, and the other two torsions are expected to have three total minima, all distinguishable. Thus, an uncoupled model would lead one to expect a total of 27 distinguishable structures. However, the total number of distinguishable structures of 1-pentyl radical is found to be only 15 as shown in Fig. 6. The 15 structures include seven pairs of mirror-image structures (which of course have the same energy and vibrational frequencies); therefore we only need to perform electronic structure calculations on eight of the 15 structures. In larger systems steric effects can lead to either a larger or smaller number of structures than would be expected based on a separable approximation.[40, 51]

In the absence of strong coupling the structures should correspond closely to minima encountered when the system is rotated about a single torsional coordinate. In this limit, $P_{j,\tau}$ assignments (and thus $M_{j,\tau}$ assignment after taking account of the torsional symmetry) may be made by starting with a particular structure, choosing a τ, and counting all structures (including the starting structure) that have similar torsional angles to the starting structure for every torsion except the τ torsion. This approach confirms the expected results of $P_{j,\tau=3} = 3$ and $P_{j,\tau=4} = 1$ for all values of j. A similar exercise for the $\tau = 1$ torsion leads to 9 structures with expected values of $P_{j,\tau=1} = 3$ and six structures (P–a⁻g⁺t, P–a⁺g⁻t, P–a⁻g⁺g⁺, P–a⁺g⁻g⁻, P–a⁻g⁺g⁻, P–a⁺g⁻g⁺) with $P_{j,\tau=1} = 1$.

Relaxed scans starting from each of these six latter structures reveal a single broad structure spanning the entire 180 degrees of the symmetry-unique $\tau = 1$ torsional degree of freedom each with a relatively large barrier—the effective barriers estimated by eqn (13) range from 451 to 654 cm⁻¹ (using $M = 2$) as compared to values of 29 to 44 cm⁻¹ (using $M = 6$) for the other 9 structures. The occurrence of these broad minima may be considered to arise from steric hindrance effects that outweigh the small barriers that one would anticipate existing between 3 expected structures in the absence of such steric effects. Thus, each of the 3 structures with broad features along the $\tau = 1$ coordinate may be thought of as aggregations of 3 expected structures and therefore these structures span a torsional subspace with a volume that is approximately 3 times as large as that spanned by the remaining 9 structures having assignments of $P_{j,\tau=1} = 3$.

In the absence of steric effects we would anticipate assignments of $P_{j,\tau=2} = 3$ for each of the structures, and such assignments would be consistent with the sum of the torsional subspace volumes of each of the structures totaling to the total volume (see eqn (30)), which serves as a convenient consistency check of possible assignments. Rigid scans along the $\tau = 2$ torsional coordinate reveal 3 distinct minima, but due to strong coupling with the $\tau = 1$ torsional degree of freedom, not all of these minima correspond closely with other structures. In particular, if we select a particular structure and look for all other structures having similar torsional angles for all torsional coordinates other than

$\tau = 2$ we find either 0 or 1 additional structures and this suggests that the simple scheme for assigning $P_{j,\tau}$ values breaks down in the presence of strong torsional coupling. For example, if we start by considering the P–a⁻g⁺t structure we find only the P–a⁻tt structure corresponds closely to the starting structure via a rotation about the $\tau = 2$ coordinate. In the presence of strong torsional coupling we need to generalize our criteria for assigning $P_{j,\tau}$ so that instead of looking only for structures having similar torsional angles to that of the structure undergoing assignment along $t - 1$ coordinates we look for structures for which the spans of the torsional minima strongly overlap with each of the spans of the torsional minima of the starting structure along $t - 1$ coordinates. Under this relaxed set of criteria we see that the P–a⁺g⁻t structure, which is one of the structures having a single broad minima along $\tau = 1$, overlaps with the torsional spans of P–a⁻g⁺t along the required $t - 1$ coordinates even though the $\tau = 1$ torsional angles of these two structures differ by about 54 degrees. Under this relaxed set of search criteria we are easily able to identify two other structures that are sufficiently similar to each structure undergoing assignment to yield assignments of $P_{j,\tau=2} = 3$ for all structures.

When employing the MS-RS method we need to identify all structures obtained by independent rotations from a reference structure. In this context, if we consider the reference structure to be P–a⁻g⁺t, the structures most consistent with independent rotation about the $\tau = 2$ coordinate are the P–a⁻tt and P–a⁺g⁻t structures. One of these is the mirror image structure of the reference structure, which shows that the concept of an independent internal rotation about a single torsional coordinate must be considered as highly approximate in the presence of strong torsional coupling. As we will see in the following, the results for the MS-RS and MS-AS methods show some consistency suggesting that both methods can, at least sometimes, yield reasonable partition functions even for cases where we have strong torsional coupling.

We also consider two variants of the strongly coupled option of the MS-AS scheme, one (denoted NS:SC = 2:2) which treats the 1–2 and 2–3 torsions as strongly coupled and one (denoted NS:SC = 1:3) which treats the 1–2, 2–3, and 3–4 torsions as

146

strongly coupled. These methods not only take account of the strong coupling, but they eliminate the need for much of the analysis presented in the proceeding four paragraphs.

In the NS:SC = 2:2 scheme, the 15 structures are divided into 3 groups with the structures in each group have the same torsional conformation for the 3–4 torsion. In particular, the group with the 3–4 torsion in a trans conformation includes the structures P–a$^-$g$^+$t, P–a$^+$g$^-$t, P–a$^+$tt, P–a$^-$tt, and P–stt; the group with the 3–4 torsion in a g$^+$ conformation includes the structures P–a$^-$g$^+$g$^+$, P–a$^+$g$^-$g$^+$, P–a$^+$tg$^+$, P–a$^-$tg$^+$, and P–stg$^+$; and the group for with the 3–4 torsion in a g$^-$ conformation includes the structures P–a$^+$g$^-$g$^-$, P–a$^-$g$^+$g$^-$, P–a$^-$tg$^-$, P–a$^+$tg$^-$, and P–stg$^-$. The Voronoi tessellation is performed considering each group separately.

In the Voronoi tessellation calculations, some indistinguishable structures are generated by symmetry. For example, if the P–a$^+$tt struture is denoted by its first three torsional angles as (159.7, 178.8, 179.9) and its corresponding indistinguishable structure is (–20.3, 178.8, 179.9) due to the 2-fold symmetry of the –CH$_2$ radical group. The angles 159.7 degrees and –20.3 degrees refer to the dihedral angle H$_a$–C$^{(1)}$–C$^{(2)}$C$^{(3)}$ and H$_b$–C$^{(1)}$–C$^{(2)}$C$^{(3)}$. However, the optimized structure has the H$_b$–C$^{(1)}$–C$^{(2)}$C$^{(3)}$ angle as -30.4 degrees. This discrepancy is caused by using a dihedral angle to represent the torsion, which also has the effect that some mirror images have slightly different volumes (e.g. the volumes of P–a$^+$tt and P–a$^+$tt have about a 1% difference). If the two mirror images have different volumes, we used the averaged volume to calculate M values.

The structure P–a$^-$g$^+$t (the global minimum) is chosen as the reference structure in the MS-RS calculations. Independent rotations starting from this reference structure generate the structures P–a$^-$g$^+$g+, P–a$^-$g$^+$g$^-$, P–a$^-$tt, and P–a$^+$g$^-$t. These five structures are used in the MS-RS calculations.

Table 8 lists information for each structure of 1-pentyl radical that is used for the partition function calculations using various schemes for M values. Table 9 lists the partition functions of 1-pentyl radical calculated by the MS-HO, MS-AS, and MS-RS methods.

Figure 7 shows the percentage differences of the harmonic oscillator partition functions of three structures relative to that of structure P–a⁻g⁺t or P–a⁺g⁻t (each harmonic oscillator partition function takes its own minimum as the zero of energy). Figure 8 shows the ratios of the partition function of 1-pentyl radical calculated by multi-structural methods to those calculated by the SS-HO approximation at the global minimum (P–a⁻g⁺t or P–a⁺g⁻t).

III.D. 1-Butanol

We label the carbon atoms in 1-butanol as $HO–H_2C^{(1)}–H_2C^{(2)}–H_2C^{(3)}–H_3C^{(4)}$. The four torsions in 1-butanol are associated with internal rotation around each of the three C–C bonds and one C–O bond. Each torsion, with the exception of the methyl torsion, is expected to generate 3 distinguishable structures, and a total of 27 distinguishable structures is expected to be generated. However, due to steric hindrance between the terminal hydroxyl and methyl groups, the expected structures $g^+g^-g^+$ and $g^-g^+g^-$ are saddle points that connects $g^+x^-g^+/g^+g^-x^+$ and $g^-x^+g^-/g^-g^+x^-$ structures, respectively. A similar effect has also been observed in alkanes.[17, 51] Therefore, 1-butanol has a total of 29 structures. The 29 structures include 14 pairs of mirror-image structures; therefore, electronic structure calculations only needed to be performed for 15 structures. Two previous conformational studies[72, 73] of 1-butanol only observed 27 structures with the structures assigned as $g^+g^-g^+$ and $g^-g^+g^-$ being similar to our $g^+x^-g^+$ and $g^-x^+g^-$ structures. The $g^+x^-g^+$ structure has torsional angles (for torsions 1–2, 2–3, and 3–4, respectively) of 60.0, 82.3, and 59.8, the $g^-g^+x^-$ structure has torsional angles of 73.4, −63.3, and 88.2, and the intervening transition state has torsional angles of 73.2, −68.9, and 81.9 degrees. The $g^+x^-g^+$ and $g^-g^+x^-$ structures lie 149 and 8 cm⁻¹ below the intervening transition state, respectively.

The structure B–tg⁺t is chosen as the reference structure in the MS-RS calculations. Starting from this reference structure, one can generate the structures B–g⁺g⁺t, B–g⁻g⁺t, B–ttt, B–tg⁻t, B–tg⁺g⁻, and B–tg⁺g⁺ by independent rotation of each C–C bond or C–O bond. These seven structures are used in the MS-RS calculations.

148

If there were no steric hindrance effect in 1-butanol such that the torsions only generated 27 structures, the parameter $M_{j,\tau}$ would be 3 for each torsion. However, it is not trivial to set reasonable integer values of $M_{j,\tau}$ for the 29 structures that satisfy eqn (30). Therefore, we use the MS-AS method with NS:SC = 1:3 to determine the $M_{j,\tau}$ values by treating only the methyl group torsion as NS.

Given that the $g^+x^-g^+/g^+g^-x^+$ $(g^-x^+g^-/g^-g^+x^-)$ structures overlap very strongly and the $g^+g^-x^+$ $(g^-g^+x^-)$ structure is extremely shallow (being bound by only 7.9 cm^{-1}) it is reasonable to only include the lower energy structure of each pair in an MS-AS calculation involving 27 structures.

Table 10 lists the information for each structure of 1-butanol that is needed for the partition function calculations. Table 11 gives the calculated conformational-rovibrational partition functions of 1-butanol.

Table 12 lists the standard state entropy of ethanol, 1-pentyl radical, and 1-butanol calculated from SS-HO, MS-HO, and MS-AS partition functions including contributions from electronic and translational degrees of freedom, and also calculated using Benson's group additivity method; the global minimum structure is used for the SS-HO method. Table 12 also contains experimentally derived values[74, 75] for comparison.

Table 13 lists the calculated correction factors Z^{int} and Z^{coup} for structures of ethanol, 1-butanol, and 1-pentyl radical.

Figure 9 shows the two cases with the largest percentage difference of structure-specific harmonic oscillator partition functions relative to that of the global minimum (each harmonic oscillator partition function takes its own minimum as the zero of energy). Figure 10 plots the temperature dependence of the ratio of the partition function of 1-butanol calculated by the multi-structural methods to that calculated by the SS-HO approximation at the global minimum.

IV. Discussion

We will begin by comparing the new MS-AS methods to accurate results of 1-D models so that we can demonstrate their accuracy for treating intra-mode anharmonicity without complications from mode-mode coupling and anharmonicities of other

vibrational modes. We have already extensively studied[14] methods to treat the intra-mode anharmonicity; herein we will only compare to the accurate values from torsional eigenvalue summation. Expansion of a torsional potential in terms of a Fourier series, along with the assumption of a constant moment of inertia, leads to a banded symmetric matrix that may be diagonalized with negligible computational expense. This technique has a long history[14, 19, 20, 76-81] and it might seem tempting to apply it whenever the additional energy evaluations needed for fitting the Fourier potential are affordable. However, there is little benefit to treating the intramode anharmonicity to a much higher degree of accuracy than we can treat the intermode anharmonicity; this is especially true in applications[19, 20] where multiple torsional modes are so treated because coupling between torsional degrees of freedom is often very important. Treatment of the inter-mode anharmonicity, which we achieve primarily by including multiple structures, is a much harder task and the primary goal of the new methods presented herein, but we begin by demonstrating that the methods also treat intramode anharmonicity well.

Table 3 clearly shows that the MS-HO approximation significantly overestimates the torsional partition function at high temperature and modestly underestimates the torsional partition function at low temperatures for the 1-D model of eqn (48). For this model torsion and most typical torsional potentials where the barriers are not very low, the MS-HO approximation is adequate for practical work at low temperatures. Due to cancellation of error, the MS-HO approximation may have quite small errors at some temperatures (e.g., 300 K for this 1-D model potential).

The MS-AS and MS-ASCB methods both use the Pitzer–Gwinn approximation based on a reference classical partition function, but they require different information about the torsional potential. They both need the energies, frequencies, and geometries of all structures that are local minima of the potential energy surface, and the MS-ASCB method also needs the locations and magnitudes of the torsional barriers. For this 1-D potential, the barriers of the deep wells are 271 cm^{-1} and 1678 cm^{-1} for each side, respectively; the shallow well has a symmetric barrier of 16 cm^{-1}. Equation (13) gives effective barriers of 1612 cm^{-1} and 40 cm^{-1} for the deep and shallow wells, respectively. Although the MS-AS and MS-ASCB methods use different effective barriers, they both

150

have errors of less than 3% for the potential of eqn (48) at temperatures above 100 K. The predominant source of errors of both methods at low temperatures (e.g., 60 K) is the Pitzer–Gwinn approximation, which only puts the quantum effects in at a harmonic level.

For the 1-D model potential of eqn (48), there is a very shallow minimum as shown in Fig. 1. On the potential energy surface of a real molecule, the geometry of such a shallow minimum may be hard to find and optimize. Also for complex molecules, finding all possible shallow minima may prove difficult, so we consider the consequences of neglecting them for this model problem. When the shallow minimum is ignored, the calculated effective barrier using eqn (13) is 364 cm^{-1} with $M = P = 2$. Table 4 shows that for $T \leq 1000$ K the two multi-structural methods (MS-HO and MS-AS) both underestimate the partition function when using two minima compared to that calculated by using three minima. At higher temperatures the MS-AS method has errors smaller than 7% when the shallow minimum is ignored. In the high-temperature limit (illustrated by 50000 K), the error of the MS-AS method is negligible even without explicitly accounting for the shallow minimum because the torsional partition function approaches a free rotor partition function, which is independent of the potential. These results suggest that accounting for shallow minima can be important if their energies are low (151.36 cm^{-1} in the 1-D model potential of eqn (48)) especially at temperatures of 400 K and lower.

The exact barrier heights on the two sides of each minimum for the 1-D torsional potential of H_2O_2 (eqn (49)) are 2545 cm^{-1} and 377 cm^{-1}, and this large difference presents a significant challenge for the MS-AS method as it assumes a single barrier height. The effective mean barrier height calculated by eqn (13) and used in the MS-AS method is 919 cm^{-1}. Although this value is quite different from the exact ones, Table 5 shows that the MS-AS method has errors no larger than 13% from 200 to 3000 K, with the largest error at 1500 K, where the error corresponds to an error of only 0.36 kcal/mol in the free energy. This 1-D case shows that accurate barrier height information does improve the accuracy of the calculated partition function through the use of the MS-ASCB method, but that the calculated partition function is not too sensitive to the barrier

heights. Because one of the two barriers on this potential energy surface is very high, the MS-HO approximation gives adequate results from 300 to 2400 K.

Ethanol is a simple molecule that has two torsions. As shown in Table 3, the two torsions around the C–O and C–C bonds have very close frequencies when modeled using internal coordinates. In the normal mode analysis, the two torsional motions are strongly coupled, and consequently the two lowest-frequency modes are mixtures of two torsional motions. The normal mode with the lowest frequency is the antisymmetric combination of two torsions, and the mode with the second lowest frequency is the symmetric combination. Therefore, even such a simple molecule as ethanol provides a case where it is impossible to assign the torsions to specific normal modes. The barrier heights calculated by eqn (13) are 1109, 329, 1206, and 379 cm^{-1} and agree very well with the normal modes optimized by the M06-2X/6-311+G(2df,2p) method, which are 1109, 386, 1195, and 359 cm^{-1}.

To apply the MS-ASCB method to ethanol, one needs to calculate the torsion angle difference $\phi_{\tau,\text{eq}.j} - \phi_{j,\tau}^{\text{L}}$ or $\phi_{j,\tau}^{\text{R}} - \phi_{\tau,\text{eq}.j}$. For the ethanol calculations, we use a single dihedral angle to represent a torsion angle although one could also construct a torsion coordinate involving a top rotating about a fixed frame from a combination of several related dihedral angles.[48-50] The $\Delta\phi^{\text{R}}$ and $\Delta\phi^{\text{L}}$ of the C–C torsion are set to 60 degrees due to the symmetry. The $\Delta\phi^{\text{R}}$ and $\Delta\phi^{\text{L}}$ of C–O is measured by the dihedral angle H-O-C-C; they are both 61.8 and degrees for structure E-t and are both 59.1 degrees for structures E-g$^+$ and E-g$^-$.

When conformational structures change by internal rotations, the other vibrational frequencies (e.g. stretching and bending modes) also change correspondingly. One of advantages of the multi-structural methods is that anharmonicities and couplings due to conformational changes are partially accounted for by the use of a different harmonic analysis at each structure. To illustrate the effect of conformational changes on partition functions, Fig. 4 shows the percentage difference of the ethanol E-g$^+$ or E-g$^-$ HO partition function from that of the global minimum E-t. Although the E-t and E-g$^+$ (or E-g$^-$) structures have quite similar conformations, this difference can be as large as 12%.

The differences are larger for 1-pentyl radical and 1-butanol. Because many conformational structures of 1-pentyl radical are quite different from the global minimum, the effects of conformational changes on partition functions are very large as shown in Fig. 7. Even larger effects are observed for 1-butanol as shown in Fig. 9. Therefore, treating torsions as separable with the frequencies of the other modes fixed at their values for the global minimum structures can introduce large errors.

When the harmonic approximation is applied to calculate partition functions in the literature, often only one structure (the global minimum) is considered. Therefore we compared the ratio of partition functions calculated by multi-structural methods to those calculated by the harmonic approximation for the global minimum. Because ethanol has three conformational structures, the partition functions calculated by multi-structural methods are larger than those calculated by the HO approximation using one structure, and the factors are between 1.9 and 3.4 in the temperature range 200–3000 K as shown in Fig. 5. Because the 1-pentyl radical and 1-butanol have many more conformational structures, the partition functions calculated by the multi-structural methods are *much* larger than the harmonic ones obtained using only the global minimum structure as shown in Fig. 8 and Fig. 10, respectively. For example, at $T = 1000$ K, the MS-AS partition function of 1-butanol is larger than that of the SS-HO approximation by a factor of 31.

Standard state entropies calculated from the SS-HO, MS-HO, and MS-AS partition functions for ethanol, 1-pentyl radical, and 1-butanol are compared to each other and to the GA method and reference data in Table 12. The reference data for ethanol is based on spectroscopic data and a reference structure treatment of anharmonicity; the reference data for 1-butanol is based on experimental heat capacities and heats of fusion and vaporization; and there is no available reference data for the 1-pentyl radical. The entropies calculated by the MS-HO method are in much better agreement with the reference data than is the single-structure HO data, and the entropies calculated by the MS-AS method give even better agreement for both ethanol and 1-butanol at the temperature studied. The entropies calculated by various parametrizations of the GA method are also listed in Table 12 for comparison. For ethanol and 1-butanol we only

calculate entropies up to 1000 K because the heat capacities C_p are available only up to 1000 K for an OH group, and extrapolation may not be reliable. All the GA calculations use the parameters from the Benson's tables[30] except some calculations for 1-pentyl radical also use the parameters from Cohen's[33] and Lay et al.'s[34] work. Benson has estimated[30] that "Values of C_P° and S° estimated from these groups are on the average within ±0.3 cal mol^{-1} K^{-1} of the measured values..." and "for heavily substituted species, deviations in C_P° and S° may go as high as ±1.5 cal mol^{-1} K^{-1}..." We find that the difference of the GA data from the MS-AS data and the reference data sometimes exceed these estimated uncertainties. The GA calculations for 1-pentyl radical obtained using Cohen's parameters agree better with the MS-AS values than those obtained using Benson's or Lay et al.'s parameters.

In the intermediate-temperature region, the values of the MS-AS partition functions of ethanol, 1-pentyl (using the 2:2 scheme), and 1-butanol (using the 1:3 scheme) are larger than those of the MS-HO partition functions. However, the MS-AS partition functions of 1-pentyl radical with all four torsions treated as nearly separable are almost the same as or lower than the MS-HO partition functions. This is because the torsion around the $C^{(1)}$–$C^{(2)}$ bond in the 1-pentyl radical has a very low barrier predicted by $M = 6$, and its torsional correction factor $f_{j,\tau}$ is already smaller than 1 in the intermediate temperature region. Figure 11 shows the temperature dependence of $f_{j,\tau}$ for several relevant cases. In the low-temperature limit the correction factors $f_{j,\tau}$ are 1, and they initially rise above 1 as temperature increases. Eventually the correction factors achieve a relative maximum and then subsequently monotonically decrease. This behavior is quite different from that predicted by the switching functions advocated in earlier work.[7]

The three sets of $M_{j,\tau}$ values (or equivalently the domain volumes) for 1-pentyl radical all have larger volumes (smaller $M_{j,\tau}$ values) for the first three pairs of structures in Table 8 than for the others, and the three sets of MS-AS partition functions have similar magnitudes. While it is difficult to judge which set of $M_{j,\tau}$ values is more accurate, this indicates that the $M_{j,\tau}$ values determined by Voronoi tessellation lead to

154

reasonable results. The ratio of the largest to the smallest of the three sets of MS-AS partition functions at 400 K is only 1.30. It is interesting to compare the effective barrier heights calculated from the three sets of $M_{j,\tau}$ values. The radical $-CH_2$ group rotation barrier is around 250 cm^{-1} for the global minimum P–a$^-$g$^+$t obtained by a relaxed scan. The effective barrier heights calculated by $M = 2.67$ (254 cm^{-1}) and $M = 2.53$ (281 cm^{-1}) have better agreement with the barrier height obtained by a relaxed scan than that calculated by $M = 2$ (451 cm^{-1}). However, for the structure P–stt, the effective barrier height obtained by a relaxed scan (around 30–40 cm^{-1}) is much lower than that calculated with $M = 3.39$ (100 cm^{-1}) and $M = 3.56$ (90 cm^{-1}), but it agrees very well with the barrier height calculated with $M = 6$ (32 cm^{-1}). Despite these differences between the effective barrier heights calculated by the three different sets of $M_{j,\tau}$ values, all of the calculated effective barrier heights fall into reasonable ranges for all the torsions considered here. The three sets of MS-AS partition functions of 1-pentyl radical have the same high–T limit because the torsional partition function is independent of the $M_{j,\tau}$ values in the high–T limit as long as eqn (30) is satisfied.

For 1-butanol the 27-structures partition functions and 29-structures partition functions have differences of less than 3% because the two addtitional structures have high energies and small subdomain volumes. This result shows that missing some structures with high energies need not lead to large errors in applying the MS-AS method.

For 1-butanol, the MS-AS partition functions and MS-RS partition functions agree with each other within about 3% for 600 K and above, but the deviation rises to 6% and 8% at 300 K and 200 K, respectively. For the 1-pentyl radical, the deviations between the MS-AS and MS-RS partition functions are larger than those for 1-butanol but are still within 10% for temperatures above 200 K when both are calculated with integer $M_{j,\tau}$. The differences between the 1-pentyl MS-RS and MS-AS partition functions when one uses the $M_{j,\tau}$ schemes designed for strong coupling are larger. With the (2:2) and (1:3) schemes, the ratios of the MS-AS to the MS-RS partition functions are 1.33 − 1.41 from 400 K to 600 K. The deviations are a consequence of the MS-RS

scheme being designed as an affordable approximation to the nearly separable MS-AS method. The levels of agreement and disagreement between the results of the methods confirm the principle behind design of the reference-structure method.

Because the MS-ASCB method uses the most information about the potential energy surface, it is expected—in the absence of cancellation of errors—to be the most accurate of the methods presented here. The good agreement observed between the results of the MS-AS and MS-ASCB methods suggests that the simpler MS-AS method is capable of providing reliable results. Finally, the comparable accuracy and reduced cost of the MS-RS method make it particularly well suited for accounting for the torsional anharmonicity of systems with a large numbers of torsions.

V. Concluding remarks

In this article, we proposed a new family of approximations called multi-structural methods for including torsional anharmonicity in thermodynamics calculations. These methods can be applied to molecules with multiple torsions coupled with each other or with other low-frequency vibrational modes. A key feature of the methods is the use of internal coordinates to correct for torsional anharmonicity so that assigning a torsion to a specific normal mode is not required in the multi-structural methods. These methods only require geometry optimizations and frequency calculations (i.e., no scans) and are easily implemented. The MS-AS method is designed to be as accurate as possible without requiring any information about the conformational barriers or the paths connecting the structures. We recommend the MS-AS method based on its good balance between computational cost, simplicity, and accuracy. The simpler MS-RS method, which is an approximation to the MS-AS method for the cases of nearly separable torsions, is also found to perform well in our tests and is recommended for large systems when the cost and effort of the MS-AS method are not affordable or not justified.

A portable and documented FORTRAN package for computing the MS partition functions conveniently is under preparation, and it will be made available at no cost when it is ready.

Appendix A

Glossary of acronyms

CHO	Classical harmonic oscillator
CM	Classical mechanical
CO	An interpolation scheme for torsional anharmonicity based on Pitzer's approximation for the moment of inertia along the curvilinear torsion (denoted C for curvilinear) and on the torsional frequency ω (denoted O for omega).
FR	Free rotor
GA	group additivity (method)
HO	Harmonic oscillator
MS	Multi-structural
MS-AS	Multi-structural method including all structures
MS-AS(I)	MS-AS method with approximation I
MS-AS(M)	MS-AS method with approximation M
MS-AS(S)	MS-AS method with approximation S
MS-ASCB	Multi-structural method including all structures and conformational barrier heights
MS-HO	Multi-structural harmonic-oscillator method
MS-RS	Multi-structural method using a reference-structure treatment involving the generation of structures by independent torsions
NS	Nearly separable torsions
QHO	Quantum mechanical harmonic oscillator
QM	Quantum mechanical
RC	Reference classical (approximation)
RPG	Reference Pitzer–Gwinn (approximation)
SC	Strongly coupled (torsions)
SRC	Segmented reference classical (approximation)

SRPG	Segmented reference Pitzer–Gwinn (approximation)
TES	Torsional eigenvalue summation, that is, evaluation of torsional partition functions by summing Boltzmann factors based on numerically computed eigenvalues of separable torsions
ZPE	Zero-point energy

Appendix B

The thermodynamic functions for the internal (i.e., neglecting translational contributions) free energy, average energy, and entropy are

$$G = -\ln(Q)/\beta \tag{B1}$$

$$E = -\frac{\partial \ln(Q)}{\partial \beta} \tag{B2}$$

$$S = k_B \ln Q - \frac{1}{T}\left(\frac{\partial \ln Q}{\partial \beta}\right)_V \tag{B3}$$

If we use the classical expression for the rotational partition function

$$Q_{\mathrm{rot},j} = \frac{\sqrt{\pi}}{\sigma_{\mathrm{rot},j}}\left(\frac{2}{\hbar^2 \beta}\right)^{3/2}\sqrt{I_A I_B I_C} \tag{B4}$$

where I_A, I_B, and I_C are the principal moments of inertia, the partial derivative of the MS-AS partition function with respect to β is

$$-\frac{\partial}{\partial \beta}\ln(Q_{\text{con-rovib}}^{\text{MS-AS}}) = \frac{1}{Q_{\text{con-rovib}}^{\text{MS-AS}}}\sum_{j=1}^{J}\left\{ e^{-\beta U_j}Q_{\text{rot},j}Q_j^{\text{HO}}Z_j\prod_{\tau=1}^{t}f_{j,\tau}\left(\frac{3}{2\beta}+U_j\right.\right.$$

$$+\sum_{m=1}^{F}\frac{\hbar\omega_{j,m}}{2}\frac{1+e^{-\beta\hbar\omega_{j,m}}}{1-e^{-\beta\hbar\omega_{j,m}}}$$ (B5)

$$-\left(g\frac{(1-Z_j^{\text{int}}Z_j^{\text{coup}})}{2t\sqrt{\beta}Z_j}\left\{\sum_{\tau=1}^{t}\frac{\bar{\omega}_{j,\tau}\sqrt{2\pi I_{j,\tau}}}{M_{j,\tau}}\frac{\text{sech}^2\left(\bar{\omega}_{j,\tau}\sqrt{2\pi I_{j,\tau}\beta/M_{j,\tau}}\right)}{\tanh\left(\bar{\omega}_{j,\tau}\sqrt{2\pi I_{j,\tau}\beta/M_{j,\tau}}\right)}\right\}\right)$$

$$\left.\left.+\sum_{\tau=1}^{t}\left(\frac{I_{j,\tau}\bar{\omega}_{j,\tau}^2}{M_{j,\tau}^2}-\frac{1}{2\beta}-\frac{I_{j,\tau}\bar{\omega}_{j,\tau}^2}{M_{j,\tau}^2}\frac{I_1(\beta I_{j,\tau}\bar{\omega}_{j,\tau}^2/M_{j,\tau}^2)}{I_0(\beta I_{j,\tau}\bar{\omega}_{j,\tau}^2/M_{j,\tau}^2)}\right)\right\}\right.$$

Note that the ZPE corresponding to the MS-AS partition function is the same as for the MS-HO method, i.e.,

$$E_0^{\text{MS-HO}} = \min_{j}\left\{E_{j,0}^{\text{HO}}+U_j\right\}$$ (B6)

where $E_{j,0}^{\text{HO}}$ is the harmonic oscillator zero-point energy of structure j with the zero of energy at its local minimum, and which is given by

$$E_{j,0}^{\text{HO}} = \frac{\hbar}{2}\sum_{m=1}^{F}\omega_{j,m}$$ (B7)

Appendix C

In this appendix, three alternative versions of the MS-AS method are presented; they are labeled MS-AS(I), MS-AS(S), and MS-AS(M).

MS-AS(I). An alternative method similar to prior work[13, 14] would be

$$f_{j,\tau}^{(I)} = \frac{\sigma_\tau}{M_{j,\tau}}\frac{q_{\tau;j}^{\text{MC-HO}}}{q_{j,\tau}^{\text{QHO}}}\tanh\left(\frac{q_{j,\tau}^{\text{FR}}}{q_{\tau;j}^{\text{MC-I}}}\right)$$ (C1)

where

$$q_{\tau;j}^{\text{MC-I}} = \sum_{i=1}^{M_{j,\tau}/\sigma_\tau}\exp\left(-\beta[U_i-U_j]\right)q_{i,\tau}^{\text{CHO}}$$ (C2)

$$q_{\tau;j}^{\text{MC}-\text{HO}} = \sum_{i=1}^{M_{j,\tau}/\sigma_\tau} \exp\left(-\beta\left[U_i - U_j\right]\right)q_{i\tau}^{\text{HO}} \tag{C3}$$

and where the sums in eqns (C2) and (C3) runs over only the minima connected to minimum j by torsion τ. However, in practice this scheme may be difficult to apply because it requires the user to identify which minima are generated by a specified torsion. Therefore, we will instead consider two simple approaches that do not have this requirement.

MS-AS(S). A simple conformation-specific interpolation function similar to those advocated previously[13] may be used to obtain correct high and low temperature limits, yielding

$$f_{j,\tau}^{(S)} = \tanh\left(\frac{\dfrac{\sigma_\tau}{M_{j,\tau}}q_{j,\tau}^{\text{FR}}}{q_{j,\tau}^{\text{CHO}}}\right) \tag{C4}$$

MS-AS(M). An alternative approach would be to seek a correction factor of the form

$$f_{j,\tau}^{(M)} = \tanh\left(\frac{N'q_{j,\tau}^{\text{FR}}}{q_\tau^{\text{MS-CHO}}}\right) \tag{C5}$$

where

$$q_\tau^{\text{MS}-\text{CHO}} = \sum_{j=1}^{J} \exp\left(-\beta U_j\right)q_{j,\tau}^{\text{CHO}} \tag{C6}$$

and where N' is chosen to get a reasonable high-temperature limit. This may be accomplished by choosing

$$N' = N^{1/t} \tag{C7}$$

where

$$N = \frac{\displaystyle\prod_{\tau=1}^{t}\sum_{j=1}^{J}e^{-\beta U_j}q_{j,\tau}^{\text{CHO}}}{\displaystyle\sum_{j=1}^{J}e^{-\beta U_j}\prod_{\tau=1}^{t}q_{j,\tau}^{\text{CHO}}} = \frac{\displaystyle\prod_{\tau=1}^{t}q_\tau^{\text{MS-CHO}}}{\displaystyle\sum_{j=1}^{J}e^{-\beta U_j}\prod_{\tau=1}^{t}q_{j,\tau}^{\text{CHO}}} \tag{C8}$$

160

Results. Partition functions calculated by the last two alternative versions for the two 1-D models and for ethanol and 1-pentyl radical are tabulated in Tables S1 to S5 of the electronic supporting information. Figs. A1–A4 plot the ratio of the partition function calculated by the multi-structural approximations to that calculated by the multi-structural HO approximation for the 1-D models, ethanol, and 1-pentyl radical. Unlike the MS-AS and MS-ASCB results, the MS-AS(S) and MS-AS(M) results are always below the MS-HO result. They agree well with the MS-HO results at low T and with the MS-AS and MS-ASCB results in the high-temperature limit. The MS-AS(M) scheme leads to every torsion approaching the free-rotor limit at the same rate, which is unnecessarily restrictive. While the MS-AS(S) scheme performs adequately, the MS-AS scheme has the potential to lead to superior results at intermediate temperatures; as a consequence, these alternative schemes are not recommended for future use.

Appendix D

Previous papers[13, 14] presented several methods that use normal mode substitution treat each torsion separately by using various schemes, e.g., CO, RPG, SPRG, and TES, and treat the other vibrational degrees of freedom based on information from one structure. Because these methods all need to identify each torsion with one of the normal modes, they are not applicable to the molecules considered here. For the systems studied in this paper, 1-pentyl radical and 1-butanol have torsional modes that are coupled with each other and with low frequency bending modes, and in ethanol the two torsional motions are completely mixed in the two lowest normal modes. Table 14 illustrates the use of the CO, SRPG, RPG, and TES approximations for ethanol where the calculations are performed by assigning the lowest normal mode frequency to C–C torsion and the second lowest normal mode frequency to C–O torsion. The normal-mode torsional frequencies and internal moment of inertial used in the CO method are calculated for each conformer instead of using an averaged value as advocated previously,[13] and the RPG method implemented here uses an effective barrier height that is taken as the average of the left and right barriers rather than that obtained using eqn (13). The TES

values were obtained by fitting 40 points along each torsion to a 10-term Fourier cosine series.

Comparison of the results in Table 14 to the MS-ASCB results in Table 7 shows that for 400 K and above there is excellent agreement of the TES results, very good agreement of the SRPG results, and good agreement of RPG results; the agreement deteriorate at lower temperatures. However, there is no straightforward way to assign the torsions to individual normal modes for 1-butanol or 1-pentyl radical, and so these methods are not generally applicable.

References

1   R. P. Feynman and A. R. Hibbs, *Quantum Mechanics and Path Integrals*; McGraw-Hill, New York, 1965.

2   R. P. Feynman, *Statistical Mechanics*; Benjamin, Reading, MA, 1972.

3   V. A. Lynch, S. L. Mielke and D. G. Truhlar, *J. Chem. Phys.*, 2004, **121**, 5148.

4   V. A. Lynch, S. L. Mielke and D. G. Truhlar, *J. Phys. Chem. A*, 2005, **109**, 10092; 2006, **110**, 5965(E).

5   S. Chempath, C. Predescu and A. T. Bell, *J. Chem. Phys.*, 2006, **124**, 234101.

6   D. R. Herschbach, *J. Chem. Phys.*, 1959, **31**, 91.

7   D. G. Truhlar, *J. Comput. Chem.*, 1991, **12**, 266.

8   J. Gang, M. J. Pilling and S. H. Robertson, *J. Chem. Soc. Faraday Trans.*, 1996, **92**, 3509.

9   A. L. L. East and L. Radom, *J. Chem. Phys.*, 1997, **106**, 6655.

10   R. B. McClurg, R. C. Flagan and W. A. Goddard, III, *J. Chem. Phys.*, 1997, **106**, 6675; 1999, **111**, 7165(E).

11   W. Witschel and C. Hartwigsen, *Chem. Phys. Lett.*, 1997, **273**, 304.

12   P. Y. Ayala and H. B. Schlegel, *J. Chem. Phys.*, 1998, **108**, 2314.

13   Y.-Y. Chuang and D. G. Truhlar, *J. Chem. Phys.*, 2000, **112**, 1221; 2004, **121**, 7036(E); 2006, **124**, 179903(E).

14   B. A. Ellingson, V. A. Lynch, S. L. Mielke and D. G. Truhlar, *J. Chem. Phys.*, 2006, **125**, 084305.

15   A. C. P. Bitencourt, M. Ragni, G. S. Maciel, V. Aquilanti and F. V. Prudente, *J. Chem. Phys.*, 2008, **129**, 154316.

16   S. Sharma, S. Raman and W. H. Green, *J. Phys. Chem. A*, 2010, **114**, 5689.

17   D. Gruzman, A. Karton and J. M. L. Martin, *J. Phys. Chem. A*, 2009, **113**, 11974.

18   T. H. Lay, L. N. Krasnoperov, C. A. Venanzi, J. W. Bozzelli and N. V. Shokhirev, *J. Phys. Chem.*, 1996, **100**, 8240.

19   T. Yamada, T. H. Lay and J. W. Bozzelli, *J. Phys. Chem. A*, 1998, **102**, 7286.

20   T. Yamada, J. W. Bozzelli and R. J. Berry, *J. Phys. Chem. A*, 1999, **103**, 5602.

21   K. S. Pitzer and W. D. Gwinn, *J. Chem. Phys.*, 1942, **10**, 428.

22   B. M. Wong and W. H. Green, *Mol. Phys.*, 2005, **103**, 1027.

23   T. F. Miller, III and D. C. Clary, *J. Chem. Phys.*, 2002, **116**, 8262.

24   V. Van Speybroeck, D. V. Neck and M. Waroquier, *J. Phys. Chem. A*, 2002, **106**, 8945.

25   P. Vansteenkiste, D. Van Neck, V. Van Speybroeck and M. Waroquier, *J. Chem. Phys.*, 2006, **124**, 044314.

26   D. A. McQuarrie, *Statistical Mechanics* Ed.; Harper & Row, New York, 1973.

27   T. F. Miller, III and D. C. Clary, *Mol. Phys.*, 2005, **103**, 1573

28   M. Tafipolsky and R. Schmid, *J. Comput. Chem.*, 2005, **26**, 1579.

29   Y. K. Sturdy and D. C. Clary, *Phys. Chem. Chem. Phys.*, 2007, **9**, 2397.

30   S. W. Benson, *Thermochemical Kinetics*, 2nd; Wiley-Interscience, New York, 1976.

31   H. E. O'Neal and S. W. Benson, *Int. J. Chem. Kinet.*, 1969, **1**, 221.

32   H. E. O'Neal and S. W. Benson, in *Free Radicals*, ed. J. H. Koshi, Wiley, New York, 1973, pp. 275.

33   N. Cohen, *J. Phys. Chem.*, 1992, **96**, 9052.

34   T. H. Lay, J. W. Bozzelli, A. M. Dean and E. R. Ritter, *J. Phys. Chem.*, 1995, **99**, 14514.

35   K. K. Irikura, in *Computational Thermochemistry*, ed. K. K. Irikura and D. J. Frurip, ACS Symposium Series Vol. 677, 1998, pp. 402.

36   V. Van Speybroeck, R. Ganib and R. J. Meier, *Chem. Soc. Rev.*, 2010, **39**, 1764.

37   K. S. Pitzer, *J. Chem. Phys.*, 1940, **8**, 711.

38   W. J. Taylor, *J. Chem. Phys.*, 1948, **16**, 257.

39   P. J. Flory and R. L. Jernigan, *J. Chem. Phys.*, 1965, **42**, 3509.

40   R. A. Scott and H. A. Scheraga, *J. Chem. Phys.*, 1966, **44**, 3054.

41   R. Janoschek and J. Kalcher, *Anorg. Allg. Chem.*, 2002, **628**, 2724.

42   G. L. Dirichlet, *J. Reine Angew. Math.*, 1850, **40**, 209.

43   G. Voronoi, *J. Reine Angew. Math.*, 1907, **133**, 97.

44   F. Aurenhammer, *ACM Computing Surveys*, 1991, **23**, 345.

45   G. Katzer and A. F. Sax, *J. Comput. Chem.*, 2005, **26**, 1438.

46   K. S. Pitzer, *J. Chem. Phys.*, 1946, **14**, 239.

47   J. E. Kilpatrick and K. S. Pitzer, *J. Chem. Phys.*, 1949, **17**, 1064.

48   T. Miyazawa and K. Fukushima, *J. Mol. Spectrosc.*, 1965, **15**, 308.

49   H. Bonadeo, E. D'Alessio and E. Silberman, *J. Mol. Spectrosc.*, 1967, **22**, 402.

50   G. Keresztury, A.-Y. Wang and J. R. Durig, *Spectrochimica Acta A*, 1992, **48**, 199.

51   G. Tasi, F. Mizukami, I. Palinko, J. Csontos, W. Gyorffy, P. Nair, K. Maeda, M. Toba, S.-i. Niwa, Y. Kiyozumi and I. Kiricsi, *J. Phys. Chem. A*, 1998, **102**, 7698.

52   D. Bond, *J. Phys. Chem. A*, 2008, **112**, 1656.

53   P. Pulay, *Mol. Phys.*, 1969, **17**, 197.

54   G. Fogarasi and P. Pulay, *Molecular Vibrational Spectra and Structure*, Ed.; Elsevier, Amsterdam, 1985.

55   C. F. Jackels, Z. Gu and D. G. Truhlar, *J. Chem. Phys.*, 1995, **102**, 3188.

56   K. A. Nguyen, C. F. Jackels and D. G. Truhlar, *J. Chem. Phys.*, 1996, **104**, 6491.

57   Y.-Y. Chuang and D. G. Truhlar, *J. Chem. Phys.*, 1997, **107**, 83.

58   E. B. Wilson, Jr., J. C. Decius and P. C. Cross, *Molecular Vibrations*, Ed.; McGraw-Hill, New York, 1955.

59   C.-L. Huang, C.-L. Liu, C.-K. Ni and J. T. Hougen, *J. Mol. Spectrosc.*, 2005, **233**, 122.

60   V. Hanninen and L. Halonen, *J. Chem. Phys.*, 2007, **126**, 064309.

61   G. Katzer and A. F. Sax, *Chem. Phys. Lett.*, 2003, **368**, 473.

62   K. L. Clarkson, K. Mehlhorn and R. Seidel, *Lect. Notes Comput. Sci.*, 1992, **577**, 463.

63   A program for convex hulls, http://www.netlib.org/voronoi/hull.html

64   Y. Zhao and D. G. Truhlar, *Theor. Chem. Acc.* , 2008, **120**, 215.

65   B. J. Lynch, P. L. Fast, M. Harris and D. G. Truhlar, *J. Phys. Chem. A*, 2000, **104**, 4811.

66   R. Krishnan, J. S. Binkley, R. Seeger and J. A. Pople, *J. Chem. Phys.*, 1980, **72**, 650.

67   T. Clark, J. Chandrasekhar, G. W. Spitznagel and P. v. R. Schleyer, *J. Comput. Chem.*, 1983, **4**, 294.

68   M. J. Frisch, G. W. Trucks, H. B. Schlegel, G. E. Scuseria, M. A. Robb, J. R. Cheeseman, G. Scalmani, V. Barone, B. Mennucci, G. A. Petersson, H. Nakatsuji, M. Caricato, X. Li, H. P. Hratchian, A. F. Izmaylov, J. Bloino, G. Zheng, J. L. Sonnenberg, M. Hada, M. Ehara, K. Toyota, R. Fukuda, J. Hasegawa, M. Ishida, T. Nakajima, Y. Honda, O. Kitao, H. Nakai, T. Vreven, J. A. Montgomery, Jr., J. E. Peralta, F. Ogliaro, M. Bearpark, J. J. Heyd, E. Brothers, K. N. Kudin, V. N. Staroverov, R. Kobayashi, J. Normand, K. Raghavachari, A. Rendell, J. C. Burant, S. S. Iyengar, J. Tomasi, M. Cossi, N. Rega, N. J. Millam, M. Klene, J. E. Knox, J. B. Cross, V. Bakken, C. Adamo, J. Jaramillo, R. E. Gomperts, O. Stratmann, A. J. Yazyev, R. Austin, C. Cammi, J. W. Pomelli, R. Ochterski, R. L. Martin, K. Morokuma, V. G. Zakrzewski, G. A. Voth, P. Salvador, J. J. Dannenberg, S. Dapprich, A. D. Daniels, O. Farkas, J. B. Foresman, J. V. Ortiz, J. Cioslowski and D. J. Fox, *Gaussian 09*, Gaussian Inc., Wallingford CT, Revision A.02, 2009.

69   I. M. Alecu, J. Zheng, Y. Zhao and D. G. Truhlar, *J. Chem. Theory Comput.*, 2010, **6**, 2872.

70   S. W. Benson, F. R. Cruickshank, D. M. Golden, G. R. Haugen, H. E. O'Neal, A. S. Rodgers, R. Shaw and R. Walsh, *Chem. Rev.*, 1969, **69**, 279.

71   J. Koput, S. Carter and N. C. Handy, *J. Phys. Chem. A*, 1998, **102**, 6325.

72   K. Ohno, H. Yoshida, H. Watanabe, T. Fujita and H. Matsuura, *J. Phys. Chem.*, 1994, **98**, 6924.

73   J. Moc, J. M. Simmie and H. J. Curran, *J. Mol. Struct.*, 2009, **928**, 149.

74   L. V. Gurvich, I. V. Veyts and C. B. Alcock, *Thermodynamic Properties of Individual Substances*, 4th, Ed.; Hemisphere Pub. Co., New York, 1989.

75   J. F. Counsell, J. L. Hales and J. F. Martin, *Trans. Faraday Soc.*, 1965, **61**, 1869.

76   E. Hirota, *J. Chem. Phys.*, 1958, **28**, 839.

77   R. M. Lees, *J. Chem. Phys.*, 1973, **59**, 2690.

78   R. Meyer, *J. Mol. Spectrosc.*, 1979, **76**, 266.

79   G. A. Guirgis, J. B. A. Barton and J. R. Durig, *J. Chem. Phys.*, 1983, **79**, 5918.

80   J. A. Kunc, *Mol. Phys.*, 2003, **101**, 413.

81   C. Y. Lin, E. I. Izgorodina and M. L. Coote, *J. Phys. Chem. A*, 2008, **112**, 1956.

Table 1 Normal-mode frequencies (cm^{-1}) calculated by M06-2X/6-311+G(2df,2p) accompanied various integration grids

Grids					
Ethanol (structure: E–t), 3 lowest frequencies					
Ultrafine[a]	224	269	423		
(99,590)[b]	224	268	423		
(99,770)[b]	247	292	423		
(99,974)[b]	238	278	422		
(96,32,64)[c]	236	275	423		
1-Pentyl radical (structure: P–stt), 5 lowest frequencies					
Ultrafine[a]	53i	84	126	225	287
(99,590)[b]	75	85	127	225	287
(99,770)[b]	64	85	128	228	287
(99,974)[b]	76	87	129	228	287
(120,974)[b]	75	87	129	228	287
(150,974)[b]	75	87	129	229	287
(96,32,64)[c]	71	87	128	228	287

[a] Ultrafine denotes the pruned (99,590) grid provided in the *Gaussian09* package.

[b] The first number indicates the number of radial quadrature nodes, and the second denotes the number of Lebedev angular quadrature nodes.

[c] A spherical product grid with the first number specifying the number of radial quadrature nodes and the next two specifying the numbers of angular quadrature nodes

Table 2 Notation for torsion angles[a]

	Abbreviation	dihedral angle range (deg)
antiperiplanar	a^+	[140, 163]
	a^-	[−163, −140]
gauche for 1-pentyl	g^+	[55, 80]
	g^-	[−80, −55]
or		
gauche for 1-butanol	g^+	[57, 76]
	g^-	[−76, −57]
cross for 1-butanol only	x^+	[80, 90]
	x^-	[-90, -80]
syn for 1-pentyl only	s	[80, 100] or [−100, −80]
trans	t	[−173, −180] and [180, 173]

[a]The dihedral angles used for torsions are $H–O–C^{(1)}–C^{(2)}$, $O–C^{(1)}–C^{(2)}–C^{(3)}$, and $C^{(1)}–C^{(2)}–C^{(3)}–C^{(4)}$ for 1-butanol, $H–C^{(1)}–C^{(2)}–C^{(3)}$, $C^{(1)}–C^{(2)}–C^{(3)}–C^{(4)}$, and $C^{(2)}–C^{(3)}–C^{(4)}–C^{(5)}$ for 1-pentyl, and H–O–C–C and O–C–C–H for ethanol.

Table 3. Calculated partition functions and their percentage errors compared to TES values for the 1-D model potential of eqn (48)

T (K)	MS-HO		MS-AS		MS-ASCB		TES
	q	% error	q	% error	q	% error	q
60	0.4776	−17	0.5247	−9	0.5356	−7	0.5751
100	1.083	−14	1.236	−2	1.229	−3	1.266
150	1.935	−10	2.174	1	2.132	−1	2.159
200	2.863	−5	3.078	2	3.006	−1	3.025
300	4.848	5	4.703	2	4.596	−0	4.600
400	6.922	16	6.106	2	5.983	0	5.979
600	11.18	35	8.447	2	8.315	0	8.303
1000	19.87	67	12.06	1	11.93	0	11.92
1500	30.83	100	15.55	1	15.44	0	15.42
2000	41.82	128	18.43	1	18.33	0	18.31
2400	50.62	149	20.46	1	20.36	0	20.34
3000	63.83	177	23.17	0	23.08	0	23.07
4000	85.87	218	27.11	0	27.03	0	27.02
7000	152.0	318	36.48	0	36.42	0	36.41
50000	1100	1007	99.43	0	99.40	0	99.40

Table 4. Percentage errors of various methods compared to TES values for the torsion potential of eqn (48) when the shallow minimum on the model potential is ignored

T (K)	MS-HO	MS-AS
60	−20	−17
100	−24	−19
150	−28	−20
200	−30	−20
300	−29	−17
400	−27	−15
600	−21	−11
1000	−8	−7
1500	7	−5
2000	20	−4
2400	30	−3
3000	43	−3
4000	63	−2
7000	111	−1
50000	453	−0

Table 5. Calculated partition functions and their percentage errors compared to TES values for the 1-D model potential of H_2O_2.

T (K)	MS-HO		MS-AS		MS-ASCB		TES
	q	% error	q	% error	q	% error	q
60	0.02036	−34	0.02061	−33	0.01999	−35	0.03071
100	0.1281	−23	0.1308	−21	0.1281	−23	0.1654
150	0.3276	−18	0.3386	−15.	0.3364	−16	0.3990
200	0.5395	−16	0.5656	−12	0.5655	−12	0.6442
300	0.9509	−15	1.03	−8	1.018	−9	1.116
400	1.345	−14	1.501	−3	1.443	−7	1.555
600	2.105	−11	2.443	4	2.223	−6	2.359
1000	3.588	−5	4.199	11	3.616	−5	3.787
1500	5.419	1	6.089	13	5.187	−4	5.383
2000	7.244	6	7.707	13	6.621	−3	6.827
2400	8.701	10	8.856	12	7.684	−3	7.893
3000	10.88	16	10.4	11	9.158	−2	9.366
4000	14.52	26	12.63	9	11.35	−2	11.56
7000	25.43	51	17.86	6	16.65	−1	16.83
50000	181.7	255	51.67	1	51.08	−0	51.17

Table 6. Information used for the ethanol partition function calculations using the MS-AS and MS-ASCB methods[a]

Torsion	$\bar{\omega}$	W^b	W^L	W^R	I	M	P
Structure E–t ($U_1 = 0$)							
C–O	258.7	328.9	385.7	385.7	0.7456	3	3
C–C	253.9	1108.6	1108.7	1108.7	2.610	3	1
Structure E–g$^+$ & E–g$^-$ ($U_2 = U_3 = 27.4$ cm^{-1})							
C–O	278.5	379.0	358.6	372.0	0.7416	3	3
C–C	264.5	1206.2	1194.9	1194.9	2.616	3	1

[a] The units are cm^{-1} for the barrier heights and frequencies and amu Å^2 for the internal moments of inertia.

[b] W is used in the MS-AS method and is calculated by eqn (13).

173

Table 7. Calculated conformational-rovibrational partition function of ethanol using multi-structural methods

T (K)	MS-HO	MS-AS	MS-ASCB
100	4.12E-104	4.47E-104	4.37E-104
150	5.45E-68	6.21E-68	6.08E-68
200	8.13E-50	9.64E-50	9.46E-50
300	1.95E-31	2.43E-31	2.39E-31
400	4.77E-22	6.06E-22	6.00E-22
600	2.94E-12	3.73E-12	3.70E-12
1000	1.62E-03	1.90E-03	1.89E-03
1500	3.60E+02	3.65E+02	3.65E+02
2000	7.76E+05	6.84E+05	6.83E+05
2400	7.65E+07	6.06E+07	6.06E+07
3000	1.74E+10	1.19E+10	1.19E+10
4000	1.56E+13	8.67E+12	8.67E+12
7000	6.07E+18	2.15E+18	2.15E+18
50000	1.13E+38	6.34E+36	6.34E+36

Table 8. Information used for the 1-pentyl radical partition function using the multi-structural method[a]

Torsion	$\bar{\omega}$	I	W^b	M	P	W^b	M	P	W^b	M	P
			NS:SC=2:2			NS:SC=1:3			NS:SC=4:0		
Structure P–a⁻g⁺t & P–a⁺g⁻t ($U = 0$)											
C(1)–C(2) 133	1.714		281	2.53	1.27	254	2.67	1.33	451	2	1
C(2)–C(3) 142	10.91		2047	2.53	2.53	1846	2.67	2.67	1458	3	3
C(3)–C(4) 99	15.98		1040	3	3	1316	2.67	2.67	1040	3	3
C(4)–C(5) 228	2.917		998	3	1	998	3	1	998	3	1
Structure P–a⁻g⁺g⁺ & P–a⁺g⁻g⁻ ($U = 27.0\ cm^{-1}$)											
C(1)–C(2) 161	1.713		426	2.48	1.24	380	2.63	1.31	654	2	1
C(2)–C(3) 131	17.09		2819	2.48	2.48	2512	2.63	2.63	1924	3	3
C(3)–C(4) 108	18.38		1418	3	3	1852	2.63	2.63	1418	3	3
C(4)–C(5) 247	3.054		1228	3	1	1228	3	1	1228	3	1
Structure P-a⁻g⁺g⁻ & P–a⁺g⁻g⁺ ($U = 349.4\ cm^{-1}$)											
C(1)–C(2) 157	1.713		382	2.56	1.28	336	2.73	1.36	625	2	1
C(2)–C(3) 132	15.88		2521	2.56	2.56	2216	2.73	2.73	1831	3	3
C(3)–C(4) 110	14.79		1188	3	3	1437	2.73	2.73	1188	3	3
C(4)–C(5) 254	3.057		1297	3	1	1297	3	1	1297	3	1
Structure P–a⁺tg⁺ & P–a⁻tg⁻ ($U = 229.8\ cm^{-1}$)											
C(1)–C(2) 126	1.670		81	4.40	2.20	107	3.84	1.92	44	6	3
C(2)–C(3) 110	14.45		533	4.40	4.40	698	3.84	3.84	1146	3	3
C(3)–C(4) 125	11.48		1177	3	3	717	3.84	3.84	1177	3	3
C(4)–C(5) 229	3.039		1049	3	1	1048	3	1	1049	3	1

Structure P–a$^+$tt & P–a$^-$tt ($U = 73.8$ cm^{-1})

C(1)–C(2)	118	1.661	76	4.28	2.14	94	3.82	1.91	38	6	3
C(2)–C(3)	119	11.40	523	4.28	4.28	655	3.82	3.82	1063	3	3
C(3)–C(4)	117	11.91	1079	3	3	664	3.82	3.82	1079	3	3
C(4)–C(5)	227	2.871	976	3	1	976	3	1	976	3	1

Structure P–a$^+$tg$^-$ & P–a$^-$tg$^+$ ($U = 257.4$ cm^{-1})

C(1)–C(2)	109	1.668	64	4.30	2.15	81	3.82	1.91	33	6	3
C(2)–C(3)	107	14.518	536	4.30	4.30	679	3.82	3.82	1098	3	3
C(3)–C(4)	123	11.34	1135	3	3	701	3.82	3.82	1135	3	3
C(4)–C(5)	228	3.040	1041	3	1	1041	3	1	1041	3	1

Structure P–stg$^+$ & P–stg$^-$ ($U = 294.9$ cm^{-1})

C(1)–C(2)	103	1.670	82	3.57	1.79	92	3.36	1.68	29	6	3
C(2)–C(3)	109	15.34	845	3.57	3.57	954	3.36	3.36	1196	3	3
C(3)–C(4)	124	11.53	1161	3	3	925	3.36	3.36	1161	3	3
C(4)–C(5)	229	3.039	1051	3	1	1051	3	1	1051	3	1

Structure P–stt ($U = 124.6$ cm^{-1})

C$^{(1)}$–C$^{(2)}$	108	1.650	90	3.56	1.78	100	3.39	1.69	32	6	3
C$^{(2)}$–C$^{(3)}$	121	11.88	816	3.56	3.56	901	3.39	3.39	1150	3	3
C$^{(3)}$–C$^{(4)}$	116	11.96	1068	3	3	837	3.39	3.39	1068	3	3
C$^{(4)}$–C$^{(5)}$	232	2.878	1024	3	1	1024	3	1	1024	3	1

---

[a] The units are cm^{-1} for barrier heights and frequencies and amu Å^2 for internal moments of inertia.

[b] W is used in the MS-AS method and is calculated by eqn (13).

Table 9. Calculated conformational-rovibrational partition function of 1-pentyl radical using multi-structural methods

T (K)	MS-HO	MS-AS			MS-RS
		$2:2^a$	$1:3^a$	$4:0^a$	
100	5.11E-190	6.02E-190	6.10E-190	5.53E-190	6.32E-190
150	1.83E-124	2.22E-124	2.27E-124	1.93E-124	2.09E-124
200	2.04E-91	2.50E-91	2.59E-91	2.11E-91	2.16E-91
300	6.69E-58	8.22E-58	8.61E-58	6.72E-58	6.45E-58
400	1.05E-40	1.28E-40	1.35E-40	1.04E-40	9.66E-41
600	1.14E-22	1.34E-22	1.42E-22	1.12E-22	1.01E-22
1000	2.20E-06	2.21E-06	2.31E-06	1.97E-06	1.78E-06
1500	2.74E+04	2.13E+04	2.20E+04	1.99E+04	1.82E+04
2000	6.18E+10	3.71E+10	3.81E+10	3.56E+10	3.29E+10
2400	4.06E+14	2.01E+14	2.05E+14	1.95E+14	1.82E+14
3000	1.37E+19	5.17E+18	5.27E+18	5.07E+18	4.78E+18
4000	6.57E+24	1.69E+24	1.71E+24	1.67E+24	1.59E+24
7000	4.08E+35	4.37E+34	4.40E+34	4.35E+34	4.22E+34
50000	7.38E+72	1.98E+70	1.98E+70	1.97E+70	1.96E+70

^{a}NS:SC

Table 10. Information used for the 1-butanol conformational-rovibrational partition function using multi-structural methods[a]

Torsion	$\bar{\omega}$	I	W^b	M	P	W^b	M	P
			NS:SC=1:3			27-structures, NS:SC=4:0		
Structure B–ttt ($U = 16.6$ cm^{-1})								
$O^{(1)}$–$C^{(1)}$	244	0.763	281	3.10	3.10	300	3	3
$C^{(1)}$–$C^{(2)}$	122	10.800	989	3.10	3.10	1057	3	3
$C^{(2)}$–$C^{(3)}$	112	11.391	881	3.10	3.10	942	3	3
$C^{(4)}$–$C^{(5)}$	231	2.832	995	3	1	995	3	1
Structure B–ttg$^+$ & B–ttg$^-$ ($U = 329.5$ cm^{-1})								
$O^{(1)}$–$C^{(1)}$	250	0.755	307	3.02	3.02	310	3	3
$C^{(1)}$–$C^{(2)}$	107	13.624	1012	3.02	3.02	1023	3	3
$C^{(2)}$–$C^{(3)}$	119	10.829	1000	3.02	3.02	1010	3	3
$C^{(4)}$–$C^{(5)}$	218	3.001	944	3	1	944	3	1
Structure B–tg$^+$t & B–tg$^-$t ($U = 0.0$ cm^{-1})								
$O^{(1)}$–$C^{(1)}$	243	0.759	273	3.12	3.12	296	3	3
$C^{(1)}$–$C^{(2)}$	143	10.368	1284	3.12	3.12	1391	3	3
$C^{(2)}$–$C^{(3)}$	98	15.608	914	3.12	3.12	990	3	3
$C^{(4)}$–$C^{(5)}$	229	2.879	994	3	1	994	3	3
Structure B–tg$^+$g$^+$ & B–tg$^-$g$^-$ ($U = 229.9$ cm^{-1})								
$O^{(1)}$–$C^{(1)}$	247	0.766	320	2.94	2.94	308	3	3
$C^{(1)}$–$C^{(2)}$	114	16.178	1433	2.94	2.94	1378	3	3
$C^{(2)}$–$C^{(3)}$	91	17.732	1008	2.94	2.94	970	3	3
$C^{(4)}$–$C^{(5)}$	220	3.007	960	3	1	960	3	1

Structure B–tg$^+$g$^-$ & B–tg$^-$g$^+$ ($U = 605.4$cm^{-1})

O$^{(1)}$–C$^{(1)}$	259	0.757	326	3.04	3.04	335	3	3
C$^{(1)}$–C$^{(2)}$	124	13.514	1345	3.04	3.04	1379	3	3
C$^{(2)}$–C$^{(3)}$	105	15.789	1116	3.04	3.04	1145	3	3
C$^{(4)}$–C$^{(5)}$	223	3.030	989	3	1	989	3	1

Structure B–g$^+$tt & B–g$^-$tt ($U = 16.1$cm^{-1})

O$^{(1)}$–C$^{(1)}$	261	0.757	320	3.09	3.09	340	3	3
C$^{(1)}$–C$^{(2)}$	128	10.938	1105	3.09	3.09	1176	3	3
C$^{(2)}$–C$^{(3)}$	112	11.538	889	3.09	3.09	946	3	3
C$^{(4)}$–C$^{(5)}$	231	2.833	1000	3	1	1000	3	1

Structure B–g$^+$tg$^+$ & B–g$^-$tg$^-$ ($U = 359.0$ cm^{-1})

O$^{(1)}$–C$^{(1)}$	252	0.760	301	3.08	3.08	318	3	3
C$^{(1)}$–C$^{(2)}$	110	13.915	1040	3.08	3.08	1100	3	3
C$^{(2)}$–C$^{(3)}$	118	10.981	949	3.08	3.08	1004	3	3
C$^{(4)}$–C$^{(5)}$	217	3.001	933	3	1	933	3	1

Structure B–g$^+$tg$^-$ & B–g$^-$tg$^+$ ($U = 314.4$ cm^{-1})

O$^{(1)}$–C$^{(1)}$	265	0.770	356	3.00	3.00	357	3	3
C$^{(1)}$–C$^{(2)}$	112	13.886	1146	3.00	3.00	1149	3	3
C$^{(2)}$–C$^{(3)}$	119	11.012	1019	3.00	3.00	1022	3	3
C$^{(4)}$–C$^{(5)}$	217	3.003	934	3	1	934	3	1

Structure B–g$^+$g$^+$t & B–g$^-$g$^-$t ($U = 40.6$ cm^{-1})

O$^{(1)}$–C$^{(1)}$	261	0.786	345	3.03	3.03	354	3	3
C$^{(1)}$–C$^{(2)}$	146	10.378	1415	3.03	3.03	1448	3	3
C$^{(2)}$–C$^{(3)}$	96	15.648	924	3.03	3.03	946	3	3
C$^{(4)}$–C$^{(5)}$	230	2.882	1000	3	1	1000	3	1

Structure B–$g^+g^+g^+$ & B-$g^-g^-g^-$ ($U = 251.2$ cm^{-1})

$O^{(1)}$–$C^{(1)}$	264	0.783	382	2.91	2.91	359	3	3
$C^{(1)}$–$C^{(2)}$	114	16.244	1471	2.91	2.91	1381	3	3
$C^{(2)}$–$C^{(3)}$	89	17.861	991	2.91	2.91	930	3	3
$C^{(4)}$–$C^{(5)}$	220	3.008	961	3	1	961	3	1

Structure B–$g^+g^+g^-$ & B-$g^-g^-g^+$ ($U = 598.4$ cm^{-1})

$O^{(1)}$–$C^{(1)}$	259	0.790	355	3.00	3.00	349	3	3
$C^{(1)}$–$C^{(2)}$	128	13.858	1514	3.00	3.00	1491	3	3
$C^{(2)}$–$C^{(3)}$	105	15.615	1154	3.00	3.00	1136	3	3
$C^{(4)}$–$C^{(5)}$	236	3.031	1113	3	1	1113	3	1

Structure B–$g^+x^-g^+$ & B-$g^-x^+g^-$ ($U = 770.4$ cm^{-1})

$O^{(1)}$–$C^{(1)}$	260	0.770	272	3.37	3.37	343	3	3
$C^{(1)}$–$C^{(2)}$	149	15.428	1785	3.37	3.37	2253	3	3
$C^{(2)}$–$C^{(3)}$	112	13.917	904	3.37	3.37	1141	3	3
$C^{(4)}$–$C^{(5)}$	284	3.021	1603	3	1	1603	3	1

Structure B–g^+g^-t & B–g^-g^+t ($U = 70.6$ cm^{-1})

$O^{(1)}$–$C^{(1)}$	254	0.767	301	3.12	3.12	326	3	3
$C^{(1)}$–$C^{(2)}$	140	10.435	1253	3.12	3.12	1355	3	3
$C^{(2)}$–$C^{(3)}$	101	15.489	966	3.12	3.12	1045	3	3
$C^{(4)}$–$C^{(5)}$	230	2.876	999	3	1	999	3	1

Structure B–$g^+g^-g^-$ & B–$g^-g^+g^+$ ($U = 343.7$ cm^{-1})

$O^{(1)}$–$C^{(1)}$	237	0.766	293	2.96	2.96	285	3	3
$C^{(1)}$–$C^{(2)}$	112	16.267	1379	2.96	2.96	1342	3	3
$C^{(2)}$–$C^{(3)}$	95	17.744	1094	2.96	2.96	1065	3	3
$C^{(4)}$–$C^{(5)}$	219	3.006	947	3	1	947	3	1

Structure B–g$^+$g$^-$x$^+$ & B–g$^-$g$^+$x$^-$ ($U = 911.5$ cm^{-1})

O$^{(1)}$–C$^{(1)}$	272	0.783	271	3.55	3.55
C$^{(1)}$–C$^{(2)}$	115	12.330	761	3.55	3.55
C$^{(2)}$–C$^{(3)}$	117	17.289	1110	3.55	3.55
C$^{(4)}$–C$^{(5)}$	202	3.012	810	3	1

[a] The units are cm^{-1} for barrier heights and frequencies and amu Å^2 for internal moments of inertia.

[b] W is used in the MS-AS method and is calculated by eqn (13).

Table 11. Calculated conformational-rovibrational partition function of 1-butanol using multi-structural methods

T (K)	MS-HO	MS-AS		MS-RS[a]
		$NS:SC=4:0$[b]	$NS:SC=1:3$	
100	1.09E-179	1.24E-179	1.25E-179	1.10E-179
150	1.28E-117	1.57E-117	1.58E-117	1.43E-117
200	2.44E-86	3.17E-86	3.20E-86	2.95E-86
300	1.25E-54	1.79E-54	1.80E-54	1.69E-54
400	2.24E-38	3.44E-38	3.48E-38	3.31E-38
600	2.39E-21	3.91E-21	3.98E-21	3.85E-21
1000	5.18E-06	7.99E-06	8.20E-06	8.12E-06
1500	1.55E+04	1.94E+04	1.99E+04	2.01E+04
2000	1.38E+10	1.35E+10	1.39E+10	1.41E+10
2400	5.11E+13	4.15E+13	4.27E+13	4.35E+13
3000	8.66E+17	5.39E+17	5.53E+17	5.65E+17
4000	1.74E+23	7.32E+22	7.49E+22	7.68E+22
7000	2.01E+33	3.49E+32	3.55E+32	3.65E+32
50000	1.00E+68	4.29E+65	4.31E+65	4.42E+65

[a]The reference structure is taken as B–$tg^{+}t$.

[b]Using only 27 structures, see text for further details.

Table 12. Standard state entropy (in cal mol^{-1} K^{-1}) calculated using SS-HO, MS-HO, and MS-AS partition functions and group additivity method[a]

T (K)	SS-HO	MS-HO	MS-AS	GA	Ref. data
ethanol					
298.15	64.79	66.85	67.47	67.10	67.31[b]
400	69.96	72.02	72.59	72.17	
600	79.26	81.33	81.68	81.16	
1000	94.99	97.06	96.85	96.28	
1-butanol					
298.15	80.04	85.97	87.17[c]	85.94	86.8[d]
400	88.54	94.78	96.07[c]	94.65	
600	104.25	110.77	111.86[c]	110.22	
1000	131.29	138.00	138.14[c]	136.48	
1-pentyl radical					
298.15	83.75	89.08	89.48[e]	86.32	
				88.48[f]	
				88.13[g]	
400	93.04	98.54	98.87[e]	95.86	
				97.87[f]	
				97.40[g]	
600	110.09	115.71	115.71[e]	112.64	
				114.55[f]	
				114.02[g]	
1000	139.20	144.88	143.95[e]	141.08	
				143.06[f]	
				142.21[g]	
1500	167.96	173.64	171.62[e]	169.22	
				171.50[f]	

[a]The SS-HO calculations only account the contribution from the global minimum and all the vibrational modes (including torsional modes) are approximated as harmonic oscillator (J, Z_j, and $f_{j,\tau}$ are all equal to 1). All the calculated entropies include electronic and translational contributions. Frequencies used in the calculations are all scaled (see text for details). The calculations by GA method use the parameters in ref.[30] except those in footnote f and g.
[b]From Ref. [74]
[c]The data are calculated using NS:SC = 3:1.
[d]Experimental data from ref.[75]
[e]The data are calculated using NS:SC = 2:2.
[f]The parameters used in the calculations were taken from Cohen[33].
[g]The parameters used in the GA calculations were taken from Lay et al[34].

Table 13. The calculated correction factors Z^{int} and Z^{coup} for structures of ethanol, 1-butanol, and 1-pentyl radical

Structure	Z^{int}	Z^{coup}	Structure	Z^{int}	Z^{coup}
ethanol			1-butanol		
E–t	0.954	1.000	B–ttt	0.920	0.937
E–g⁺/E–g⁻	0.974	0.993	B–ttg⁺/B–ttg⁻	0.790	0.962
			B–tg⁺t/B–tg⁻t	0.886	0.941
1-pentyl radical			B–tg⁺g⁺/B–tg⁻g⁻	1.024	0.758
P–a⁻g⁺t⁻/P–a⁺g⁻t⁺	0.834	0.935	B–tg⁺g⁻/B–tg⁻g⁺	0.642	0.948
P–a⁻g⁺g⁺/P–a⁺g⁻g⁻	1.115	0.737	B–g⁺tt/B–g⁻tt	0.912	0.938
P–a⁻g⁺g⁻/P–a⁺g⁻g⁺	0.721	0.928	B–g⁺tg⁺/B–g⁻tg⁻	0.789	0.954
P–a⁺g⁺g⁺/P–a⁻g⁻g⁻	0.785	0.944	B–g⁺tg⁻/B–g⁻tg⁺	0.818	0.946
P–a⁺tt/P–a⁻tt	0.866	0.935	B–g⁺g⁺t/B–g⁻g⁻t	0.922	0.909
P–a⁺tg⁻/P–a⁻tg⁺	0.700	0.945	B–g⁺g⁺g⁺/B–g⁻g⁻g⁻	1.027	0.744
P–stg⁺/P–stg⁻	0.608	0.938	B–g⁺g⁺g⁻/B–g⁻g⁻g⁺	0.770	0.908
P–stt	0.783	0.933	B–g⁺x⁻g⁺/B–g⁻x⁺g⁻	0.716	0.917
			B–g⁺g⁻t/B–g⁻g⁺t	0.868	0.936
			B–g⁺g⁻g⁻/B–g⁻g⁺g⁺	1.020	0.759
			B- g⁺g⁻x⁺/B–g⁻g⁺x⁻	0.554	0.934

Table 14. Partition function of ethanol calculated by various approximations[a]

T (K)	CO	SRPG	RPG	TES
100	4.30E-104	5.77E-104	6.80E-104	7.03E-104
150	5.64E-68	7.79E-68	8.74E-68	8.54E-68
200	8.38E-50	1.16E-49	1.29E-49	1.25E-49
300	1.99E-31	2.77E-31	3.02E-31	2.95E-31
400	4.78E-22	6.71E-22	7.25E-22	7.13E-22
600	2.82E-12	3.96E-12	4.21E-12	4.22E-12
1000	1.40E-03	1.94E-03	2.02E-03	2.05E-03
1500	2.74E+02	3.66E+02	3.77E+02	3.84E+02
2000	5.26E+05	6.76E+05	6.93E+05	7.07E+05
2400	4.72E+07	5.97E+07	6.08E+07	6.18E+07
3000	9.56E+09	1.17E+10	1.19E+10	1.21E+10
4000	7.14E+12	8.46E+12	8.54E+12	8.67E+12
7000	1.87E+18	2.09E+18	2.09E+18	2.12E+18
50000	6.04E+36	6.14E+36	6.14E+36	6.17E+36

[a]All the frequencies in the CO, SRPG, RPG calculations are scaled by a factor $\lambda = 0.970$ for M06-2X/6-311+G(2df,2p) method,[69] and λ^2 is used to scale the 1-D potentials used in TES calculations.
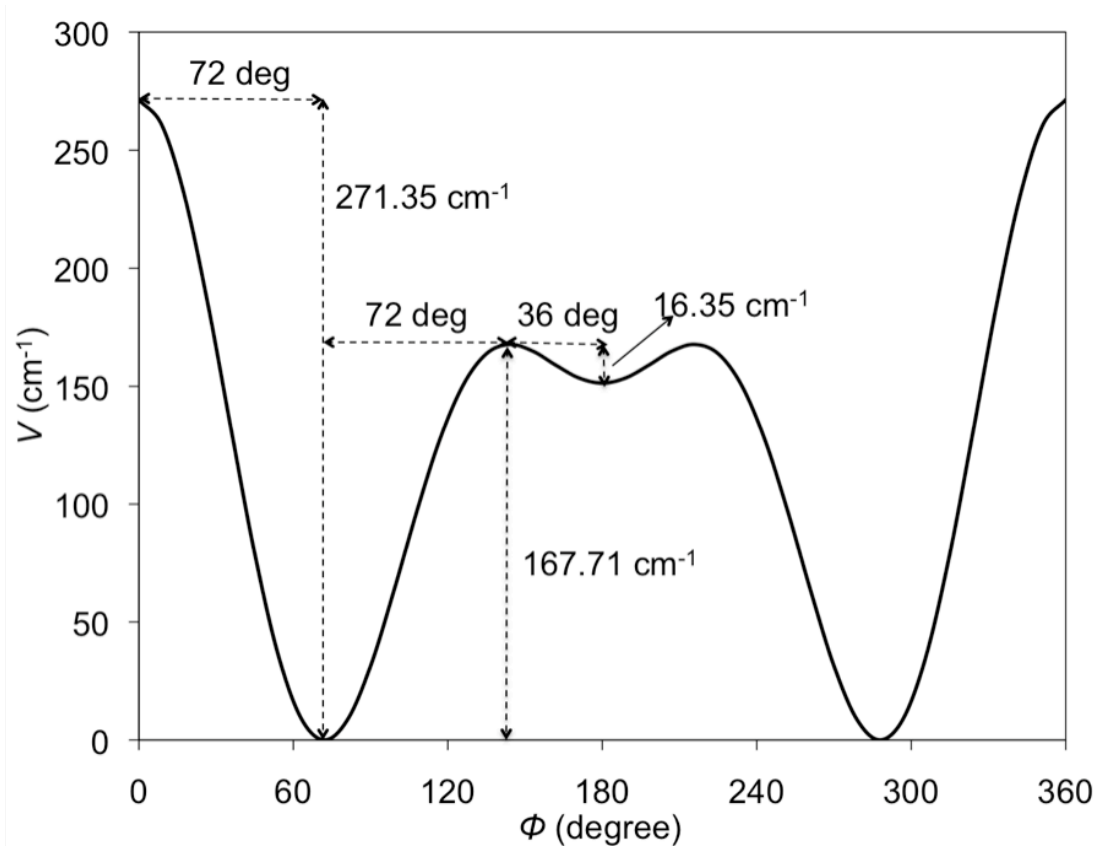
Fig. 1. A model potential (eqn (48)) representing a torsional motion.
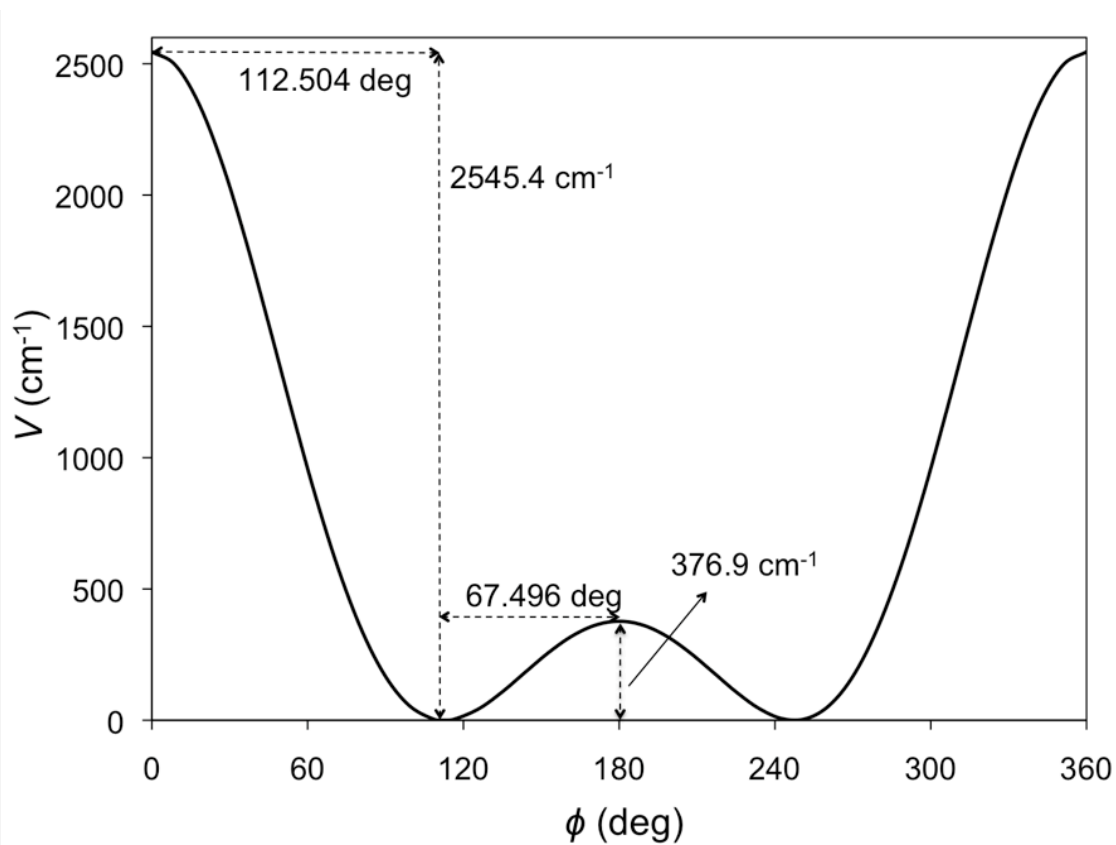
Fig. 2 The potential energy curve (eqn (49)) of the 1-D torsional motion in H_2O_2
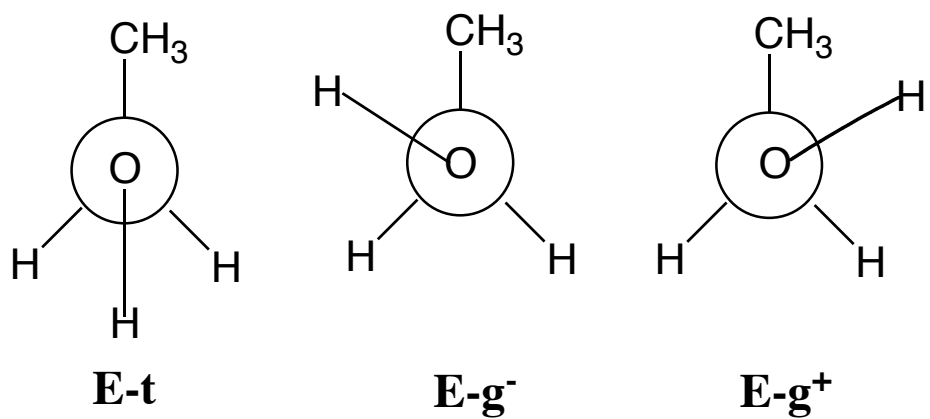
Fig. 3. Newman projections of the three structures of ethanol. Structure E–t is the global minimum and structures E–g⁻ and E–g⁺ are isoenergetic but distinguishable. Note that E denotes ethanol, t denotes trans, and g denotes gauche.
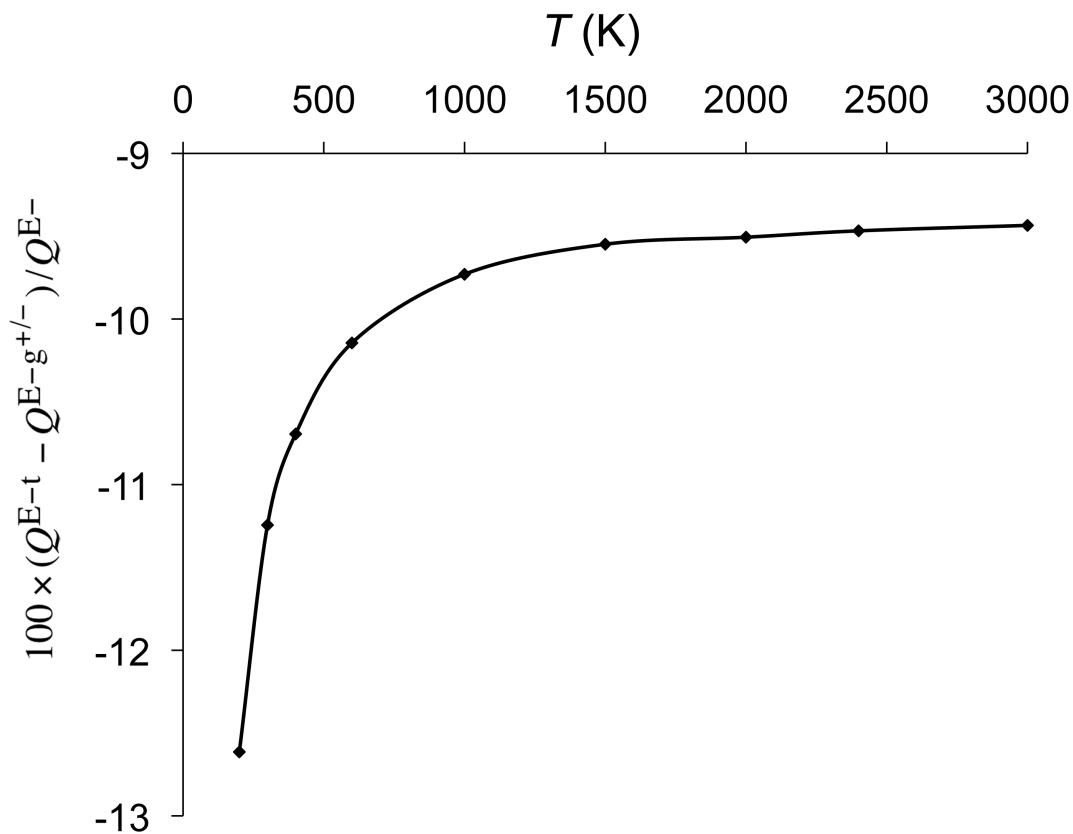
Fig. 4. Percentage difference between partition functions of structures E–t and E–g⁻ (or E–g⁺) using the harmonic approximation. The zero of energy is at each structure's local minimum.
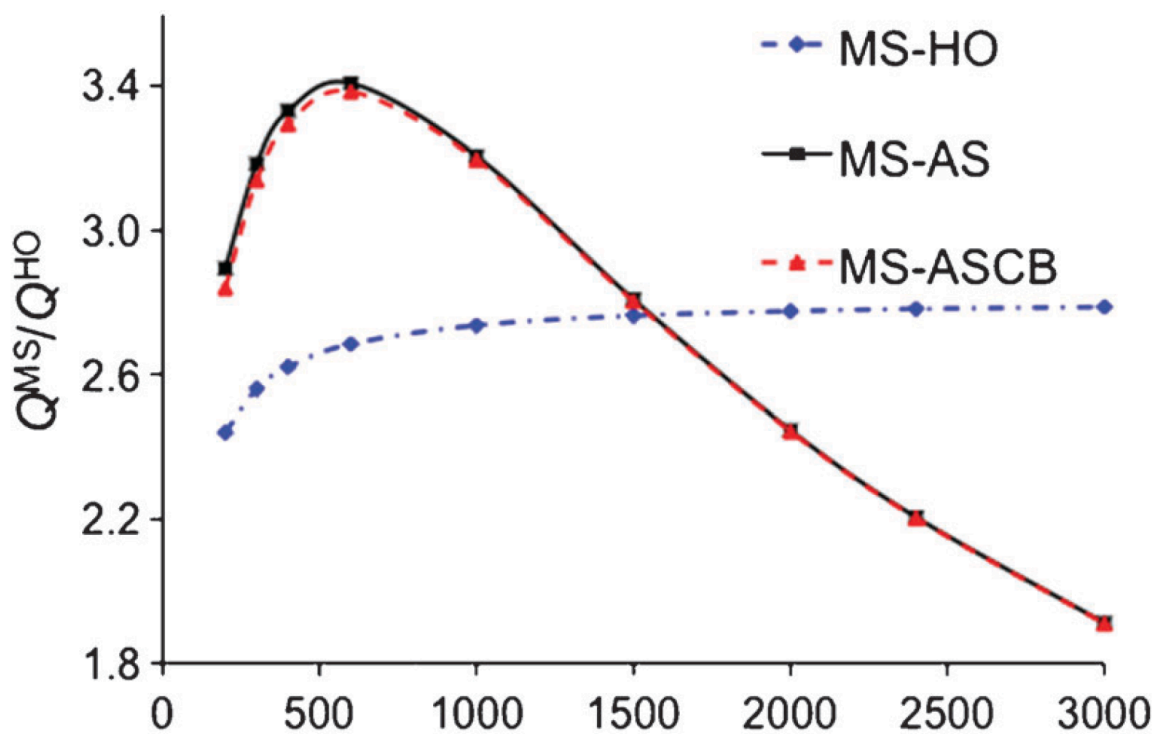
Fig. 5 Ratio of the rovibrational partition function of ethanol calculated by multi-structural methods to that calculated by the single-structure HO approximation at the global minimum.
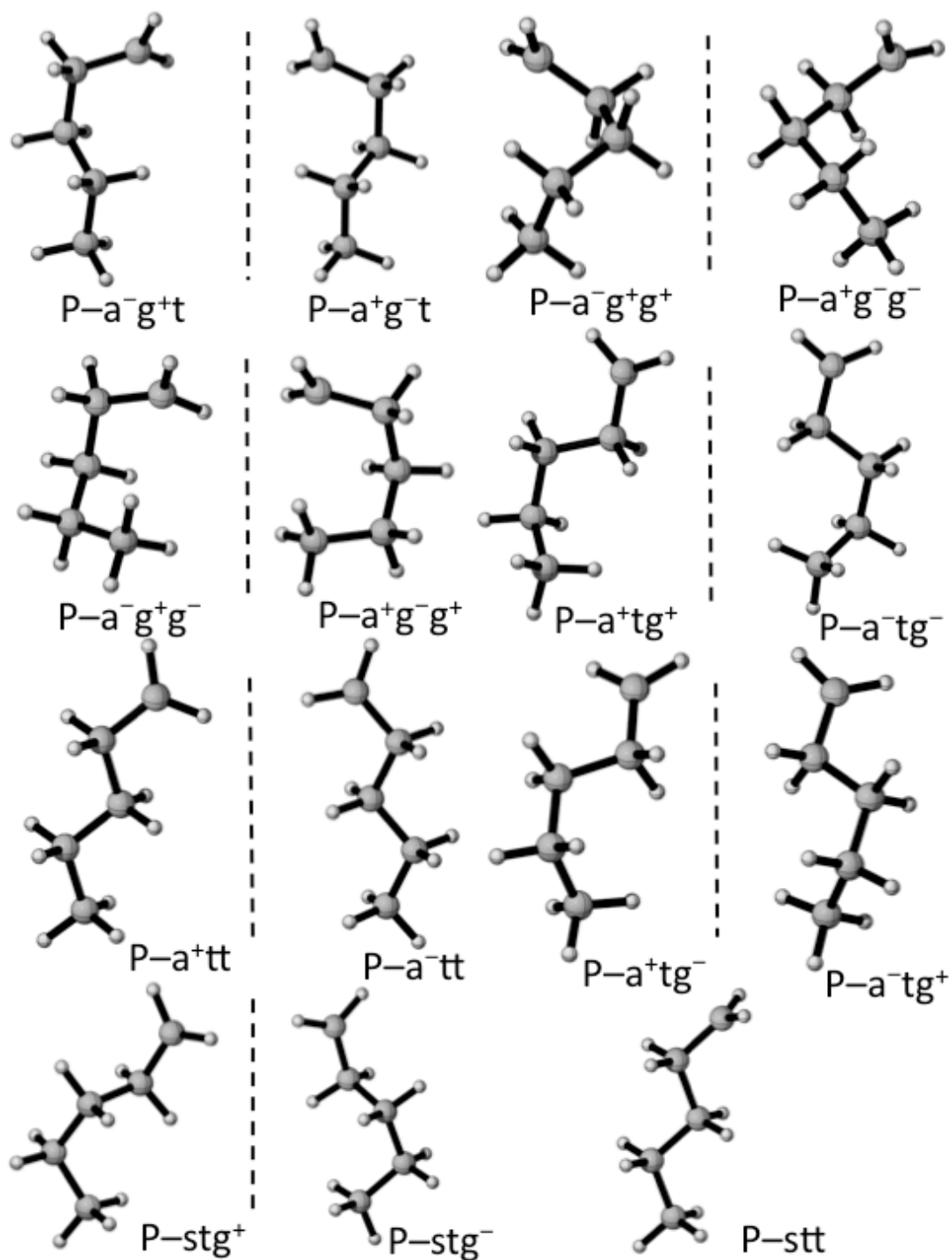
Fig. 6. Fifteen structures of the 1-pentyl radical. Structures separated by a dashed vertical line are mirror images, e.g., P–a⁻g⁺t and P–a⁺g⁻t.
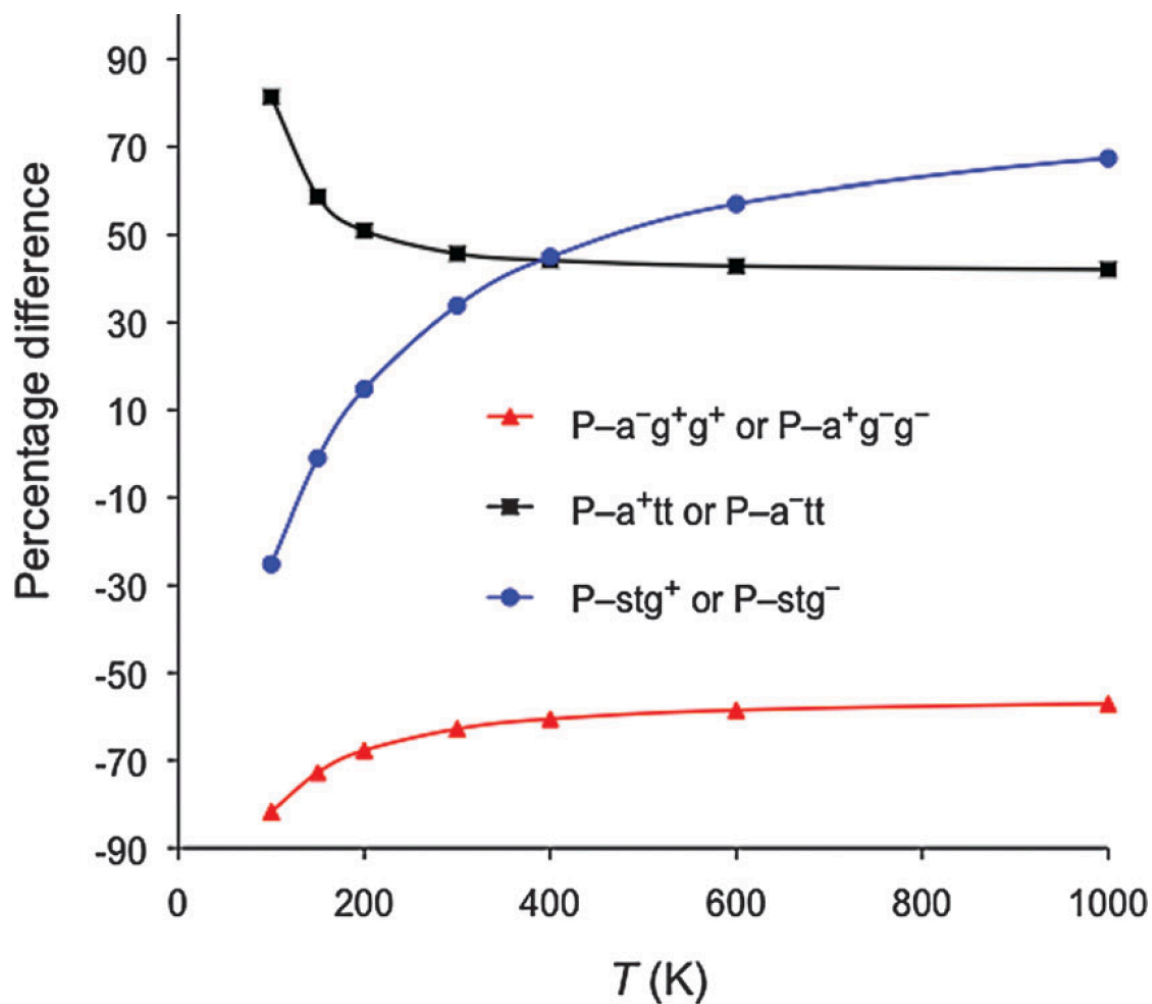
Fig. 7. Percentage difference between harmonic oscillator partition functions of the global minimum structure and selected other structures of the 1-pentyl radical. The zero of energy is at each structure's local minimum. The three cases with the largest difference are presented in this figure.
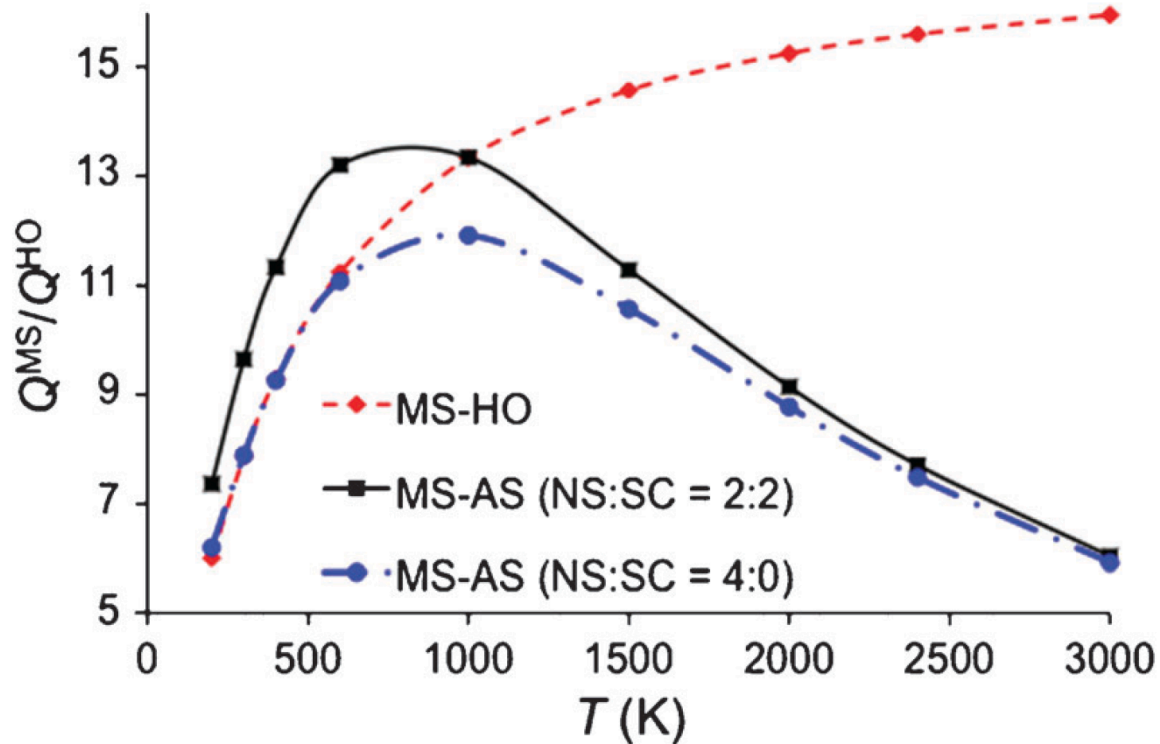
Fig. 8 Ratio of the partition function of the 1-pentyl radical calculated by multi-structural methods to that calculated by the single-structure HO approximation using the global minimum structure.
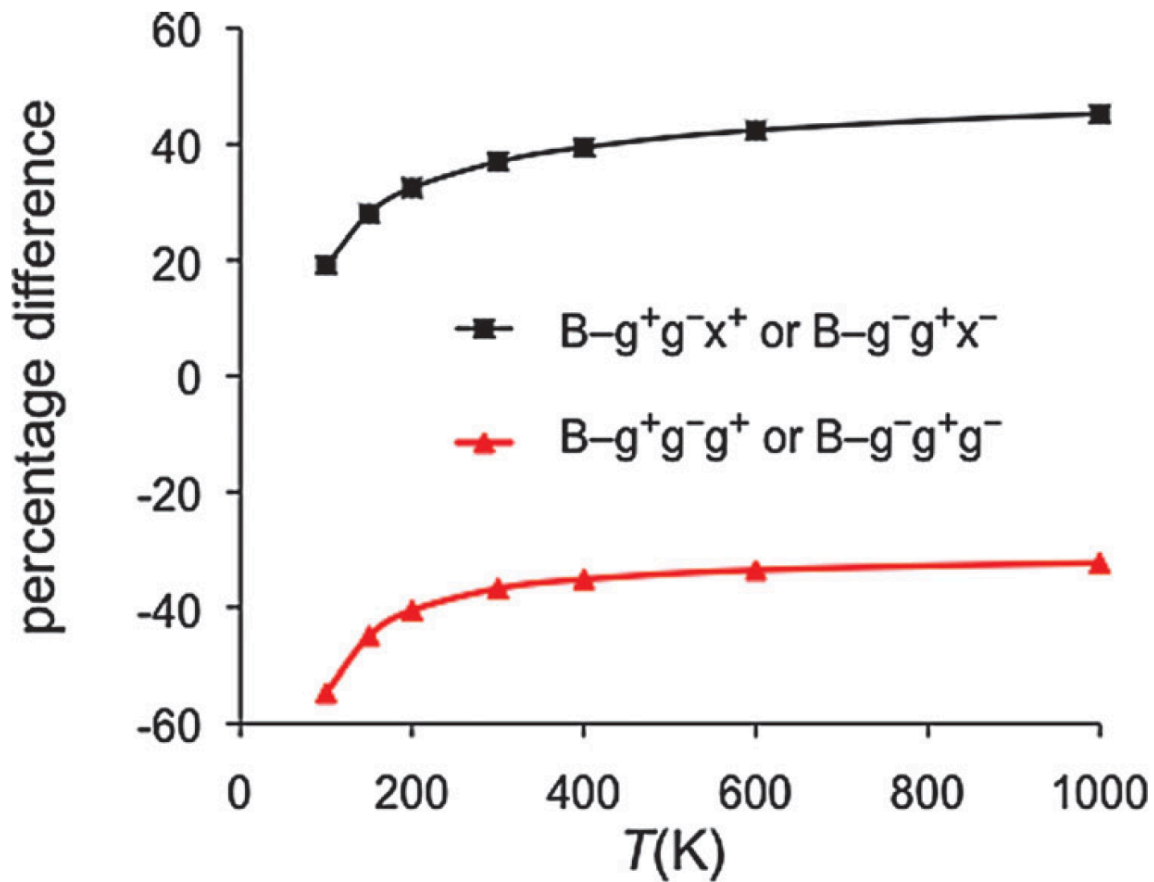
Fig. 9 Percentage difference between harmonic oscillator partition functions of selected 1- butanol structures and the harmonic oscillator partition functions of the global minimum. The zero of energy is at each structure's local minimum. The two cases with the largest differences are presented in this figure.
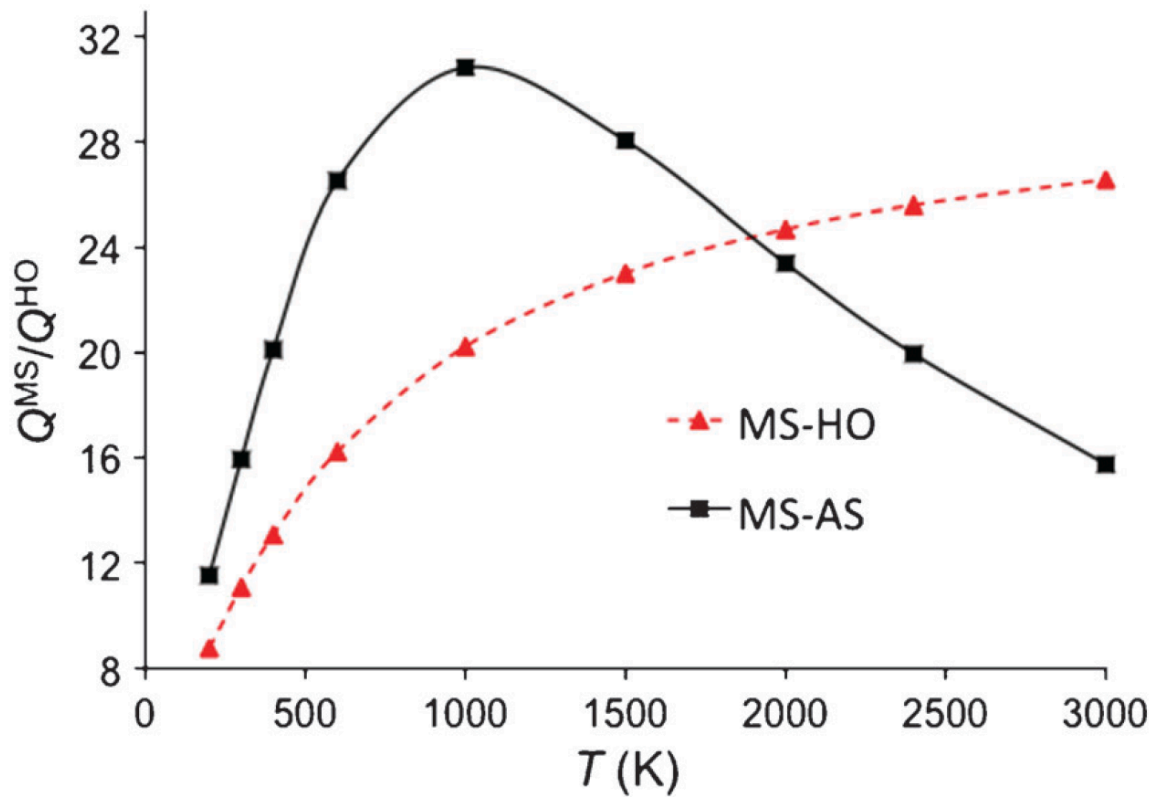
Fig. 10 Ratio of the partition function of 1-butanol calculated by multi-structural methods with NS:SC=1:3 to that calculated by the single-structure HO approximation at the global minimum.
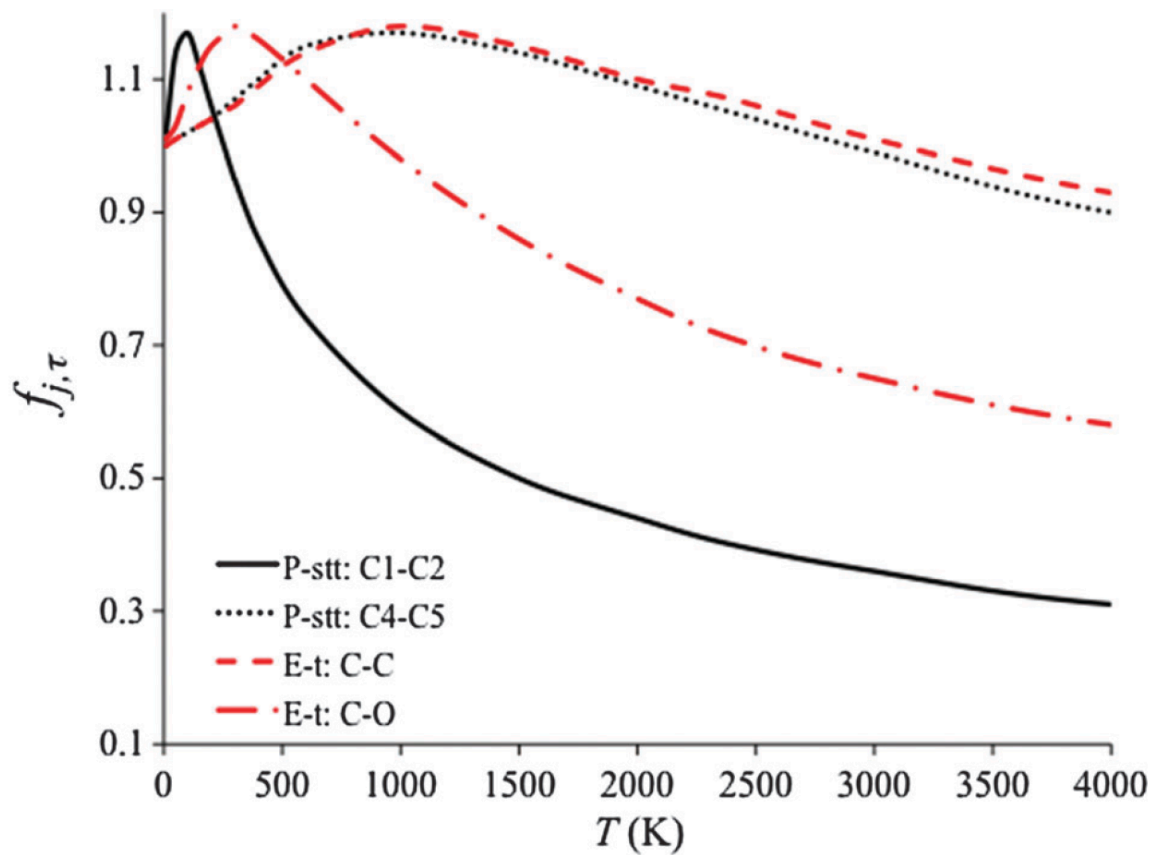
Fig. 11. Temperature dependence for the $f_{j,\tau}$ for several relevant cases.
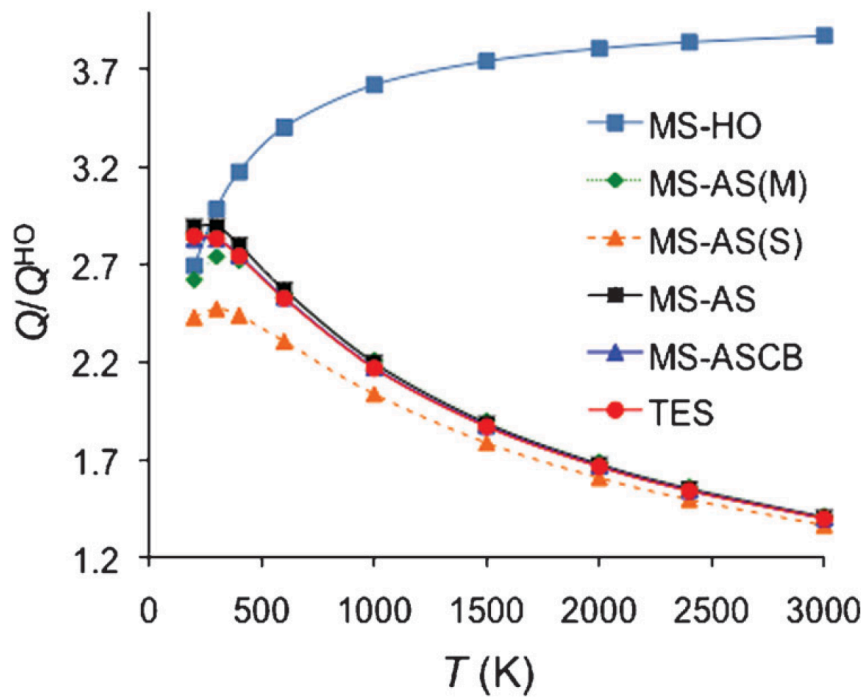
Fig. A1 Ratios of the partition function of the 1-D potential of eqn (48) calculated by multi-structural methods or the TES method to that calculated by the single-structural HO approximation at the global minimum.
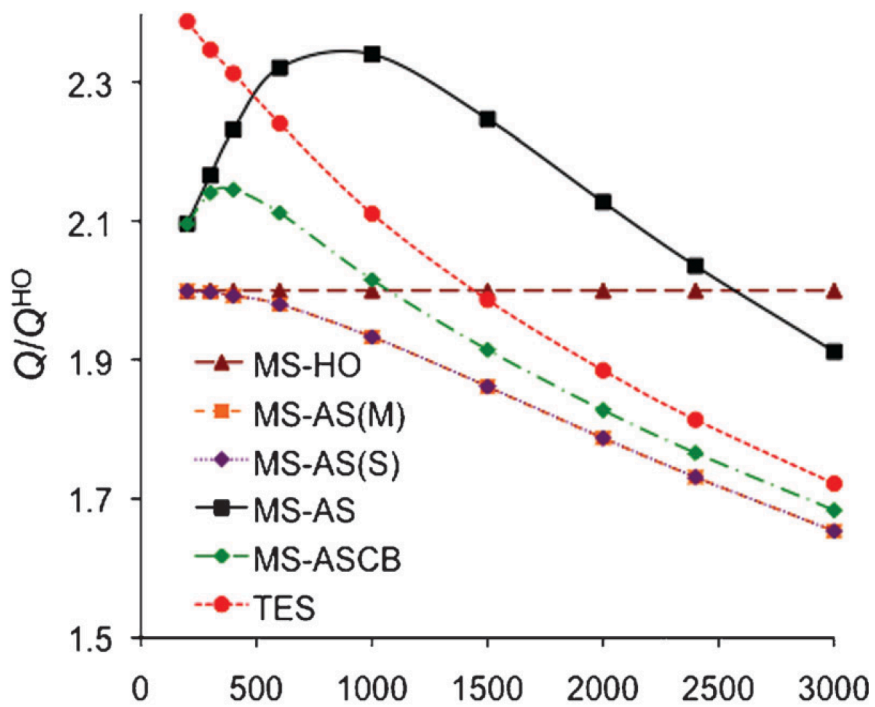
Fig. A2 Ratios of partition functions of the 1-D potential of H_2O_2 calculated by multi-structural methods or the TES method to those calculated by the single-structural HO approximation at the global minimum.
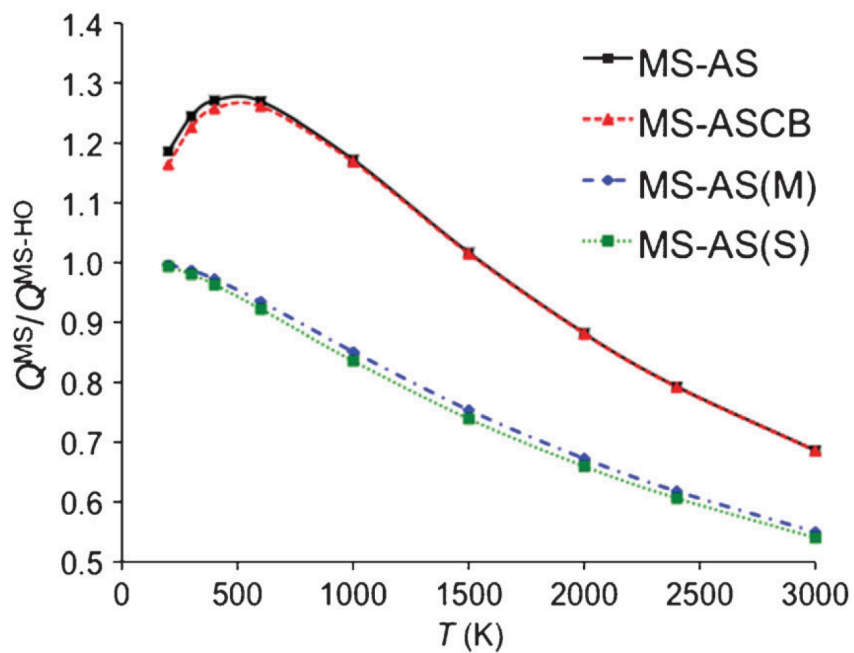
Fig. A3 Ratio of the partition functions for ethanol calculated by multi-structural methods including torsional anharmonicity to those calculated by the MS-HO approximation at the global minimum.
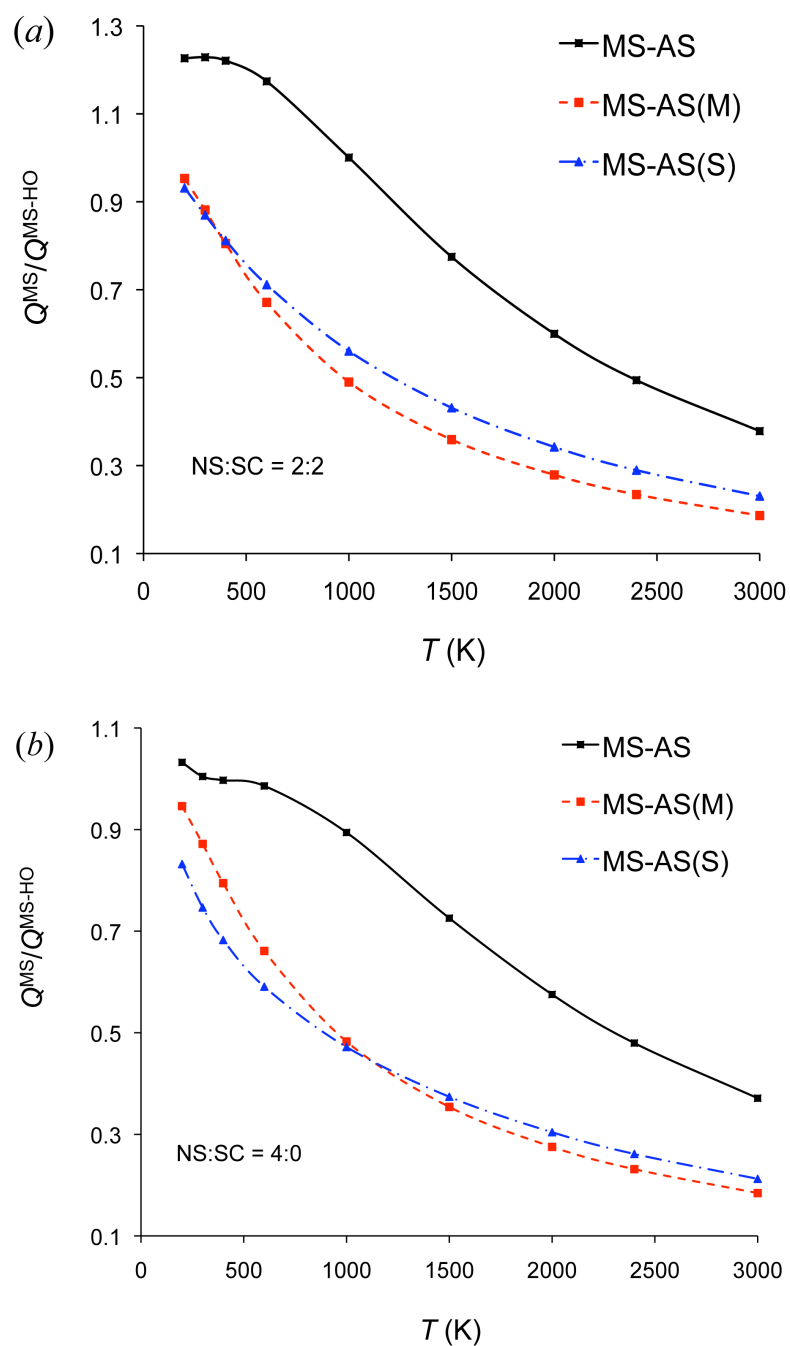
Fig. A4. Ratios of partition functions for 1-pentyl radical calculated by the multi-structural methods including torsional anharmonicity to those calculated by the MS-HO approximation. Note the calculations used $M_{j,\tau}$ parameters predicted by the scheme NS:SC = 2:2 for (*a*) and NS:SC = 4:0 for (*b*).

Chapter 7.   Statistical thermodynamics of 1-butanol, 2-methyl-1-propanol, and butanal

Prasenjit Seal, Ewa Papajak, Tao Yu, and Donald G. Truhlar

Department of Chemistry and Supercomputing Institute, University of Minnesota, Minneapolis, Minnesota 55455-0431

The purpose of the present investigation is to calculate partition functions and thermodynamic quantities, viz., entropy, enthalpy, heat capacity, and Gibbs free energies, for 1-butanol, 2-methyl-1-propanol, and butanal in the vapor phase. We employed the multi-structural (MS) anharmonicity method and electronic structure calculations including both explicitly correlated coupled cluster theory and density functional theory. The calculations are performed using all structures for each molecule and employing both the local harmonic approximation (MS-LH) and the inclusion of torsional anharmonicity (MS-T). The results obtained from the MS-T calculations are in excellent agreement with experimental data taken from the Thermodynamics Research Center data series and the *CRC Handbook of Chemistry and Physics*, where available. They are also compared with Benson's empirical group additivity values, where available; in most cases the present results are more accurate than the group additivity values. In other cases where experimental data (but not group additivity values) are available, we also obtain good agreement with experiment. This validates the accuracy of the electronic structure calculations when combined with the MS-T method for estimating the thermodynamic properties of systems with multiple torsions, and it increases our confidence in the predictions made with this method for molecules and temperatures where experimental or empirical data are not available.

I. INTRODUCTION

Butanol, 2-methyl-1-propanol, and butanal play important roles in alternative-fuel combustion.[1–5] Therefore accurate estimation of the thermodynamic properties of these systems is essential. One can, in favorable cases and for certain conditions, obtain these properties either experimentally or by a statistical mechanical approach. Since it is very difficult and often impossible to measure thermodynamic properties of substances for a wide range of temperature by experimental means, it is necessary to calculate them by employing reliable theoretical-methods, validated by experimental data. In the present article we consider four properties, entropy (S_T°), heat capacity ($C_P^\circ(T)$), enthalpy (H_T°), free energy (G_T°), that are needed to calculate thermal reaction rate constants and chemical equilibrium constants. We validate the method where experimental or empirical data is available, and we make predictions for the remaining cases.

Limited experimental data is available.[6-9] Parks[6] presented heat capacity and free energy data for crystalline and liquid *n*-butyl alcohol at low temperatures. Strömsöe *et al.*[8] reported vapor-phase heat capacity for various aliphatic alcohols including 1-butanol and 2-methyl-1-propanol; these heat capacities were measured in a flow calorimeter at atmospheric pressure in a temperature range of about 300–600 K. For butanal, Tjebbes[7] estimated the heats of combustion and heats of formation experimentally. Benson's empirical group additivity (GA) method[9] has widely been used by researchers to estimate thermodynamic quantities for systems with no available experimental results. The GA method is empirical and is based on fitting a limited number of experimental data for a limited number of systems. Its reliability and accuracy is questionable when applied to systems not contained in its training set, but the accuracy is high for cases for which it represents a convenient fit to available experimental data.

The recently developed internal-coordinate multi-structural (MS) approximation[10] can be used to compute partition functions and other thermodynamic quantities of systems with multiple structures and torsional (T) anharmonicity, and it has recently been applied successfully to hydrocarbons.[11,12] Other works on coupled torsions includes the work of Miller and Clary[13] and that of Waroquier and coworkers.[14] Miller and Clary

developed a torsional path integral Monte Carlo algorithm to calculate the conformational thermodynamics of molecules; their treatment provides a coupled, anharmonic description of the torsional contributions to the partition functions, a harmonic treatment of the other internal modes, and an *ab initio* description of the potential energy surface. Waroquier and coworkers developed an internal-coordinate scheme for coupling neighboring torsions.

The MS-T method developed in our group combines both MS anharmonicity and T anharmonicity. In the low-temperature limit, where the MS anharmonicity is most important, the MS-T method reduces to the local-harmonic (LH) approximation, while in the high-temperature limit, it gives the free-rotor result and thus includes the T anharmonicity effect. In this work, we have included anharmonicity in three ways:

1. Scaling of harmonic frequencies by empirical factors[15] that depend on the electronic model chemistry. This is done in order to reduce the error in zero-point energies, which are calculated by the LH approximation.
2. Using all structures for a particular system. The presence of multiple local minima on a potential energy surface is an anharmonic effect.
3. Inclusion of torsions and their coupling to one another and to overall rotation.

In the present study, we focus our attention on the determination of various thermodynamic properties of 1-butanol, 2-methyl-1-propanol, and butanal in the gas-phase. We employed three Minnesota density functionals, M06-2X,[16] M08-SO,[17] and M08-HX,[17] along with the explicitly correlated coupled-cluster (CC) wave function method in order to determine standard state entropies, heat capacities, enthalpies, and Gibbs free energies. Even at temperatures below the boiling point, all the calculations are performed for a pure ideal gas at a pressure of 1 bar. Molecular dissociation is not included.

II. COMPUTATIONAL DETAILS

The geometry optimizations and frequency calculations for 1-butanol were performed with M06-2X,[16] M08-HX,[17] and M08-SO[17] with the 6-311+G(2df,2p) basis set.[18] The 6-311+G(2df,2p) basis is the same as MG3S[19] for H, C and O, and we will use

the shorter name "MG3S". For 2-methyl-1-propanol, geometries and frequencies were calculated with M08-HX/MG3S, and for butanal they were calculated by M08-HX with the minimally augmented correlation-consistent triple-zeta basis set, i.e., maug-cc-pVTZ.[20] We also performed single-point calculations with the F12a explicit correlation extension of coupled cluster theory with single and double excitations and a quasiperturbative treatment of connected triple excitations (CCSD(T)-F12a)[21] and the jul-cc-pVTZ[20] basis sets for the one-electron part of the basis set.

All the density functional calculations were carried out with the *Gaussian 09*[22] suite of programs, and the CCSD(T)-F12a results were obtained using *Molpro*.[23] The density functional frequency calculations involve 99 radial shells and 974 angular points per shell and are scaled by standard scaling factors[15] of 0.970 for M06-2X/MG3S, 0.973 for M08-HX/MG3S, 0.983 for M08-SO/MG3S, and 0.976 for M08-HX/maug-cc-pVTZ.

The MS-T method for the partition functions and thermodynamic quantities takes into account all the conformational structures of a system and improves over the harmonic results by using torsional factors.[10] In the local harmonic (LH) approximation, the conformational-rotational-vibrational partition functions can be written as

$$
Q_{\text{con-rovib}}^{\text{MS-LH}} = \sum_{j=1}^{J} Q_{\text{rot},j} \exp\left(-\beta U_j\right) Q_j^{\text{HO}} \tag{1}
$$

where j labels a structure, J is the number of structures, the term "con" means conformational, "rovib" denotes rotational-vibrational, $Q_{\text{rot},j}$ is the rotational partition function of structure j, which includes the rotational symmetry number, σ_j, in the denominator, and Q_j^{HO} is the normal-mode local-harmonic-oscillator vibrational partition function calculated at structure j. Including the torsional factors in Eq. (1), the partition function becomes

$$
Q_{\text{con-rovib}}^{\text{MS-T}} = \sum_{j=1}^{J} Q_{\text{rot},j} \exp\left(-\beta U_j\right) Q_j^{\text{HO}} Z_j \prod_{\tau=1}^{t} f_{j,\tau} \tag{2}
$$

where Z_j is a factor that is designed to ensure that the MS-T approach reaches the high-temperature limit, $f_{j,\tau}$ is an internal-coordinate torsional anharmonicity function,

and τ is the torsional motion. The MS-T and MS-LH methods are implemented in the *MSTor* program.[24]

The total partition function is the product of the contributions of electronic, translational, and conformational-rotational-vibrational factors. From the partition function we can calculate entropy, heat capacity, enthalpy, and free energy using the *MSTor* program.[24]

III. RESULTS AND DISCUSSION

III.A. Structure and energetics of 1-butanol, 2-methyl-1-propanol, and butanal

The lowest-energy structures of 1-butanol, 2-methyl-1-propanol, and butanal are shown in Fig. 1. In 1-butanol, there are four torsions, namely O2–C3, C3–C4, C4–C5 and C5–C6. Of these, internal rotations around C5–C6 do not generate distinguishable conformers, and hence only the other three torsions, i.e., O2–C3, C3–C4, and C4–C5, produce structures that are distinguishable.

The naming convention for the structures is given in Table I. This table was prepared following the IUPAC convention[25] with slight modifications. We introduced "g±" and "a±" ranges to be "(±75, ±90)" and "(±90, ±105)", respectively. The density functional calculations with each of the three functionals yield 29 structures for 1-butanol with 14 pairs of mirror images and one structure (**TTT**) that does not have any distinguishable mirror image owing to the plane of symmetry. Note that structures having torsional angles that are all 180° or 0° (excluding the –CH$_3$ torsions) have indistinguishable mirror images due to the presence of a plane of symmetry; hence we should take into account only one structure. In case of 2-methyl-1-propanol, we have nine structures of which four have distinguishable mirror images; the other has the anti-periplanar (**TT**) arrangement. These nine structures are generated by rotating the molecule around O14–C7 and C5–C7; the other two rotations, viz., C1–C5 and C5–C10 contain –CH$_3$ and thus do not contribute any new structures. For butanal the torsions around C1–C4 and C4–C7, produce seven distinguishable structures, and torsion around

C7–C10 does not produce more structures. Among these seven structures, we have three pairs of mirror images and one structure (**CT**) with torsional angles of 0° and 180°. The rotational symmetry numbers for all the structures are one because they have no rotational symmetry axis.

Table II lists all the structures with their names and both zero-point-exclusive and zero-point-inclusive relative conformational energies. Although we performed geometry optimizations and frequency calculations using MO8-HX, M08-SO, and M06-2X for 1-butanol, Table II only shows the data for M08-HX since the coupled cluster calculations were carried out with M08-HX geometries, and hence this provides a better comparison to the coupled cluster results. The results for the other two functionals are in supplementary material.[26] Inspection of Table II reveals some noteworthy features of the results. For 1-butanol, the zero-point-exclusive relative conformational energies calculated using the M08-HX functional are lower than those obtained with CCSD(T)-F12a for 18 of the total of 27 non-zero relative energy values. In contrast, for 2-methyl-1-propanol, the zero-point-exclusive relative conformational energies in 4 out of 7 cases are lower when calculated with the coupled cluster method than when M08-HX was used. For 1-butanol and 2-methyl-1-propanol, the most stable geometry is the same in both density functional and coupled cluster methods. In case of butanal, however, the lowest energy structures are different and all the relative conformational energies are lower according to coupled cluster than the density functional ones.

Some of the torsions in these molecules are strongly coupled (SC). In an ideal situation, where all torsions are independent, alcohols would have 3^n structures where n is the number of torsions that each generate 3 distinguishable structures. Since n is 3 for 1-butanol and 2 for 2-methyl-1-propanol, ideal torsions would generate 27 and 9 structures, respectively. We do have nine structures in the latter case; however, due to coupling between O2–C3 and C4–C5, we identified 29 distinguishable structures for 1-butanol. This is attributed to steric hindrance[10] between terminal –OH and –CH$_3$ groups. In particular, the expected **G$^-$G$^+$G$^-$** and **G$^+$G$^-$G$^+$** structures become saddle points connecting **G$^-$G$^+$a$^-$/G$^-$g$^+$G$^-$** and **G$^+$G$^-$a$^+$/G$^+$g$^-$G$^+$**, respectively. Hence, instead of 27 structures, we have 29. Earlier studies[27,28] based on the conformational analysis of 1-

butanol have taken into account only 27 structures. Of the four torsions present in 1-butanol, three of them, i.e., O2–C3, C3–C4, and C4–C5 are SC and one (C5–C6) involving the $-CH_3$ group is nearly separable (NS). In case of 2-methyl-1-propanol, two torsions (O14–C7 and C5–C7) are SC, and the other two, viz., C1–C5 and C5–C10 with $-CH_3$ group are NS in nature.

It is harder to count the number of ideal structures for butanal, but we find seven structures, which is clearly nonideal since seven, like 29, is a prime number. Butanal has two SC torsions (C1–C4 and C4–C7) which generate distinguishable structures, and the one containing the $-CH_3$ group, C7–C10 is NS.

III.B. Conformational-rotational-vibrational partition functions of 1-butanol, 2-methyl-1-propanol, and butanal

Tables III–V present the conformational-rotational-vibrational partition functions for 1-butanol, 2-methyl-1-propanol, and butanal, respectively. For 1-butanol, the structure with the lowest zero-point-exclusive energy also has the lowest zero-point-inclusive energy. The zero of energy for calculating the partition functions is taken to be the zero-point-exclusive energy of this structure. In case of 2-methyl-1-propanol and butanal, the zero-point-exclusive and zero-point-inclusive energies yield different minimum-energy structures. For 2-methyl-1-propanol, we have taken the zero-point-exclusive energy of the $\mathbf{T^-G^-}$, $\mathbf{T^+G^+}$ structures as the zero of energy to calculate the partition functions; for butanal, the zero-point-exclusive energies of $\mathbf{C^-G^-}$ and $\mathbf{C^+G^+}$ are taken to be the zero of energy for calculating the partition functions.

To calculate the partition functions, one requires local periodicity[10] ($M_{j,\tau}$) parameters. For NS torsions involving the CH_3 group, $M_{j,\tau}$ is three. However, for the torsions that are SC, we use the Voronoi tessellation method (VTM).[10, 24] We use three-dimensional VTM for 1-butanol, two-dimensional VTM for butanal, and assign integer values for 2-methyl-1-propanol.

Table III illustrates that the partition functions (Q) obtained with M08-HX/MG3S are larger than those obtained with CCSD(T)-F12a at all temperatures above 298 K in

both the MS-LH and MS-T approximations. Similar behavior is observed when using M08-SO/MG3S, where we found that the density functional calculations give a larger Q at all temperatures studied here. However, the third density functional, M06-2X, gives smaller Q values than the coupled cluster in both the approximations for all temperature values. In Tables IV and V, the partition functions obtained with M08-HX/MG3S and M08-HX/maug-cc-pVTZ for 2-methyl-1-propanol and butanal, respectively have smaller Q values than CCSD(T)-F12a irrespective of the temperatures used. Figure 2 shows the percent deviation in Q between M08-HX results and the coupled cluster method. This deviation is calculated as

$$\frac{Q_{\text{CCSD(T)-F12a}} - Q_{\text{M08-HX}}}{Q_{\text{M08-HX}}} \times 100\%$$

(3)

The figure shows that we have a similar trend for alcohols where the percent deviation decreases with increase in temperature and starts to saturate at about 1500 K. The Q values for 1-butanol obtained from coupled cluster and density functional calculations are quite close to each other, and the deviation is 7% or less, whereas for 2-methyl-1-propanol, the percentage ranges up to 16%. The difference in Q values obtained with density functionals and coupled cluster methods for butanal, on the other hand, is quite large, up to 40% (see Fig. 2). As we increase the temperature, the Q values for butanal calculated using density functional and coupled cluster methods get closer.

III.C. Thermodynamic quantities: Standard state entropy, heat capacity, enthalpy, and free energies of 1-butanol, 2-methyl-1-propanol, and butanal

In order to obtain the standard state entropy, heat capacity, enthalpy, and free energies, we made use of Eqs. (3)–(7) of Ref. 29. The results are tabulated in Tables VI–XIV. We also applied Benson's GA parameters[9] to estimate entropies and heat capacities, and they are tabulated in these tables along with the density functional and coupled cluster results. For the calculations of entropy values from Benson's GA data at temperatures above 298 K, we made use of the following equation.

$$S_T^\circ = S_{T_0}^\circ + \int_{T_0}^{T} \frac{C_P^\circ(T)}{T} dT$$

(4)

208

The standard heat capacity ($C_P^\circ(T)$) values obtained from the GA tables at available temperatures are fitted to a cubic polynomial and then used in Eq. (4) in order to get entropy values at the desired temperatures. The experimental data are taken from the TRC data series[30] and *CRC Handbook of Chemistry and Physics*.[31] Since Benson's empirical parameters are based on the thermodynamic functions found in the American Petroleum Institute (API)[32] tables that correspond to a standard state of 1 atm; in the present work, we correct those values to a standard state of 1 bar. The results from TRC data series and CRC tables are already for a standard state of 1 bar.

Tables VI–VIII give the standard state entropies of 1-butanol, 2-methyl-1-propanol, and butanal, respectively. In all cases, the entropies calculated with MS-LH approximations are smaller than those calculated with the MS-T approximation for temperatures ranging from 200 K to 1000 K, however, beyond 1000 K the MS-LH entropies are larger than the MS-T ones, as shown in Fig. 3. The estimated entropy values obtained from Benson's empirical GA parameters[9] agree only within 4.1 cal mol^{-1} K^{-1} with those obtained from density functional and coupled cluster methods. The experimental data taken from TRC and CRC data series, on the other hand, agrees well with the computed entropy values. It is very encouraging that for 1-butanol the torsional corrections at high temperatures (1500 K and 2000 K) bring the theory into close agreement with the experimental data.

The heat capacities are given in Tables IX–XI along with Benson's GA values and experimental results. We have computed the $C_P^\circ(T)$ for density functional and coupled cluster methods using a finite difference approximation to

$$C_P^\circ(T) = \frac{dH_T^\circ}{dT}$$

(5)

The $C_P^\circ(T)$ values calculated using MS-LH approach are less than those calculated using MS-T in the temperature regime up to ~450 K while beyond that they become larger, as seen in Fig. 4. Benson's GA value for the heat capacity agree well with those calculated from the MS-T approach beyond 400 K, while for 300 and 400 K, they are closer to the LH approximation. For 1-butanol, at temperatures greater than or equal to 600 K, the

theoretical values are within 0.7 cal mol^{-1} K^{-1} of the experiment.[30] In case of 2-methyl-1-propanol, the computed $C_P^\circ(T)$ values have ~3 cal mol^{-1} K^{-1} difference with experimental results[8] at low temperatures, however, as the temperature increases, the difference gradually decreases and the computed $C_P^\circ(T)$ values almost match with experiment.

The mean unsigned errors in standard state entropies and heat capacities were also calculated and are presented in Tables VI–XI. The tables show that our values agree better with the experimental data than Benson's GA values in almost all the cases. The only exception observed is $C_P^\circ(T)$ values for 1-butanol (see Table IX), where Benson's GA values are slightly better in agreement with the experimental results than those obtained from the MS-T method with M08 or coupled cluster.

Finally, we calculated the standard state enthalpy and Gibbs free energies, and the results are in Tables XII–XIV. These tables reveal that at temperatures of 200–800 K, the enthalpy, H_T°, is almost same in the MS-LH and MS-T approximations. However, at and above 1000 K, the difference increases. The free energy, G_T°, on the other hand, shows less difference between the values obtained with the MS-LH and MS-T approximations than is observed for H_T°. The free energy results show the importance of torsional anharmonicity at high temperatures.

IV. CONCLUSIONS

In the present work, we have calculated the partition functions and four thermodynamic quantities (entropy, enthalpy, heat capacity, and Gibbs free energy) for 1-butanol, 2-methyl-1-propanol, and butanal by applying the recently developed MS-LH and MS-T approximations. Our results for the thermodynamic properties agree well with the experimental values obtained from the TRC data series[30] and CRC tables,[31] where such data are available. The present investigation demonstrates the quantitative importance of torsional anharmonicity in these systems, particularly at high temperatures. The computed thermodynamic quantities agree with the empirical group additivity data

of Benson only within 4.1 cal mol^{-1} K^{-1}; this demonstrates the unreliability of group additivity.

The present investigation illustrates that high-level electronic structure calculations combined with MS statistical thermodynamic methods can be used reliably for calculating various thermodynamic properties of more complex systems with multiple torsions. Therefore we can use this statistical mechanical approach to predict thermodynamic quantities even for molecules or temperatures where there are no experimental data or group additivity data.

REFERENCES

[1] C. –W. Zhou, J. M. Simmie, and H. J. Curran, Combustion and Flame **158**, 726 (2011).

[2] S. S. Vasu, D. F. Davidson, R. K. Hanson, and D. M. Golden, Chem. Phys. Lett. **497**, 26 (2010).

[3] M. D. Hurley, T. J. Wallington, L. Laursen, M. S. Javadi, O. J. Nielsen, T. Yamanaka, and M. Kawasaki, J. Phys. Chem. A **113**, 7011 (2009).

[4] D. H. Semmes, A. R. Ravishankara, C. A. Gump-Perkins, and P. H. Wine, Int. J. Chem. Kinet. **17**, 303 (1985).

[5] J. A. Kerr and D. W. Sheppard, Environ. Sci. Technol. **15**, 960 (1981).

[6] G. S. Parks, J. Am. Chem. Soc. **47**, 338 (1925).

[7] J. Tjebbes, Acta Chem. Scand. **14**, 180 (1960).

[8] E. Strömsöe, H. G. Rönne, and A. L. Lydersen, J. Chem. Eng. Data **15**, 286 (1970).

[9] S. W. Benson, *Thermochemical Kinetics*, 2nd ed. (Wiley-Interscience, New York, 1976).

[10] J. Zheng, T. Yu, E. Papajak, I. M. Alecu, S. L. Mielke, and D. G. Truhlar, Phys. Chem. Chem. Phys. **13**, 10885 (2011).

[11] T. Yu, J. Zheng and D. G. Truhlar, Chem. Sci. **2**, 2199 (2011).

[12] J. Zheng, T. Yu, and D. G. Truhlar, Phys. Chem. Chem. Phys. **13**, 19318 (2011).

[13] T. F. Miller III and D. C. Clary, Phys. Chem. Chem. Phys. **6**, 2563 (2004). T. F. Miller III and D. C. Clary, Mol. Phys. **103**, 1573 (2005).

[14] P. Vansteenkiste, V. Van Speybroeck, E. Pauwels, and M. Waroquier, Chem. Phys. **314**, 109 (2005). K. Van Cauter, V. Van Speybroeck, P. Vansteeenkiste, M.-F. Reyniers, and M. Waroquier, ChemPhysChem **7**, 131 (2006).

[15] I. M. Alecu, J. Zheng, Y. Zhao, and D. G. Truhlar, J. Chem. Theor. Comput. **6**, 2872 (2010).

[16] Y. Zhao and D. G. Truhlar, Theor. Chem. Acc. **120**, 215 (2008).

[17] Y. Zhao and D. G. Truhlar, J. Chem. Theory Comput. **4**, 1849 (2008).

[18] R. Krishnan, J. S. Binkley, R. Seeger, and J. A. Pople, J. Chem. Phys. **72**, 650 (1980); T. Clark, J. Chandrasekhar, G. W. Spitznagel, and P. v. R. Schleyer, J. Comp. Chem.

4, 294 (1983); M. J. Frisch, J. A. Pople, and J. S. Binkley, J. Chem. Phys. **80**, 3265 (1984).

[19] B. J. Lynch, Y. Zhao, and D. G. Truhlar, J. Phys. Chem. A **107**, 1384 (2003).

[20] E. Papajak and D. G. Truhlar, J. Chem. Theor. Comput. **6**, 597 (2010); E. Papajak and D. G. Truhlar, *ibid*. **7**, 10 (2011).

[21] T. B. Adler, G. Knizia, and H.-J. Werner, J. Chem. Phys. **127**, 221106 (2007); G. Knizia, T. B. Adler, and H. –J. Werner, J. Chem. Phys. **130**, 054104 (2009); F. R. Manby, J. Chem. Phys. **119**, 4607 (2003).

[22] M. J. Frisch, G. W. Trucks, H. B. Schlegel, G. E. Scuseria, M. A. Robb, J. R. Cheeseman, G. Scalmani, V. Barone, B. Mennucci, G. A. Petersson, H. Nakatsuji, M. Caricato, X. Li, H. P. Hratchian, A. F. Izmaylov, J. Bloino, G. Zheng, J. L. Sonnenberg, M. Hada, M. Ehara, K. Toyota, R. Fukuda, J. Hasegawa, M. Ishida, T. Nakajima, Y. Honda, O. Kitao, H. Nakai, T. Vreven, Jr., J. A. Montgomery, J. E. Peralta, F. Ogliaro, M. Bearpark, J. J. Heyd, E. Brothers, K. N. Kudin, V. N. Staroverov, R. Kobayashi, J. Normand, K. Raghavachari, A. Rendell, J. C. Burant, S. S. Iyengar, J. Tomasi, M. Cossi, N. Rega, N. J. Millam, M. Klene, J. E. Knox, J. B. Cross, V. Bakken, C. Adamo, J. Jaramillo, R. Gomperts, R. E. Stratmann, O. Yazyev, A. J. Austin, R. Cammi, C. Pomelli, J. W. Ochterski, R. L. Martin, K. Morokuma, V. G. Zakrzewski, G. A. Voth, P. Salvador, J. J. Dannenberg, S. Dapprich, A. D. Daniels, Ö. Farkas, J. B. Foresman, J. V. Ortiz, J. Cioslowski, and D. J. Fox, *Gaussian 09*, Revision A.02, Gaussian, Inc., Wallingford CT, 2009.

[23] H.-J. Werner, P. J. Knowles, F. R. Manby, M. Schütz, P. Celani, G. Knizia, T. Korona, R. Lindh, A. Mitrushenkov, G. Rauhut, T. B. Adler, R. D. Amos, A. Bernhardsson, A. Berning, D. L. Cooper, M. J. O. Deegan, A. J. Dobbyn, F. Eckert, E. Goll, C. Hampel, A. Hesselmann, G. Hetzer, T. Hrenar, G. Jansen, C. Köppl, Y. Liu, A. W. Lloyd, R. A. Mata, A. J. May, S. J. McNicholas, W. Meyer, M. E. Mura, A. Nicklaß, P. Palmieri, K. Pflüger, R. Pitzer, M. Reiher, T. Shiozaki, H. Stoll, A. J. Stone, R. Tarroni, T. Thorsteinsson, M. Wang, and A. Wolf, *Molpro*, University of Birmingham, Birmingham, 2010.1, 2010.

[24] J. Zheng, S. L. Mielke, K. L. Clarkson, and D. G. Truhlar, *MSTor* computer program, version 2011, University of Minnesota, Minneapolis, 2011.

[25] *Basic terminology of stereochemistry, (IUPAC Recommendations 1996)*, 68, 2193 (PAC, 1996).

[26] See supplementary material at for all the structures and corresponding zero-point-exclusive and zero-point-inclusive relative conformational energies for 1-butanol obtained with M08-SO and M06-2X density functionals and MG3S basis set.

[27] K. Ohno, H. Yoshida, H. Watanabe, T. Fujita, and H. Matsuura, J. Phys. Chem. **98**, 6924 (1994).

[28] J. Moc, J. M. Simme, and H. J. Curran, J. Mol. Struct. **928**, 149 (2009).

[29] T. Yu, J. Zheng, and D. G. Truhlar, Phys. Chem. Chem. Phys. DOI:10.1039/C1CP22578B.

[30] TRC Data Series: M. Frenkel, G. J. Kabo, K. N. Marsh, G. N. Roganov, and R. C. Wilhoit, *Thermodynamics of Organic Compounds in the Gas State*, Vol. II, (CRC Press, Boca Raton, FL, 1994).

[31] *CRC Handbook of Chemistry and Physics*, 91st ed. (CRC press, Boca Raton, 2011).

[32] API Tables: *Selected Values of Properties of Hydrocarbons and Related Compounds*, American Petroleum Institute Research Project 44, Carnegie Press (Carnegie Institute of Technology, Pittsburgh, 1953).

TABLE I. Name conventions and labeling of structures[a]

Name convention	Abbreviation	Dihedral angle range (in deg)[b]
cis	**C**	0
cis±	**C$^\pm$**	(0, ±30)
gauche±	**G$^\pm$**	(±30, ±75)[c]
	g$^\pm$	(±75, ±90)
anti±	**a$^\pm$**	(±90, ±105)
	A$^\pm$	(±105, ±150)
trans±	**T$^\pm$**	(±150, ±180)
trans	**T**	180

[a]The dihedral angles used for torsions are H1–O2–C3–C4, O2–C3–C4–C5, and C3–C4–C5–C6 for 1-butanol; H15–O14–C7–C5 and O14–C7–C5–H6 for 2-methyl-1-propanol; O2–C1–C4–C7 and C1–C4–C7–C10 for butanal.

[b](x, y) means $x < \tau < y$.

[c]This includes both $-75 < \tau < -30$ and $30 < \tau < 75$.

TABLE II. Names of structures and their relative conformational energies (in kcal/mol)

Compound	Structures	Relative conformational energy		
		M08-HX[a]		CCSD(T)-F12a[b, c]
		Zero-point-exclusive	Zero-point-inclusive	
1-butanol	$T^-G^+T^-$, $T^+G^-T^+$	0.00	0.00	0.00
	$T^+G^+G^+$, $T^-G^-G^-$	0.05	0.37	0.48
	$G^+G^+T^-$, $G^-G^-T^+$	0.19	0.21	0.14
	$G^+G^-T^-$, $G^-G^+T^+$	0.20	0.29	0.12
	$G^+G^+G^+$, $G^-G^-G^-$	0.23	0.49	0.63
	$G^+G^-G^-$, $G^-G^+G^+$	0.33	0.62	0.76
	TTT	0.37	0.32	0.20
	$G^+T^+T^+$, $G^-T^-T^-$	0.40	0.37	0.19
	$G^+T^-G^-$, $G^-T^+G^+$	0.82	0.89	0.83
	$T^+T^+G^+$, $T^-T^-G^-$	0.82	0.89	0.89
	$G^+T^+G^+$, $G^-T^-G^-$	0.99	1.02	0.95
	$T^+g^+G^-$, $T^-g^-G^+$	1.32	1.34	1.66
	$G^+G^+G^-$, $G^-G^-G^+$	1.32	1.40	1.55
	$G^+g^-G^+$, $G^-g^+G^-$	1.44	1.71	1.87
	$G^-G^+a^-$, $G^+G^-a^+$	1.96	2.19	2.33
2-methyl-1-propanol	T^-G^-, T^+G^+	0.00	0.00	0.00
	G^-G^+, G^+G^-	0.11	0.20	0.03
	G^-G^-, G^+G^+	0.13	0.20	0.07
	TT	0.22	0.34	0.37
	G^+T^-, G^-T^+	0.28	0.48	0.35
Butanal	C^-G^-, C^+G^+	0.00	0.03	0.03
	CT	0.10	0.00	0.00
	A^+G^-, A^-G^+	1.05	0.95	0.67
	A^-T^-, A^+T^+	1.20	1.10	0.71

[a]The basis set used for M08-HX is MG3S for 1-butanol and 2-methyl-1-propanol and maug-cc-pVTZ for butanal.

[b]CCSD(T)-F12a/jul-cc-pVTZ//M08-HX/MG3S for 1-butanol and 2-methyl-1-propanol

[c]CCSD(T)-F12a/jul-cc-pVTZ//M08-HX/maug-cc-pVTZ for butanal

TABLE III. Calculated conformational-rotational-vibrational partition function of 1-butanol[a]

T (K)	MS-LH				MS-T			
	M06-2X[b]	M08-SO[b]	M08-HX[b]	CCSD(T)-F12a[c]	M06-2X[b]	M08-SO[b]	M08-HX[b]	CCSD(T)-F12a[c]
200	4.97E−86	1.35E−85	1.20E−85	1.22E−85	6.40E−86	1.75E−85	1.55E−85	1.60E−85
250	3.87E−67	8.90E−67	7.98E−67	7.95E−67	5.24E−67	1.21E−66	1.09E−66	1.09E−66
298	7.70E−55	1.60E−54	1.44E−54	1.41E−54	1.09E−54	2.26E−54	2.04E−54	2.02E−54
300	2.07E−54	4.28E−54	3.87E−54	3.79E−54	2.93E−54	6.07E−54	5.49E−54	5.43E−54
400	3.32E−38	6.01E−38	5.50E−38	5.32E−38	5.01E−38	9.08E−38	8.31E−38	8.11E−38
600	3.15E−21	5.03E−21	4.68E−21	4.50E−21	5.07E−21	8.04E−21	7.46E−21	7.22E−21
800	5.28E−12	7.96E−12	7.46E−12	7.20E−12	8.49E−12	1.26E−11	1.17E−11	1.14E−11
1000	6.25E−06	9.14E−06	8.61E−06	8.34E−06	9.63E−06	1.37E−05	1.29E−05	1.25E−05
1500	1.80E+04	2.54E+04	2.41E+04	2.35E+04	2.29E+04	3.09E+04	2.91E+04	2.84E+04
2000	1.57E+10	2.18E+10	2.08E+10	2.04E+10	1.59E+10	2.10E+10	1.98E+10	1.94E+10
2400	5.79E+13	7.98E+13	7.63E+13	7.50E+13	4.88E+13	6.38E+13	6.03E+13	5.91E+13

[a]The zero of energy is at the lowest-energy classical equilibrium structure.

[b]The basis set used for M08-HX, M08-SO, and M06-2X is MG3S.

[c]CCSD(T)-F12a/jul-cc-pVTZ//M08-HX/MG3S

217

TABLE IV. Calculated conformational-rotational-vibrational partition function of 2-methyl-1-propanol[a]

T (K)	MS-LH		MS-T	
	M08-HX[b]	CCSD(T)-F12a[c]	M08-HX[b]	CCSD(T)-F12a[c]
200	1.37E–85	1.44E–85	1.76E–85	1.85E–85
250	6.76E–67	6.99E–67	9.05E–67	9.36E–67
298	1.00E–54	1.03E–54	1.39E–54	1.42E–54
300	2.66E–54	2.73E–54	3.70E–54	3.79E–54
400	2.93E–38	2.97E–38	4.29E–38	4.36E–38
600	1.92E–21	1.94E–21	2.99E–21	3.02E–21
800	2.70E–12	2.72E–12	4.22E–12	4.25E–12
1000	2.90E–06	2.91E–06	4.36E–06	4.38E–06
1500	7.35E+03	7.37E+03	9.29E+03	9.32E+03
2000	6.05E+09	6.06E+09	6.18E+09	6.19E+09
2400	2.16E+13	2.17E+13	1.86E+13	1.86E+13

[a]The zero of energy is at the lowest-energy classical equilibrium structure ($\mathbf{G}^-\mathbf{T}^-$ in Table II).

[b]The basis set used for M08-HX is MG3S.

[c]CCSD(T)-F12a/jul-cc-pVTZ//M08-HX/MG3S

TABLE V. Calculated conformational-rotational-vibrational partition function of butanal[a]

T (K)	MS-LH		MS-T	
	M08-HX[b]	CCSD(T)-F12a[c]	M08-HX[b]	CCSD(T)-F12a[c]
200	1.47E−70	2.02E−70	1.66E−70	2.33E−70
250	5.93E−55	8.25E−55	7.04E−55	9.97E−55
298	8.86E−45	1.22E−44	1.10E−44	1.54E−44
300	2.01E−44	2.78E−44	2.50E−44	3.51E−44
400	5.42E−31	7.25E−31	7.28E−31	9.84E−31
600	7.06E−17	8.85E−17	1.03E−16	1.30E−16
800	3.53E−09	4.23E−09	5.26E−09	6.31E−09
1000	4.30E−04	5.00E−04	6.31E−04	7.31E−04
1500	3.91E+04	4.34E+04	5.08E+04	5.61E+04
2000	4.12E+09	4.46E+09	4.58E+09	4.93E+09
2400	4.33E+12	4.64E+12	4.25E+12	4.52E+12

[a]The zero of energy is at the lowest-energy classical equilibrium structure ($\mathbf{C^-G^-}$ in Table II).

[b]The basis set used for M08-HX is maug-cc-pVTZ.

[c]CCSD(T)-F12a/jul-cc-pVTZ//M08-HX/maug-cc-pVTZ

TABLE VI. Standard state entropy (in cal mol⁻¹ K⁻¹) of 1-butanol

T (K)	MS-LH				MS-T				Benson's GA[c]	Expt.[d]
	M06-2X[a]	M08-SO[a]	M08-HX[a]	CCSD(T)-F12a[b]	M06-2X[a]	M08-SO[a]	M08-HX[a]	CCSD(T)-F12a[b]		
200	76.84	77.17	77.02	76.76	77.78	78.11	77.96	77.73		77.52
250	81.72	82.08	81.95	81.74	82.78	83.13	83.02	82.83		
298	86.08	86.46	86.35	86.17	87.23	87.60	87.49	87.34	88.14	86.42
300	86.26	86.64	86.53	86.35	87.41	87.78	87.68	87.52	88.32	86.58
400	94.84	95.25	95.15	95.03	96.09	96.47	96.37	96.26	96.86	95.02
600	110.78	111.24	111.16	111.09	111.90	112.29	112.19	112.12	112.44	110.73
800	125.14	125.63	125.55	125.51	125.89	126.27	126.18	126.12	126.31	124.72
1000	137.99	138.51	138.44	138.41	138.30	138.69	138.59	138.54	138.68	137.17
1500	164.84	165.39	165.32	165.30	164.02	164.43	164.34	164.31		163.01
2000	186.08	186.65	186.58	186.57	184.31	184.73	184.64	184.62		183.39
2400	200.23	200.81	200.74	200.73	197.81	198.23	198.14	198.12		
MUE(6)[e]	0.36	0.51	0.46	0.48	1.03	1.41	1.31	1.21	1.69	
MUE(9)[f]	0.81	1.01	0.98	1.01	0.93	1.31	1.21	1.11		

[a]The basis set used for M08-HX, M08-SO and M06-2X is MG3S.

[b]CCSD(T)-F12a/jul-cc-pVTZ//M08-HX/MG3S

[c]using Benson's data from Ref. 9 and adding 0.026 cal mol⁻¹ K⁻¹ to convert from a standard pressure of 1 atm to a standard pressure of 1 bar

[d]taken from Ref. 30

[e]the mean unsigned errors (MUE) in standard state entropies (cal mol⁻¹ K⁻¹) corresponding to six temperatures where our computed results, Benson's empirical GA values, and experimental data are all available

[f]the mean unsigned errors (MUE) in standard state entropies (cal mol⁻¹ K⁻¹) corresponding to nine temperatures where our computed results and experimental data are all available

TABLE VII. Standard state entropy (in cal mol^{-1} K^{-1}) of 2-methyl-1-propanol

T (K)	MS-LH		MS-T		Benson's GA[c]
	M08-HX[a]	CCSD(T)-F12a[b]	M08-HX[a]	CCSD(T)-F12a[b]	
200	74.32	74.27	75.18	75.13	
250	79.18	79.14	80.14	80.11	
298	83.55	83.52	84.59	84.57	87.64
300	83.73	83.70	84.77	84.75	87.82
400	92.35	92.33	93.49	93.47	96.30
600	108.38	108.37	109.43	109.43	111.90
800	122.79	122.79	123.53	123.52	125.81
1000	135.69	135.68	136.01	136.00	138.20
1500	162.57	162.57	161.83	161.83	
2000	183.83	183.83	182.17	182.16	
2400	197.99	197.97	195.68	195.68	

[a]The basis set used for M08-HX is MG3S.

[b]CCSD(T)-F12a/jul-cc-pVTZ//M08-HX/MG3S

[c]using Benson's data from Ref. 9 and adding 0.026 cal mol^{-1} K^{-1} to convert from a standard pressure of 1 atm to a standard pressure of 1 bar

TABLE VIII. Standard state entropy (in cal mol^{-1} K^{-1}) of butanal

T (K)	MS-LH		MS-T		Benson's GA[c]	Expt.[d]
	M08-HX[a]	CCSD(T)-F12a[b]	M08-HX[a]	CCSD(T)-F12a[b]		
200	72.51	73.32	73.12	73.98		
250	77.18	77.82	77.98	78.66		
298	81.28	81.77	82.22	82.73		82.14
300	81.44	81.93	82.39	82.89	84.17	
400	89.31	89.60	90.41	90.69	84.33	
600	103.54	103.67	104.59	104.69	92.05	
800	116.20	116.26	116.98	117.03	105.92	
1000	127.48	127.52	127.94	127.96	118.22	
1500	150.91	150.93	150.59	150.59	129.18	
2000	169.37	169.38	168.36	168.35		
2400	181.63	181.64	180.14	180.13		
UE[e]	0.86	0.37	0.084	0.59	2.03	

[a]The basis set used for M08-HX is maug-cc-pVTZ.

[b]CCSD(T)-F12a/jul-cc-pVTZ//M08-HX/maug-cc-pVTZ

[c]using Benson's data from Ref. 9 and adding 0.026 cal mol^{-1} K^{-1} to convert from a standard pressure of 1 atm to a standard pressure of 1 bar

[d]taken from Ref. 31

[e]the unsigned errors (UE) in standard state entropies (cal mol^{-1} K^{-1}) corresponding to 298 K temperature where our computed result, Benson's empirical GA, and the experimental value are all available

TABLE IX. Heat capacity (in cal mol⁻¹ K⁻¹) of 1-butanol

T (K)	MS-LH				MS-T				Benson's GA[c]	Expt.[d]
	M06-2X[a]	M08-SO[a]	M08-HX[a]	CCSD(T)-F12a[b]	M06-2X[a]	M08-SO[a]	M08-HX[a]	CCSD(T)-F12a[b]		
200	20.57	20.70	20.85	20.99	21.14	21.23	21.40	21.54		19.42
250	23.36	23.49	23.58	23.77	23.91	23.99	24.10	24.28		
298	26.42	26.54	26.61	26.79	26.90	26.97	27.03	27.20	26.48	25.82
300	26.55	26.67	26.74	26.93	27.03	27.10	27.15	27.33		25.95
400	33.42	33.54	33.58	33.75	33.57	33.60	33.61	33.74	32.99	33.02
600	45.47	45.58	45.61	45.72	44.62	44.62	44.62	44.68	44.12	44.54
800	54.30	54.42	54.43	54.51	52.61	52.63	52.62	52.68	52.27	52.71
1000	60.86	60.97	60.98	61.03	58.57	58.61	58.61	58.66	58.38	58.78
1500	71.07	71.14	71.15	71.18	67.97	68.02	68.03	68.06		68.24
2000	76.33	76.38	76.38	76.40	72.86	72.91	72.91	72.94		73.08
2400	78.78	78.82	78.82	78.83	75.15	75.19	75.20	75.22		
MUE(5)[e]	1.03	1.15	1.19	1.32	0.52	0.53	0.56	0.63	0.36	
MUE(9)[f]	1.49	1.60	1.64	1.75	0.59	0.60	0.63	0.69		

[a] The basis set used for M08-HX, M08-SO and M06-2X is MG3S.
[b] CCSD(T)-F12a/jul-cc-pVTZ//M08-HX/MG3S
[c] using Benson's data from Ref. 9
[d] taken from Ref. 30
[e] the mean unsigned errors (MUE) in heat capacities (cal mol⁻¹ K⁻¹) corresponding to five temperatures where our computed results, Benson's empirical GA values, and experimental data are all available
[f] the mean unsigned errors (MUE) in heat capacities (cal mol⁻¹ K⁻¹) corresponding to nine temperatures where our computed results and experimental data are all available

223

TABLE X. Heat capacity (in cal mol^{-1} K^{-1}) of 2-methyl-1-propanol

T (K)	MS-LH		MS-T		Benson's GA[c]	Expt.[d]
	M08-HX[a]	CCSD(T)-F12a[b]	M08-HX[a]	CCSD(T)-F12a[b]		
200	20.37	20.43	20.84	20.89		
250	23.35	23.41	23.83	23.88		
298	26.51	26.56	26.96	27.00		
300	26.65	26.70	27.09	27.14	26.21	
390.55	32.97	33.01	33.18	33.21	32.40	35.52
397.65	33.46	33.49	33.65	33.68	32.86	35.17
400	33.62	33.66	33.80	33.83	32.93	
406.95	34.10	34.13	34.25	34.28	33.44	35.30
416.95	34.78	34.81	34.89	34.92	34.07	35.41
424.05	35.26	35.29	35.34	35.37	34.51	35.79
441.85	36.44	36.46	36.45	36.47	35.60	36.69
451.25	37.05	37.08	37.03	37.05	36.17	37.40
474.35	38.52	38.55	38.40	38.42	37.53	38.79
477.75	38.74	38.76	38.60	38.62	37.73	38.91
501.55	40.20	40.22	39.95	39.97	39.08	40.08
525.85	41.63	41.65	41.28	41.29	40.40	41.64
546.35	42.80	42.82	42.35	42.37	41.48	42.77
582.95	44.79	44.81	44.18	44.19	43.35	44.46
600	45.68	45.70	44.99	45.00	44.26	
602.55	45.81	45.83	45.11	45.12	44.30	45.81
800	54.48	54.49	52.96	52.97	52.46	
1000	61.00	61.01	58.87	58.87	58.52	
1500	71.15	71.15	68.14	68.14		
2000	76.38	76.38	72.97	72.98		
2400	78.82	78.82	75.24	75.24		
MUE(14)[e]	0.58	0.57	0.65	0.63	1.49	

[a] The basis set used for M08-HX is MG3S.

[b] CCSD(T)-F12a/jul-cc-pVTZ//M08-HX/MG3S

[c] using Benson's data from Ref. 9

[d] taken from Ref. 8

[e] the mean unsigned errors (MUE) in heat capacities (cal mol^{-1} K^{-1}) corresponding to 14 temperatures where our computed results, Benson's empirical GA values, and experimental data are all available

224

TABLE XI. Heat capacity (in cal mol^{-1} K^{-1}) of butanal

T (K)	MS-LH		MS-T		Benson's GA[c]	Expt.[d]
	M08-HX[a]	CCSD(T)-F12a[b]	M08-HX[a]	CCSD(T)-F12a[b]		
200	19.78	19.16	20.64	19.95		
250	22.16	21.32	23.03	22.07		
298	24.62	23.81	25.36	24.45		24.71
300	24.73	23.92	25.46	24.55	24.19	
400	30.25	29.68	30.54	29.92	29.54	
600	40.23	39.96	39.65	39.38	39.19	
800	47.72	47.57	46.53	46.38	46.36	
1000	53.30	53.21	51.68	51.60	51.65	
1500	61.88	61.84	59.66	59.64		
2000	66.21	66.19	63.69	63.69		
2400	68.20	68.18	65.55	65.55		
UE[e]	0.090	0.90	0.65	0.26		

[a] The basis set used for M08-HX is maug-cc-pVTZ.

[b] CCSD(T)-F12a/jul-cc-pVTZ//M08-HX/maug-cc-pVTZ

[c] using Benson's data from Ref. 9

[d] taken from Ref. 31

[e] the unsigned errors (UE) in standard state entropies (cal mol^{-1} K^{-1}) corresponding to 298 K temperature where our computed result and the experimental value are both available

TABLE XII. Standard state enthalpy and free energies (in kcal/mol) of 1-butanol

T (K)	H_T°							
	MS-LH				MS-T			
	M06-2X[a]	M08-SO[a]	M08-HX[a]	CC[b]	M06-2X[a]	M08-SO[a]	M08-HX[a]	CC[b]
200	86.7	87.1	86.7	86.7	87.1	86.8	86.7	86.7
250	87.8	88.2	87.8	87.8	88.2	87.9	8	87.9
298	89.0	89.3	89.1	89.0	89.5	89.1	89.2	89.1
300	89.1	89.4	89.1	89.1	89.5	89.2	89.2	89.2
400	92.1	92.4	92.1	92.1	92.6	92.2	92.3	92.2
600	100.14	100.3	100.1	100.1	100.5	100.10	100.2	100.1
800	110.1	110.4	110.1	110.2	110.5	109.9	109.9	109.9
1000	121.7	121.9	121.7	121.8	121.7	121.0	121.1	121.1
1500	155.0	155.2	155.0	155.1	154.0	152.9	153.0	153.0
2000	192.0	192.2	192.1	192.1	189.6	188.3	188.4	188.4
2400	223.1	223.2	223.1	223.2	219.4	217.9	218.0	218.0

T (K)	G_T°							
200	71.7	71.3	71.3	71.3	71.6	71.2	71.2	71.2
250	67.7	67.3	67.4	67.4	67.6	67.2	67.2	67.2
298	63.7	63.3	63.3	63.3	63.5	63.1	63.1	63.1
300	63.5	63.1	63.1	63.2	63.3	62.9	62.9	62.9
400	54.5	54.0	54.1	54.1	54.1	53.7	53.7	53.8
600	33.9	33.3	33.4	33.4	33.3	32.8	32.8	32.9
800	10.3	9.6	9.7	9.8	9.5	8.9	9.0	9.0
1000	−16.1	−16.8	−16.7	−16.7	−16.9	−17.6	−17.5	−17.5
1500	−92.1	−93.1	−92.9	−92.9	−92.8	−93.7	−93.5	−93.4
2000	−180.0	−181.3	−181.1	−181.0	−180.0	−181.1	−180.9	−180.8
2400	−257.3	−258.9	−258.6	−258.6	−256.5	−257.8	−257.5	−257.4

[a] The basis set used for M08-HX, M08-SO and M06-2X is MG3S.

[b] CCSD(T)-F12a/jul-cc-pVTZ//M08-HX/MG3S

TABLE XIII. Standard state enthalpy ad free energies (in kcal/mol) of 2-methyl-1-propanol

| T (K) | H°_T | | | | G°_T | | | |
| | MS-LH | | MS-T | | MS-LH | | MS-T | |
	M08-HX[a]	CC[b]	M08-HX[a]	CC[b]	M08-HX[a]	CC[b]	M08-HX[a]	CC[b]
200	86.1	86.1	86.2	86.2	71.3	71.3	71.2	71.2
250	87.2	87.2	87.3	87.3	67.4	67.4	67.3	67.3
298	88.4	88.4	88.6	88.5	63.5	63.5	63.3	63.3
300	88.5	88.5	88.6	88.6	63.4	63.4	63.2	63.2
400	91.5	91.5	91.7	91.6	54.6	54.5	54.3	54.2
600	99.5	99.5	99.6	99.6	34.5	34.5	33.9	33.9
800	109.6	109.5	109.4	109.4	11.3	11.3	10.6	10.6
1000	121.1	121.1	120.6	120.6	-14.6	-14.6	-15.4	-15.4
1500	154.5	154.4	152.7	152.6	-89.4	-89.4	-90.1	-90.1
2000	191.5	191.5	188.1	188.0	-176.2	-176.2	-176.3	-176.3
2400	222.6	222.5	217.7	217.7	-252.6	-252.6	-251.9	-251.9

[a]The basis set used for M08-HX is MG3S.

[b]CCSD(T)-F12a/jul-cc-pVTZ//M08-HX/MG3S

TABLE XIV. Standard state enthalpy and free energies (in kcal/mol) of butanal

T (K)	H_T°				G_T°			
	MS-LH		MS-T		MS-LH		MS-T	
	M08-HX[a]	CC[b]	M08-HX[a]	CC[b]	M08-HX[a]	CC[b]	M08-HX[a]	CC[b]
200	72.0	72.1	72.1	72.2	57.5	57.4	57.5	57.4
250	73.1	73.1	73.2	73.2	53.8	53.6	53.7	53.5
298	74.2	74.2	74.4	74.3	50.0	49.8	49.9	49.7
300	74.3	74.2	74.4	74.4	49.8	49.6	49.7	49.5
400	77.0	76.9	77.2	77.1	41.3	41.1	41.1	40.8
600	84.1	83.9	84.3	84.1	22.0	21.7	21.5	21.3
800	92.9	92.7	92.9	92.7	−0.021	−0.31	−0.66	−0.95
1000	103.1	102.8	102.8	102.5	−24.4	−24.7	−25.2	−25.5
1500	132.1	131.8	130.8	130.5	−94.3	−94.6	−95.0	−95.3
2000	164.2	163.9	161.8	161.5	−174.5	−174.8	−174.9	−175.2
2400	191.2	190.9	187.7	187.4	−244.8	−245.1	−244.7	−245.0

[a]The basis set used for M08-HX is maug-cc-pVTZ.

[b]CCSD(T)-F12a/jul-cc-pVTZ//M08-HX/maug-cc-pVTZ

Figure Captions

FIG. 1. Structures of (a) 1-butanol, (b) 2-methyl-1-propanol, and (c) butanal.

FIG. 2. The percent deviations of the partition function values (as defined in Eq. (3)) between CCSD(T)-F12a and M08-HX results of 1-butanol, 2-methyl-1-propanol, and butanal obtained by MS-LH and MS-T approximations.

FIG. 3. The ratio of the standard state entropies of 1-butanol, 2-methyl-1-propanol, and butanal obtained using MS-LH and MS-T approximations at various temperatures.

FIG. 4. The ratio of the heat capacities of 1-butanol, 2-methyl-1-propanol, and butanal obtained using MS-LH and MS-T approximations at various temperatures.

(a)

(b)

(c)

FIG. 1

H

C

O
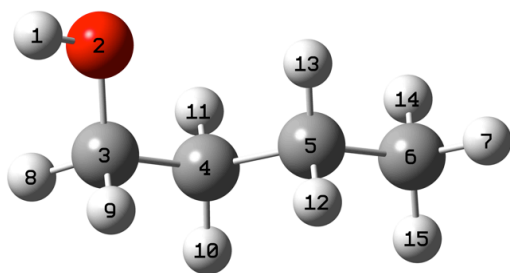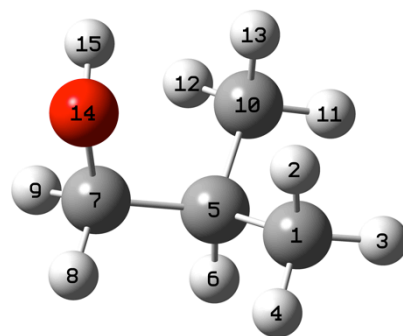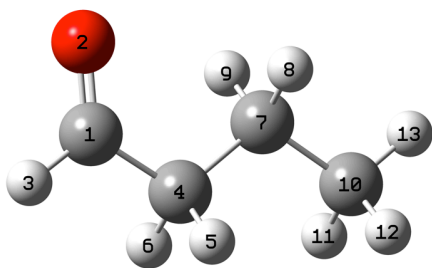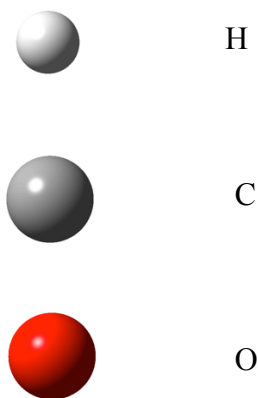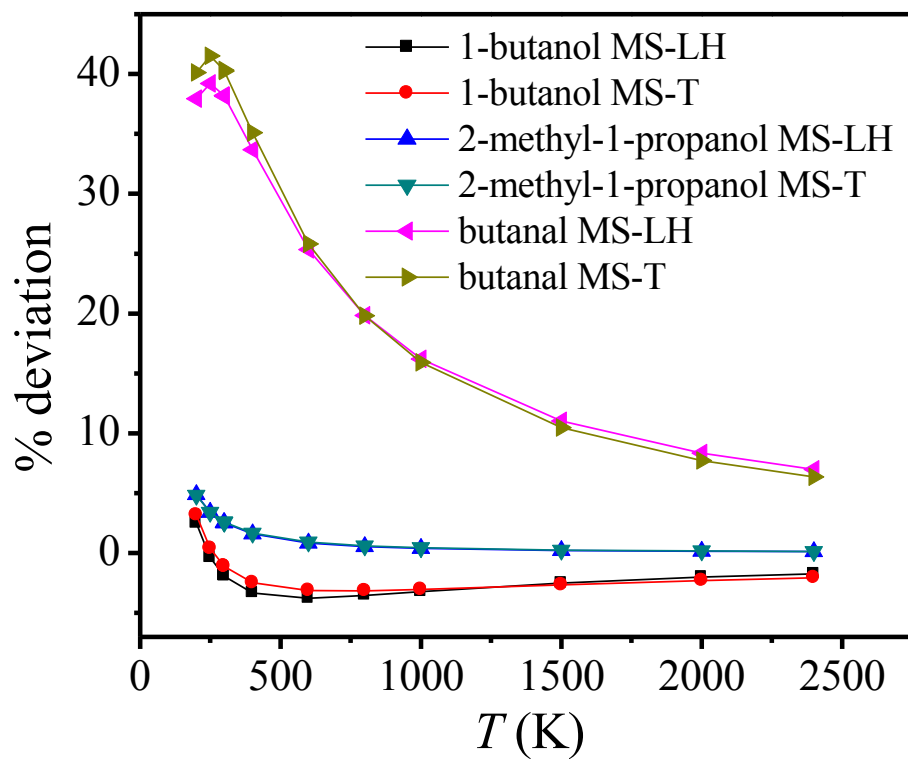
FIG. 2
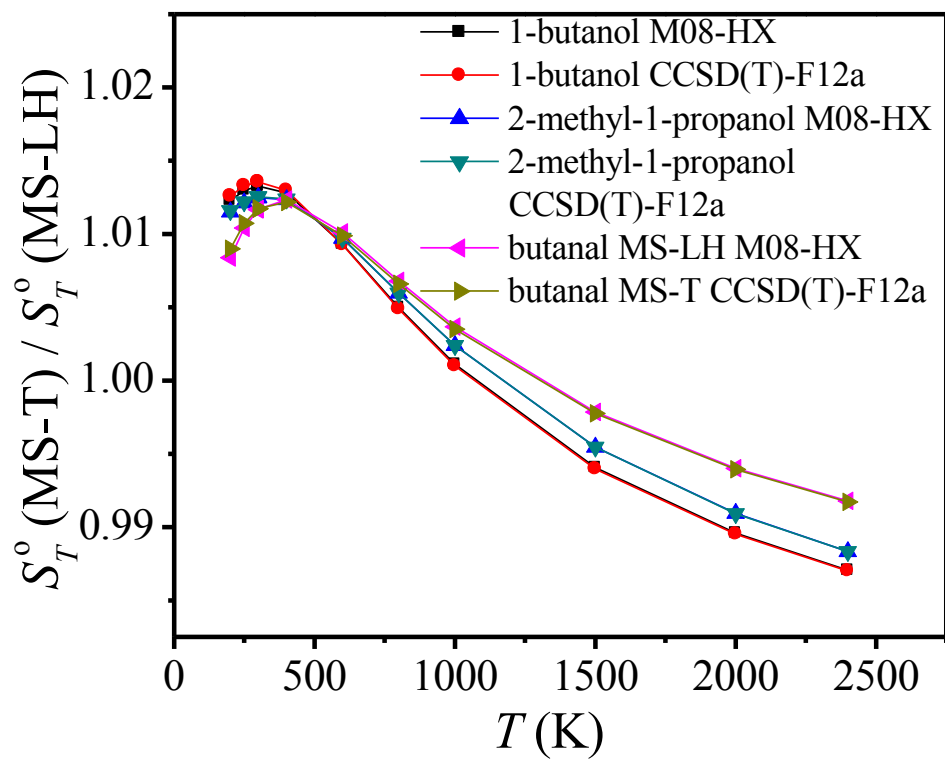
FIG. 3
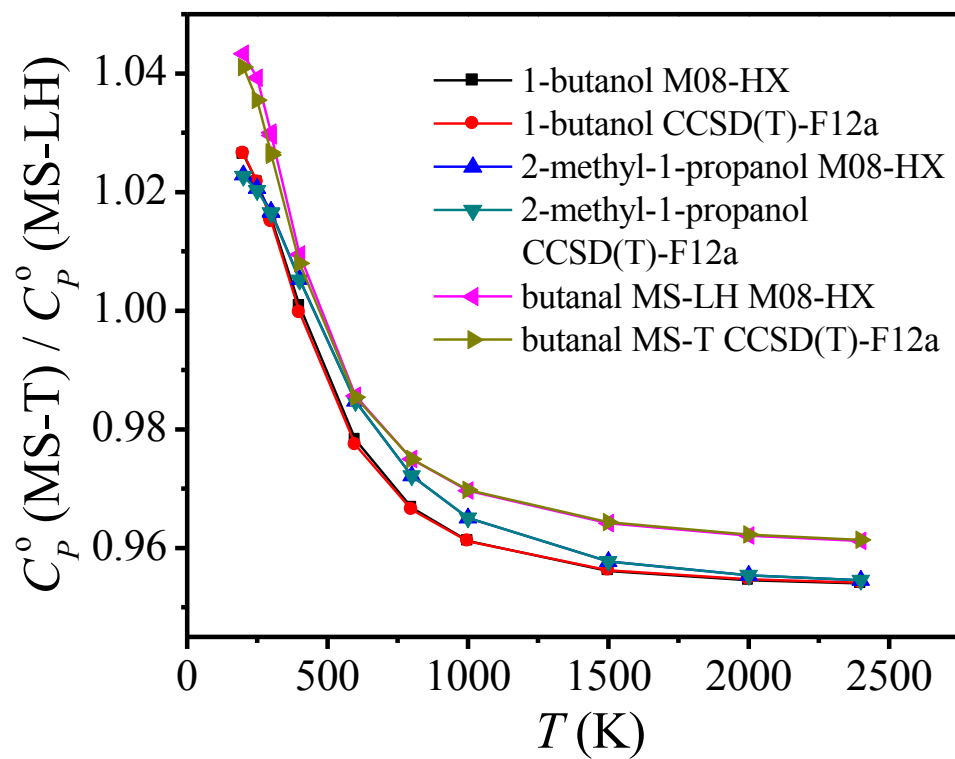
FIG. 4

Chapter 8.   Thermochemistry of Radicals Formed by Hydrogen Abstraction from 1-Butanol, 2-Methyl-1-Propanol, and Butanal

Ewa Papajak, Prasenjit Seal, Xuefei Xu, and Donald G. Truhlar*
*Department of Chemistry and Minnesota Supercomputing Institute,
University of Minnesota,
Minneapolis, MN 55455-0431 USA*

We calculate the standard state entropy, heat capacity, enthalpy, and Gibbs free energy for thirteen radicals important for the combustion chemistry of biofuels. These thermochemical quantities are calculated from recently proposed methods for calculating partition functions of complex molecules by taking into account their multiple conformational structures and torsional anharmonicity. The radicals considered in this study are those obtained by hydrogen abstraction from 1-butanol, 2-methyl-1-propanol, and butanal. Electronic structure calculations for all conformers of the radicals were carried out using both density functional theory and explicitly correlated coupled cluster theory with quasipertubative inclusion of connected triple excitations. The heat capacity and entropy results are compared with available group additivity data, and trends in enthalpy and free energy as a function of radical center are discussed for the isomeric radicals.

I. INTRODUCTION

Small oxygen-containing radicals are present in the atmosphere and are regarded as responsible for health menaces and ozone depletion. Most reactions taking place in the troposphere involve or produce radicals. Radicals are also central to the investigation of fossil-fuel and alternative-fuel combustion, where they are important as intermediates. Therefore reliable prediction of the thermodynamic properties of radicals is required for understanding both atmospheric chemistry and energy production. Yet, thermodynamic

234

data is much more plentiful for stable molecules than for radicals because radicals are difficult to investigate experimentally. Moreover, experimental techniques usually cover only small ranges of temperature, so when results are needed for broad temperature ranges, they usually can be obtained, if at all, only by interpolation or extrapolation, which can be unreliable. Modern theoretical methods based on the calculation of Born-Oppenheimer potential energy surfaces by electronic structure theory combined with a quantum statistical mechanical treatment of molecular partition functions do not have such limitations.

We recently developed a statistical mechanical method, called the multi-structural method with torsional anharmonicity[1] (MS-T) that uses electronic structure theory to calculate thermodynamic properties of molecules and radicals having multiple conformations. We made initial applications to hydrocarbons (n-hexane,[2] 2-methylpentane,[2] n-heptane,[3] and 2-methylhexane[3]), alcohols (ethanol,[1,4] 1-butanol,[1,5,6] and 2-methyl-1-propanol[5]), an aldehyde (butanal[5]), hydrocarbon radicals (1-pentyl,[1,7] 2-pentyl,[7] seven isomeric hexyls,[2] 2-cyclohexyl ethyl,[8] and 2-ethylcyclohexan-1-yl[8]), and oxygenated radicals (1-butoxyl,[9] 4-hydroxy-1-butyl,[9] and 4-hydroxy-2-butyl[9]). In the present article, we consider the oxygenated radicals produced by hydrogen abstraction from 1-butanol, 2-methyl-1-propanol, and butanal:

- five radicals of 1-butanol: 1-butoxyl radical, 1-hydroxy-1-butyl radical, 1-hydroxy-2-butyl radical, 4-hydroxy-2-butyl radical, and 4-hydroxy-1-butyl radical;
- four radicals of 2-methyl-1-propanol: 2-methyl-1-propoxyl radical, 1-hydroxy-2-methyl-1-propyl radical, 3-hydroxy-2-methyl-2-propyl radical, and 3-hydroxy-2-methyl-1-propyl radical;
- four radicals of butanal: butanoyl radical, 1-oxo-2-butyl radical, 4-oxo-2-butyl radical, and 4-oxo-1-butyl radical.

We show the radicals and their names in Figure 1. Since most of them have a large number of conformational minima due to internal rotation (up to 19 pairs of mirror images yielding 38 distinguishable structures), we compute partition functions of all the

235

radicals by employing the MS-T method incorporating all the conformers, which are also called structures.

The purpose of this study is to

- demonstrate the systematic application of the statistical mechanical method to families of radicals more complex than any treated previously;
- provide reliable thermodynamic data that can be used for atmospheric and combustion models;
- investigate enthalpy trends in the radicals that have the same chemical composition but different location of the radical center;
- compare the results of the multi-structural statistical mechanics method to thermodynamic properties calculated using Benson's group additivity rules for entropy and heat capacity.

Group additivity (GA) is widely used to compute thermodynamic properties of unknown molecules by using available data on similar compounds. In GA schemes, thermodynamic properties, such as entropy, enthalpy, and heat capacity, are estimated as additive sums of contributions from their component groups. The values for the contributions one uses to calculate a property of an unknown system are empirically established and depend on the atomic numbers of the atoms and their bonded neighbors. Due to its empiricism and to the neglect of general intergroup interactions, group additivity is more reliable for molecules typical of those well represented in the training set than it is for radicals and less studied species. Numerous group additivity schemes have been developed;[10–16] however, Benson's version[17] is the most widely used. Large sets of parameters for stable molecules have been expanded and improved over the years by Benson and coworkers and other researchers.[17–21] Literature on additivity rules for radicals is scarcer, but group additivity values are available for hydrocarbon radicals[22–26] and for some oxygen-containing radicals[27–30]. In this work, we compare our results to those calculated by Benson's group additivity using parameters from references 17, 28, and 29.

II. COMPUTATIONAL DETAILS

Conformational geometry optimizations and frequency calculations for all the conformations of all the radicals were performed using the *Gaussian 09*[31] program with the *MN-GFM*[32] density functional extension. Stationary point searches were carried out with the M08-HX density functional[33] and the MG3S basis set[34] for 1-butanol and 2-methyl-1-propanol radicals and with M08-HX and the minimally augmented correlation consistent polarized valence-triple-ζ (maug-cc-pVTZ) basis set[35–38] in the case of butanal radicals. Note that for the elements in this study (C, H, and O), the MG3S basis set is the same as the 6-311+G(2df,2p) basis set of Pople and coworkers.[39] After the initial conformational minima were found using an ultrafine grid for the density functional integrations, all the unique geometries were refined with an even finer grid having 99 radial points and 974 angular points and tight convergence criteria with a maximum force threshold of 0.000015 E_h/a_0 or 0.000015 E_h /rad and a maximum displacement of 0.000060 a_0 or 0.000060 rad (note: 1 E_h = 1 hartree; 1 a_0 = 1 bohr; 1 rad = 1 radian). Frequency calculations were performed for the refined structures. All frequencies were scaled by standard scale factors[40] of 0.973 and 0.976 for M08-HX/MG3S and M08-HX/maug-cc-pVTZ calculations, respectively. (This scale factor is the one that brings the zero point energy computed with harmonic oscillator formulas close to the experimental zero point energy, and it is used throughout this article except for the SS-HO results section III. D.)

In order to improve the accuracy of the conformational energy values from electronic structure calculations, single-point energy calculations were performed using explicitly correlated coupled cluster theory with single and double excitations and a quasiperturbative treatment of connected triple excitations. In particular, we used the CCSD(T)-F12a method[41] with the jul-cc-pVTZ basis set[38] as the one-electron basis set for alcohol-derived radicals and the jun-cc-pVTZ basis set[42] as the one-electron basis set for butanal-derived radicals. CCSD(T)-F12a calculations are coupled cluster calculations that employ a conventional expansion in Slater determinants formed from a one-electron Gaussian basis and augment this with excitation amplitudes corresponding to excitations into explicitly correlated functions[43–53] containing short-range correlation. The basis set

convergence with respect to the one-electron basis is much faster than for conventional CCSD(T) calculations such that the jul-cc-pVTZ and jun-cc-pVTZ basis sets should yield results close to the complete basis set limit.

The coupled cluster calculations were carried out using the *Molpro 09* program suite.[55] These single-point energy calculations were used to upgrade the thermodynamics calculations, and in the results section we compare the upgraded calculations to the results obtained by using M08-HX/MG3S energies.

The partition function calculations were carried out using the *MSTor* computer program.[56,57] In this program, the total partition function Q is calculated as a product of the translational (Q_{trans}), electronic (Q_{elec}), and conformational–rotational–vibrational ($Q_{con-rovib}$), partition functions:[1]

$$Q = Q_{trans}Q_{elec}Q_{con-rovib} \tag{1}$$

In the present article, we employ two multi-structural (MS) approximations to the $Q_{con-rovib}$ term that we described in reference 1. Both of them calculate the conformational-rotational-vibrational partition function as a sum over the contributions of all conformational structures for a given molecule, but they differ in how the individual contributions are put together.

In the first method, called the MS local quasiharmonic (MS-LQ) method, we calculate the contribution to the partition function for each structure as a product of the classical approximation to the rotational partition function and a local quasiharmonic oscillator approximation to the vibrational partition function. The quasiharmonic approximation uses the harmonic oscillator formulas, but with scaled frequencies, where the scaling corrects in an approximate way for anharmonicity as well as for the systematic overestimation in the higher frequencies by the electronic structure calculations. Therefore the MS-LQ (formerly called MS-LQ for "local harmonic" because the formulas are based on the harmonic oscillator) results are partially anharmonic. In the second method, called MS-T, we improve upon the MS-LQ partition function by including factors for torsional anharmonicity. For a molecule with t torsions, there are $t + 1$ factors for each structure.[1] The first factor ensures that the partition function reaches the correct free-rotor limit in the high-temperature limit. The other

factors adjust the harmonic result for the anharmonicity of each of the t internal-coordinate torsions.

Subsequently, based on the partition functions just described, which will be called $Q_{\text{elec}}, Q_{\text{con-rovib}}^{\text{MS-QH}}$, and $Q_{\text{con-rovib}}^{\text{MS-T}}$, the standard state thermodynamic functions (enthalpy H_T°, heat capacity C_P°, entropy S_T°, and Gibbs free energy G_T°) are computed based on the total partition function by standard formulas:

$$H_T^\circ = -\frac{\partial \ln Q}{\partial \beta} + k_B T \tag{2}$$

$$C_P^\circ (T) = -\left(\frac{\partial H^\circ}{\partial T}\right)_P \tag{3}$$

$$S_T^\circ = k_B + k_B \ln Q - \frac{1}{T}\left(\frac{\partial \ln Q}{\partial (1/(k_B T))}\right)_V \tag{4}$$

and

$$G_T^\circ = H_T^\circ - T S_T^\circ \tag{5}$$

where $^\circ$ denotes the standard state (1 bar pressure), k_B is Boltzmann's constant, T is temperature, and Q is the partition function with the zero of energy at the vibrational zero point exclusive energy of the structure of the radical that has the lowest zero-point-inclusive energy. (This structure is called the global minimum (GM) and the choice of zero of energy is a special case of our general convention that partition functions without a tilde have their zero of energy at the local minimum of the Born-Oppenheimer potential energy surface.) The thermodynamic quantities above have been computed for a range of temperature and are given in the results section and in the supplementary material. In the case of enthalpy and Gibbs free energy, we list H_T° and G_T° values, where the subscript T refers to temperature. Note that, since our calculations are carried out for the gas phase, the thermodynamic data listed for the low temperatures (below the boiling or melting point) refer to the vapor phase above the liquid or solid.

III. RESULTS AND DISCUSSION

Figure 2 depicts the notation that we adopted for specific ranges of dihedral angles in order to label the conformational structures of the radicals. We follow the recommendations of International Union of Pure and Applied Chemistry (IUPAC) on nomenclature of the torsion angles.[58] Thus **T**, **T⁺,** and **T⁻** stand for "trans" and correspond to 180° exactly, (+150° to +180°), and (−150° to −180°), respectively. **C**, **C⁺**, and **C⁻** stand for "cis" and correspond to angles of exactly 0°, (0° to +30°), and (0° to −30°), respectively. Similarly, "gauche" and "anti" span the ranges of (±30°, ±90°) and (±90°, ±150°). In order to differentiate those gauche angles that are far from the typical ±60° and closer to ±90°, we chose to split the "gauche" range into two sub-ranges: **G±** (±30°, ±75°) and **g±** (±75°, ±90°). A similar division was made for the "anti" configuration by assigning **a±** to (±90°, ±105°) angle values and **A±** to those within (±105°, ±150°).

When labeling conformational structures we always start from the first torsion on the O-side of the chain and move by one bond along the chain. For example, structure **C⁺T⁻G⁺** of the 1-hydroxy-1-butyl radical corresponds to the conformer in which the first ($H–O–C–C$) torsional angle is +24.8°, the second ($O–C–C–C$) torsional angle is -173.0°, and the third ($C–C–C–C$) torsional angle is +65.0°. Rotation around the fourth bond, ($C–C–C–H$), does not produce distinguishable structures and is therefore omitted in labeling of the conformational structures.

All the alcohol-derived radicals considered in this article have the chemical formula C_4H_9O. Similarly, all the butanal-derived radicals have the same molecular composition (C_4H_7O). If the enthalpies and free energies of these radicals are computed with respect to a common zero of energy they may be considered a measure of relative stability of the isomeric radicals. That is why we defined the absolute zero of energy as the zero-point exclusive energy of the lowest energy structure of the GM. In the case of alcohol-derived radicals the GM is the **T⁺G⁻, T⁻G⁺** structure of 1-hydroxy-2-methyl-1-propyl radical, whereas for aldehyde-derived radicals, the **CT** structure of butanoyl radical is the GM. For other uses, some readers may wish to convert the zero of energy to either the equilibrium structure or the ground-state level of a particular radical of interest. That

can easily be done with the data provided in our tables because we give the Born-Oppenheimer energy and zero-point inclusive energy of every structure of every radical in Tables I – VII.

In Tables I – VII we list the conformational structures for all the radicals, and Tables VIII – XIII provide their computed thermodynamics properties for three temperature values for H_T° and G_T° and three-to-six temperatures for S_T° and $C_P^{\circ}(T)$. Supplementary material includes data for a wider range of temperature.[59] Where GA parameters are available, we compare our results to values computed using these parameters.

III.A. 1-Butanol radicals

We have identified nine distinguishable conformers (four pairs of mirror images plus one symmetrical structure **TT**) for the 1-butoxyl radical, 36 conformers (18 pairs of mirror images) each for the 1-hydroxy-1-butyl and 1-hydroxy-2-butyl radicals, and 38 conformers (19 pairs of mirror images) each for the 1-hydroxy-3-butyl and 1-hydroxy-4-butyl radicals. Tables I – V list all of the conformers along with their equilibrium energy (sometimes called the Born-Oppenheimer energy, the zero-point exclusive energy, the classical energy, the electronic energy or the electronic energy including nuclear repulsion) and their zero-point-inclusive energy (which may also be called the 0 K energy or ground-vibrational-state energy). The equilibrium energies are presented both as calculated by M08-HX/MG3S and as calculated by CCSD(T)-F12a/jul-cc-pVTZ//M08-HX/MG3S (where, as usual, A//B denotes a single-point energy calculation by method A at a geometry optimized by method B), and the zero-point-inclusive energies are presented only as calculated by M08-HX/MG3S with scaled frequencies.

The five lowest-energy structures of each radical are illustrated in Figure 3. The M08-HX/MG3S and CCSD(T)-F12a/jul-cc-pVTZ methods identify different structures as having the lowest equilibrium energy for the 1-hydroxy-1-butyl and 1-hydroxy-2-butyl radicals, whereas they identify the same lowest-equilibrium-energy structure for the other three radicals produced from 1-butanol. Another noteworthy difference in the predictions of the two methods is that in the cases of the 1-hydroxy-2-butyl and 1-hydroxy-4-butyl

radicals the variation in the conformational energy is significantly lower in the coupled cluster calculations than in the density functional calculations.

Table VIII provides the thermodynamics properties of the five 1-butanol radicals. Where group additivity coefficients are available, Table IX compares them to those obtained in this study. For 1-butoxyl radical, 4-hydroxy-2-butyl radical, and 4-hydroxy-1-butyl radical, there are two sets of parameters available for calculations of heat capacity and entropy by group additivity. The values in the column on the left were obtained using parameters taken from the second edition of Benson's book on thermochemical kinetics.[17] The values on the right were obtained using a combination of parameters by Benson[17] and more recently established parameters taken from Khan *et al.*[28] and Sabbe *et al.*[29] With one exception (M08-HX/MG3S results for 1-hydroxy-3-butyl) all of the heat capacity values computed by GA are lower than those computed in the present work. The coupled cluster results vary slightly more from the group additivity ones than do the DFT results. The heat capacities differ by as much as 1.67 cal/mol. In the case of entropy we find better agreement of DFT and CC results with group additivity for radicals than we found previously[1,5] for 1-butanol, with mean error in the present case averaging 1.6 cal/mol and the highest error being 3.5 cal·mol^{-1}·K^{-1}.

Comparing Gibbs free energy values for the radicals, all relative to the same zero of energy, one can also draw conclusions on their relative stability. Comparison of G_{298}° of the alcohol radicals leads to the conclusion that 1-hydroxy-1-butyl radical is the most stable product of the hydrogen abstraction from 1-butanol. It has a significantly lower G_{T}° than all the other radicals, by 2.7–10.8 kcal·mol^{-1} at 298 K, 2.1–12.7 kcal·mol^{-1} at 800 K, and 0.9–16.2 kcal·mol^{-1} at 2000 K. The Gibbs free energy increases in the following order : 1-hydroxy-1-butyl < 4-hydroxy-2-butyl < 1-hydroxy-2-butyl < 4-hydroxy-1-butyl < 1-butoxyl radical.

The impact of anharmonicity and multi-structural effects on the calculated relative stability is discussed in section III. D.

III.B. 2-Methyl-1-propanol radicals

We found 3 conformers (1 pair of mirror images plus 1 symmetrical structure T) for the 2-methyl-1-propoxyl radical, 12 conformers (6 pairs of mirror images) for the 1-hydroxy-2-methyl-1-propyl radical, 8 conformers (4 pairs of mirror images) for the 3-hydroxy-2-methyl-2-propyl radical, and 18 conformers (9 pairs of mirror images) for the 3-hydroxy-2-methyl-1-propyl radical. Up to five lowest-energy structures of each radical are illustrated in Figure 4. Table VI lists all of the conformers and their classical M08-HX/MG3S, zero-point-corrected M08-HX/MG3S, and the CCSD(T)-F12a/jul-cc-pVTZ single point conformational energy values. In the case of 2-methyl-1-propanol radicals prediction of the lowest energy structure based on M08-HX/MG3S and CCSD(T)-F12a/jul-cc-pVTZ energy values differs slightly (by 0.04 kcal/mol) only for one case: 3-hydroxy-2-methyl-1-propyl radical.

Tables X summarizes the thermodynamics properties of the 2-methyl-1-propanol radicals. Variation in the Gibbs free energy values for these radicals is less than what we observed in the case of 1-butanol radicals. G values increase as the radical center is located farther away from –OH group along the heavy-atom chain

$$\dot{O}-C-C-(C)_2 > O-\dot{C}-C-(C)_2 > O-C-\dot{C}-(C)_2 > O-C-C-(C)(\dot{C})$$. Figure 6 depicts

comparison of G_T° at 298 K of the alcohol radicals. 1-hydroxy-2-methyl-1-propyl radical is the most stable product of the hydrogen abstraction from 2-methyl-1-propanol and the most stable among the alcohol derived radicals in this study. For the 2-methyl-1-propanol radicals the Gibbs free energy increases in the following order : 1-hydroxy-2-methyl-1-propyl < 3-hydroxy-2-methyl-2-propyl < 3-hydroxy-2-methyl-1-propyl < 2-methyl-1-propoxyl radical. The importance of anharmonicity and multi-structural effects in these calculations is discussed in section III. D.

Table XI compares heat capacity and entropy values computed in this work to the group additivity values, considering large variation within the GA values computed with different parameters, it shows very good agreement.

III.C. Butanal radicals

We have optimized 7 conformers (3 pairs of mirror images plus 1 symmetrical CT structure) for the butanoyl radical, 6 conformers (2 pairs of mirror images and two different structures superimposable with their own images) for the 1-oxo-2-butyl radical, 7 conformers (3 pairs of mirror images and one **CT** symmetrical structure) for the 4-oxo-2-butyl radical, and 14 conformers (7 pairs of mirror images) for the 4-oxo-1-butyl radical. Figure 5 illustrates up to five lowest-energy structures of each radical of butanal. Table VII lists all of the conformers and their classical M08-HX/maug-cc-pVTZ, zero-point-corrected M08-HX/maug-cc-pVTZ, and the CCSD(T)-F12a/jun-cc-pVTZ single-point conformational energy values. Similarly to 2-methyl-1-propanol radicals, prediction of the lowest energy structure for butanal based on M08-HX/maug-cc-pVTZ and CCSD(T)-F12a/jun-cc-pVTZ energy values agrees for all but one case: butanoyl radical with an 0.05 kcal/mol difference in conformational energy.

Table XII depicts the standard state thermodynamic properties, viz., enthalpy, heat capacity, entropy and free energies for the butanal-derived radicals under consideration at temperatures 298, 800, and 2000 K. The highest free energy belongs to butanoyl radical and the lowest to the 4-oxo-1-butyl radical. The table reveals the fact that the values vary little with respect to the methods used. Table XIII compares heat capacity and entropy values computed in this work to the group additivity values showing very good agreement of our results with the GA using recent parameters.

The relative stability of the butanal radicals as estimated from MS-T Gibbs free energy decreases in the following order: butanoyl > 1-oxo-2-butyl > 4-oxo-2-butyl > 4-oxo-1-butyl radical.

III.D. Importance of anharmonicity and multi-structure effects on the relative stability of radicals

Comparison of the stability of various chemical species (reagents, intermediate products, transition states) is one of the most common applications of computational methods in mechanistic studies of chemical reactions. Stability of the transition states relative to the reactants controls branching ratios in the case of multiple possible reactive

paths. Stability of the intermediate products of reactions involving many steps may affect which isomeric product will form or which mechanism of the reaction is favorable. Differences in the stability of the radicals has been shown to affect which reactive site is going to be substituted in chain reactions with radical-like transition states. Therefore, the estimation of relative stabilities of isomeric radicals and other species is ubiquitous and consequential in the chemistry literature. This relative stability is commonly estimated in the literature as the zero-point corrected and/or –uncorrected electronic energy of their lowest energy conformers. If frequency calculation is affordable for a system in question Gibbs free energy values (again, most often only for the lowest energy conformer) are used as a measure of the relative stability. Anharmonicity and torsional effects are assumed to have negligible effect on the stability of the species.

In order to evaluate the importance of including multiple conformational structures as well as the torsional anharmonicity effects on the partition function, and consequently on the Gibbs free energy at 298 K, Figures 6 and 7 compare trends in the relative stability of the radicals. Gibbs free energy values computed by the MS-T method (shown in green) are the most computationally extensive because they take into account all the conformational minima and correct for anharmonicity. The other columns use quantities that are calculated for the single, lowest energy structure, which saves a certain amount of work and computational time. Red columns depict the trend in the Born-Oppenheimer electronic energy of the radicals and constitute the least expensive, but also the crudest way of estimating relative stability of different species in this figure. In blue we show the same energy values, but corrected by the scaled vibrational zero-point energy. The scaling factors used here (unlike the rest of the paper) are those that correct the systematic errors partially inherent in a given electronic structure method (M08-HX/MG3S for alcohol-derived radicals and M08-HX/maug-cc-pVTZ for those derived from aldehyde) and partially due to the harmonic approximation of the vibrational motion. The scaling factors used here are those that bring frequencies closest to the experimental results. The purple columns show trends in the single structure Gibbs free energies of radicals, where frequencies are scaled to match the best harmonic frequency. This method is called the single structure harmonic approximation (SS-QH) in our

figures. The predictions of relative stability of radicals from different methods differ by up to about 1 kcal·mol^{-1} for alcohol-derived radicals and by up to about 2 kcal·mol^{-1} for the butanal-derived radicals. Furthermore, the predictions of the relative stability of the isomeric radicals from SS-QH and MS-T approximations differ significantly. For example, according to SS-QH butanoyl and 1-oxo-2-butyl radicals have nearly equal Gibbs free energy values as shown in Figure 7. However, MS-T predicts an over 2 kcal·mol^{-1} difference in free energy, which suggests abstraction from C1 produces a more favorable radical than abstraction from C2. In the case of alcohol-derived radicals in Figure 6 the conclusions on the relative stability of the radicals is actually reverse using MS-T and SS-QH for 1-hydroxy-1-butyl and 3-hydroxy-2-methyl-2-propyl radicals.

IV. CONCLUSIONS

In this study, we have computed the thermodynamic data for five radicals of 1-butanol, four radicals of 2-methyl-1-propanol, and four radicals of butanal. We incorporated all conformational stationary points for each molecule by using the multiple-structure local quasiharmonic (MS-QH) approximation and the multi-structural method with torsional anharmonicity (MS-T). Benson's group additivity (GA) values for heat capacities and entropies

(C_P° and S_T°) agree reasonably well with our results when one considers the empirical nature of GA: to within 2 cal·mol^{-1}·K^{-1} for S_T° and 1 cal·mol^{-1}·K^{-1} for C_P°. We also calculate enthalpies and free energies. The results obtained from DFT reproduce those from coupled cluster theory to within ~0.08 kcal·mol^{-1} for H°, ~0.08 cal·mol^{-1}·K^{-1} for C_p°, ~0.05 cal·mol^{-1}·K^{-1} for S_T°, and 0.1 kcal·mol^{-1} for G_T°. We show that anharmonicity and multiple-structure effects have appreciable effect on the thermodynamic properties of radicals.

References

[1] J. Zheng, T. Yu, E. Papajak, I. M. Alecu, S. L. Mielke, and D. G. Truhlar, Phys. Chem. Chem. Phys. **13**, 10885 (2011).

[2] J. Zheng, T. Yu, and D. G. Truhlar, Phys. Chem. Chem. Phys. **13**, 19318 (2011)

[3] T. Yu, J. Zheng, and D. G. Truhlar, Phys. Chem. Chem. Phys., **14**, 482 (2011)

[4] J. Zheng and D. G. Truhlar, Faraday Discuss., in press.

[5] P. Seal, E. Papajak, T. Yu, and D. G. Truhlar, J. Chem. Phys. **136**, 034306 (2012).

[6] P. Seal, E. Papajak, J. Zheng, and D. G. Truhlar, J. Phys. Chem. Lett. **3**, 264 (2012).

[7] T. Yu, J. Zheng, and D. G. Truhlar, Chem. Sci., **2**, 2199 (2011).

[8] T. Yu, J. Zheng, and D. G. Truhlar, J. Phys. Chem. A **116**, 297 (2012).

[9] X. Xu, E. Papajak, J. Zheng, and D. G. Truhlar, Phys. Chem. Chem. Phys. 14, 4204 (2012).

[10] J. Platt, J. Chem. Phys. **15**, 419 (1947)

[11] J. Platt, J. Phys. Chem. **56**, 328 (1952)

[12] J. Greenshields and F. Rossini, J. Phys. Chem. **62**, 271 (1958).

[13] G. Somayajulu and B. Zwolinski, J. Trans. Faraday Soc. **62**, 2327 (1966).

[14] T. -P. Thinh, J. -L. Duran, and R. Ramalho, Ind. Eng. Process Des. Dev. **10**, 576 (1971).

[15] T. –P. Thinh and T. Trong, Can. J. Chem. **54**, 344 (1976).

[16] R. Joshi, J. Macromol. Sci.-Chem. **A4**, 1819 (1970).

[17] S. W. Benson, *Thermochemical Kinetics*, 2nd ed. (Wiley-Interscience, New York, 1976).

[18] N. Cohen, S. Benson, Chem. Rev. **93**, 2419 (1993)

[19] N. Cohen, J. Phys. Chem. Ref. Data **25**, 1411 (1996).

[20] T. H. Lay and J. W. Bozzelli, J. Phys. Chem. A **101**, 9505 (1997).

[21] N. Sebbar, J. W. Bozzelli, H. Bockhorn, J. Phys. Chem. A **108**, 8353-8366 (2004).

[22] H. O'Neal, S. Benson, In Free Radicals; J. K. Kochi, Ed.; Wiley: New York, 1973; pp 275.

[23] T. Ni, R. Caldwell, L. Melton, J. Am. Chem. Soc. **111**, 457 (1989).

[24] N. Cohen, J. Phys. Chem. **96**, 9052 (1992).

[25] M. K. Sabbe, F. De Vieeschower, M.-F. Reyniers, M. Waroquier, and G. B. Marin, J. Phys. Chem. A **112**, 12235 (2008).

[26] V. V. Turovtsev, Y. D. Orlov, Y. A. Lebedev, Russ. J. Phys. Chem. A **83** 245 (2009).

[27] I. Marsi, B. Viskolcz, L. Seres, J. Phys. Chem. A **104**, 4497 (2000).

[28] S. S. Khan, X. Yu, J. R. Wade, D. Malmgren, and L. J. Broadbelt J. Phys. Chem. **113**, 5176 (2009).

[29] M. K. Sabbe, M. Saeys, M.-F. Reyniers, and G. B. Marin J. Phys. Chem. A **109**, 7466 (2005)

[30] J. M. Hudzik, J. W. Bozzelli, J. Phys. Chem. A **114**, 7984 (2010).

[31] M. J. Frisch, G. W. Trucks, H. B. Schlegel, G. E. Scuseria, M. A. Robb, J. R. Cheeseman, G. Scalmani, V. Barone, B. Mennucci, G. A. Petersson, H. Nakatsuji, M. Caricato, X. Li, H. P. Hratchian, A. F. Izmaylov, J. Bloino, G. Zheng, J. L. Sonnenberg, M. Hada, M. Ehara, K. Toyota, R. Fukuda, J. Hasegawa, M. Ishida, T. Nakajima, Y. Honda, O. Kitao, H. Nakai, T. Vreven, Jr., J. A. Montgomery, J. E. Peralta, F. Ogliaro, M. Bearpark, J. J. Heyd, E. Brothers, K. N. Kudin, V. N. Staroverov, R. Kobayashi, J. Normand, K. Raghavachari, A. Rendell, J. C. Burant, S. S. Iyengar, J. Tomasi, M. Cossi, N. Rega, N. J. Millam, M. Klene, J. E. Knox, J. B. Cross, V. Bakken, C. Adamo, J. Jaramillo, R. Gomperts, R. E. Stratmann, O. Yazyev, A. J. Austin, R. Cammi, C. Pomelli, J. W. Ochterski, R. L. Martin, K. Morokuma, V. G. Zakrzewski, G. A. Voth, P. Salvador, J. J. Dannenberg, S. Dapprich, A. D. Daniels, Ö. Farkas, J. B. Foresman, J. V. Ortiz, J. Cioslowski, and D. J. Fox, *Gaussian 09*, Revision A.02, Gaussian, Inc., Wallingford CT, 2009.

[32] Z. Zhao, R. Peverati, K. Yang, and D. G. Truhlar, *MN-GFM* version 5.2 computer program module, University of Minnesota, Minneapolis, 2011.

[33] Y. Zhao, N. E. Schultz, and D. G. Truhlar, J. Chem. Theory Comput. **4**, 1849 (2008).

[34] B. J. Lynch, Y. Zhao, and D. G. Truhlar, J. Phys. Chem. A **107**, 1384 (2003).

[35] T. H. Jr. Dunning, J. Chem. Phys. **90**, 1007 (1989).

[36] R. A. Kendall, T. H. Jr. Dunning, R. J. Harrison, J. Chem. Phys. **96**, 6796 (1992).

[37] E. Papajak, H. R. Leverentz, J. Zheng, and D. G. Truhlar, J. Chem. Theory Comput. **5**, 1197 (2009); **5**, 3330 (2009).

[38] E. Papajak and D. G. Truhlar, J. Chem. Theory Comput. **6**, 597 (2010).

[39] R. Krishnan, J. S. Binkley, R. Seeger, and J. A. Pople, J. Chem. Phys. **72**, 650 (1980); T. Clark, J. Chandrasekhar, G. W. Spitznagel, and P. v. R. Schleyer, J. Comp. Chem. **4**, 294 (1983); M. J. Frisch, J. A. Pople, and J. S. Binkley, J. Chem. Phys. **80**, 3265 (1984).

[40] I. M. Alecu, J. Zheng, Y. Zhao, and D. G. Truhlar, J. Chem. Theory Comput. **6**, 2872 (2010).

[41] G. Knizia, T. B. Adler, and H.-J. Werner, J. Chem. Phys. **130**, 054104 (2009).

[42] E. Papajak and D. G. Truhlar, J. Chem. Theory Comput. **7**, 10 (2011).

[43] W. Kutzelnigg Theor. Chim. Acta **68**, 445 (1985).

[44] W. Kutzelnigg, W. Klopper, J. Chem. Phys., **94**, 1985, (1991).

[45] W. Klopper, W. Kutzelnigg, Chem. Phys. Lett. **134**, 17 (1987).

[46] W. Klopper, C. C. M. J. Samson, Chem. Phys. **116**, 6397 (2002).

[47] F. R. Manby, J. Chem. Phys. **119**, 4607 (2003).

[48] S. Ten-no, F. R. Manby, J. Chem. Phys. **119**, 5358 (2003).

[49] S. J. Ten-no, Chem. Phys. **121**, 117 (2004).

[50] E. F. Valeev, Chem. Phys. Lett. **395**, 190 (2004).

[51] E. F. Valeev and C. L. Jansen, Chem. Phys. Lett. **121**, 1214 (2004).

[52] S. Ten-no, Chem. Phys. Lett. **121**, 117 (2004).

[53] H. –J. Werner, T. B. Adler, and F. R. Manby, J. Chem. Phys. **126**, 164102 (2007).

[54] T. D. Crawford, C. D. Sherrill, E. F. Valeev, J. T. Fermann, R. A. King, M. L. Leininger, S. T. Brown, C. L. Janssen, E. T. Seidl, J. P. Kenny, and W. D. J. Allen, J. Comp. Chem. **28**, 1610 (2007).

[55] H.-J. Werner, P. J. Knowles, F. R. Manby, M. Schütz, P. Celani, G. Knizia, T. Korona, R. Lindh, A. Mitrushenkov, G. Rauhut, T. B. Adler, R. D. Amos, A. Bernhardsson, A. Berning, D. L. Cooper, M. J. O. Deegan, A. J. Dobbyn, F. Eckert, E. Goll, C. Hampel, A. Hesselmann, G. Hetzer, T. Hrenar, G. Jansen, C. Köppl, Y. Liu, A. W. Lloyd, R. A. Mata, A. J. May, S. J. McNicholas, W. Meyer, M. E. Mura, A. Nicklaß, P. Palmieri, K. Pflüger, R. Pitzer, M. Reiher, T. Shiozaki, H. Stoll, A. J. Stone, R. Tarroni, T.

Thorsteinsson, M. Wang, and A. Wolf, *Molpro* computer program, version 2010.1 (University of Birmingham, Birmingham, 2010).

[57] J. Zheng, S. L. Mielke, K. L. Clarkson, and D. G. Truhlar, Computer Phys. Commun., to be published.

[58] G. P. Moss, Pure Appl. Chem. *68*, 2193 (1996). *See* page 2220.

[59] See Supplementary Material Document for all the structures and corresponding zero-point-exclusive and zero-point- inclusive relative conformational energies for 1-butanol obtained with M08-SO and M06-2X density functionals and MG3S basis set.

A.

1-butoxyl radical
$[2 \cdot 4 + 1]$

B.

1-hydroxy-1-butyl radical
$[2 \cdot 18]$

C.

1-hydroxy-2-butyl radical
$[2 \cdot 18]$

D.

4-hydroxy-2-butyl radical
$[2 \cdot 19]$

E.

4-hydroxy-1-butyl radical
$[2 \cdot 19]$

F.

2-methyl-1-propoxyl radical
$[2 \cdot 1 + 1]$

G.

1-hydroxy-2-methyl-1-propyl radical
$[2 \cdot 6]$

H.

3-hydroxy-2-methyl-2-propyl radical
$[2 \cdot 4]$

I.

3-hydroxy-2-methyl-1-propyl radical
$[2 \cdot 9]$

J.

butanoyl radical
(also called
butyryl radical or
1-oxo-1-butyl radical)
$[2 \cdot 3 + 1]$

K.

1-oxo-2-butyl radical
$[2 \cdot 2 + 1 + 1]$

L.

4-oxo-2-butyl radical
$[2 \cdot 3 + 1]$

M.

4-oxo-1-butyl radical
$[2 \cdot 7]$
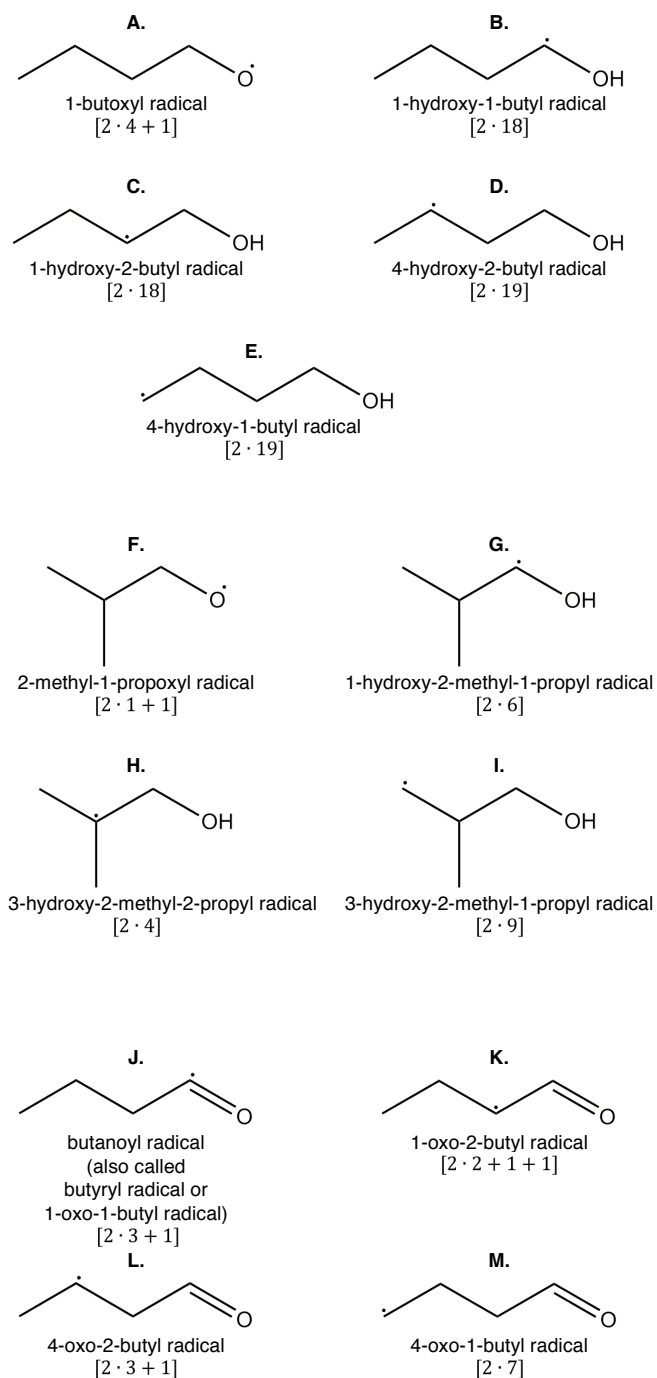
FIG. 1. Structures and names of radicals of 1-butanol, 2-methyl-1-propanol, and butanal studied in this work. The totals in the parentheses $[2 \cdot a + b + c]$ indicate the number of distinguishable conformational structures included in the calculations in our partition function calculations, where a is a number of pairs of mirror images, and $b \neq 1$ and $c \neq 1$ indicate existence of one (when $b = 1$ and $c = 0$) or two (when $b = 1$ and $c = 1$) conformers that are superimposable with their own mirror images.

251
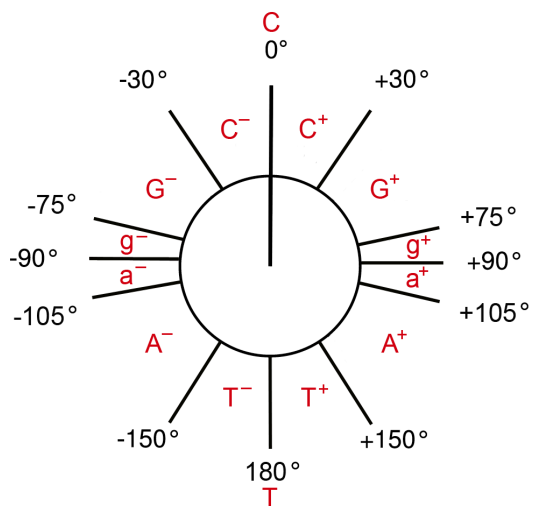
FIG. 2. Labeling scheme used in this article to define structures by their dihedral angles.

1-Butoxyl Radical

G+T−, G−T+   G+G+, G−G−   g+G−, g−G+   TT   T+G+, T−G−

1-Hydroxy-1-butyl Radical

T+G+G+, T−G−G−   G+G+G−, G−G−G+   T+G−G−, T−G+G+   C+G−G−, C−G+G+   T+G−T+, T−G+T−

1-Hydroxy-2-butyl Radical

G+G+G+, G−G−G−   G+G+T−, G−G−T+   G+T−T+, G−T+T−   G+G+a−, G−G−a+   G+T−G−, G−T+G+

4-Hydroxy-2-butyl Radical

G+G−T+, G−G+T−   G+G−G−, G−G+G+   G−G+G+, G+G−G−   G+G−A+, G−G+A−   G+G+T+, G−G+T−

4-Hydroxy-1-butyl Radical

G−G+G−G−, G+G−G+G+   G+G−G−C−, G−G+G+C+   T−G+G+G+, T+G−G−G−   T+G−T+C−, T−G+T−C+   G+G+G+C+, G−G−G−C−
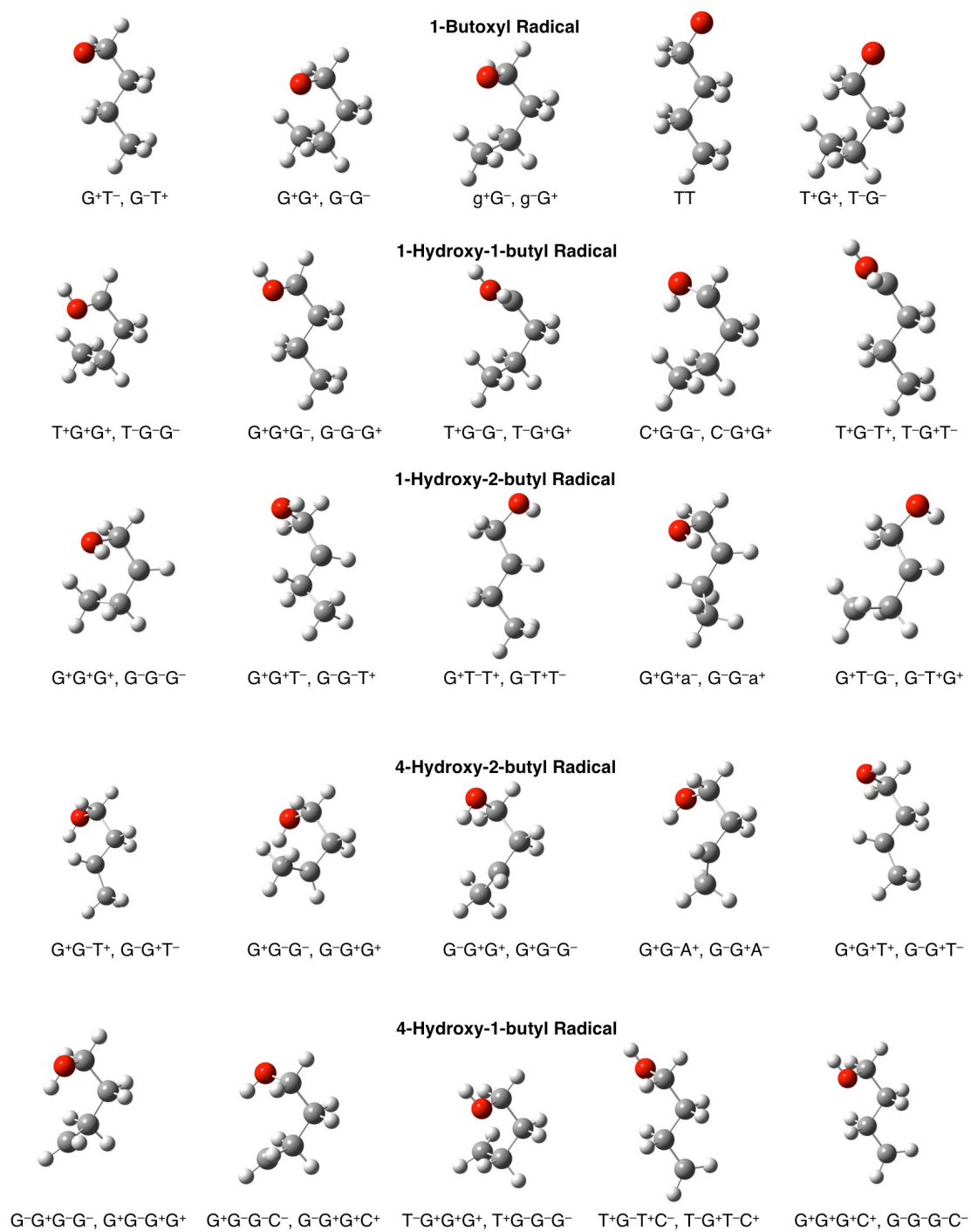
FIG. 3 Lowest energy conformers for 1-butanol radicals.

2-methyl-1-propoxyl Radical

G^+, G^- T

1-hydroxy-2-methyl-1-propyl Radical

T^+G^-, T^-G^+ T^+G^+, T^-G^- C^-G^-, C^+G^+ C^-G^+, C^+G^- $T+T+$, $T-T-$

3-hydroxy-2-methyl-2-propyl Radical

Tg^+, Tg^- T^-T^-, T^+T^+ G^+T^-, G^-T^+ G^+G^-, G^-G^+

3-hydroxy-2-methyl-1-propyl Radical

$G^-T^-G^+$, $G^+T^+G^-$ $G^+G^+G^-$, $G^-G^-G^+$ $G^+G^+g^-$, $G^-G^-g^+$ $T^-G^-G^+$, $T^+G^+G^-$ $T^+G^+G^+$, $T^-G^-G^-$
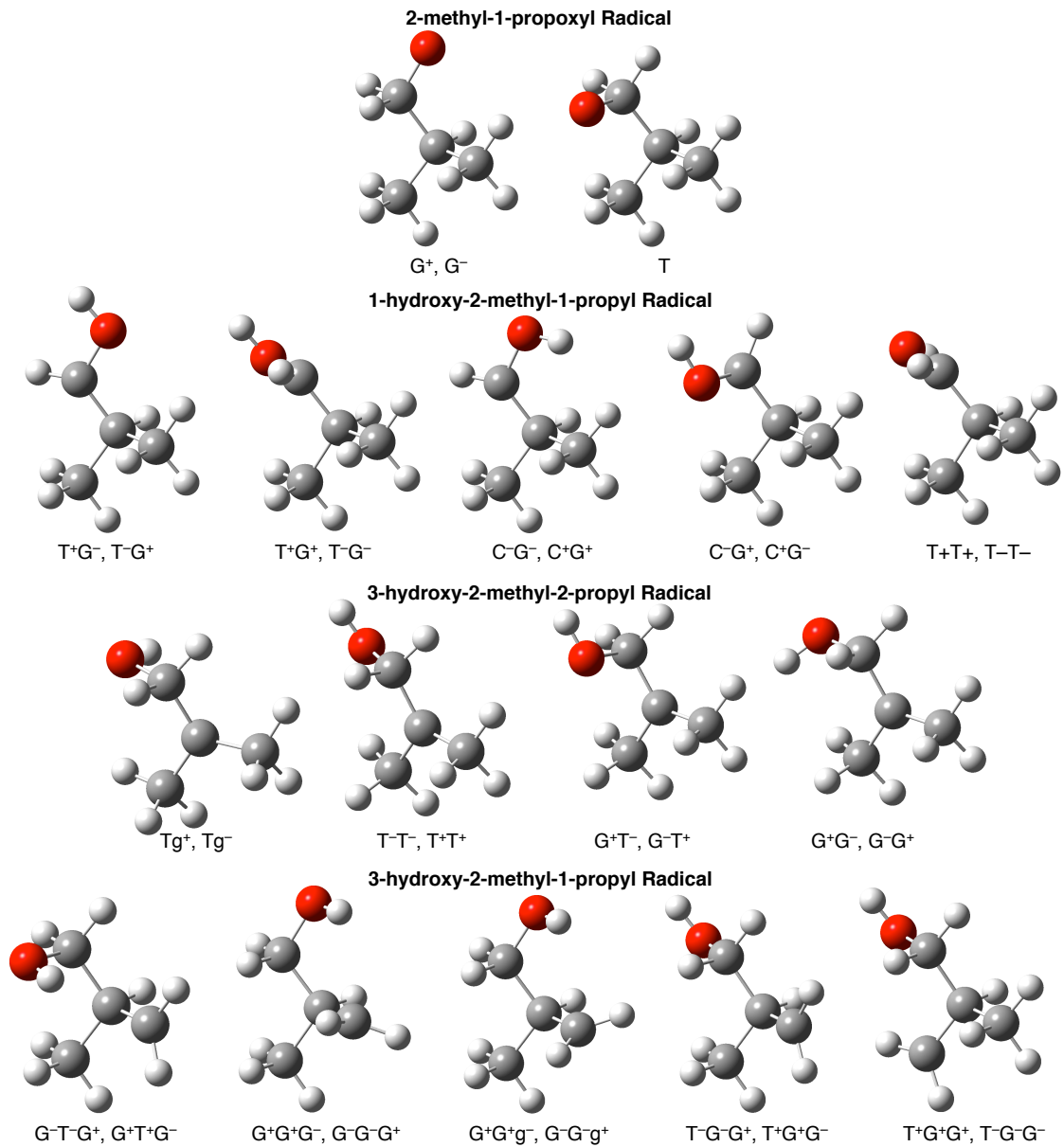
FIG. 4. Lowest energy conformers for 2-methyl-1-propanol radicals.

Butanoyl Radical

C⁺G⁺, C⁻G⁻   CT   T⁻G⁺, T⁺G⁻   A⁻T⁻, A⁺T⁺

1-oxo-2-butyl Radical

C⁻A⁺, C⁺A⁻   CC   T⁺A⁺, T⁻A⁻   TC

4-oxo-2-butyl Radical

CT   C⁻G⁺, C⁺G⁻   a⁻g⁺, a⁺g⁻   A⁻T⁺, A⁺T⁻

4-oxo-1-butyl Radical

C⁺T⁻T⁻, C⁻T⁺T⁺   C⁺G⁺G⁻, C⁻G⁻G⁺   C⁺G⁺T⁻, C⁻G⁻T⁺   A⁻G⁺C⁺, A⁺G⁻C⁻   A⁻G⁻T⁺, A⁺G⁺T⁻
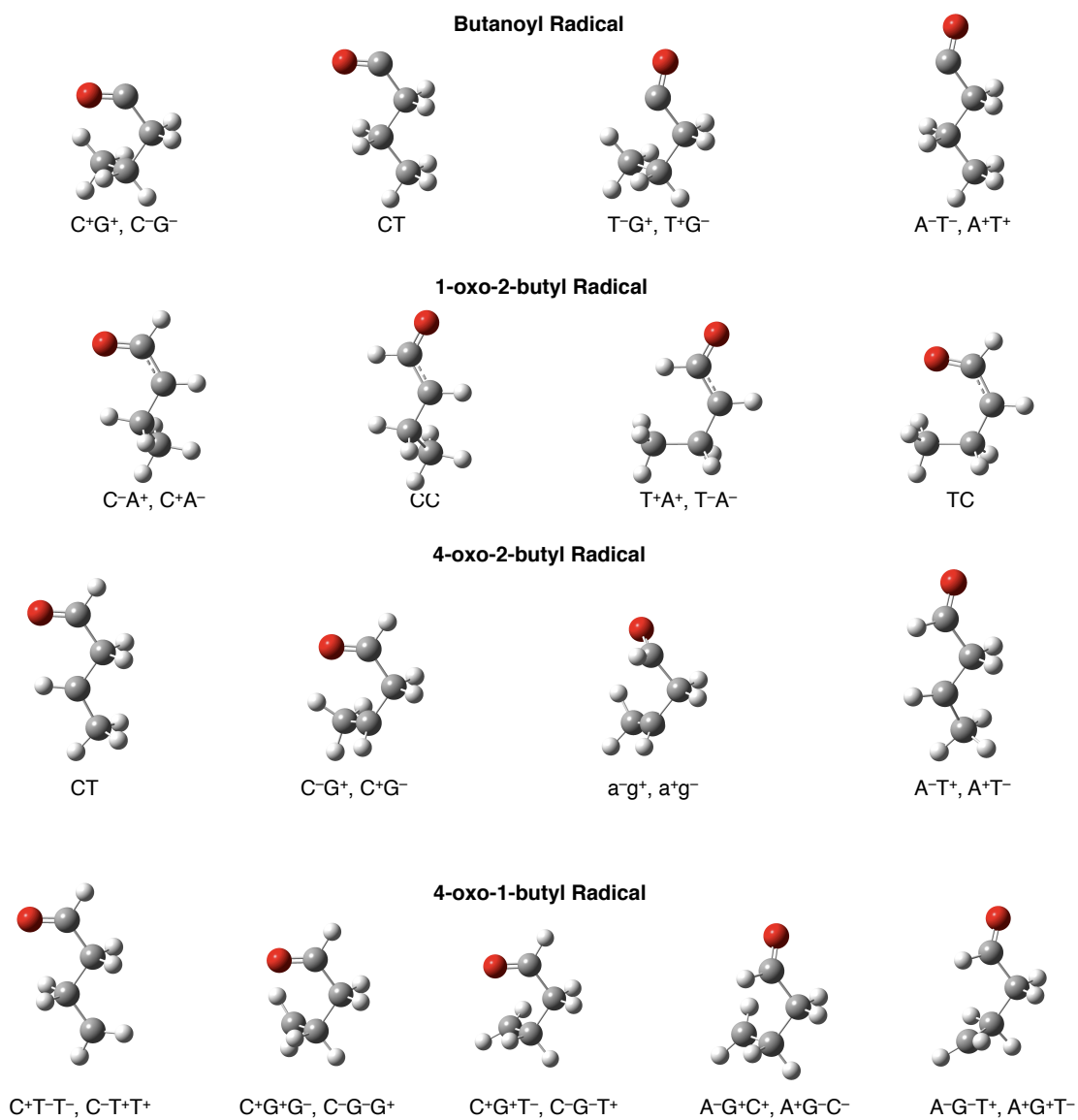
FIG. 5. Lowest energy conformers for butanal radicals.
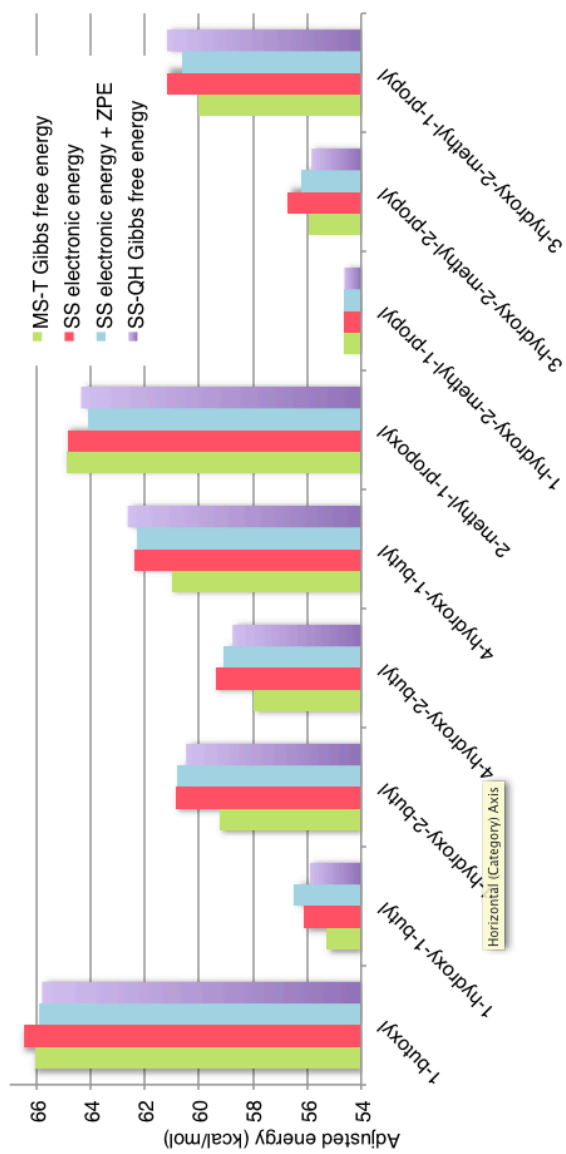
FIG. 6. Relative stability of 1-butanol and 2-methyl-1-propanol radicals. In green is the standard Gibbs free energy (G_{298}°) calculated using the MS-T method. Red columns illustrate the trends in CCSD(T)-F12a/jul-cc-pVTZ//M08-HX/MG3S electronic energy for the lowest energy conformational structures for every radical. Blue columns depict the same energy values as the red ones plus M08-HX/MG3S zero-point vibrational energy scaled by 0.973. In purple we show the single structure quasiharmonic approximation to the G_{298}°, where the frequencies are scaled by 0.984. In order to compare trends in values (rather than absolute electronic energy and Gibbs free energy values), all column heights were adjusted for the second, third, and fourth columns so that they match G_{298}° for 1-hydroxy-2-methyl-1-propyl radical. Thus the G_{298}° values are unadjusted, but the other three sets of values are adjusted.

256
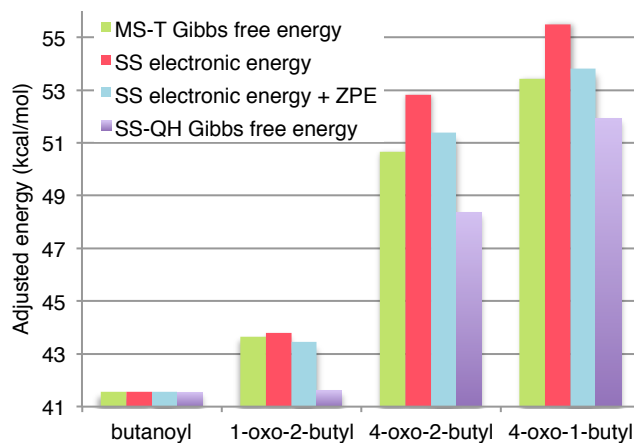
FIG. 7. Relative stability of butanal radicals. Red columns illustrate the trends in CCSD(T)-F12a/jul-cc-pVTZ//M08-HX/MG3S electronic energy for the lowest energy conformational structures for every radical. Blue columns depict the same energy values as the red ones plus M08-HX/MG3S zero-point vibrational energy scaled by 0.976. In purple we show the single structure quasiharmonic approximation to the G_{298}° , where the frequencies are scaled by 0.990. In order to compare trends in values (rather than absolute electronic energy and Gibbs free energy values), all column heights were adjusted for the second, third, and fourth columns so that they match G_{298}° for butanoyl radical. Thus the G_{298}° values are unadjusted, but the other three sets of values are adjusted.

TABLE I. Energy (kcal/mol, relative to the lowest energy structure of 1-hydroxy-2-methyl-1-propyl) of conformers of the 1-butoxyl radical.

Structure	equilibrium[a]	0 K[b]
G^+T^-, G^-T^+	11.868	86.401
G^+G^+, G^-G^-	12.364	87.229
g^+G^-, g^-G^+	12.394	87.535
TT	12.198	86.464
T^+G^+, T^-G^-	12.676	87.591

[a]CCSD(T)-F12a/jul-cc-pVTZ//M08-HX/MG3S electronic energy. The equilibrium energy is the Born-Oppenheimer energy at the local minimum of the potential energy surface.

[b]CCSD(T)-F12a/jul-cc-pVTZ//M08-HX/MG3S electronic energy plus M08-HX/MG3S zero-point vibrational energy scaled by 0.973.

TABLE II. Energy (kcal/mol, relative to the lowest energy structure of 1-hydroxy-2-methyl-1-propyl) of conformers of the 1-hydroxy-1-butyl radical.

Structure	equilibrium[a]	0 K[b]
T⁺G⁺G⁺, T⁻G⁻G⁻	1.493	76.997
T⁺G⁺T⁻, T⁻G⁻T⁺	1.318	76.749
T⁺G⁻G⁻, T⁻G⁺G⁺	1.500	76.941
C⁺G⁻G⁻, C⁻G⁺G⁺	1.883	77.361
T⁺G⁻T⁺, T⁻G⁺T⁻	1.220	76.656
T⁺T⁺G⁻, T⁻T⁻G⁺	1.818	77.128
T⁺T⁺T⁺, T⁻T⁻T⁻	1.496	76.733
C⁺G⁺G⁺, C⁻G⁻G⁻	1.854	77.240
C⁺T⁻G⁺, C⁻T⁺G⁻	1.963	77.294
C⁺g⁻T⁻, C⁻g⁺T⁺	1.697	77.117
C⁺g⁺G⁻, C⁻g⁻G⁺	2.103	77.511
T⁺g⁻G⁺, T⁻g⁺G⁻	1.956	77.392
C⁺T⁻T⁻, C⁻T⁺T⁺	1.680	76.916
C⁺g⁻G⁺, C⁻g⁺G⁻	2.387	77.874
C⁺G⁺T⁻, C⁻G⁻T⁺	1.667	77.025
T⁺T⁺G⁺, T⁻T⁻G⁻	2.073	77.400
T⁺g⁺G⁻, T⁻g⁻G⁺	2.314	77.730
C⁺T⁻G⁻, C⁻T⁺G⁺	2.202	77.548

[a]CCSD(T)-F12a/jul-cc-pVTZ//M08-HX/MG3S electronic energy. The equilibrium energy is the Born-Oppenheimer energy at the local minimum of the potential energy surface.

[b]CCSD(T)-F12a/jul-cc-pVTZ//M08-HX/MG3S electronic energy plus M08-HX/MG3S zero-point vibrational energy scaled by 0.973.

TABLE III. Energy (kcal/mol, relative to the lowest energy structure of 1-hydroxy-2-methyl-1-propyl) of conformers of the 1-hydroxy-2-butyl radical.

Structure	equilibrium[a]	0 K[b]
G⁺G⁺G⁺, G⁻G⁻G⁻	6.241	81.323
G⁺G⁺T⁻, G⁻G⁻T⁺	5.913	80.850
G⁺T⁻T⁺, G⁻T⁺T⁻	6.084	80.896
G⁺G⁺a⁻, G⁻G⁻a⁺	6.219	81.235
G⁺T⁻G⁻, G⁻T⁺G⁺	6.386	81.383
T⁻G⁺G⁺, T⁺G⁻G⁻	6.992	81.904
G⁺A⁻g⁺, G⁻A⁺g⁺	6.595	81.540
G⁺g⁺G⁻, G⁻g⁻G⁺	6.929	81.930
G⁻a⁺G⁻, G⁺a⁻G⁺	6.645	81.734
T⁻G⁺T⁻, T⁺G⁻T⁺	6.889	81.513
T⁻G⁺a⁻, T⁺G⁻a⁺	7.030	81.926
G⁺T⁻G⁺, G⁻T⁺G⁻	7.059	82.050
G⁺G⁻T⁻, G⁻G⁺T⁺	7.059	81.444
G⁺G⁻G⁻, G⁺G⁺G⁺	7.364	81.961
G⁺G⁻G⁻, G⁻G⁺G⁺	7.399	82.427
T⁻T⁻T⁺, T⁺T⁺T⁻	7.602	82.491
T⁺T⁺G⁺, T⁻T⁻G⁻	7.661	82.255
T⁺G⁺G⁻, T⁻G⁻G⁺	7.477	82.493

[a]CCSD(T)-F12a/jul-cc-pVTZ//M08-HX/MG3S electronic energy. The equilibrium energy is the Born-Oppenheimer energy at the local minimum of the potential energy surface.

[b]CCSD(T)-F12a/jul-cc-pVTZ//M08-HX/MG3S electronic energy plus M08-HX/MG3S zero-point vibrational energy scaled by 0.973.

TABLE IV. Energy (kcal/mol, relative to the lowest energy structure of 1-hydroxy-2-methyl-1-propyl) of conformers of the 4-hydroxy-2-butyl radical.

Structure	equilibrium[a]	0 K[b]
G⁺G⁻T⁺, G⁻G⁺T⁻	4.778	79.604
G⁺G⁻G⁻, G⁻G⁺G⁺	5.327	80.263
G⁻G⁺G⁺, G⁺G⁻G⁻	5.055	79.919
G⁺G⁻A⁺, G⁻G⁺A⁻	5.276	80.067
G⁺G⁺T⁺, G⁻G⁻T⁻	5.645	80.222
T⁻G⁺T⁺, T⁺G⁻T⁻	5.641	80.313
G⁺G⁺G⁺, G⁻G⁻G⁻	6.189	80.936
T⁻G⁺g⁻, T⁺G⁻g⁺	5.746	80.551
T⁺T⁺T⁺, T⁻T⁻T⁻	5.703	80.183
G⁺G⁺g⁻, G⁻G⁻g⁺	5.863	80.716
G⁺T⁻T⁻, G⁻T⁺T⁺	5.755	80.199
G⁺T⁺T⁺, G⁻T⁻T⁻	5.765	80.232
T⁺G⁺G⁺, T⁻G⁻G⁻	6.336	80.980
G⁺T⁺G⁻, G⁻T⁻G⁺	5.798	80.527
G⁺T⁻G⁺, G⁻T⁺G⁻	5.844	80.552
T⁻T⁻G⁺, T⁺T⁺G⁻	5.979	80.597
T⁻G⁺G⁻, T⁺G⁻G⁺	6.808	81.641
G⁺G⁺G⁻, G⁻G⁻G⁺	6.833	81.616
G⁺g⁻C⁺, G⁻g⁺C⁻	6.959	81.984

[a]CCSD(T)-F12a/jul-cc-pVTZ//M08-HX/MG3S electronic energy. The equilibrium energy is the Born-Oppenheimer energy at the local minimum of the potential energy surface.

[b]CCSD(T)-F12a/jul-cc-pVTZ//M08-HX/MG3S electronic energy plus M08-HX/MG3S zero-point vibrational energy scaled by 0.973.

TABLE V. Energy (kcal/mol, relative to the lowest energy structure of 1-hydroxy-2-methyl-1-propyl) of conformers of the 4-hydroxy-1-butyl radical.

Structure	equilibrium[a]	0 K[b]
G⁻G⁺G⁻G⁻, G⁺G⁻G⁺G⁺	7.778	82.783
G⁺G⁻G⁻C⁻, G⁻G⁺G⁺C⁺	8.315	83.278
T⁻G⁺G⁺G⁺, T⁺G⁻G⁻G⁻	8.105	82.849
T⁺G⁻T⁺C⁻, T⁻G⁺T⁻C⁺	8.162	82.729
G⁺G⁺G⁺C⁺, G⁻G⁻G⁻C⁻	8.193	82.725
T⁻G⁺T⁺C⁻, T⁺G⁻T⁻C⁺	8.378	83.056
G⁻G⁻T⁺C⁻, G⁺G⁺T⁻C⁺	8.288	82.832
G⁺G⁺T⁻C⁻, G⁻G⁻T⁺C⁺	8.290	82.817
T⁺T⁺G⁺C⁺, T⁻T⁻G⁻C⁻	8.488	83.119
G⁺T⁺G⁻C⁻, G⁻T⁻G⁺C⁺	8.564	83.254
G⁺T⁺G⁺G⁺, G⁻T⁻G⁻G⁻	8.608	83.235
G⁺G⁻T⁻C⁻, G⁻G⁺T⁺C⁺	8.490	83.088
G⁻G⁺T⁺C⁻, G⁺G⁻T⁻C⁺	8.532	83.082
T⁻T⁻T⁺C⁻, T⁺T⁺T⁻C⁺	8.545	82.972
G⁺T⁺T⁻C⁻, G⁻T⁻T⁺C⁺	8.511	83.020
G⁺T⁺T⁺C⁻, G⁻T⁻T⁻C⁺	8.561	82.981
G⁻G⁻g⁺G⁺, G⁺G⁺g⁻G⁻	9.567	84.219
T⁻T⁺T⁺g⁻, T⁺T⁻T⁻g⁺	8.750	83.314
T⁻G⁺g⁻C⁺, T⁺G⁻g⁺C⁻	9.526	84.138

[a]CCSD(T)-F12a/jul-cc-pVTZ//M08-HX/MG3S electronic energy. The equilibrium energy is the Born-Oppenheimer energy at the local minimum of the potential energy surface.
[b]CCSD(T)-F12a/jul-cc-pVTZ//M08-HX/MG3S electronic energy plus M08-HX/MG3S zero-point vibrational energy scaled by 0.973.

TABLE VI. Energy (kcal/mol, relative to the lowest energy structure of 1-hydroxy-2-methyl-1-propyl) of conformers of the 2-methylpropan-1-ol radical.

Structure	equilibrium[a]	0 K[b]
2-methyl-1-propoxyl		
G⁻, G⁺	10.210	84.607
T	10.391	84.753
1-hydroxy-2-methyl-1-propyl		
T⁺G⁻, T⁻G⁺	0.000	75.106
T⁺G⁺, T⁻G⁻	0.118	75.212
C⁻G⁻, C⁺G⁺	0.341	75.487
T⁺T⁺, T⁻T⁻	0.522	75.762
C⁻G⁺, C⁺G⁻	0.505	75.592
G⁺T⁻, G⁻T⁺	0.932	76.133
3-hydroxy-2-methyl-2-propyl		
Tg⁺, Tg⁻	2.092	76.728
T⁻T⁻, T⁺T⁺	3.095	77.553
G⁺T⁻, G⁻T⁺	2.924	77.369
G⁺G⁻, G⁻G⁺	3.536	77.942
3-hydroxy-2-methyl-1-propyl		
G⁻T⁻G⁺, G⁺T⁺G⁻	6.554	81.132
G⁺G⁺G⁻, G⁻G⁻G⁺	6.518	81.101
G⁺G⁺g⁻, G⁻G⁻g⁺	6.536	80.933
T⁻G⁻G⁺, T⁺G⁺G⁻	6.900	81.293
T⁺G⁺G⁺, T⁻G⁻G⁻	7.000	81.392
G⁺G⁻G⁺, G⁻G⁺G⁻	6.949	81.319
G⁻G⁻G⁺, G⁺G⁺G⁻	6.980	81.382
G⁺T⁺C⁻, G⁻T⁻C⁺	7.534	82.040
T⁻T⁻C⁻, T⁺T⁺C⁺	7.618	82.112

[a]CCSD(T)-F12a/jul-cc-pVTZ//M08-HX/MG3S electronic energy. The equilibrium energy is the Born-Oppenheimer energy at the local minimum of the potential energy surface.

[b]CCSD(T)-F12a/jul-cc-pVTZ//M08-HX/MG3S electronic energy plus M08-HX/MG3S zero-point vibrational energy scaled by 0.973.

TABLE VII. Energy (kcal/mol, relative to the lowest energy structure of 1-hydroxy-2-methyl-1-propyl) of conformers of the butanal radicals.

Structure	equilibrium[a]	0 K[b]
butanoyl		
C^+G^+, C^-G^-	0.053	61.910
CT	0.000	61.729
T^-G^+, T^+G^-	0.374	61.993
A^-T^-, A^+T^+	0.616	62.180
1-oxo-2-butyl		
C^-A^+, C^+A^-	2.241	63.625
CC	4.521	65.891
T^+A^+, T^-A^-	2.904	64.155
TC	3.890	65.286
4-oxo-2-butyl		
CT	11.457	71.269
C^-G^+, C^+G^-	11.598	71.820
a^-g^+, a^+g^-	11.281	71.558
A^-T^+, A^+T^-	12.217	72.102
4-oxo-1-butyl		
$C^+T^-T^-$, $C^-T^+T^+$	13.944	73.995
$C^+G^+T^-$, $C^-G^-T^+$	14.512	74.569
$C^+G^+G^-$, $C^-G^-G^+$	14.131	74.384
$A^-T^-C^+$, $A^+T^+C^-$	14.951	74.965
$A^-T^-C^-$, $A^+T^+C^+$	15.006	74.971
$A^-G^+C^+$, $A^+G^-C^-$	14.613	74.633
$A^-G^-T^+$, $A^+G^+T^-$	15.114	75.208

[a]CCSD(T)-F12a/jun-cc-pVTZ//M08-HX/maug-cc-pVTZ electronic energy. The equilibrium energy is the Born-Oppenheimer energy at the local minimum of the potential energy surface.

[b]CCSD(T)-F12a/jun-cc-pVTZ//M08-HX/ maug-cc-pVTZ electronic energy plus M08-HX/ maug-cc-pVTZ zero-point vibrational energy scaled by 0.976.

TABLE VIII. Standard state thermodynamic properties, viz., enthalpy (H_T° in kcal·mol^{-1}), heat capacities ($C_P^\circ(T)$ in cal K^{-1} mol^{-1}), entropy (S_T° in cal K^{-1} mol^{-1}), and Gibbs free energies (G_T° in kcal·mol^{-1}) of 1-butanol-derived radicals. The zero of energy for this table is the zero-point-exclusive energy of the **T⁺G⁻** or **T⁻G⁺** structures of 1-hydroxy-2-methyl-1-propyl.

T (K)	MS-T		MS-T	
	M08-HX[a]	CC[b]	M08-HX[a]	CC[b]
		1-butoxyl radical		
	H_T°		$C_P^\circ(T)$	
298	91.761	91.741	26.444	26.749
800	111.758	111.785	50.328	50.353
2000	186.201	186.240	68.888	68.891
	S_T°		G_T°	
298	86.288	86.161	66.047	66.065
800	123.665	123.652	12.826	12.863
2000	179.199	179.197	-172.197	-172.154
		1-hydroxy-1-butyl radical		
	H_T°		$C_P^\circ(T)$	
298	82.127	82.203	26.630	26.709
800	101.831	101.922	49.282	49.304
2000	174.742	174.856	67.619	67.633
	S_T°		G_T°	
298	90.368	90.306	55.198	55.292
800	127.260	127.232	0.022	0.136
2000	181.633	181.623	-188.525	-188.390
		1-hydroxy-2-butyl radical		
	H_T°		$C_P^\circ(T)$	
298	86.981	86.548	26.312	26.466
800	106.552	106.158	49.222	49.270
2000	179.493	179.137	67.643	67.663
	S_T°		G_T°	
298	91.771	91.643	59.633	59.238
800	128.357	128.314	3.867	3.507

2000	182.725	182.713		-185.957	-186.289

4-hydroxy-2-butyl radical

	H_T°			$C_P^\circ(T)$	
298	85.649	85.373		26.061	25.822
800	105.131	104.827		49.180	49.196
2000	178.126	177.858		67.705	67.732

	S_T°			G_T°	
298	91.906	91.933		58.261	57.977
800	128.287	128.240		2.501	2.235
2000	182.680	182.659		-187.233	-187.462

4-hydroxy-1-butyl radical

	H_T°			$C_P^\circ(T)$	
298	88.661	88.115		26.492	26.138
800	108.480	107.872		49.772	49.749
2000	182.086	181.498		68.236	68.262

	S_T°			G_T°	
298	90.907	91.011		61.571	60.994
800	127.946	127.904		6.123	5.549
2000	182.815	182.784		-183.545	-184.070

[a]The basis set used for M08-HX is MG3S.
[b]CCSD(T)-F12a/jul-cc-pVTZ//M08-HX/ MG3S

TABLE IX. Comparison in the $C_P^\circ(T)$ and S_T° values between our computed results and group additivity data for 1-butoxyl radical, 4-hydroxy-2-butyl radical, and 4-hydroxy-1-butyl radical (in cal K^{-1} mol^{-1})

T (K)	$C_P^\circ(T)$			S_T°		
	CC (MS-T)	GA[a]	GA[b]	CC (MS-T)	GA[a,c]	GA[b,c]
			1-butoxyl radical			
300	26.868	25.09	25.90	86.340	85.84	86.06
400	32.854	31.54	31.84	94.892	93.96	94.34
600	42.967	42.29	42.15	110.229	108.89	109.28
800	50.353	50.16	49.90	123.652	122.19	122.52
1000	55.883	55.85	55.54	135.508	134.03	134.30
			4-hydroxy-2-butyl radical			
300	25.929	26.14	25.64	92.106	89.64	92.09
400	31.633	32.15	31.06	100.332	98.05	100.24
600	41.781	42.14	41.11	115.162	113.02	114.84
800	49.196	49.46	48.62	128.240	126.20	127.72
1000	54.702	54.88	54.31	139.826	137.85	139.21
1500	63.295		63.09	163.800		163.13
			4-hydroxy-1-butyl radical			
300	26.257	26.28	26.49	91.186	88.61	90.92
400	32.266	32.39	32.01	99.558	97.03	99.32
600	42.421	42.46	41.83	114.655	112.17	114.26
800	49.749	49.69	49.06	127.904	125.42	127.31
1000	55.201	55.08	54.52	139.607	137.12	138.88
1500	63.775		63.02	163.778		162.78

[a]Group additivity parameters were taken from reference 17.
[b]Group additivity parameters were taken from references 17, 28, and 29.
[c]Entropy values obtained from group additivity were corrected by adding 0.026 cal mol^{-1} K^{-1} to convert from a standard pressure of 1 atm to a standard pressure of 1 bar.

TABLE X. Standard state thermodynamic properties, viz., enthalpy (H_T° in kcal·mol^{-1}),
heat capacities ($C_P^\circ(T)$ in cal K^{-1} mol^{-1}), entropy (S_T° in cal K^{-1} mol^{-1}), and Gibbs free
energies (G_T° in kcal·mol^{-1}) of 2-methyl-1-propanol-derived radicals. The zero of energy
for this table is the zero-point-exclusive energy of the **T⁺G⁻** or **T⁻G⁺** structures of 1-
hydroxy-2-methyl-1-propyl.

T (K)	MS-T			MS-T	
	M08-HX[a]	CC[b]		M08-HX[a]	CC[b]
2-methyl-1-propoxyl radical					
	H_T°			$C_P^\circ(T)$	
298	89.569	89.576		26.518	26.544
800	109.887	109.896		50.999	51.000
2000	184.804	184.816		69.127	69.129
	S_T°			G_T°	
298	82.905	82.894		64.864	64.874
800	120.875	120.871		13.187	13.200
2000	176.822	176.820		-168.840	-168.824
1-hydroxy-2-methyl-1-propyl radical					
	H_T°			$C_P^\circ(T)$	
298	80.612	80.554		27.640	27.492
800	100.672	100.579		49.660	49.627
2000	173.729	173.618		67.645	67.639
	S_T°			G_T°	
298	86.946	87.041		54.703	54.616
800	124.599	124.618		0.993	0.885
2000	179.116	179.119		-184.502	-184.620
3-hydroxy-2-methyl-2-propyl radical					
	H_T°			$C_P^\circ(T)$	
298	82.736	82.487		27.661	26.804
800	102.775	102.366		50.453	50.365
2000	178.066	177.641		69.964	69.979
	S_T°			G_T°	
298	88.752	89.111		56.288	55.933
800	126.255	126.243		1.771	1.371
2000	182.345	182.318		-186.624	-186.996

3-hydroxy-2-methyl-1-propyl radical

	H_T°			$C_P^\circ(T)$	
298	87.102	86.312		26.745	26.831
800	107.889	106.337		49.920	49.943
2000	184.983	179.656		67.764	67.771

	S_T°			G_T°	
298	88.313	88.248		60.766	60.014
800	125.736	125.721		6.497	5.761
2000	180.428	180.424		-180.467	-181.192

[a]The basis set used for M08-HX is MG3S.
[b]CCSD(T)-F12a/jul-cc-pVTZ//M08-HX/ MG3S

TABLE XI. Comparison in the $C_P^\circ(T)$ and S_T° values between our computed results and group additivity data for 2-methyl-1-propoxyl radical and 3-hydroxy-2-methyl-1-propyl radical (in cal K^{-1} mol^{-1}).

T (K)	$C_P^\circ(T)$			S_T°		
	CC (MS-T)	GA[a]	GA[b]	CC (MS-T)	GA[a,c]	GA[b,c]
		2-methyl-1-propoxyl radical				
300	26.867	24.82	19.43	88.492	85.34	85.81
400	32.930	31.48	24.38	97.053	93.41	92.10
600	42.880	42.43	32.06	112.392	108.36	103.52
800	49.920	50.35	37.52	125.736	121.71	113.54
1000	55.145	55.99	41.33	137.454	133.59	122.34
		3-hydroxy-2-methyl-1-propyl radical				
300	26.953	26.01	25.47	88.428	88.11	90.29
400	32.996	32.33	31.44	97.010	96.48	98.46
600	42.916	42.60	41.59	112.369	111.64	113.24
800	49.943	49.88	48.93	125.721	124.95	126.25
1000	55.163	55.22	54.35	137.443	136.69	137.79
1500	63.426		62.95	161.535		161.61

[a]Group additivity parameters were taken from reference 17.
[b]Group additivity parameters were taken from references 17, 28, and 29.
[c]Entropy values obtained from group additivity were corrected by adding 0.026 cal mol^{-1} K^{-1} to convert from a standard pressure of 1 atm to a standard pressure of 1 bar.

TABLE XII. Standard state thermodynamic properties, viz., enthalpy (H_T° in kcal·mol^{-1}), heat capacities ($C_P^\circ(T)$ in cal K^{-1} mol^{-1}), entropy (S_T° in cal K^{-1} mol^{-1}), and Gibbs free energies (G_T° in kcal·mol^{-1}) of butanal-derived radicals. The zero of energy for this table is the zero-point-exclusive energy of the lowest energy structure of **CT** conformer of the butanoyl radical.

T (K)	MS-T			MS-T	
	M08-HX[a]	CC[b]		M08-HX[a]	CC[b]
			butanoyl radical		
	H_T°			$C_P^\circ(T)$	
298	66.604	66.611		23.081	23.013
800	83.852	83.838		43.190	43.170
2000	147.320	147.305		58.508	58.513
	S_T°			G_T°	
298	84.050	84.094		41.557	41.551
800	116.320	116.318		-9.204	−9.217
2000	163.698	163.693		-180.077	−180.082
			1-oxo-2-butyl radical		
	H_T°			$C_P^\circ(T)$	
298	67.078	68.338		23.405	23.288
800	84.701	85.948		44.240	44.264
2000	149.225	150.513		59.083	59.112
	S_T°			G_T°	
298	82.838	82.829		42.392	43.655
800	115.785	115.738		-7.926	−6.642
2000	164.004	163.987		-178.783	−177.462
			4-oxo-2-butyl radical		
	H_T°			$C_P^\circ(T)$	
298	75.085	76.537		24.518	23.833
800	92.488	93.811		43.176	43.083
2000	155.885	157.155		58.429	58.406
	S_T°			G_T°	
298	86.457	86.821		49.322	50.665
800	119.135	119.196		-2.820	−1.546

2000	166.453	166.468		-177.022	−175.782

4-oxo-1-butyl radical

	H_T°			$C_P^\circ(T)$	
298	78.051	79.276		24.743	24.121
800	95.591	96.674		43.316	43.222
2000	158.986	160.040		58.395	58.394
	S_T°			G_T°	
298	86.415	86.768		52.299	53.419
800	119.352	119.378		0.110	1.171
2000	166.652	166.649		-174.318	-173.259

[a]The basis set used for M08-HX is maug-cc-pVTZ.
[b]CCSD(T)–F12a/jun-cc-pVTZ//M08-HX/maug-cc-pVTZ

TABLE XIII. Comparison of the $C_P^\circ(T)$ and S_T° values in this study to the group additivity results for 1-oxo-2-butyl radical and 4-oxo-1-butyl radical (in cal K^{-1} mol^{-1})

T (K)	$C_P^\circ(T)$			S_T°		
	CC (MS-T)	GA[a]	GA[b]	CC (MS-T)	GA[a,c]	GA[b,c]
		1-oxo-2-butyl radical				
300	23.397	23.80		82.985	83.99	
400	28.796	29.05		90.459	91.58	
600	37.810	37.74		103.931	105.08	
800	44.264	44.06		115.738	116.85	
1000	48.924	48.71		126.137	127.21	
1500	55.800	55.87		147.438	148.45	
		4-oxo-1-butyl radical				
300	24.209	24.69	24.15	86.929	84.81	87.32
400	28.848	29.69	29.10	94.516	92.61	94.96
600	37.113	37.68	37.08	107.836	106.23	108.35
800	43.222	43.81	43.25	119.378	117.95	119.90
1000	47.771	48.21	47.68	129.522	128.23	130.05
1500	54.810		55.04	150.359		150.90

[a]Group additivity parameters were taken from reference 17.
[b]Group additivity parameters were taken from references 17, 28, and 29.
[c]Entropy values obtained from group additivity were corrected by adding 0.026 cal mol^{-1} K^{-1} to convert from a standard pressure of 1 atm to a standard pressure of 1 bar.

[1] J. Zheng, T. Yu, E. Papajak, I. M. Alecu, S. L. Mielke, and D. G. Truhlar, Phys. Chem. Chem. Phys. **13**, 10885 (2011).

[2] J. Zheng, T. Yu, and D. G. Truhlar, Phys. Chem. Chem. Phys. **13**, 19318 (2011)

[3] T. Yu, J. Zheng, and D. G. Truhlar, Phys. Chem. Chem. Phys., **14**, 482 (2011)

[4] J. Zheng and D. G. Truhlar, Faraday Discuss., in press.

[5] P. Seal, E. Papajak, T. Yu, and D. G. Truhlar, J. Chem. Phys. **136**, 034306 (2012).

[6] P. Seal, E. Papajak, J. Zheng, and D. G. Truhlar, J. Phys. Chem. Lett. **3**, 264 (2012).

[7] T. Yu, J. Zheng, and D. G. Truhlar, Chem. Sci., **2**, 2199 (2011).

[8] T. Yu, J. Zheng, and D. G. Truhlar, J. Phys. Chem. A **116**, 297 (2012).

[9] X. Xu, E. Papajak, J. Zheng, and D. G. Truhlar, Phys. Chem. Chem. Phys. 14, 4204 (2012).

[10] J. Platt, J. Chem. Phys. **15**, 419 (1947)

[11] J. Platt, J. Phys. Chem. **56**, 328 (1952)

[12] J. Greenshields and F. Rossini, J. Phys. Chem. **62**, 271 (1958).

[13] G. Somayajulu and B. Zwolinski, J. Trans. Faraday Soc. **62**, 2327 (1966).

[14] T. -P. Thinh, J. -L. Duran, and R. Ramalho, Ind. Eng. Process Des. Dev. **10**, 576 (1971).

[15] T. –P. Thinh and T. Trong, Can. J. Chem. **54**, 344 (1976).

[16] R. Joshi, J. Macromol. Sci.-Chem. **A4**, 1819 (1970).

[17] S. W. Benson, *Thermochemical Kinetics*, 2nd ed. (Wiley-Interscience, New York, 1976).

[18] N. Cohen, S. Benson, Chem. Rev. **93**, 2419 (1993)

[19] N. Cohen, J. Phys. Chem. Ref. Data **25**, 1411 (1996).

[20] T. H. Lay and J. W. Bozzelli, J. Phys. Chem. A **101**, 9505 (1997).

[21] N. Sebbar, J. W. Bozzelli, H. Bockhorn, J. Phys. Chem. A **108**, 8353-8366 (2004).

[22] H. O'Neal, S. Benson, In Free Radicals; J. K. Kochi, Ed.; Wiley: New York, 1973; pp 275.

[23] T. Ni, R. Caldwell, L. Melton, J. Am. Chem. Soc. **111**, 457 (1989).

[24] N. Cohen, J. Phys. Chem. **96**, 9052 (1992).

[25] M. K. Sabbe, F. De Vieeschower, M.-F. Reyniers, M. Waroquier, and G. B. Marin, J. Phys. Chem. A **112**, 12235 (2008).

[26] V. V. Turovtsev, Y. D. Orlov, Y. A. Lebedev, Russ. J. Phys. Chem. A **83** 245 (2009).

[27] I. Marsi, B. Viskolcz, L. Seres, J. Phys. Chem. A **104**, 4497 (2000).

[28] S. S. Khan, X. Yu, J. R. Wade, D. Malmgren, and L. J. Broadbelt J. Phys. Chem. **113**, 5176 (2009).

[29] M. K. Sabbe, M. Saeys, M.-F. Reyniers, and G. B. Marin J. Phys. Chem. A **109**, 7466 (2005)

[30] J. M. Hudzik, J. W. Bozzelli, J. Phys. Chem. A **114**, 7984 (2010).

[31] M. J. Frisch, G. W. Trucks, H. B. Schlegel, G. E. Scuseria, M. A. Robb, J. R. Cheeseman, G. Scalmani, V. Barone, B. Mennucci, G. A. Petersson, H. Nakatsuji, M. Caricato, X. Li, H. P. Hratchian, A. F. Izmaylov, J. Bloino, G. Zheng, J. L. Sonnenberg, M. Hada, M. Ehara, K. Toyota, R. Fukuda, J. Hasegawa, M. Ishida, T. Nakajima, Y. Honda, O. Kitao, H. Nakai, T. Vreven, Jr., J. A. Montgomery, J. E. Peralta, F. Ogliaro, M. Bearpark, J. J. Heyd, E. Brothers, K. N. Kudin, V. N. Staroverov, R. Kobayashi, J. Normand, K. Raghavachari, A. Rendell, J. C. Burant, S. S. Iyengar, J. Tomasi, M. Cossi, N. Rega, N. J. Millam, M. Klene, J. E. Knox, J. B. Cross, V. Bakken, C. Adamo, J. Jaramillo, R. Gomperts, R. E. Stratmann, O. Yazyev, A. J. Austin, R. Cammi, C. Pomelli, J. W. Ochterski, R. L. Martin, K. Morokuma, V. G. Zakrzewski, G. A. Voth, P. Salvador, J. J. Dannenberg, S. Dapprich, A. D. Daniels, Ö. Farkas, J. B. Foresman, J. V. Ortiz, J. Cioslowski, and D. J. Fox, *Gaussian 09*, Revision A.02, Gaussian, Inc., Wallingford CT, 2009.

[32] Z. Zhao, R. Peverati, K. Yang, and D. G. Truhlar, *MN-GFM* version 5.2 computer program module, University of Minnesota, Minneapolis, 2011.

[33] Y. Zhao, N. E. Schultz, and D. G. Truhlar, J. Chem. Theory Comput. **4**, 1849 (2008).

[34] B. J. Lynch, Y. Zhao, and D. G. Truhlar, J. Phys. Chem. A **107**, 1384 (2003).

[35] T. H. Jr. Dunning, J. Chem. Phys. **90**, 1007 (1989).

[36] R. A. Kendall, T. H. Jr. Dunning, R. J. Harrison, J. Chem. Phys. **96**, 6796 (1992).

[37] E. Papajak, H. R. Leverentz, J. Zheng, and D. G. Truhlar, J. Chem. Theory Comput. **5**, 1197 (2009); **5**, 3330 (2009).

[38] E. Papajak and D. G. Truhlar, J. Chem. Theory Comput. **6**, 597 (2010).

[39] R. Krishnan, J. S. Binkley, R. Seeger, and J. A. Pople, J. Chem. Phys. **72**, 650 (1980); T. Clark, J. Chandrasekhar, G. W. Spitznagel, and P. v. R. Schleyer, J. Comp. Chem. **4**, 294 (1983); M. J. Frisch, J. A. Pople, and J. S. Binkley, J. Chem. Phys. **80**, 3265 (1984).

[40] I. M. Alecu, J. Zheng, Y. Zhao, and D. G. Truhlar, J. Chem. Theory Comput. **6**, 2872 (2010).

[41] G. Knizia, T. B. Adler, and H.-J. Werner, J. Chem. Phys. **130**, 054104 (2009).

[42] E. Papajak and D. G. Truhlar, J. Chem. Theory Comput. **7**, 10 (2011).

[43] W. Kutzelnigg Theor. Chim. Acta **68**, 445 (1985).

[44] W. Kutzelnigg, W. Klopper, J. Chem. Phys., **94**, 1985, (1991).

[45] W. Klopper, W. Kutzelnigg, Chem. Phys. Lett. **134**, 17 (1987).

[46] W. Klopper, C. C. M. J. Samson, Chem. Phys. **116**, 6397 (2002).

[47] F. R. Manby, J. Chem. Phys. **119**, 4607 (2003).

[48] S. Ten-no, F. R. Manby, J. Chem. Phys. **119**, 5358 (2003).

[49] S. J. Ten-no, Chem. Phys. **121**, 117 (2004).

[50] E. F. Valeev, Chem. Phys. Lett. **395**, 190 (2004).

[51] E. F. Valeev and C. L. Jansen, Chem. Phys. Lett. **121**, 1214 (2004).

[52] S. Ten-no, Chem. Phys. Lett. **121**, 117 (2004).

[53] H. –J. Werner, T. B. Adler, and F. R. Manby, J. Chem. Phys. **126**, 164102 (2007).

[54] T. D. Crawford, C. D. Sherrill, E. F. Valeev, J. T. Fermann, R. A. King, M. L. Leininger, S. T. Brown, C. L. Janssen, E. T. Seidl, J. P. Kenny, and W. D. J. Allen, J. Comp. Chem. **28**, 1610 (2007).

[55] H.-J. Werner, P. J. Knowles, F. R. Manby, M. Schütz, P. Celani, G. Knizia, T. Korona, R. Lindh, A. Mitrushenkov, G. Rauhut, T. B. Adler, R. D. Amos, A. Bernhardsson, A. Berning, D. L. Cooper, M. J. O. Deegan, A. J. Dobbyn, F. Eckert, E. Goll, C. Hampel, A. Hesselmann, G. Hetzer, T. Hrenar, G. Jansen, C. Köppl, Y. Liu, A. W. Lloyd, R. A. Mata, A. J. May, S. J. McNicholas, W. Meyer, M. E. Mura, A. Nicklaß, P. Palmieri, K. Pflüger, R. Pitzer, M. Reiher, T. Shiozaki, H. Stoll, A. J. Stone, R. Tarroni, T.

Thorsteinsson, M. Wang, and A. Wolf, *Molpro* computer program, version 2010.1 (University of Birmingham, Birmingham, 2010).

[56] J. Zheng, S. L. Mielke, K. L. Clarkson, and D. G. Truhlar, *MSTor* computer program, version 2011–2 (University of Minnesota, Minneapolis, 2011).

[57] J. Zheng, S. L. Mielke, K. L. Clarkson, and D. G. Truhlar, Computer Phys. Commun., to be published.

[58] G. P. Moss, Pure Appl. Chem. *68*, 2193 (1996). *See* page 2220.

[59] See Supplementary Material Document for all the structures and corresponding zero-point-exclusive and zero-point- inclusive relative conformational energies for 1-butanol obtained with M08-SO and M06-2X density functionals and MG3S basis set.

Chapter 9. Kinetics of the Hydrogen Abstraction from Carbon-3 of 1-Butanol by Hydroperoxyl Radcial: Multi-Structural Variational Transition-State Calculations of a Reaction with 262 Conformational of the Transition State

Prasenjit Seal, Ewa Papajak, and Donald G. Truhlar *

Department of Chemistry and Supercomputing Institute, University of Minnesota, Minneapolis, Minnesota 55455-0431

We estimated rate constants for the hydrogen abstraction from carbon-3 of 1-butanol by hydroperoxyl radical, a critically important reaction in combustion chemistry. We employed the recently developed multi-structural variational transition-state theory (MS-VTST), which utilizes a multi-faceted dividing surface that allows us to include the contributions of multiple structures for reacting species and transition states. First multi-configurational Shepard interpolation—based on molecular-mechanics-guided interpolation of electronic-structure Hessian data obtained by the M08 HX/jun cc-pVTZ electronic model chemistry—was used to

obtain the portion of the potential energy surface needed for single-structure variational transition state theory rate constants including multidimensional tunneling; then the M08-HX/MG3S electronic model chemistry was used to calculate multi-structural torsional anharmonicity factors to complete the MS-VTST rate constant calculations. Our results
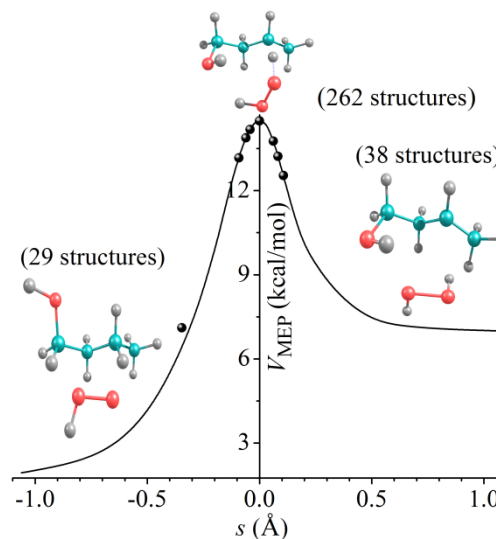
indicate that neglect of multi-structural anharmonicity would lead to errors of factors of 3, 46, and 171 at 200, 1000, and 2400 K for this reaction.

Recent years have witnessed the emergence of 1-butanol as a promising candidate for new generation fuels.[1–13] Several features make 1-butanol a possible replacement of ethanol as a transport liquid fuel component; these include its high energy content, low vapor pressure, intoxicity to human health,[8,9] and decreased NO_x emission.[10] Wallner and co-workers[7] found that 1-butanol performs as well as ethanol in a direct-injection spark-ignition engine with an advantage of less fuel consumption; this further increases the interest in studying the combustion chemistry of 1-butanol in engines. Some recent research has also shown the potential of converting 1-butanol to alternative jet fuels.[12,13]

There have been several investigations of 1-butanol kinetics, both theoretical[1,4–6] and experimental.[2,3] Very recently, Karwat et al.[2] provided insights to the low-temperature combustion chemistry of 1-butanol by ignition and speciation studies. Earlier, Vasu et al.[3] reported high-temperature rate constants of the •OH radical with 1-butanol using shock tube and laser absorption. Simmie and co-workers[1] carried out theoretical work using VTST.

Hydrogen (H) abstraction by small radicals like •OH, •H, •Cl, •CH3, $•O_2H$ plays an especially important role at high temperature. The $•O_2H$ radical is an important species at intermediate temperatures in ignition, and its H abstraction reactions are an important source of H_2O_2, whose decomposition to form two •OH radicals is also important. Therefore, the reaction of 1-butanol with $•O_2H$ is important. The objective of the present Letter is to provide reliable theoretical rate constants for the H-atom abstraction from carbon-3 of 1-butanol by hydroperoxyl radical ($•O_2H$) to yield 4-hydroxy-2-butyl radical and hydrogen peroxide:

$$CH_3CH_2CH_2CH_2OH + •O_2H \rightarrow CH_3C•HCH_2CH_2OH + H_2O_2 \qquad (R1)$$
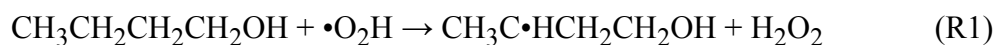
Although there have been a number of studies of the abstraction of hydrogen atoms from 1-butanol by other radicals, particularly, •OH,[1–4] we found only one result with

•O_2H. Black et al.[5] reported barrier heights for the site-specific abstraction of H atom from different sites of 1-butanol by •O_2H.

Theory. The thermal rate constant is calculated by[14]

$$k^{\text{MS-CVT/SCT}} = F^{\text{MS-T}}(T)k^{\text{SS-CVT/SCT}}(T) \tag{1}$$

where $k^{\text{SS-CVT/SCT}}(T)$ and $k^{\text{MS-CVT/SCT}}(T)$ are the canonical variation theory (CVT) rate constants[15–17] in the single-structure[15–19] (SS) and multi-structural[14] (MS) approximations, respectively, employing multidimensional small-curvature tunneling (SCT),[20] and the factor, $F^{\text{MS-T}}(T)$ accounts for the multiple-structure and torsional anharmonicity effects. Because $k^{\text{SS-CVT/SCT}}$ is based on scaled[21] frequencies, it includes some nontorsional anharmonicity, but it does not include multi-structural anharmonicity due to multiple structures and torsions. We call $F^{\text{MS-T}}(T)$, the multi-structural torsional anharmonicity factor ratio, and it can be written in terms of multi-structural anharmonicity factors for reactant (R) and transition states (‡) as

$$F^{\text{MS-T}}(T) = \frac{F^{\ddagger}_{\text{MS-T}}}{F^{\text{R}}_{\text{MS-T}}} \tag{2}$$

The anharmonicity factors $F^{\chi}_{\text{MS-T}}$ of eq 2 can be factored as

$$F^{\chi}_{\text{MS-T}} = F^{\chi}_{\text{MS-LH}}F^{\chi}_{\text{T}} \tag{3}$$

where χ is R or ‡, MS-LH denotes the multiple-structure local harmonic approximation, and F^{χ}_{T} accounts for torsional anharmonicity. We calculate these factors as

$$F^{\chi}_{\text{MS-LH}} = \frac{Q^{\text{MS-LH}}_{\chi,\,\text{con-rovib}}(T)}{Q^{\text{SS-HO}}_{\chi,\,\text{rovib, GM}}(T)} \tag{4}$$

$$F^{\chi}_{\text{T}} = \frac{Q^{\text{MS-T}}_{\chi,\,\text{con-rovib}}(T)}{Q^{\text{MS-LH}}_{\chi,\,\text{con-rovib}}(T)} \tag{5}$$

where Q is the partition function for a given system, "con" denotes conformational, "rovib" denotes rotational-vibrational, GM denotes the global minimum geometry of a

reagent or the transition state (TS, also denoted as ‡), and SS-HO denotes the single-structure harmonic oscillator approximation. We can re-write eq 2 with the help of eqs 4 and 5 as

$$F^{MS-T}(T) = \frac{Q^{MS-T}_{\ddagger, \text{con-rovib}}(T) \, Q^{SS-HO}_{R, \text{rovib, gm}}(T)}{Q^{MS-T}_{R, \text{con-rovib}}(T) \, Q^{SS-HO}_{\ddagger, \text{rovib, gm}}(T)} \qquad (6)$$

In the present study, we followed a four-step procedure to obtain the MS-VTST thermal rate constants.

1. Structure Search. In the first step, we generated initial guesses of all the structures of the reactant (1-butanol), products (4-hydroxy-2-butyl radical and hydrogen peroxide), and transition state (TS). The geometry optimizations were performed with the M08-HX[22]/MG3S[23] electronic model chemistry using the ultrafine grid in the *Gaussian 09* program[24] with the MN-GFM.[25] Then those optimized geometries were used for further optimization and vibrational frequency calculations with an integral grid of 99 radial shells and 974 angular points per shell.

The torsion angles that we used in searching for distinguishable structures are H5–O6–C1–C2, O6–C1–C2–C3, and C1–C2–C3–C4 for 1-butanol and 4-hydroxy-2-butyl radical and H10–O8–C1–C2, O8–C1–C2–C3, C1–C2–C3–C4, C2–C3–H17–O12, C3–H17–O12–O13, and H17–O12–O13–H14 for the TS (see Figure 1). When all torsions are independent and ideal, *t* three fold torsions (excluding methyl groups) would generate 3^t structures. Since *t* is 3 for 1-butanol and 4-hydroxy-2-butyl radical and 6 for the TS, ideal torsions would generate 27 structures for 1-butanol and the product radical and 729 structures for the TS. However, the torsions are not ideal, and we found 29, 38, and 262 structures.

The naming of the structures is based on the scheme explained in ref 26. For 1-butanol, the **T⁻G⁺T⁻** conformer and its mirror image are the GM structures. The **G⁺G⁻T⁺**, **G⁻G⁺T⁻** structures of 4-hydroxy-2-butyl radical have the lowest zero-point-exclusive and inclusive energies, and hence it is the GM structure of the product radical. For the TS, among 262 conformers we found that the **G⁺G⁻T⁺G⁺C⁺g⁻** conformer and its mirror

image have the lowest zero-point-inclusive and exclusive energies and is the GM structure. These GM structures are presented in Figure 1.

The relative conformational energies for each of the structures are given in Table S1 and S2 of the Supporting Information. Although the relative conformational energies for 1-butanol and 4-hydroxy-2-butyl radical lie within a range of 2.25 kcal/mol, for the TS the range is 7.45 kcal/mol.

2. Multi-structural (MS) Partition Functions and Anharmonicity Factors (F). The second step is to determine Q and the F factors for the reactant, products, and TS; these were calculated with the Hessians from the formatted checkpoint files of the above optimizations by using the *MSTor* program.[27] The M08-HX/MG3S density functional frequencies are scaled by a standard scaling factor[21] of 0.973 to account for nontorsional anharmonicity and higher-order correlation effects. For 1-butanol, 4-hydroxy-2-butyl radical, and the TS, the Voronoi tessellation method[27,28] was used to calculate the local periodicity parameters, $M_{j,\tau}$,[28] where j labels a structure and τ labels a torsional coordinate. We used three-dimensional Voronoi calculations for 1-butanol and 4-hydroxy-2-butyl radical and six-dimensional for transition state. The $M_{j,\tau}$ for 1-butanol, 4-hydroxy-2-butyl radical, and the TS are given in Table S1 and S2 of the Supporting Information.

3. Validations of density functional results. The third step consists of validating the density functionals to be used for the dynamics calculations. In the present study, we choose the combination of three Minnesota density functionals, i.e., M06-2X,[29] M08-SO,[22] and M08-HX and five basis sets, viz. MG3S[23] (same as 6-311+G(2df,2p)[30–32] basis for H, C and O), ma-TZVP,[33] maug-cc-pVTZ,[34] jun-cc-pVTZ,[35] and maug-cc-pVQZ.[35] The reason for choosing these methods is their good performance for reactive barrier heights.[36] We also performed coupled cluster (CCSD(T)-F12a)[37–39] single-point calculations with the *Molpro* program.[40] Dual-level methods have also been used where the corresponding energies are given by

$$E_{\text{jun-jun}} = E_{\text{CCSD(T)-F12a/jun-cc-pVDZ}} \tag{7}$$

$$+ \left(E_{\text{MP2-F12/jun-cc-pVTZ}} - E_{\text{MP2-F12/jun-cc-pVDZ}} \right)$$

$$E_{\text{jun-jun(HL)}} = E_{\text{CCSD(T)-F12a/jun-cc-pVTZ}} \qquad (8)$$

$$+ \left(E_{\text{MP2-F12/jun-cc-pVQZ}} - E_{\text{MP2-F12/jun-cc-pVTZ}} \right)$$

These methods are called jun-jun and jun-jun (HL), respectively.

The mean unsigned error (MUE) is defined as the average of the absolute values of these the errors of zero-point-exclusive forward ($V_f^{\ddagger}$) and reverse ($V_r^{\ddagger}$) barrier heights and energy of reaction, ΔU, where "error" is assessed relative to the benchmark jun-jun (HL) results at the same geometry. Table 1 gives the zero-point-exclusive barrier heights, and reaction energies based on 19 electronic model chemistries. The table shows that the smallest errors in $V_f^{\ddagger}$, $V_r^{\ddagger}$, and ΔU are given by the M08-HX/jun-cc-pVTZ, M08-HX/ma-TZVP, and M08-SO/maug-cc-pVQZ methods, respectively. The MUE is smallest (0.09 kcal/mol) for M08-HX/jun-cc-pVTZ, and hence we choose this method for dynamics calculations. For comparison to the single-point energies in Table 2, we note that the consistently optimized values of $V_f^{\ddagger}$, $V_r^{\ddagger}$, and ΔU with M08-HX/jun-cc-pVTZ are 14.50, 2.60, and 11.90 kcal/mol. The zero-point-inclusive forward and reverse barrier heights for M08-HX/jun-cc-pVTZ are found to be 12.89 and 2.16 kcal/mol.

Recently, Simmie and co-workers[5] reported forward barrier heights for the abstraction of hydrogen atom from all possible sites of 1-butanol by $\bullet O_2H$ as calculated by several methods. Our computed results obtained with jun-jun (HL) method for the forward barrier height agree well with their G3 data,[5] but their B3LYP, M05-2X, MP2, and CBS-Q3 results underestimate the barrier heights.

4. Dynamics calculations for the rate constant. In the final step, the electronic model chemistry with the smallest MUE was used to determine thermal rate coefficients via multi-configuration Shepard interpolation (MCSI),[41–45] using single-structure (SS) VTST[15-17] with a curvilinear dividing surface[18,19] and a multidimensional small-

curvature tunneling.[20] The MEP (V_{MEP}) and ground-state vibrationally adiabatic potential, V_a^G, were obtained with the MCSI[46] and MC-TINKERATE[47] programs, and the rate constants were estimated using MC-TINKERATE[47] and POLYRATE[48,49] programs.

Results. The partition functions for the reacting species and TS were calculated in order to determine multi-structural anharmonicity factors (*F*). These *F* factors were then used to obtain forward and reverse MS-VTST rate constants[47] for the reaction. Table 2 provides the final F_{MS-T} factors of 1-butanol, 4-hydroxy-2-butyl radical, H_2O_2, and the TS. The partition functions and other *F* factors for these systems are given in the Supporting Information. Tale 2 shows where some F_{MS-T} factors pass through a maximum. Maxima were also observed for F_T, while F_{MS-LH} shows a gradual increase (see Table S3, S4, and S6 of the Supporting Information). In Table 2, we also tabulated the ratio, F^{MS-T}, which is large and increases gradually.

For estimating the rate constants, we choose M08-HX/jun-cc-pVTZ frequencies and Hessians. The MCSI algorithm was used to find the minimum energy reaction path. Let *s* denote the reaction coordinate (*s*) scaled to a reduced mass of 1 amu. To obtain the potential energy surface in the vicinity of the minimum energy path, we follow same strategy as proposed in the work of Albu et al.[42] The points in Figure 2a were taken at $s = 0.0$ Å (Point 1: saddle point geometry), $s = -0.061$ Å (Point 2: one quarter down from the saddle point along the MCMM-0 reaction path on the dynamical bottleneck side), $s = 0.061$ Å (Point 3: one quarter down from the saddle point along the MCMM-1 path on the side opposite to the dynamical bottleneck side), $s = -0.092$ Å (Point 4: one half down from the saddle point along the MCMM-2 path on the dynamical bottleneck side), and so forth. The details of the total reaction path are given in the Supporting Information. This procedure results in a V_{MEP} profile that is well converged. Figures 2a and 2b show V_{MEP} and V_a^G respectively, as functions of *s*. The V_a^G profile is not well converged in the foothills but this has little effect on the combustion rate constants because the representative tunneling energies[50] (tabulated in Table 3) are above 104.7 kcal/mol for *T* ≥ 400 K.

Table 3 and Fig. 3 present the SS-VTST and MS-VTST forward and reverse rate constants. The figure illustrates that up to 400 K, the SS-VTST and MS-VTST rate constants are within a factor of three. Beyond 500 K, we obtain large deviations in rate constants, reaching a factor of 147 by 2000 K and then increasing further. This shows the importance of torsional factors at high temperatures. The MS-VTST rate constants fit well with the following physically motivated four-parameter expressions[51]

$$k_{R1}^{MS\text{-}CVT/SCT}(\text{forward}) = 1.54 \times 10^{-13} \left(\frac{T}{300}\right)^{2.56} \times e^{-\frac{12.92(T+197.26)}{R(T^2+197.26^2)}} \tag{9}$$

$$k_{R1}^{MS\text{-}CVT/SCT}(\text{reverse}) = 2.54 \times 10^{-16} \left(\frac{T}{300}\right)^{2.54} \times e^{-\frac{13.05(T+188.86)}{R(T^2+188.86^2)}} \tag{10}$$

where R is the gas constant.

Table 3 also gives the activation energies, E_a for the forward and reverse reaction in Table 3. The activation energies are calculated from eqs 9 and 10 and the definition:

$$E_a = -R\frac{d(\ln k)}{d(1/T)} \tag{11}$$

The activation energies vary by 26.8 kcal/mol over the temperature range studied.

Summary. We estimated the thermal rate constants for hydrogen abstraction from carbon-3 of 1-butanol by $\bullet O_2H$ by employing the recently developed MS-VTST method[14] for the temperature range 200–4000 K. The MS-VTST approach is a convenient way to include contributions of more than one structure for reagents and transition states, thereby yielding rate constants for complex reactions with multiple torsions. We applied the MCSI method[41–45] to obtain the portion of the potential energy surface needed to calculate the variational effect and tunneling contributions. To the best of our knowledge, there are no experimental and theoretical rate constant data for this reaction. Our results indicate that torsional factors are very important at higher temperatures, and neglecting these factors would lead to an error of a factor as large of 171 at 2400 K.

Supporting Information.

Optimized Cartesian coordinates of the six lowest-energy structures of 1-butanol, 4-hydroxy-2-butyl radical, and the transition states and of hydroperoxyl radical and hydrogen peroxide; relative conformational energies and local periodicities; conformational-rotational-vibrational partition functions and anharmonicity factors; and details of the reaction path. This material is available free of charge via the Internet at http://pubs.acs.org.

References

 (1) Zhou, C.–W.; Simmie, J. M.; Curran, H. J. Rate Constants for Hydrogen-Abstraction by $\overset{\cdot}{O}H$ from *n*-Butanol. *Combust. Flame* **2011**, *158*, 726–731.

(2) Karwat, D. M. A.; Wagnon, S. W.; Teini, P. D.; Wooldridge, M. S. On the Chemical Kinetics of *n*-Butanol: Ignition and Speciation Studies. *J. Phys. Chem. A* **2011**, *115*, 4909–4921.

(3) Vasu, S. S.; Davidson, D. F.; Hanson, R. K.; Golden, D. M. Measurements of the Reaction of OH with *n*-Butanol at High-Temperatures. *Chem. Phys. Lett.* **2010**, *497*, 26–29.

(4) Moc, J.; Simmie, J. M. Hydrogen Abstraction from *n*-Butanol by the Hydroxyl Radical: High Level Ab Initio Study of the Relative Significance of Various Abstraction Channels and the Role of Weakly Bound Intermediates. *J. Phys. Chem. A* **2010**, *114*, 5558–5564.

(5) Black, G.; Simmie, J. M. Barrier Heights for H-Atom Abstraction by $H\overset{\cdot}{O}_2$ from *n*-Butanol–A Simple Yet Exacting Test for Model Chemistries?. *J. Comput. Chem.* **2010**, *31*, 1236–1248.

(6) Moc, J.; Simmie, J. M.; Curran, H. J. The Elimination of Water from a Conformationally Complex Alcohol: A Computational Study of the Gas Phase Dehydration of *n*-Butanol. *J. Mol. Struct.* **2009**, *928*, 149–157.

(7) Wallner, T.; Miers, S. A.; McConnell, S. *Proc. Spring Tech. Conf.*; ASME Internal Combustion Engine Division: Chicago, USA, 2008.

(8) Jacobson, M. Z. Effects of Ethanol (E85) Versus Gasoline Vehicles on Cancer and Mortality in the United States. *Environ. Sci. Technol.* **2007**, *41*, 4150–4157.

(9) Fargione, J.; Hill, J.; Tilman, D.; Polasky, S.; Hawthorne, P. Land Clearing and the Biofuel Carbon Debt. *Science* **2008**, *319*, 1235–1238.

(10) Golombok, M.; Tierney, S. Effect of Oxygenates on Water Uptake in Hydrocarbon Fuels. *Ind. Eng. Chem. Res.* **1997**, *36*, 5023–5027.

(11) Westbrook, C. K. Chemical Kinetics of Hydrocarbon Ignition in Practical Combustion Systems. *Proc. Combust. Inst.* **2000**, *28*, 1563–1577.

(12) Wright, M. E.; Harvey, B. G.; Quintana, R. L. Highly Efficient Zirconium-Catalyzed Batch Conversion of 1-Butene: A New Route to Jet Fuels. *Energy Fuels* **2008**, *22*, 3299–3302.

(13) Harvey, B. G.; Quintana, R. L. Synthesis of Renewable Jet and Diesel Fuels from 2-Ethyl-1-Hexene. *Energy Environ. Sci.* **2010**, *3*, 352–357.

(14) Yu, T.; Zheng, J.; Truhlar, D. G. Multi-Structural Variational Transition State Theory: Kinetics of the 1,4-Hydrogen Shift Isomerization of the Pentyl Radical with Torsional Anharmonicty. *Chem. Sci.* **2011**, *2*, 2199–2213.

(15) Garrett, B. C.; Truhlar, D. G. Criterion of Minimum State Density in the Transition State Theory of Bimolecular Reactions. *J. Chem. Phys.* **1979**, *70*, 1593–1598.

(16) Truhlar, D. G.; Garrett, B. C. Variational Transition-State Theory. *Acc. Chem. Res.* **1980**, *13*, 440–448.

(17) Truhlar, D. G.; Isaacson, A. D.; Garrett, B. C. *Theory of Chemical Reaction Dynamics*; Baer, M., Ed.; CRC Press: Boca Raton, FL, 1985; Vol. 4, pp 65–137.

(18) Jackels, C. F.; Gu, Z.; Truhlar, D. G. Reaction-Path Potential and Vibrational Frequencies in Terms of Curvilinear Internal Coordinates. *J. Chem. Phys.* **1995**, *102*, 3188–3201.

(19) Fernandez-Ramos, A.; Ellingson, B. A.; Garrett, B. C.; Truhlar, D. G. Variational Transition State Theory with Multidimensional Tunneling. In *Reviews in Computational Chemistry*; Lipkowitz, K. B., Cundari, T. R., Eds.; Wiley-VCH: Hoboken, NJ, 2007; Vol. 23, pp 125–232.

(20) Liu, Y.–P.; Lynch, G. C.; Truong, T. N.; Lu, D.–h.; Truhlar, D. G. Molecular Modeling of the Kinetic Isotope Effect for the [1,5]-Sigmatropic Rearrangement of *cis*-1,3-Pentadiene. *J. Am. Chem. Soc.* **1993**, *115*, 2408–2415.

(21) Alecu, I. M.; Zheng, J.; Zhao, Y.; Truhlar, D. G. Computational Thermochemistry: Scale Factor Databases and Scale Factors for Vibrational Frequencies Obtained from Electronic Model Chemistries. *J. Chem. Theor. Comput.* **2010**, *6*, 2872–2887.

(22) Zhao, Y.; Truhlar, D. G. Exploring the Limit of Accuracy of the Global Hybrid Density Functional for Main-Group Thermochemistry, Kinetics, and Noncovalent Interactions. *J. Chem. Theory Comput.* **2008**, *4*, 1849–1868.

(23) Lynch, B. J.; Zhao, Y.; Truhlar, D. G. Effectiveness of Diffuse Basis Functions for Calculating Relative Energies by Density Functional Theory. *J. Phys. Chem. A* **2003**, *107*, 1384–1388.

(24) Frisch, M. J.; Trucks, G. W.; Schlegel, H. B.; Scuseria, G. E.; Robb, M. A.; Cheeseman, J. R.; Scalmani, G.; Barone, V.; Mennucci, B.; Petersson, G. A. et al. Gaussian 09, revision A.1; Gaussian, Inc.: Wallingford, CT, 2009.

(25) Zhao, Y.; Peverati, R.; Yang, K.; Truhlar, D. G. *MN-GFM* version 5.2 computer program module, University of Minnesota, Minneapolis, 2011.

(26) Seal, P.; Papajak, E.; Yu, T.; Truhlar, D. G. Statistical Thermodynamics of 1-Butanol, Methyl-1-Propanol, and Butanal. submitted, *J. Chem. Phys.* **2011**.

(27) Zheng, J.; Mielke, S. L.; Clarkson, K. L.; Truhlar, D. G. MSTor computer program, version 2011, University of Minnesota, Minneapolis, 2011.

(28) Zheng, J.; Yu, T.; Papajak, E.; Alecu, I. M.; Mielke, S. L. Truhlar, D. G. Practical Methods for Including Torsional Anharmonicity in Thermochemical Calculations on Complex Molecules: The Internal-Coordinate Multi-Structural Approximation. *Phys. Chem. Chem. Phys.* **2011**, *13*, 10885–10907.

(29) Zhao, Y.; Truhlar, D. G. The M06 Suite of Density Functionals for Main Group Thermochemistry, Kinetics, Noncovalent Interactions, Excited States, and Transition Elements: Two New Functionals and Systematic Testing of Four M06 Functionals and Twelve Other Functionals. *Theor. Chem. Acc.* **2008**, *120*, 215–241.

(30) Krishnan, R.; Binkley, J. S.; Seeger, R.; Pople, J. A. Self-Consistent Molecular Orbital Methods. XX. A Basis Set for Correlated Wave Functions. *J. Chem. Phys.* **1980**, *72*, 650–654.

(31) Clark, T.; Chandrasekhar, J.; Spitznagel, G. W.; Schleyer, P. v. R. Efficient Diffuse Function-Augmented Basis Sets for Anion Calculations. III. The 3-21+G Basis Set for First-Row Elements, Li–F. *J. Comp. Chem.* **1983**, *4*, 294–301.

(32) Frisch, M. J.; Pople, J. A.; Binkley, J. S. Self-Consistent Molecular Orbital Methods 25. Supplementary Functions for Gaussian Basis Sets. *J. Chem. Phys.* **1984**, *80*, 3265–3269.

(33) Zheng, J.; Xu, X.; Truhlar, D. G. Minimally Augmented Karlsruhe Basis Sets. *Theor. Chem. Acc.* **2011**, *128*, 295–305.

(34) Papajak, E.; Truhlar, D. G. Efficient Diffuse Basis Sets for Density Functional Theory *J. Chem. Theor. Comput.* **2010**, *6*, 597–601.

(35) Papajak, E.; Truhlar, D. G. Convergent Partially Augmented Bases for Post-Hartree-Fock Calculations of Molecular Properties and Reaction Barrier Heights *J. Chem. Theor. Comput.* **2011**, *7*, 10–18.

(36) Xu, X.; Alecu, I. M.; Truhlar, D. G. How Well Can Modern Density Functionals Predict Intermolecular Distances at Transition State. *J. Chem. Theory Comput.* **2011**, *7*, 1667–1676.

(37) Adler, T. B.; Knizia, G.; Werner, H.–J. A Simple and Efficient CCSD(T)-F12 Approximation. *J. Chem. Phys.* **2007**, *127*, 221106–221109.

(38) Knizia, G.; Adler, T. B.; Werner, H.–J. Simplified CCSD(T)-F12 Methods: Theory and Benchmarks. *J. Chem. Phys.* **2009**, *130*, 054104–054123.

(39) Manby, F. R. Density Fitting in Second-Order Linear-r_{12} Møller–Plesset Perturbation Theory. *J. Chem. Phys.* **2003**, *119*, 4607–4613.

(40) Werner, H.–J.; Knowles, P. J.; Manby, F. R.; Schütz, M.; Celani, P.; Knizia, G.; Korona, T.; Lindh, R.; Mitrushenkov, A.; Rauhut, G. et al. Molpro, University of Birmingham, Birmingham, 2010.1, 2010.

(41) Kim, Y.; Corchado, J. C.; Villa, J.; Xing, J.; Truhlar, D. G. Multiconfiguration Molecular Mechanics Algorithm for Potential Energy Surfaces of Chemical Reactions. *J. Chem. Phys.* **2000**, *112*, 2718–2735.

(42) Albu, T. V.; Corchado, J. C.; Truhlar, D. G. Molecular Mechanics for Chemical Reactions: A Standard Strategy for Using Multiconfiguration Molecular Mechanics for Variational Transition State Theory with Optimized Multidimensional Tunneling. *J. Phys. Chem. A* **2001**, *105*, 8465–8487.

(43) Lin, H.; Zhao, Y.; Tishchenko, O.; Truhlar, D. G. Multi-Configuration Molecular Mechanics Based on Combined Quantum Mechanical and Molecular Mechanical Calculations. *J. Chem. Theory Comput.* **2006**, *2*, 1237–1254.

(44) Tischenko, O.; Truhlar, D. G. Optimizing the Performance of the Multiconfiguration Molecular Mechanics Method. *J. Phys. Chem. A* **2006**, *110*, 13530–13536.

(45) Tishchenko, O.; Truhlar, D. G. Non-Hermitian Multiconfiguration Molecular Mechanics. *J. Chem. Theory Comput.* **2009**, *5*, 1454–1461.

(46) Tishchenko, O.; Higashi, M.; Albu, T. V.; Corchado, J. C.; Kim, Y.; Villà, J.; Xing, J.; Lin, H.; Truhlar, D. G. MCSI, version 2010, University of Minnesota, Minneapolis, 2010.

(47) Albu, T. V.; Tishchenko, O.; Corchado, J. C.; Kim, Y.; Villà, J.; Xing, J.; Lin, H.; Higashi, M.; Truhlar, D. G. MC-TINKERATE, version 2010, University of Minnesota, Minneapolis, 2010.

(48) Zheng, J.; Zhang, S.; Lynch, B. J.; Corchado, J. C.; Chuang, Y.–Y.; Fast, P. L.; Hu, W.–P.; Liu, Y.–P.; Lynch, G. C.; Nguyen, K. A. et al. POLYRATE-version 2010-A, University of Minnesota, Minneapolis, 2010.

(49) Lu, D.–h.; Truong, T. N.; Melissas, V. S.; Lynch, G. C.; Liu, Y.–P.; Garrett, B. C.; Steckler, R.; Isaacson, A. D.; Rai, S. N.; Hancock, G. C. et al. POLYRATE 4: A New Version of a Computer Program for the Calculation of Chemical Reaction Rates for Polyatomics. *Comput. Phys. Commun.* **1992**, *71*, 235–262.

(50) Garrett, B. C.; Truhlar, D. G. Critical Tests of Variational Transition State Theory and Semiclassical Tunneling Methods for Hydrogen and Deuterium Atom Transfer Reactions and Use of the Semiclassical Calculations To Interpret the Overbarrier and Tunneling Dynamics. *J. Phys. Chem.* **1991**, *95*, 10374–10379.

(51) Zheng, J.; Truhlar, D. G. Kinetics of Hydrogen-Transfer Isomerizations of Butoxyl Radicals. *Phys. Chem. Chem. Phys.* **2010**, *12*, 7782–7793.

Table 1. Forward and Reverse Classical Barrier Heights and Classical Energies of Reaction for the Hydrogen Abstraction from Carbon-3 of 1-Butanol[a] (in kcal/mol)

Electronic model chemistry	$V_f^{\ddagger}$	$V_r^{\ddagger}$	ΔU	MUE[b]
M06-2X/MG3S	12.42	0.58	11.84	1.44
M08-HX/MG3S	14.04	1.85	12.18	0.59
M08-SO/MG3S	14.33	2.62	11.71	0.15
M06-2X/ma-TZVP	13.41	1.07	12.34	1.11
M08-HX/ma-TZVP	15.95	2.83	13.12	0.92
M08-SO/ma-TZVP	16.43	3.37	13.06	1.24
M06-2X/maug-cc-pVTZ	12.73	1.40	11.33	1.22
M08-HX/maug-cc-pVTZ	14.81	2.94	11.87	0.16
M08-SO/maug-cc-pVTZ	15.73	3.65	12.08	0.78
M06-2X/jun-cc-pVTZ	12.52	1.17	11.35	1.36
M08-HX/jun -cc-pVTZ	14.50	2.60	11.90	0.09
M08-SO/jun -cc-pVTZ	15.50	3.36	12.14	0.62
M06-2X/maug-cc-pVQZ	13.26	1.53	11.74	0.86
M08-HX/maug-cc-pVQZ	15.71	3.55	12.15	0.76
M08-SO/maug-cc-pVQZ	15.83	3.99	11.83	0.84
CCSD(T)-F12a/jun-cc-pVDZ	14.43	2.01	12.42	0.48
CCSD(T)-F12a/jun-cc-pVTZ	14.39	2.48	11.90	0.17
jun-jun	13.96	2.54	11.42	0.40
jun-jun (HL)	14.56	2.74	11.82	0.00

[a] In order to perform a consistent comparison, all results in this table are calculated at the same set of three geometries, namely those obtained by the M08-HX/MG3S method. "In the context of the present table, "classical" means zero-point-exclusive.

[b] The mean unsigned errors in the three energetic quantities are calculated with respect to the jun-jun (HL) method.

Table 2. Multi-structural Torsional Anharmonicity Factors for the H-Abstraction from Carbon-3 of 1-Butanol by $\cdot O_2H^a$

T (K)	Multi-structural anharmonicity factors						
	$F_{MS\text{-}T}^{R}$	$F_{MS\text{-}T}^{P1}$	$F_{MS\text{-}T}^{P2}$	$F_{MS\text{-}T}^{P}$	$F_{MS\text{-}T}^{\ddagger}$	$F_{forward}^{MS\text{-}T}$	$F_{reverse}^{MS\text{-}T}$
200	9.43	12.35	2.00	24.70	3.45	0.37	0.14
250	11.80	17.55	2.00	35.10	5.16	0.44	0.15
298.15	13.96	22.55	2.00	45.10	8.69	0.62	0.19
300	14.04	22.74	2.00	45.48	8.88	0.63	0.19
400	18.10	31.76	2.00	63.52	31.59	1.74	0.50
500	21.41	38.37	2.00	76.74	95.17	4.44	1.24
600	23.92	42.72	2.00	85.44	220.1	9.20	2.57
800	26.77	46.48	2.00	92.96	661.6	24.71	7.12
1000	27.50	46.32	2.00	92.64	1257	45.73	13.57
1300	26.37	42.94	2.00	85.88	2121	80.45	24.70
1500	24.93	39.96	2.00	79.92	2553	102.4	31.95
1800	22.47	35.35	2.00	70.70	2943	130.9	41.63
2000	20.81	32.46	2.02	65.57	3055	146.8	46.60
2400	17.78	27.37	2.02	55.29	3038	170.8	54.95
3000	14.08	21.41	2.02	43.25	2702	191.9	62.49
4000	9.84	14.78	2.02	29.85	1997	202.9	66.92

[a] $F_{MS\text{-}T}^{P}$ in the table is the product of the F factors for the two products, 4-hydroxy-2-butyl radical (P1) and H_2O_2 (P2).

Table 3. Forward and Reverse SS-VTST and MS-VTST Thermal Rate Constants (in cm^3 molecule^{-1} sec^{-1}) for the H-Abstraction from Carbon-3 of 1-Butanol by $\cdot O_2H$, the Activation Energy, E_a (in kcal/mol) of the Forward and Reverse Reaction, and the SCT Representative Tunneling Energy[a]

T (K)	Forward rate coefficients		E_a for the forward reaction	Reverse rate coefficients		E_a for the reverse reaction	SCT representative tunneling energy
	$k^{SS\text{-}CVT/SCT}$	$k^{MS\text{-}CVT/SCT}$		$k^{SS\text{-}CVT/SCT}$	$k^{MS\text{-}CVT/SCT}$		
200	6.36E−28	2.33E−28	7.65	1.00E−30	1.40E−31	8.29	103.39
250	1.02E−25	4.49E−26	10.87	2.58E−28	3.87E−29	11.52	104.04
298.15	3.49E−24	2.17E−24	13.30	1.16E−26	2.20E−27	13.90	104.12
300	3.92E−24	2.48E−24	13.38	1.32E−26	2.51E−27	13.98	104.13
400	5.63E−22	9.83E−22	16.60	2.52E−24	1.26E−24	17.03	104.74
500	1.53E−20	6.80E−20	18.34	7.71E−23	9.56E−23	18.64	106.44
600	1.55E−19	1.43E−18	19.35	8.18E−22	2.10E−21	19.56	107.29
800	4.13E−18	1.02E−16	20.51	2.21E−20	1.57E−19	20.62	108.10
1000	3.69E−17	1.69E−15	21.31	1.95E−19	2.64E−18	21.37	108.13
1300	3.24E−16	2.61E−14	22.42	1.66E−18	4.10E−17	22.45	108.15
1500	9.62E−16	9.85E−14	23.18	4.85E−18	1.55E−16	23.20	108.17
1800	3.43E−15	4.49E−13	24.38	1.70E−17	7.08E−16	24.39	108.19
2000	6.21E−15	9.12E−13	25.22	3.04E−17	1.42E−15	25.22	108.19
2400	7.64E−15	1.31E−12	26.96	3.69E−17	2.03E−15	26.95	108.20
3000	2.32E−14	4.45E−12	29.70	1.11E−16	6.94E−15	29.67	108.20
4000	8.53E−14	1.73E−11	34.44	4.03E−16	2.70E−14	34.38	108.20

[a] Includes variational effects, torsional anharmonicity, and tunneling.

Figure Captions:

Figure 1. Global minimum structures of (a) 1-butanol, (b) transition state leading to the formation of 4-hydroxy-2-butyl radical, and (c) 4-hydroxy-2-butyl radical.

Figure 2. Estimated (a) V_{MEP} and (b) ground-state vibrationally adiabatic potential, V_a^G, plotted against the reaction coordinate, s, scaled to a reduced mass of 1 amu, for the H abstraction from carbon-3 of 1-butanol by $\cdot O_2H$ to form 4-hydroxy-2-butyl radical. Points 2–7 in Figure 2a are the non-stationary Shepard points that we consider to calculate the reaction path by following ref 42. Point 1 is the saddle point.

Figure 3. Calculated forward and reverse rate constants obtained by the MS-VTST method for the H-atom abstraction from carbon-3 of 1-butanol by $\cdot O_2H$ to form 4-hydroxy-2-butyl radical and hydrogen peroxide.
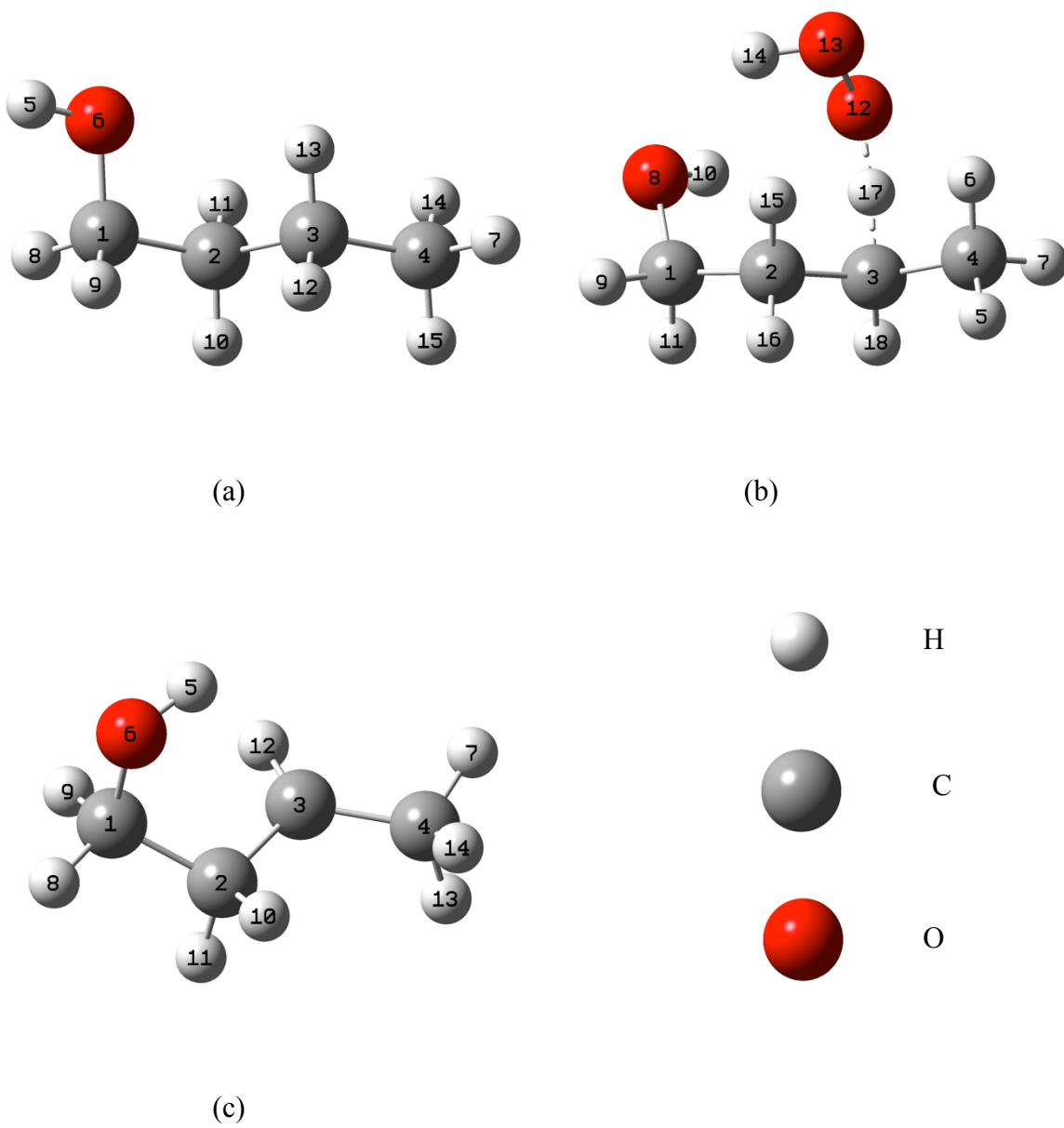
(a)

(b)

(c)

H

C

O

Figure 1

Figure 2

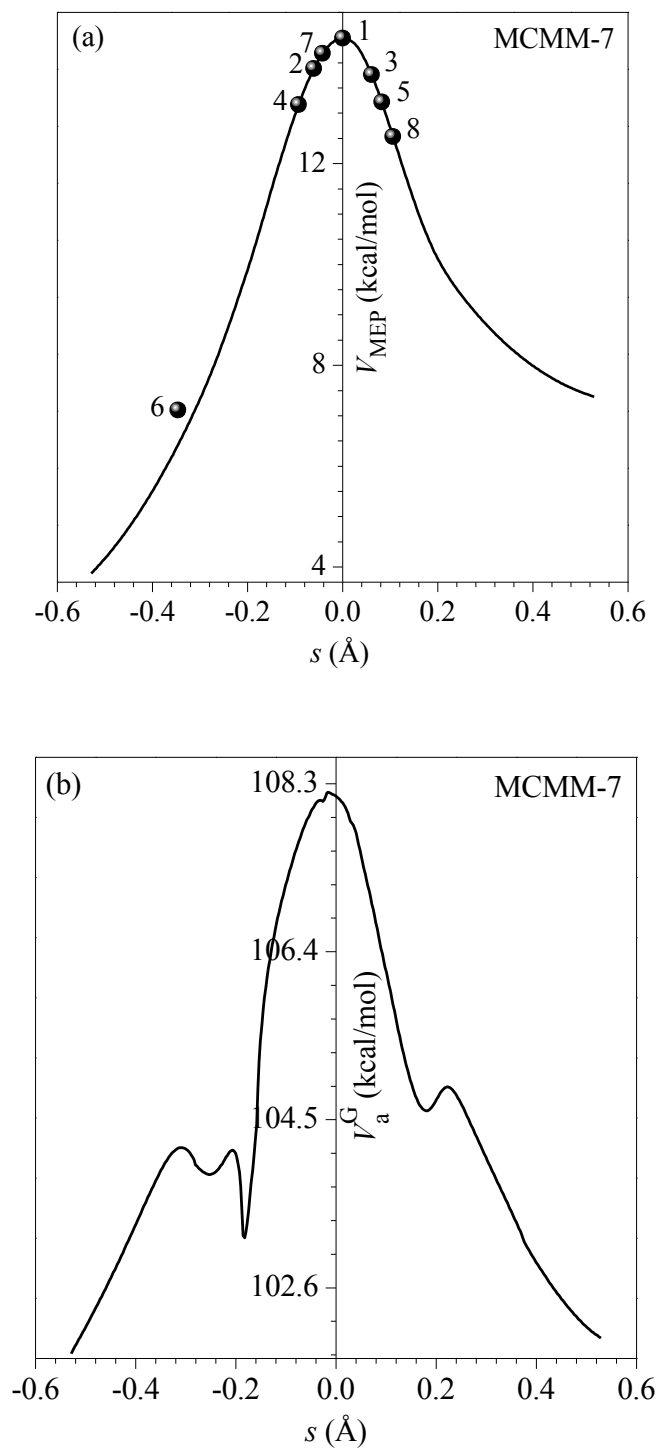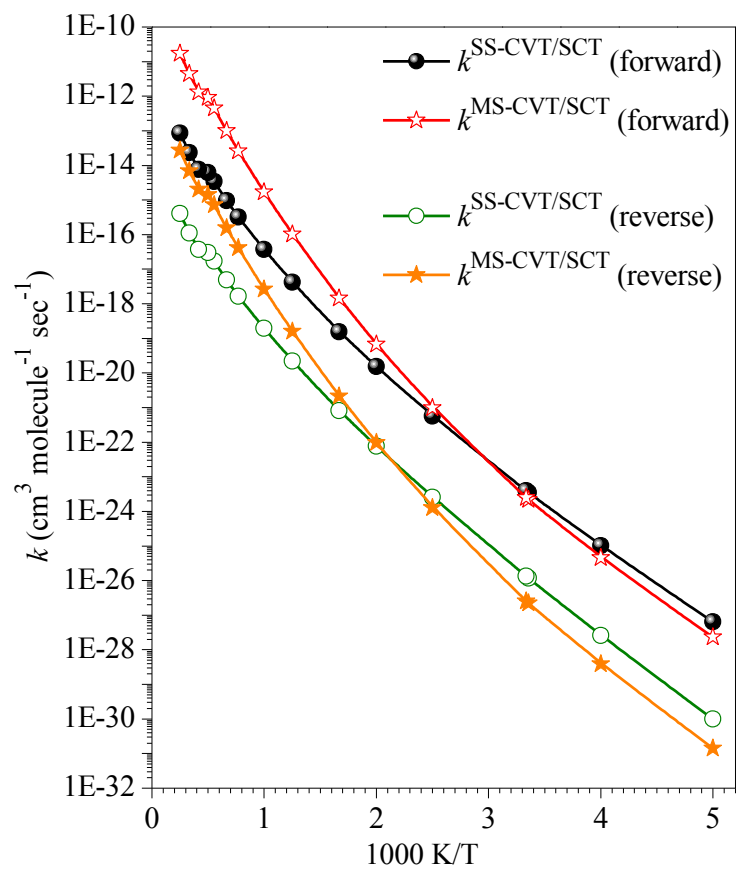**Figure 3**

Chapter 10. Multi-Structural Variational Transition State Theory: Kinetics of the 1,5-Hydrogen Shift Isomerization of the 1-Butoxyl Radical Including All Structures and Torsional Anharmonicity

Xuefei Xu, Ewa Papajak, Jingjing Zheng, and Donald G. Truhlar *

Department of Chemistry and Supercomputing Institute, University of Minnesota, Minneapolis, MN 55455-0431 USA

We investigate the statistical thermodynamics and kinetics of the 1,5-hydrogen shift isomerization reaction of 1-butoxyl radical and its reverse isomerization. The partition functions and thermodynamic functions (entropy, enthalpy, heat capacity, and Gibbs free energy) are calculated using the multi-structural torsional (MS-T) anharmonicity method including all structures for three species (reactant, product, and transition state) involved in the reaction. The calculated thermodynamic quantities have been compared to those estimated by the empirical group additivity (GA) method. The kinetics of the unimolecular isomerization reaction was investigated using multi-structural canonical variational transition state theory (MS-CVT) including both multiple-structure and torsional (MS-T) anharmonicity effects. In these calculations, multidimensional tunneling (MT) probabilities were evaluated by the small-curvature tunneling (SCT) approximation and compared to results obtained with the zero-curvature tunneling (ZCT) approximation. The MS-CVT/MT (MT can be ZCT or SCT) rate constants were reported for both forward and reverse reactions. Comparison with the rate constants obtained by the single-structural harmonic oscillator (SS-HO) approximation shows the importance of anharmonicity in the rate constants of these reactions, and the effect of multi-structural anharmonicity is found to be very large. Whereas the tunneling effect increases the rate constants, the MS-T anharmonicity decreases them at all temperatures. The two effects counteract each other at temperature 385 K and 264 K for forward and reverse reactions,

respectively, and tunneling dominates the lower temperatures while MS-T anharmonicity has a larger effect at higher temperatures. The multi-structural torsional anharmonicity effect reduces the final reverse reaction rate constants by a much larger factor than it does to the forward ones as a result of the existence of more low-energy structures of the product 4-hydroxy-1-butyl radical than the reactant 1-butoxyl radical. As a consequence there is also a very large effect on the equilibrium constant. The neglect of multi-structural anharmonicity will lead to large errors in the estimation of reverse reaction rate constants.

1. Introduction

Alkoxyl radicals as key intermediate species play important roles in both combustion and atmospheric chemistry.[1] Once formed, the relative rates and branching ratios of their subsequent reactions,[2] which could be decomposition, isomerization, and reactions with other molecules or radicals, will strongly affect the distribution of final products. Hence, both the knowledge of the thermodynamics of these radicals and accurate measurement or calculation of the kinetics of these radical reactions are very important for developing mechanisms of combustion and atmospheric processes. However, the corresponding experimental studies of the statistical thermodynamics and reaction kinetics of reactive radicals are very hard, especially in the gas phase.

In present work, we present a theoretical and computational study of the 1,5-hydrogen shift isomerization reaction of 1-butoxyl radical. The 1-butoxyl radical is an important radical in the combustion of the biofuel 1-butanol. As the dominant reaction channel of 1-butoxyl radical, the 1,5-hydrogen shift isomerization rate has been investigated by both experimental[3] and theoretical[4] methods. Due to the short lifetime and difficulty of detections of radicals, the experimental isomerization rate is usually obtained indirectly and over a limited temperature range. For example, Cassanelli et al.[3d] measured the branching ratio between the 1,5-hydrogen shift isomerization reaction of 1-butoxyl and the reaction of 1-butoxyl with O_2 as a function of oxygen concentration at atmospheric pressure over the temperature range 250–318 K, then converted the rate constant ratio to an absolute rate constant for isomerization reaction by using the

temperature-dependent absolute rate constant of the O_2 reaction. Heiss and Sahetchian[3b] derived the isomerization rate of 1-butoxyl radical over 343–503 K from the ratio of the isomerization rate to decomposition rate of 1-butoxyl and the known decomposition rate. Theoretical modeling extends the rate constant estimation to a larger temperature range, and——if accurate enough—can provide either a check on the experimental results or an improvement on them. In previous theoretical studies, Somnitz[4e] obtained consistent results with Cassanelli et al.'s experimental rate constants at low temperature by using RRKM theory including tunneling contributions calculated with the assumption of conservation of vibrational energy and with a fully coupled multiple-channel master equation (ME). A study[4f] by two of us employed single-structure variational transition state theory (SS-VTST)[5] with the small-curvature tunneling[6] (SCT) approximation and concluded that Somnitz had underestimated the tunneling. However the SS-VTST calculated rate constants[4f] have large deviations from Cassanelli et al.'s results at low temperature, and the same divergence is noticed in the study of Davis and Francisco[4g] with a small-curvature parabolic approximation for tunneling[7] and G4[8] electronic structure calculations. These discrepancies could result in part from both the two studies not accounting for the anharmonicity in calculations of partition functions. In addition, in a later section we will mention that Davis and Francisco[4g] also significantly overestimated tunneling with the parabolic tunneling approximation and underestimated tunneling with the Wigner method[9] at low temperature.

Both the reactant 1-butoxyl radical and the product 4-hydroxy-1-butyl have more than one torsion. The presence of multiple torsional degrees of freedom often results in multiple minima on the potential energy surface, which results in multiple-structure anharmonicity. The reactant 1-butoxyl radical has three torsional motions. One of them is the torsion of a methyl group, which does not generate additional distinguishable structures, and each of other two torsional motions can generate three (one trans (T) and two gauche (G)) structures, so that ideally $3 \times 3 = 9$ distinguishable structures would be generated for 1-butoxyl. In previous theoretical studies which only considered a single structure, Somnitz[4e] and Méreau[4b] used a GT structure for 1-butoxyl (in Figure 1, this is the structure in which the O-C-C-C torsion is gauche, and the C-C-C-C torsion is trans);

two of us[4f] and Davis and Francisco[4g] used only the TT structure (fourth structure in Figure 1). In the present study, as discussed more fully below, we located ten conformers (five pairs of mirror images) with the M08-SO density functional. The ten conformers are close to each other in energy, and the largest energy difference, before including zero point energy, is only 0.69 kcal/mol. Because the structures are all low in energy, they can all play an important role in calculations of partition functions. We found that the ratio between the partition functions calculated with the multi-structural torsional approximation[10] (MS-T), including both multiple-structure anharmonicity and torsional anharmonicity, and those calculated in the single-structure harmonic-oscillator (SS-HO) approximation is as much as a factor of 11.5 for 1-butoxyl. The inaccuracy in partition functions calculations that do not include multiple-structure anharmonicity leads to large errors in the theoretical prediction of thermochemical properties (such as equilibrium constants) and rate constants.

The work in 2003 by Vereecken and Peeters[4c] is so far the only theoretical study incorporating multiple conformers of the reactant and the transition state for the 1,5-H-shift isomerization reaction of 1-butoxyl. They reported that the temperature dependence of the rate constant was substantially influenced by using a multirotamer treatment. However they were mainly interested in atmospheric chemistry at a temperature of 298 K, and they neglected torsional anharmonicity.

In the present article we consider temperatures up to 2400 K, where torsional anharmonicity can be very important, and we include both multiple-structure anharmonicity and torsional anharmonicity in calculations of partition functions. We report standard state thermochemical properties (for an ideal gas at 1 bar) for the reactant, product, and transition state of the 1,5-hydrogen shift isomerization reaction of 1-butoxyl radical. The calculated thermochemical properties will be compared to those obtained by the group additivity (GA) method.[11] Multi-structural canonical variational transition state theory including a multidimensional treatment of tunneling (MS-CVT/MT)[12] will be used to obtain accurate forward and reverse rate constants of this reaction.

2. Computational methods

2.1. Electronic structure calculations

The M08-SO[13] density functional combined with the MG3S[14] basis set (which is the same as the 6-311+G(2df,2p) for H, C, and O) has been shown to be a very accurate combination of density functional and basis set for estimation of barrier heights and reaction energies of hydrogen-atom transfer reactions,[15] and this combination has also been shown to perform well for predicting transition state structures.[16] The validity of the M08-SO/MG3S method for the present reaction was examined in a previous study,[4f] in which the best estimate of the classical barrier height (obtained by the CCSD(T)/CBS method) was 11.89 kcal/mol, and M08-SO/MG3S was shown to yield 12.15 kcal/mol. Therefore, we will use M08-SO/MG3S for all electronic structure calculations in the present work, in particular, for conformer searching and optimization and for energy and frequency calculations. A locally modified version, *MN-GFM5.0,*[17a] of *Gaussian09.a02*[17b] that contains additional Minnesota functionals is used. The grid for density functional integrations has 99 radial shells around each atom and 974 angular points in each shell.

All vibrational frequencies were scaled by a factor of 0.983, determined previously,[18] to account for nontorsional anharmonicity and to yield a more accurate zero point energy (ZPE). Including ZPE in the barrier height calculated with the lowest-energy structures of reactant (or product) and transition state yields 10.72 kcal/mol for the forward reaction and 14.82 kcal/mol for the reverse reaction.

2.2. Dynamics calculations

2.2.1. MS-CVT/MT theory

The MS-CVT/MT method has been described in Ref.12. Calculations employing this method begin with the well-known[5] single-structure (SS) canonical variational transition state theory including multidimensional treatment of tunneling (CVT/MT). Then one adds vibrational anharmonicity (multiple-structures and torsional anharmonicity) to the rate constant calculations by multiplying by a multi-structural torsional factor F^{MS-T}. In this way the MS-CVT/MT rate constant is expressed as

$$k^{\text{MS-CVT/MT}} = F^{\text{MS-T}}(T)\kappa^{\text{MT}}(T)k^{\text{CVT}}(T) \tag{1}$$

where k^{CVT} in eqn (1) is the single-structure CVT rate constant,[5a,19] which minimizes the calculated generalized transition state (GT) rate constant (k^{GT}) for each temperature. For a unimolecular reaction, this is given in the harmonic oscillator (HO) approximation by

$$k^{\text{CVT}} = \min_s k^{\text{GT}}(T,s) = \frac{1}{\beta h}\frac{Q_{\text{el}}^{\text{GT}}(T)Q_{\text{rovib}}^{\text{GT}}(T,s_*^{\text{CVT}})}{Q_{\text{el}}^{\text{R}}(T)Q_{\text{rovib}}^{\text{R}}(T)}\exp\left(-\beta V_{\text{MEP}}(s_*^{\text{CVT}})\right) \tag{2}$$

where β is $(k_B T)^{-1}$, k_B is Boltzmann's constant, h is Planck's constant, s is the signed distance along the minimum energy path (MEP), s_*^{CVT} is the value of s that minimizes the rate constant, $Q_{\text{el}}^{\text{GT}}$ and $Q_{\text{rovib}}^{\text{GT}}$ are respectively the electronic and rotational–vibrational partition functions of the generalized transition states $= s_*^{\text{CVT}}$, Q_{el}^{R} and $Q_{\text{rovib}}^{\text{R}}$ are the electronic and rotational–vibrational partition functions of the reactant, and $V_{\text{MEP}}(s_*^{\text{CVT}})$ is the potential energy at $s = s_*^{\text{CVT}}$. All symmetry numbers for rotations are included in rotational partition functions.

The factor κ^{MT} in eqn (1) is the transmission coefficient, which corrects for quantum effects (tunneling and nonclassical reflection) on the reaction coordinate. In MS-VTST, we assume that the transmission coefficient is the ground-state transimission coefficient taken as the ratio of the thermally averaged ground-state quantal transmission probability to the thermally averaged ground-state classical transmission probability,[20] where "ground-state" here refers to vibrational and rotational modes transverse to the reaction coordinate. The ground-state vibrationally adiabatic potential curve, V_a^{G}, governs the tunneling motion,

$$V_a^{\text{G}} = V_{\text{MEP}}(s) + \varepsilon^{\text{G}}(s) \tag{3}$$

where $\varepsilon^G(s)\varepsilon^G(s)$ denotes the local zero-point vibrational energy of the bound modes transverse to the reaction coordinate at s. Because $\varepsilon^G\varepsilon^G$ depends on s, it means that we already include one effect of the nonseparability of the reaction coordinate in the quantal treatment; thus tunneling calculations based on eqn (3) are labeled as multidimensional. In the present work, we will consider two multidimensional tunneling approximations: zero-curvature tunneling (ZCT)[21] and small-curvature tunneling (SCT).[6] Therefore, MT is either ZCT or SCT.

The product of $\kappa^{MT}\kappa^{MT}\kappa^{MT}$ and $k^{CVT}k^{CVT}$ is called the SS-HO CVT/MT rate constant (where HO denotes harmonic because in eqn (2), Q_{rovib}^R and Q_{rovib}^{GT} Q_{rovib}^{GT} are taken as a product of a rotational partition function and a vibrational one that can be calculated using the harmonic formalism (strictly speaking it is quasiharmonic because the scale factor described in section 2.1 accounts approximately for nontorsional anharmonicity)). This single-structure harmonic approximation is reasonable if neither the generalized TS nor the reactant include any torsional motion and if they both have only one conformer. However, in most cases we have to consider torsional anharmonicity and multiple-structure anharmonicity in partition functions, and this may have an important influence on the final computed rate constants. There are many methods for correcting harmonic partition functions, such as applying a one-dimensional (1-D) hindered-rotor (HR) approximation[22] to each torsional mode separately and more complicated methods including mode-mode coupling in the treatment of anharmonicity, for example, Feynman path integral methods[23] and the Pitzer-Gwinn approximation.[22a,24] MS-CVT/MT includes anharmonicity by multiplying by a multi-structural torsional factor F^{MS-T} as shown in eqn (1); this factor is calculated by the multi-structural method for torsional anharmonicity (MS-T), which is specifically designed for systems with multiple conformers and with multiple torsions coupled with each other and/or with other low-frequency vibrational modes. The MS-T method[10] uses internal-coordinate correction factors to the harmonic treatment, and it avoids assigning specific normal modes as separable torsions. For the present MS-T calcuations, we included all structures

(AS). The full name of the AS version of the MS-T method is MS-AS-T, but here we shorten it to MS-T.

The first step in using MS-T methods is to find all conformers generated by internal rotations or ring structure isomerizations for both the reactant and the transition state. Since we will also calculate the reverse rate constants, we also consider the product. Then one calculates the corresponding MS-T conformational–rotational–vibrational partition functions via

$$Q_{\text{con−rovib}}^{\text{MS−T}} = \sum_{j=1}^{J} Q_j^{\text{rot}} \exp(-\beta U_j) Q_j^{\text{HO}} Z_j \prod_{\tau=1}^{t} f_{j,\tau}$$

(4)

where j labels the distinguishable structures of the investigated species (reactant, product, or transition state), J is the total number of structures, U_j denotes the potential energy of structure j relative to the lowest-potential-energy structure in the relevant set, which is always numbered as $j = 1$, with $U_1 = 0$ by definition, Q_j^{rot} is the classical rotational partition function of structure j, Q_j^{HO} is the usual normal-mode local-harmonic-oscillator vibrational partition function calculated at structure j, Z_j is a factor for guiding the MS-T scheme to the correct high-temperature limit (within the parameters of the model), and $f_{j,\tau}$ is a torsional anharmonicity function, based on internal coordinates, that, in conjunction with Z_j, adjusts the harmonic partition function of structure j for the presence of the torsional motion τ.

For each species, we define the ratio of the calculated MS-T conformational–rotational–vibrational partition function $Q_{\text{con−rovib}}^{\text{MS−T}}$ to $Q_{\text{rovib,1}}^{\text{SS−HO}}$ which is single-structure harmonic rotational–vibrational partition function of the lowest-potential-energy structure 1, as the MS-T anharmonic factor $F_{\text{MS−T}}^{\alpha}$ of that species (α is either a reactant or product or TS):

$$F_{\text{MS-T}}^{\alpha} = \frac{Q_{\text{con-rovib},\alpha}^{\text{MS-T}}(T)}{Q_{\text{rovib},1,\alpha}^{\text{SS-HO}}(T)}$$

(5)

The multi-structural torsional factor $F^{\text{MS-T}}$ in eqn (1) is then obtained as the ratio of $F_{\text{MS-T}}^{\alpha} F_{\alpha}^{\text{MS-T}}$ factors of the transition state and reactant. We therefore obtain

$$F^{\text{MS-T}} = \frac{F_{\text{MS-T}}^{\text{TS}}(T)}{F_{\text{MS-T}}^{\text{R}}(T)}$$

(6)

The MS-T anharmonic factors of eqns (5) and (6) introduce both multiple-structure and torsional anharmonicity effects. We can decompose the ratios of eqn (5) into a multiple-structure, local-harmonic component $F_{\text{MS-LH}}^{\alpha} F_{\alpha}^{\text{MS-LH}}$ and a torsional component F_{T}^{α} F_{α}^{T} to clarify their respective contributions,

$$F_{\text{MS-T}}^{\alpha} = F_{\text{MS-LH}}^{\alpha}(T) F_{\text{T}}^{\alpha}(T) = \left(\frac{Q_{\text{con-rovib},\alpha}^{\text{MS-LH}}(T)}{Q_{\text{rovib},1,\alpha}^{\text{SS-HO}}(T)} \right) \left(\frac{Q_{\text{con-rovib},\alpha}^{\text{MS-T}}(T)}{Q_{\text{con-rovib},\alpha}^{\text{MS-LH}}(T)} \right)$$

(7)

where $Q_{\text{con-rovib},\alpha}^{\text{MS-LH}}(T) Q_{\text{con-rovib},\alpha}^{\text{MS-LH}}(T)$ is the multiple-structure local-harmonic partition function obtained by setting all of the Z_j and $f_{j,\tau}$ equal to unity in eqn (4); this includes anharmonicity from the multiple structures but treats torsions in the vicinity of each local minimum as harmonic oscillators with infinitely high barriers between the structures. (As already mentioned in conjunction with the SS-HO approximation, the MS-LH method is actually quasiharmonic, not strictly harmonic, because of the frequency scaling factors.)

2.2.2. Thermodynamic calculations with MS-T method

The thermodynamic quantities for one mole of an ideal gas at a standard state pressure of one bar, the Gibbs free energy (G_T°), average energy (E_T°), enthalpy (H_T°), entropy (S_T°), and heat capacity at constant pressure ($C_P^\circ(T)$), can be calculated as

$$G_T^\circ = -\frac{\ln Q}{\beta} + k_B T \tag{8}$$

$$E_T^\circ = -\frac{\partial \ln Q}{\partial \beta} \tag{9}$$

$$H_T^\circ = E_T^\circ + P^\circ V = E_T^\circ + RT \tag{10}$$

$$S_T^\circ = k_B \ln Q - \frac{1}{T}\left(\frac{\partial \ln Q}{\partial \beta}\right) \tag{11}$$

$$C_P^\circ(T) = \left(\frac{\partial H_T^\circ}{\partial T}\right)_P \tag{12}$$

where P is pressure, V is volume, the little circle denotes standard state, and Q is the total partition functions including translational, electronic and conformational–vibrational–rotational contributions.

2.2.3. Computational details

Four main steps were carried out to calculate thermochemical properties with the MS-T method and MS-CVT/MT forward and reverse reaction rate constants with potential energy surfaces calculated by the M08-SO/MG3S method:

1. We performed an exhaustive search for all conformational structures (local minima of the potential energy) of the reactant and product and for all saddle point structures of the transition state. We calculated the ideal-gas partition functions, entropy, heat capacity, enthalpy, and Gibbs free energy for the standard state (1 bar pressure), and we calculated F_{MS-T}^α factors using all generated conformers by the *MSTor* program.[25] The multi-structural torsional factor F^{MS-T} was calculated using eqn (6).

2. For each conformer λ of the transition state ($\lambda = 1, 2, \ldots, C$), we calculate a ground-state energy by

$$V_{a,\lambda}^{G} = V_{\lambda}^{TS} + \varepsilon_{\lambda}^{G,TS}$$

(13)

Where V_{λ}^{TS} is the potential energy relative to that of the lowest-energy structure of the reactant, and $\varepsilon_{\lambda}^{G,TS}$ is the zero point energy. Then we used the transition state structure with the lowest $V_{a,\lambda}^{G}$ V_a^G and the reactant and product well structures connected to this transition state by its MEP to construct V_{MEP} V_{MEP} and V_a^G V_a^G curves by the MCSI method[26] using the *MCSI* program.[27]

3. Based on the generated V_{MEP} V_{MEP} and V_a^G curves in step 2, we calculated κ^{MT} κ^{MT} and k^{CVT} k^{CVT} in eqn (1) for the temperature range 200–2400 K by using the *MC-TINKERATE* program.[28] The global-minimum structures of the reactant and the transition state were used to calculate SS-HO partition functions in calculation of k^{CVT} with eqn (2).

4. The forward rate constants $k^{MS-CVT/MT}$ over the 200–2400 K range were obtained using eqn (1). The corresponding $k^{MS-CVT/MT}$ $k^{MS-CVT/MT}$ reverse rate constants were calculated by using the partition function of the product instead of that of the reactant.

In the MCSI calculations of the potential energy surface and vibrationally adiabatic potential energy curve (steps 2 and 3 above), we used the energies, gradients, and Hessians of the saddle point, well structures in the reactant and product valleys, and 18 nonstationary Shepard points close to the MEP. This data was calculated by the M08-SO/MG3S method. The locations of the first six nonstationary Shepard points were obtained in a similar way to that presented in a previous paper,[26b] and the other 12 nonstationary Shepard points were added for smoothing the V_a^G V_a^G curve. Ten of the 18 non-stationary Shepard points were located on the 1-butoxyl side of the saddle point with energies 0.31, 0.62, 1.60, 2.28, 3.25, 4.73, 6.23, 7.77, 9.41, and 9.76 kcal/mol below the

transition state; and the other eight were located on the 4-hydroxy-1-butyl side with energies 0.89, 1.54, 2.99, 4.60, 6.07, 6.26, 7.69, and 9.48 kcal/mol below the transition state. The Euler steepest-descents integrator (ESD) was used with a step size of 0.0053 Å to follow the MEP, and the RODS[29] algorithm was used to refine the energies and frequencies along the path. The parameters for the molecular mechanics force field used in the MCSI calculations are those of the modified MM3 force field,[30] and the modified parameters are given in Supporting Information.

In all calculations of partition functions and the V_a^G V_a^G curve, the harmonic frequencies obtained from M08-SO/MG3S electronic structure calculations were scaled by an empirical factor of 0.983^{18} to reduce the average error in zero point energies calculated by the local harmonic approximation. The use of the scaling factor introduces anharmonicity into the low-temperature results.

3. Results and discussion

3.1. Conformers, partition functions, and anharmonicity of stationary points (reactant, product, and transition state)

Information about the conformers of the reactant (1-butoxyl) and product (4-hydroxy-1-butyl) and their partition functions and MS-T factors is presented in Tables 1–5. There are ten distinguishable structures (five pairs of mirror images) for 1-butoxyl radical and 37 distinguishable structures (18 pairs of mirror images plus one symmetric structure with a mirror plane) for 4-hydroxy-1-butyl radical. The five lowest-energy structures of reactant and product are shown in Figures 1 and 2.

3.1.1 1-butoxyl

As stated in the Introduction, nine distinguishable structures generated by two torsions (O-C-C-C and C-C-C-C) were expected for 1-butoxyl, but we found ten. The naming convention for labeling the structures is given in Table 1. The lowest-energy structures are G^-T^+ and G^+T^-, which are a pair of mirror images.

In the present investigations with the M08-SO density functional, the all-trans symmetric structure TT expected originally splits into two mirror images T^-T^- and T^+T^+ with similar geometries, and in particular the two torsion angles are ±178.1 and ±179.3 respectively. The two minima correspond to almost the same geometry on the potential energy surface. We considered including only one of them in the MS-T partition function calculations, using nine structures instead of ten, and this gives results differing from those obtained using all ten structures by 17% at 200 K, 11% at 1000 K, 7% at 1500 K, and 5% at 2400 K (the M value for the T^-T^- structure is 4.25 for ten structures and 3.04 for nine). But all structures are present, so in the final calculations we used all ten.

The energy difference between the lowest and highest of the ten structures is very small, less than 0.69 (or 1.02) kcal/mol when zero-point-energy is excluded (or included); hence the conformational–rotational–vibrational partition functions considering all ten structures ($Q_{con-rovib}^{MS-LH}$, $Q_{con-rovib}^{MS-T}$) are much larger than the single-structure rotational–vibrational partition functions calculated with the lowest-energy structure ($Q_{rovib,1}^{SS-HO}$) as shown in Table 3. The multi-structural torsional factors F_{MS-T}^{R} and their components F_{MS-LH}^{R} and F_{T}^{R} of 1-butoxyl calculated with eqn (7) are shown in Table 5. They indicate that both multiple-structure and torsional anharmonicity increase the partition functions of 1-butoxyl except for at temperature 2400 K where torsional anharmonicity very slightly decreases the partition functions, and the final MS-T conformational–rotational–vibrational partition functions $Q_{con-rovib}^{MS-T}$ are as much as 4.98–11.46 times larger than $Q_{rovib,1}^{SS-HO}$ over the 200–2400 K temperature range. The F_{MS-LH}^{R} factor is larger than F_{T}^{R} at each temperature studied here.

3.1.2. 4-hydroxy-1-butyl

The four torsions of the product, 4-hydroxy-1-butyl, are H-O-C-C, O-C-C-C, C-C-C-C, and C-C-C-H, and they generate 37 low-energy distinguishable structures (18 pairs of mirror images plus one symmetric structure with a mirror plane). These structures have very similar energies, in particular the energy differences between the 37 structures are smaller than 1.92 (or 1.57) kcal/mol when zero-point-energy is excluded (or included). The lowest-energy structures are $G^-G^+G^-T^+$ and $G^+G^-G^+T^-$, which are 1.35 kcal/mol lower in energy than the all trans structure that was sometimes taken as the lowest-energy structure in previous work.

As a result of large number of conformers, multi-structural torsional anharmonicity, especially anharmonicity introduced by multiple structures, has a remarkable effect on the partition functions of 4-hydroxy-1-butyl radical as shown in Table 4. The F_{MS-T}^P given in Table 5 are as large as 30.4–119.9 over the temperature range 200–2400 K, while F_{MS-LH}^P are as large as 22.5–201.5. Due to the mode-mode coupling, the torsional anharmonicity at temperatures higher than 800 K has a negative effect on partition functions; thus it leads to F_T^P values smaller than unity.

3.1.3 Transition state

The transition state of the 1,5-H shift reaction of 1-butoxyl is a six-member ring structure without torsions; therefore, only two distinguishable structures (one pair of mirror images) were located in the present work, and these are shown in Figure 3. Thus, for the transition state, there is no torsional anharmonicity, and $Q_{con-rovib,TS}^{MS-LH}$ $Q_{con-rovib,TS}^{MS-LH}(T)$ are exactly equal to $Q_{con-rovib,TS}^{MS-T}Q_{con-rovib,TS}^{MS-T}(T)$, which is twice as large as the SS-HO rotational–vibrational partition function for each temperature. The calculated total partition functions Q_{TS}^{MS-T} and $Q_{con-rovib,TS}^{MS-T}Q_{con-rovib,TS}^{MS-T}(T)$ of the

transition state for temperature 200–2400 K and the multi-structural torsional factors are shown in Table 6. Due to an absence of torsion motion and only two degenerate conformers, $F_T^{TS} F_{TS}^T$ is 1, and $F_{MS-LH}^{TS} F_{TS}^{MS\text{-}T}$ and $F_{MS-T}^{TS} F_{TS}^{MS\text{-}LH}$ are equal to each other and have a value of 2 at all temperatures.

3.2 Thermodynamics quantities

As shown in equations $(8)-(12)$, all the thermodynamics quantities are determined by the total partition functions. The multi-structural torsional anharmonicity which plays important role in calculations of partition function will directly affect the accuracy of these thermodynamics quantities. Tables 7–9 list the calculated temperature-dependent standard-state (one bar) ideal-gas entropy S_T°, heat capacity $C_P^\circ(T)$, relative enthalpy $H_T^\circ - H_0^\circ$, and relative Gibbs free energy $G_T^\circ - H_0^\circ$ using multi-structural torsional partition functions for 1-butoxyl, 4-hydroxy-1-butyl, and the transition state that interconnects them. For comparison, those entropy and heat capacity obtained by Benson's group additivity (GA) method[11] are given for 1-butoxyl and 4-hydroxy-1-butyl. The heat capacities obtained by Davis and Francisco[4g] using the G4 method with a single structure are also shown in Tables 7–9.

The heat capacities calculated with the MS-T method considering both multiple-structure and torsional anharmonicity are in reasonable agreement with those obtained by the GA method for 1-butoxyl and 4-hydroxy-1-butyl. Although for 1-butoxyl, the MS-LH method only considering multiple-structure anharmonicity gives $C_P^\circ(T)$ values closer to the GA values for 300 and 400 K, the MS-LH method overestimates the heat capacities at most temperatures for both 1-butoxyl and 4-hydroxy-1-butyl. The heat capacities obtained by Davis and Francisco are based on considering only a single structure, and they have a large deviation from those calculated by MS methods in the present work and from the empirical GA results for 1-butoxyl. For 4-hydroxy-1-butyl and the transition state, Davis and Francisco's results are similar to our MS-LH heat capacities.

Similarly, the entropies calculated with MS methods are in reasonable agreement with GA results. Although, MS-T entropies have a deviation of 2–3 cal mol^{-1} K^{-1} from the GA entropies at some temperatures, the MS-T results may be more reliable than the empirical GA values and the MS-LH results.

3.3. Multi-structural torsional factors and anharmonicity of the reactions

The multi-structural torsional anharmonicity factors ($F^{\text{MS-T}}$, $F^{\text{MS-LH}}F^{\text{MS-T}}$, and $F^{\text{T}}F^{\text{T}}$) for rate calculations of the forward or reverse reaction are obtained using eqn (6) and are shown in Table 10. The smaller number of structures of the transition state as compared to the reactant and product lead to $F^{\text{MS-T}}F^{\text{MS-T}}$ factors smaller than unity for both the forward and reverse reactions. Therefore the multi-structural torsional anharmonicity reduces the final thermal rate constants. The $F^{\text{MS-T}}F^{\text{MS-T}}$ factor of the forward reaction decreases gradually from 0.40 at 200 K to 0.17 at 1000 K, and then it increases gently to 0.25 at 2400 K. The $F^{\text{MS-T}}F^{\text{MS-T}}$ factors of the reverse reaction are much smaller than those of the forward reaction because there are much more conformers of the product than of the reactant, and they are 0.066, 0.017, and 0.029 for temperatures of 200, 800, and 2400 K. From Table 10, one can notice that multiple-structure anharmonicity has larger effects on partition functions than torsional anharmonicity in the present case.

3.4. CVT/MT rate constants and transmission coefficients

The forward and reverse barrier heights and the reaction energy calculated using the lowest-energy structures of reactant, product, and transition state are 12.59, 17.26, and −4.67 kcal/mol respectively by the M08-SO/MG3S method before including ZPE. The calculated barrier heights are larger than those (12.15 kcal/mol for forward reaction and 15.92 kcal/mol for reverse reaction by the M08-SO/MG3S method) in previous work by two of us,[4f] because we now use those more stable conformers for the reactant and product. Table 11 compares the calculated enthalpy of reaction and enthalpy of activation obtained by the MS-T method in the present work, with those obtained by Davis and

Francisco[4g] using the G4 method and only considering a single structure, and those estimated by GA method.

The calculated potential energy along the minimum energy path, V_{MEP} V_{MEP}, and the ground-state vibrationally adiabatic potential curve V_a^{G} are shown in Figure 4. Using these curves, the single-structure harmonic (in fact it should be quasiharmonic because the scaling factor is used in zero point energy calculations) CVT rate constants k^{CVT} and corresponding transmission coefficient κ^{MT} (MT can be ZCT or SCT) for both forward and reverse reactions are evaluated. Figure 5 plots the common logarithm of the ZCT and SCT transmission coefficients as functions of $1000/T$. As we expected, κ^{ZCT} are much smaller than κ^{SCT} at low temperatures because ZCT underestimates the tunneling, and the difference between them decreases when the temperature increases. At $T = 300$ K, we get $\kappa^{\mathrm{ZCT}} = 3.3$, and $\kappa^{\mathrm{SCT}} = 11.0$; both of them are smaller than the previous work by two of us[4f] where $\kappa^{\mathrm{ZCT}} = 5.3$ and $\kappa^{\mathrm{SCT}} = 40.9$, but larger than Somnitz's estimation[4e] for tunneling, which corresponds to $\kappa = 2.7$. Davis and Fransisco[4g] significantly overestimated tunneling ($\kappa = 120$) with the parabolic tunneling approximation for G4 data set, and they underestimated tunneling ($\kappa = 3.5$) with the Wigner method.

The present work predicts only a small variational effect with the rate constant ratio of CVT to TST ranging from 0.90 to 0.97. In our previous work[4f] this rate ratio ranged from 0.83 to 0.90. Since the previous work[4f] was based on straight direct dynamics calculations whereas the present work involves the MCSI method, the previous work should be more accurate for the variational effect, but fortunately the difference between the two treatments is less than 8%.

The single-structure $k^{\mathrm{CVT/MT}}$ (MT can be ZCT or SCT) rate constants including tunneling are obtained as a product of k^{CVT} and κ^{MT}, and are plotted in Figure 6 as functions of $1000/T$ along with k^{CVT} rate constants for forward and reverse reactions.

As shown in Figure 6, the forward reaction has larger rate constants than the reverse reaction. Tunneling increases the reaction rate constants especially at low temperature.

3.5. MS-CVT/MT rate constants

The above calculations provide the factors needed in eqn (1) to calculate the thermal rate constants: κ, $F^{\text{MS-T}}$ and k^{CVT}. Figure 7 shows that the tunneling and anharmonicity effects have opposite effects on the rate constants for the 1,5-hydrogen shift isomerization reaction of 1-butoxyl, and the former increase the rate (positive logarithm), while the later reduce the rate (negative logarithm). At low temperature, $T <$ 385 K, the tunneling is a larger effect for the forward reaction; for higher temperature than 385 K, multi-structural torsional anharmonicity has the larger effect for the forward reaction rate. The large number of low-energy conformers of the product has the consequence that the anharmonic effect is larger for the reverse reaction at even lower temperatures ($T > 264$ K). Therefore, both tunneling and multi-structural torsional anharmonicity effects are very important for accurate rate constants calculations if one considers a wide temperature range.

The final $k^{\text{MS-CVT/MT}}$ rate constants including these two important effects are obtained using eqn (1), and they are plotted as functions of temperature in Figure 8. In Figure 8, the $k^{\text{CVT/SCT}}$ obtained by single-structure method in present work and the previous theoretical and experimental results are also given for comparisons. The $k^{\text{MS-CVT/SCT}}$ rate constants at several temperatures are shown in Table 12. As shown in Figure 8, the single-structure $k^{\text{CVT/SCT}}$ rate constants in the present work agree very well with experimental results of Heiss et al.[3b] and Cassanelli et al.[3d] Due to larger estimated tunneling contributions, the previous single-structure CVT/SCT rate constants obtained by two of us,[4f] have a large deviation from the present $k^{\text{CVT/SCT}}$ results at low temperature. Another contributing factor to the difference is that we use a more stable reactant structure in present calculations. Comparison of the present $k^{\text{CVT/SCT}}$ rate constants and single-structure rate constants obtained by Somnitz[4e] shows that Somnitz

overestimated the rate constants at high temperature and underestimated tunneling at low temperature, but he had rate constants similar to our $k^{\text{CVT/SCT}}$ rate constants and Cassanelli et al.'s experimental results at 250–300 K. Although these theoretical rate constants by the single-structure method are in good agreement with experimental results, one must realize that these single-structure methods neglect the important multi-structural torsional anharmonicity effects. When multi-structural torsional anharmonicity is considered, the final $k^{\text{MS-CVT/MT}}$ k^{MS-CVT/MT} (MT can be either ZCT or SCT) rate constants are much smaller than the ones obtained by single-structure methods. There is a large deviation of the MS-CVT/MT results for the forward reaction from the experimental data, but our smaller $k^{\text{MS-CVT/SCT}}$ k^{MS-CVT/SCT}results are still located within the error range of Cassanelli et al.'s experiments. Due to the underestimation of tunneling by the ZCT method, the $k^{\text{MS-CVT/ZCT}}$ rate constants are much smaller than those from $k^{\text{MS-CVT/SCT}}$ at low temperatures. As we mentioned in the introduction, so far all the experimental rate constants reported for 1-butoxyl isomerization reaction were determined by relative rate technique, and this introduced large uncertainties in results. Therefore, we believe that the real rate constants may be closer to our $k^{\text{MS-CVT/SCT}}$ k^{MS-CVT/SCT}results.

The importance of multi-structural torsional anharmonicty is especially remarkable for the reverse reaction as we discussed in the beginning of this subsection. Figure 9 shows a large difference between the single-structure and multi-structural rate constants for the reverse reaction. The calculated $k^{\text{MS-CVT/MT}}$ k^{MS-CVT/MT}rate constants for both forward and reverse reactions are fitted to the modified Arrhenius equation [4f]

$$k = A\left(\frac{T}{300}\right)^n \exp\left[-\frac{E(T+T_0)}{R(T^2+T_0^2)}\right]$$

$$(14)$$

which has four fitting parameters. The corresponding Arrhenius activation energy is

$$E_a = E \frac{T^4 + 2T_0 T^3 - T_0^2 T^2}{(T^2 + T_0^2)^2} + nRT \tag{15}$$

The fitted parameters and calculated activation energies for both forward and reverse reactions are listed in Tables 13 and 14. Table 14 shows that the activation energy increases nonlinearly with temperature, which shows clearly that T_0 must be nonzero.

As a result of a different extent of multi-structural torsional anharmonicity on the forward and reverse reactions, the equilibrium constant of the reaction which is the ratio of the forward to reverse rate constants, is also affected by the multi-structrural torsional anharmonicity.

4. Concluding Remarks

Multi-structural canonical variational transition state theory including a multidimensional treatment of tunneling (MS-CVT/MT) has been applied to the 1,5-hydrogen shift isomerization reaction of 1-butoxyl. The presence of several torsion motions leads to multiple minima (ten and 37) on potential energy surfaces for both reactant and product. The mirror image structures of the six-member ring transition state are included in this work. All conformers of stationary points have been used in calculations of partition functions including multi-structural torsional anharmonicity (we used MS-T conformational–rotational–vibrational partition functions). The thermochemical properties (entropy, enthalpy, relative heat capacity, and relative Gibbs free energies) at a standard state of reactant 1-butoxyl, product 4-hydroxy-1-butyl, and their transition state as an ideal gas have been calculated using the total MS-T partition functions, and been compared to those obtained by Benson's group additivity method and G4 method that only considering a single structure. The MS-T conformational–rotational–vibrational partition functions have been used to obtain a multi-structural torsional factor $F^{\text{MS-T}}$ for the final rate constants calculations. The multidimensional zero-curvature tunneling (ZCT) and small-curvature tunneling (SCT) have been used for calculating transmission coefficients (κ). The single-structure harmonic (quasiharmonic) k^{CVT} rate constants were calculated on the potential

energy surface obtained by multi-configuration Shepard interpolation (MCSI) method using the lowest-energy structures for reactant, product and transition state. Based on $F^{\text{MS}-\text{T}}$, κ^{MT}, and k^{CVT} k^{CVT}, the final $k^{\text{MS}-\text{CVT/MT}}$ $\text{k}^{\text{MS-CVT/MT}}$ (MT can be ZCT or SCT) rate constants including both multi-structural torsional anharmonicity and multidimensional tunneling are obtained for both forward and reverse reactions.

The multi-structural torsional anharmonicty is found to be very important for the accurate rate constants, especially for reverse reaction because of more low-energy conformers located for product. The reaction rate constants using single-structural harmonic oscillator approximation are reduced by factors of 0.17 to 0.40 for the forward reaction and by factors of 0.017–0.066 for the reverse reaction. As a consequence there is also a very large effect on the equilibrium constant. A much larger effect is observed for multiple-structure anharmonicity than for torsional anharmonicity.

The tunneling effect and MS-T anharmonicity counteract each other at temperature 385 K and 264 K for the forward and reverse reaction respectively, and tunneling dominates the low temperatures while MS-T anharmonicity dominates higher temperatures.

The final $k^{\text{MS}-\text{CVT/SCT}}$ $\text{k}^{\text{MS-CVT/SCT}}$ rate constants considering both small-curve tunneling and MS-T anharmonicity are believed to be more accurate rate constants.

5. Acknowledgment

References

[1] (a) K. Y. Choo, S. W. Benson, Int J Chem Kinet 1981, 13, 833; (b) B. J. Finlayson-Pitts, J. N. Pitts Jr., *Chemistry of the Upper and Lower Atmosphere*, Academic Press, San Diego, 2000; (c) R. Atkinson, J. Arey, Chem. Rev. 2003, 103, 4605.

[2] R. Atkinson, Atmos. Environ. 2007, 41, 8468

[3] (a) P. Morabito, J. Heicklen, Bull. Chem. Soc. Jpn., 1987, 60, 2641; (b) A. Heiss, K. Sahetchian, Int. J. Chem. Kinet. 1996, 28, 531; (c) H. Hein, A. Hoffmann and R. Zellner, Phys. Chem. Chem. Phys. 1999, 1, 3743; (d) P. Cassanelli, D. Johnson, R. A. Cox, Phys. Chem. Chem. Phys. 2005, 7, 3702.

[4] (a) H. Somnitz, R. Zellner, Phys. Chem. Chem. Phys. 2000, 2, 1907; (b) R. Méreau, M.T. Rayez, F. Caralp, J.C. Rayez, Phys. Chem. Chem. Phys. 2000, 2, 1919; (c) L.Vereecken, J. Peeters, J. Chem. Phys. 2003, 119, 5159; (d) R. Méreau, M.-T. Rayez, F. Caralp, J.-C. Rayez, Phys. Chem. Chem. Phys. 2003, 5, 4828; (e) H. Somnitz, Phys. Chem. Chem. Phys. 2008, 10, 965; (f) J. Zheng, D. G. Truhlar, Phys. Chem. Chem. Phys. 2010, 12, 7782; (g) A. C. Davis, J. S. Francisco, J. Am. Chem. Soc. 2011, DOI: 10.1021/ja204806b

[5] (a) B. C. Garrett and D. G. Truhlar, J. Chem. Phys. 1979, 70, 1593; (b) D. G. Truhlar and B. C. Garrett, Acc. Chem. Res. 1980, 13, 440; (c) D. G. Truhlar, A. D. Isaacson, R. T. Skodje and B. C. Garrett, J. Phys. Chem. 1982, 86, 2252; (d) D. G. Truhlar and B. C. Garrett, Annu. Rev. Phys. Chem. 1984, 35, 159; (e) A. Fernandez-Ramos, B. A. Ellingson, B. C. Garrett and D. G. Truhlar, in *Reviews in Computational Chemistry*, eds. T. R. Cundari and K. B. Lipkowitz, Wiley-VCH, Hoboken, NJ, 2007, vol. 23, P. 125.

[6] (a) D.-h. Lu, T. N. Truong, V. S. Melissas, G. C. Lynch, Y.-P. Liu, B. C. Garrett, R. Steckler, A. D. Isaacson, S. N. Rai, G. C. Hancock, J. G. Lauderdale, T. Joseph and D. G. Truhlar, Comput. Phys. Commun. 1992, 71, 235; (b) Y.-P. Liu, G. C. Lynch, T. N. Truong, D.-h. Lu, D. G. Truhlar and B. C. Garrett, J. Am. Chem. Soc. 1993, 115, 2408.

[7] (a) R. T. Skodje, D. G. Truhlar and B. C. Garrett, J. Phys. Chem. 1981, 85, 624; (b) R. T. Skodje and D. G. Truhlar, J. Phys. Chem. 1981, 85, 3019.

[8] L. A. Curtiss, P. C. Redfern, and K. Raghavachari, J. Chem. Phys. 2007, 126, 084108.

[9] Z. Wigner, Z. Phys. Chem. B 1932, 19, 203.

[10] (a) J. Zheng, T. Yu, E. Papajak, I. M. Alecu, S. L. Mielke, and D. G. Truhlar, Phys. Chem. Chem. Phys. 2011, 13, 10885. (b) J. Zheng, T. Yu, and D. G. Truhlar, Phys. Chem. Chem. Phys. 2011, 13, 19318; (c) T. Yu, J. Zheng, and D. G. Truhlar, Phys. Chem. Chem. Phys. 2011, DOI:10.1039/C1CP22578B.

[11] (a) S. W. Benson, *Thermochemical Kinetics*, 2nd ed. (Wiley-Interscience, New York, 1976); (b) T. Ni, R. A. Caldwell, and L. A. Melton, J. Am. Chem. Soc., 1989, 111, 457; (c) N. Cohen, J. Phys. Chem. 1992, 96, 9052.

[12] (a) T. Yu, J. Zheng, and D. G. Truhlar, Chem. Sci. 2011, 2, 2199; (b) I. M. Alecu, and D. G. Truhlar, J. Phys. Chem. A. in press.

[13] Y. Zhao, and D. G. Truhlar, J. Chem. Theory Comput. 2008, 4, 1849.

[14] (a) R. Krishnan, J. S. Binkley, R. Seeger, J. A. Pople, J. Chem. Phys. 1980, 72, 650; (b) T. Clark, J. Chandrasekhar, G. W. Spitznagel, P. v. R. Schleyer, J. Comp. Chem. 1983, 4, 294; (c) M. J. Frisch, J. A. Pople, J. S. Binkley, J. Chem. Phys. 1984, 80, 3265; (d) L. A. Curtiss, K. Raghavachari, C. Redfern, V. Rassolov, J. A. Pople, J. Chem. Phys. 1998, 109, 7764; (e) P. L. Fast, M. L. Sanchez, D. G. Truhlar, Chem. Phys. Letter 1999, 306, 407; (f) B. J. Lynch, Y. Zhao, D. G. Truhlar, J. Phys. Chem. A. 2003, 107, 1384.

[15] J. Zheng, Y. Zhao, and D. G. Truhlar, J. Chem. Theory Comput. 2009, 5, 808.

[16] X. Xu, I. M. Alecu, and D. G. Truhlar, J. Chem. Theory Comput. 2011, 7, 1667.

[17] (a) K. Yang, Y. Zhao, and D. G. Truhlar, *MN-GFM: Minnesota Gaussian Functional Module*, version 5.0; University of Minnesota: Minneapolis, MN, 2011.

[18] I. M. Alecu, J. Zheng, Y. Zhao, and D. G. Truhlar, J. Chem. Thery Comput. 2010, 6, 2872.

[19] (a) B. C. Garrett, D. G. Truhlar, J. Phys. Chem. 1979, 83, 1052; B. C. Garrett, D. G. Truhlar, J. Phys. Chem. 1983, 87, 4553 (E); (b) B. C. Garrett, D. G. Truhlar, J. Phys. Chem. 1979, 83, 3058.

[20] (a) D. C. Chatfield, R. S. Friedman, D. G. Truhlar, B. C. Garrett, D. W. Schwenke, Faraday. Dis. Chem. Soc. 1991, 91, 289; (b) D. C. Chatfield, R. S. Friedman, D. G. Truhlar, B. C. Garrett, D. W. Schwenke, J. Am. Chem. Soc. 1991, 113, 486.

[21] (a) D. G. Truhlar and A. Kuppermann, J. Chem. Phys. 1970, 52, 3842; J. Amer. Chem. Soc. 1971, 93, 1840; (b) B. C. Garrett, D. G. Truhlar, R. S. Grev, and A. W. Magnuson, J. Phys. Chem. 1980, 84, 1730; 1983, 87, 4554(E); (c) D. G. Truhlar, A. D. Isaacson, B. C. Garrett, in The Theory of Chemical Reaction Dynamics, ed. M. Baer (CRC Press, Boca Raton, FL, 1985), Vol. 4, pp. 65.

[22] (a) K. S. Pitzer, W. D. Gwinn, J. Chem. Phys. 1942, 10, 428; (b) K. S. Pitzer, J. Chem. Phys. 1946, 14, 239; (c) D. G. Truhlar, J. Comput. Chem. 1991, 12, 266.

[23] (a) R. P. Feynman, A. R. Hibbs, Quantum Mechanics and Path Integrals, McGraw-Hill: New York, 1965;(b) R. Q. Topper, Adv. Chem. Phys. 1999, 105, 117; (c) S. L. Mielke, J. Srinivasan, D. G. Truhlar, J. Chem. Phys. 2000, 112, 8768; (d) S. L. Mielke, D. G. Truhlar, J. Chem. Phys. 2001, 114, 621; (e) J. A. Miller, Faraday Discuss. 2001, 119, 461; (f) S. L. Mielke, D. G. Truhlar, Chem. Phys. Lett. 2003, 378, 317; (g) V. A. Lynch, S. L. Mielke, D. G. Truhlar, J. Chem. Phys. 2004, 121, 5148; (h)V. A. Lynch, S. L. Mielke, D. G. Truhlar, J. Phys. Chem. A 2005, 109, 10092.

[24] A. D. Isaacson, D. G. Truhlar, J. Chem. Phys. 1981, 75, 4090.

[25] J. Zheng, S. L. Mielke, K. L. Clarkson, and D. G. Truhlar, Comput. Phys. Commun., submitted.

[26] (a) Y. Kim, J. C. Corchado, J. Villa, J. Xing, and D. G. Truhlar, J. Chem. Phys. 2000, 112, 2718; (b) T. V. Albu, J. C. Corchado, and D. G. Truhlar, J. Phys. Chem. A 2001, 105, 8465; (c) O. Tishchenko, and D. G. Truhlar, J. Chem. Theory Comput. 2007, 3, 938; (d) M. Higashi, and D. G. Truhlar, J. Chem. Theory Comput. 2008, 4, 790; (e) O. Tishchenko, and D. G. Truhlar, J. Chem. Theory Comput. 2009, 5, 1454; (f) O. Tishchenko, and D. G. Truhlar, J. Chem. Phys. 2009, 130, 024105.

[27] (a) O. Tishchenko, M. Higashi, T. V. Albu, J. C. Corchado, Y. Kim, J. Vill, J. Xing, H. Lin, and D. G. Truhlar, MCSI-version 2010-1 University of Minnesota, Minneapolis, MN, 2010. (b) J. W. Ponder, TINKER-version 3.5, Washington University, St. Louis, MO, 1997.

[28] (a) T. V. Albu, O. Tishchenko, J. C. Corchado, Y. Kim, J. Villà, J. Xing, H. Lin, M. Higashi, and D. G. Truhlar, MC-TINKERATE-version 2008, University of Minnesota, Minneapolis, MN, 2008;(b) J. C. Corchado, Y.-Y. Chuang, P. L. Fast, J. Villà, W.-P. Hu, Y.-P. Liu, G. C. Lynch, K. A. Nguyen, C. F. Jackels, V. S. Melissas, B. J. Lynch, I. Rossi, E. L. Coitiño, A. Fernandez-Ramos, J. Pu, T. V. Albu, R. Steckler, B. C. Garrett, A. D. Isaacson, and D. G. Truhlar, POLYRATE-version 9.1, University of Minnesota, Minneapolis, MN, 2002.

[29] J. Villà and D. G. Truhlar, Theor. Chem. Acc. 1997, 97, 317.

[30] (a) N. L. Allinger, Y. H. Yuh, J. H. Lii, J. Am. Chem. Soc., 1989, 111, 8551; (b) J. H. Lii, N. L. Allinger, J. Am. Chem. Soc. 1989, 111,8566; (c) J. H. Lii, N. L. Allinger, J. Am. Chem. Soc. 1989, 111, 8576; (d) N. L. Allinger, H. J. Geise, W. Pyckhout, L. A. Paquette, and J. C. Gallucci, J. Am. Chem. Soc. 1989, 111, 1106; (e) N. L. Allinger, F. Li, and L. Yan, J. Comput. Chem., 1990, 11, 848; (f) N. L. Allinger, F. Li, L. Yan, and J. C. Tai, J. Comput. Chem. 1990, 11, 868.

Table 1 Name convention and labeling of structures

Name convention	Abbreviation	Dihedral angle range (in deg)
trans	$\mathbf{T}$	180
trans±	$\mathbf{T}^{\pm}$	($\pm$150, $\pm$180)
anti±	$\mathbf{A}^{\pm}$	($\pm$105, $\pm$150)
	$\mathbf{a}^{\pm}$	($\pm$90, $\pm$105)
gauche±	$\mathbf{g}^{\pm}$	($\pm$75, $\pm$90)
	$\mathbf{G}^{\pm}$	($\pm$30, $\pm$75)
cis±	$\mathbf{C}^{\pm}$	($\pm$0, $\pm$30)
cis	$\mathbf{C}$	0

Table 2 Name of structures and their relative conformational energies (in kcal/mol).

Structures	Relative conformational M08-SO[c] energy	
	Zero-point-exclusive	Zero-point-inclusive
1-butoxyl[a]		
G⁻T⁺, G⁺T⁻	0.00	0.00
G⁻G⁻, G⁺G⁺	0.17	0.54
g⁻G⁺, g⁺G⁻	0.22	0.71
T⁻T⁻, T⁺T⁺	0.44	0.28
T⁻G⁻, T⁺G⁺	0.69	1.02
4-hydroxy-1-butyl[b]		
G⁻G⁺G⁻T⁺, G⁺G⁻G⁺T⁻	0.00	0.00
G⁻G⁺G⁺T⁻, G⁺G⁻G⁻T⁺	0.41	0.30
T⁺G⁻G⁻T⁺, T⁻G⁺G⁺T⁻	0.43	0.14
G⁻G⁻G⁻T⁺, G⁺G⁺G⁺T⁻	0.77	0.43
T⁺G⁻T⁺ T⁺, T⁻G⁺T⁻T⁻	0.79	0.37
T⁺G⁻T⁻T⁻, T⁻G⁺T⁺T⁺	0.81	0.32
G⁻G⁻T⁺T⁻, G⁺G⁺T⁻T⁺	0.92	0.45
G⁻G⁻T⁺T⁺, G⁺G⁺T⁻T⁻	0.92	0.46
T⁺T⁻G⁺T⁻, T⁻T⁺G⁻T⁺	0.98	0.58
G⁻T⁻G⁺T⁻, G⁺T⁺G⁻T⁺	1.09	0.72
G⁻T⁻G⁻T⁺, G⁺T⁺G⁺T⁻	1.13	0.73
G⁻G⁺T⁺T⁻, G⁺G⁻T⁻T⁺	1.17	0.75
G⁻G⁺T⁺T⁺, G⁺G⁻T⁻T⁻	1.20	0.72
G⁻T⁻T⁺T⁺, G⁺T⁺T⁻T⁻	1.32	0.83
T⁺T⁺T⁻T⁻, T⁻T⁻T⁺T⁺	1.35	0.69
G⁺T⁺T⁺T⁺, G⁻T⁻T⁻T⁻	1.35	0.80
G⁻G⁻g⁺G⁺, G⁺G⁺g⁻G⁻	1.61	1.19
TTTg⁺, TTTg⁻ [d]	1.71	1.31
T⁺G⁻g⁺T⁺, T⁻G⁺g⁻T⁻	1.92	1.57

[a]First torsion angle in the structure abbreviations for 1-butoxyl indicates O-C-C-C angle, while the second indicates the C-C-C-C angle

[b]First torsion angle in the structure abbreviation for 4-hydroxy-1-butyl indicates H-O-C-C angle, the second indicates the O-C-C-C angle, the third is the C-C-C-C torsion angle, and the forth is the C-C-C-H torsion.

[c]The basis set used for M08-SO is MG3S.

[d]The two mirror images are indistinguishable structures, and they will be accounted as one structure in calculations of partition functions.

Table 3 Calculated total partition functions with the multi-structural method, conformational–rotational–vibrational partition function of 1-butoxyl radical, and single-structure harmonic rotational–vibrational partition function of the lowest-energy structure of 1-butoxyl radical.[a]

T (K)	$Q^{\text{MS–LH}}$	$Q^{\text{MS–T}}$	$Q_{\text{con–rovib}}^{\text{MS–LH}}$	$Q_{\text{con–rovib}}^{\text{MS–T}}$	$Q_{\text{rovib,1}}^{\text{SS–HO}}$
200	1.12E-68	1.32E-68	6.12E-76	7.21E-76	1.45E-76
250	1.18E-51	1.46E-51	3.68E-59	4.55E-59	7.63E-60
298.15	1.67E-40	2.15E-40	3.36E-48	4.33E-48	6.35E-49
300	3.83E-40	4.94E-40	7.58E-48	9.78E-48	1.43E-48
400	2.07E-25	2.88E-25	2.00E-33	2.78E-33	3.32E-34
600	8.15E-10	1.23E-09	2.85E-18	4.30E-18	4.15E-19
800	3.15E-01	4.83E-01	5.36E-10	8.22E-10	7.30E-11
1000	1.65E+05	2.46E+05	1.60E-04	2.39E-04	2.09E-05
1500	1.77E+14	2.32E+14	6.09E+04	7.98E+04	7.55E+03
2000	1.01E+20	1.12E+20	1.63E+10	1.81E+10	1.97E+09
2400	3.07E+23	2.97E+23	3.03E+13	2.94E+13	3.61E+12

[a]Geometries, energies, and frequencies were calculated by the M08-SO/MG3S method. The zero of energy for the partition function calculations is the lowest-energy classical equilibrium structure energy (G^-T^+ which is the same as the G^+T^- energy).

Table 4 Calculated total partition functions with the multi-structural method, conformational–rotational–vibrational partition function of 4-hydroxy-1-butyl radical, and single structure harmonic rotational–vibrational partition function of the lowest-energy structure of 4-hydroxy-1-butyl radical.[a]

T (K)	$Q^{\text{MS–LH}}$	$Q^{\text{MS–T}}$	$Q_{\text{con–rovib}}^{\text{MS–LH}}$	$Q_{\text{con–rovib}}^{\text{MS–T}}$	$Q_{\text{rovib},1}^{\text{SS–HO}}$
200	1.02E-68	1.38E-68	5.64E-76	7.65E-76	2.51E-77
250	1.79E-51	2.44E-51	5.65E-59	7.71E-59	1.74E-60
298.15	3.64E-40	4.92E-40	7.41E-48	1.00E-47	1.74E-49
300	8.44E-40	1.14E-39	1.69E-47	2.29E-47	3.94E-49
400	7.73E-25	9.99E-25	7.55E-33	9.76E-33	1.20E-34
600	5.64E-09	6.39E-09	2.00E-17	2.27E-17	2.06E-19
800	3.11E+00	3.04E+00	5.37E-09	5.24E-09	4.37E-11
1000	2.03E+06	1.71E+06	2.00E-03	1.69E-03	1.41E-05
1500	2.89E+15	1.71E+15	1.04E+06	6.14E+05	5.99E+03
2000	1.84E+21	7.95E+20	3.21E+11	1.39E+11	1.67E+09
2400	5.77E+24	2.00E+24	6.39E+14	2.21E+14	3.17E+12

[a] Geometries, energies, and frequencies were calculated by the M08-SO/MG3S method. The zero of energy for the partition function calculations is the lowest-energy classical equilibrium structure energy ($G^-G^+G^-T^+$ which is the same as the $G^+G^-G^+T^-$ energy).

Table 5 Multi-structural torsional factors of 1-butoxyl and 4-hydroxy-1-butyl

T (K)	1-butoxyl			4-hydroxy-1-butyl		
	$F_{\text{MS-T}}^{\text{R}}$	$F_{\text{MS-LH}}^{\text{R}}$	F_{T}^{R}	$F_{\text{MS-T}}^{\text{P}}$	$F_{\text{MS-LH}}^{\text{P}}$	F_{T}^{P}
200	4.98	4.23	1.18	30.44	22.46	1.36
250	5.96	4.83	1.24	44.38	32.53	1.36
298.15	6.82	5.29	1.29	57.54	42.54	1.35
300	6.85	5.31	1.29	58.03	42.94	1.35
400	8.36	6.02	1.39	81.61	63.17	1.29
600	10.35	6.87	1.51	110.16	97.23	1.13
800	11.26	7.34	1.53	119.92	122.71	0.98
1000	11.46	7.65	1.50	119.46	141.90	0.84
1500	10.58	8.07	1.31	102.54	173.12	0.59
2000	9.19	8.29	1.11	82.97	191.52	0.43
2400	8.13	8.40	0.97	69.73	201.51	0.35

Table 6 Calculated total partition functions and conformational−rotational−vibrational partition function with multi-structural torsional method and multi-structural torsional factors of transition state.

T(K)	Q^{MS-T}	$Q^{MS-T}_{con-rovib,TS}$	F^{TS}_{MS-T}	F^{TS}_{MS-LH}	F^{TS}_{T}
200	1.47E-67	7.99E-75	2	2	1
250	3.91E-51	1.22E-58	2	2	1
298.15	2.16E-40	4.35E-48	2	2	1
300	4.80E-40	9.50E-48	2	2	1
400	7.08E-26	6.82E-34	2	2	1
600	6.75E-11	2.36E-19	2	2	1
800	1.22E-02	2.07E-11	2	2	1
1000	3.91E+03	3.82E-06	2	2	1
1500	2.04E+12	7.21E+02	2	2	1
2000	7.44E+17	1.28E+08	2	2	1
2400	1.73E+21	1.89E+11	2	2	1

a. Geometries, energies, and frequencies were calculated by the M08-SO/MG3S method.

Table 7 Standard state (1 bar) entropy (in cal mol^{-1} K^{-1}), heat capacity (in cal mol^{-1} K^{-1}), relative enthalpy (in kcal/mol), and relative Gibbs free energy (in kcal/mol) of ideal gas for 1-butoxyl radical.

T (K)	S_T°			$C_P^\circ(T)$			
	MS-LH	MS-T	GA^a	MS-LH	MS-T	GA^a	Ref.4g^b
200	76.12	76.84		19.85	20.57		17.6
250	80.81	81.69		22.41	23.14		
298.15	85.00	86.01	83.85	25.32	25.97		22.7
300	85.16	86.17	84.02	25.44	26.09	25.09	22.8
400	93.38	94.52	92.17	32.00	32.28	31.54	28.6
600	108.61	109.70	107.05	43.37	42.75	42.29	38.6
800	122.29	123.10	121.48	51.71	50.41	50.16	46.1
1000	134.53	134.99	132.67	57.94	56.18	55.85	51.8
1500	160.09	159.69	161.49	67.62	65.26		
2000	180.28	179.16		72.47	69.84		
2400	193.70	192.08		74.63	71.88		

T (K)	$H_T^\circ - H_0^\circ$			$G_T^\circ - H_0^\circ$	
	MS-LH	MS-T		MS-LH	MS-T
200	2.91	2.99		-12.32	-12.38
250	3.96	4.08		-16.24	-16.35
298.15	5.11	5.26		-20.23	-20.39
300	5.16	5.31		-20.39	-20.54
400	8.03	8.23		-29.32	-29.58
600	15.62	15.78		-49.55	-50.04
800	25.17	25.14		-72.66	-73.34
1000	36.17	35.82		-98.37	-99.17
1500	67.84	66.44		-172.29	-173.10
2000	103.00	100.34		-257.57	-257.97
2400	132.45	128.72		-332.43	-332.28

a. Using group values from Ref.11, and for entropy, adding 0.026 cal mol^{-1} K^{-1} to convert from a standard pressure of 1 atm to a standard pressure of 1 bar

b.   The data is obtained from Ref.4g, where single-structure method was used for G4 data set.

Table 8 Standard state (1 bar) entropy (in cal mol^{-1} K^{-1}), heat capacity (in cal mol^{-1} K^{-1}), relative enthalpy (in kcal/mol), and relative Gibbs free energy (in kcal/mol) of ideal gas for 4-hydroxy-1-butyl radical.

	S_T°			$C_P^\circ(T)$			
T (K)	MS-LH	MS-T	GA[a]	MS-LH	MS-T	GA[a]	Ref.4g[a]
200	80.76	81.53		21.93	21.34		20.6
250	85.92	86.52		24.445	23.63		
298.15	90.46	90.90	89.94	27.27	26.28		26.3
300	90.63	91.07	90.11	27.39	26.38	26.01	26.4
400	99.34	99.46	98.45	33.66	32.32	31.97	32.7
600	115.15	114.58	113.63	44.36	42.47	42.01	43.5
800	129.03	127.84	126.77	52.09	49.76	49.34	51.3
1000	141.30	139.54	138.83	57.81	55.15	54.77	57.1
1500	166.63	163.67	166.61	66.75	63.58		
2000	186.54	182.60		71.39	67.93		
2400	199.76	195.17		73.56	69.96		

	$H_T^\circ - H_0^\circ$			$G_T^\circ - H_0^\circ$	
T (K)	MS-LH	MS-T		MS-LH	MS-T
200	3.30	3.34		-12.85	-12.97
250	4.46	4.46		-17.02	-17.18
298.15	5.70	5.66		-21.27	-21.45
300	5.76	5.71		-21.45	-21.62
400	8.81	8.64		-30.95	-31.15
600	16.67	16.18		-52.44	-52.59
800	26.35	25.44		-76.89	-76.86
1000	37.37	35.95		-103.96	-103.61
1500	68.76	65.88		-181.23	-179.67
2000	103.41	98.87		-269.72	-266.39
2400	132.43	126.47		-347.05	-341.99

a. Using group values from Ref.11, and for entropy, adding 0.026 cal mol^{-1} K^{-1} to convert from a standard pressure of 1 atm to a standard pressure of 1 bar.

b. The data is obtained from Ref.4g, where single structure method was used for G4 data set.

Table 9 Standard state (1 bar) entropy (in cal mol^{-1} K^{-1}), heat capacity (in cal mol^{-1} K^{-1}), relative enthalpy (in kcal/mol), and relative Gibbs free energy (in kcal/mol) of ideal gas calculated by MS-T method for transition state

T (K)	S_T°	$C_P^\circ(T)^a$	$H_T^\circ - H_0^\circ$	$G_T^\circ - H_0^\circ$
200	68.09	15.57/15.2	2.15	-11.47
250	71.91	18.85	3.01	-14.97
298.15	75.52	22.36/21.8	4.00	-18.52
300	75.66	22.50/22.0	4.04	-18.66
400	83.16	29.96/29.3	6.67	-26.60
600	97.77	42.18/41.4	13.96	-44.71
800	111.13	50.62/49.9	23.29	-65.62
1000	123.11	56.64/56.0	34.04	-89.07
1500	148.00	65.61	64.88	-157.11
2000	167.55	70.06	98.92	-236.18
2400	180.52	72.09	127.38	-305.86

a. The values after slash are from Ref.4g, where single-structure method was used for G4 data set.

Table 10 The calculated multi-structural torsional factors for rate calculations of forward reaction and reverse reaction

T(K)	Forward reaction			Reverse reaction		
	F^{MS-T}	F^{MS-LH}	F^T	F^{MS-T}	F^{MS-LH}	F^T
200	0.402	0.473	0.849	0.066	0.089	0.738
250	0.336	0.415	0.809	0.045	0.061	0.733
298.15	0.293	0.378	0.776	0.035	0.047	0.739
300	0.292	0.377	0.774	0.034	0.047	0.740
400	0.239	0.332	0.720	0.025	0.032	0.774
600	0.193	0.291	0.663	0.018	0.021	0.883
800	0.178	0.272	0.652	0.017	0.016	1.023
1000	0.175	0.262	0.667	0.017	0.014	1.188
1500	0.189	0.248	0.763	0.020	0.012	1.688
2000	0.218	0.241	0.902	0.024	0.010	2.308
2400	0.246	0.238	1.033	0.029	0.010	2.890

Table 11 Standard state enthalpy of reaction and enthalpy of activation (kcal/mol)

T(K)	Enthalpy of reaction			Enthalpy of activation	
	Present	Ref.4g[a]	GA[b]	Present	Ref.4g[a]
Forward reaction					
0	-4.10	-3.4		10.72	10.4
298	-3.70	-3.0	-3.25	9.46	9.5
1000	-3.97	n.a.	-3.35	8.94	n.a.
2000	-5.58	n.a.		9.30	n.a.
Reverse reaction					
0	4.10	3.4		14.82	n.a
298	3.70	3.0	3.25	13.16	n.a.
1000	3.97	n.a.	3.35	12.91	n.a.
2000	5.58	n.a.		14.87	n.a.

a. Davis and Francisco's single structure G4 method.
b. Using group values from Ref.11

Table 12 The $k^{MS-CVT/SCT}$ $k^{MS\text{-}CVT/MT}$ rate constants(s^{-1})

T(K)	Forward reaction	Reverse reaction
298	5.66E+04[a]	9.17E+00
1000	7.35E+08	9.96E+06
2000	1.16E+10	4.95E+08

a. The experimental rate constant at 298 K is 1.76E+05 s^{-1} by Atkinson,[2] 2.0E+05 s^{-1} at 1 atm by Cassanelli et al.,[3d] and 1.1E+05 s^{-1} by Hein et al.[3c] after accounting for any pressure fall-off under their experimental conditions (they obtained rate constant of (3.5 ± 2)E+04 s^{-1} at 295±3 K and 50 mbar pressure).

Table 13 The parameters in the fits to $k^{\text{MS-CVT/MT}}$ rate constants, where MT is ZCT or SCT

	Forward reaction		Reverse reaction	
	$k^{\text{MS-CVT/ZCT}}$	$k^{\text{MS-CVT/SCT}}$	$k^{\text{MS-CVT/ZCT}}$	$k^{\text{MS-CVT/SCT}}$
A (s^{-1})	2.033E+09	1.514E+09	4.737E+07	2.672E+07
n	1.704	1.787	2.366	2.561
E (kcal/mol)	5.755	5.045	8.274	7.295
T_0 (K)	104.62	157.88	88.43	124.79
RMSR	0.009	0.012	0.009	0.007

Table 14 E_a (kcal/mol) calculated by MS-CVT/SCT method

T (K)	Forward reaction	Reverse reaction
200	4.45	8.04
250	5.69	9.45
298.15	6.53	10.30
300	6.56	10.32
400	7.59	11.28
600	8.56	12.25
800	9.18	13.02
1000	9.75	13.82
1500	11.24	15.98
2000	12.84	18.29
2400	14.16	20.21
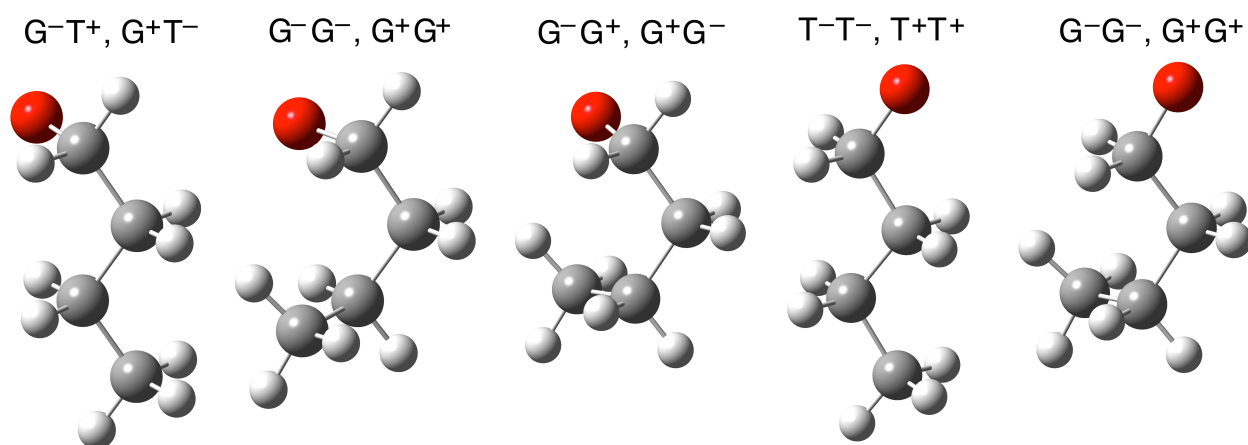
Fig. 1 All conformers of 1-butoxyl radical. Conformations are depicted here in the order of increasing zero-point-exclusive M08-SO/MG3S energy.
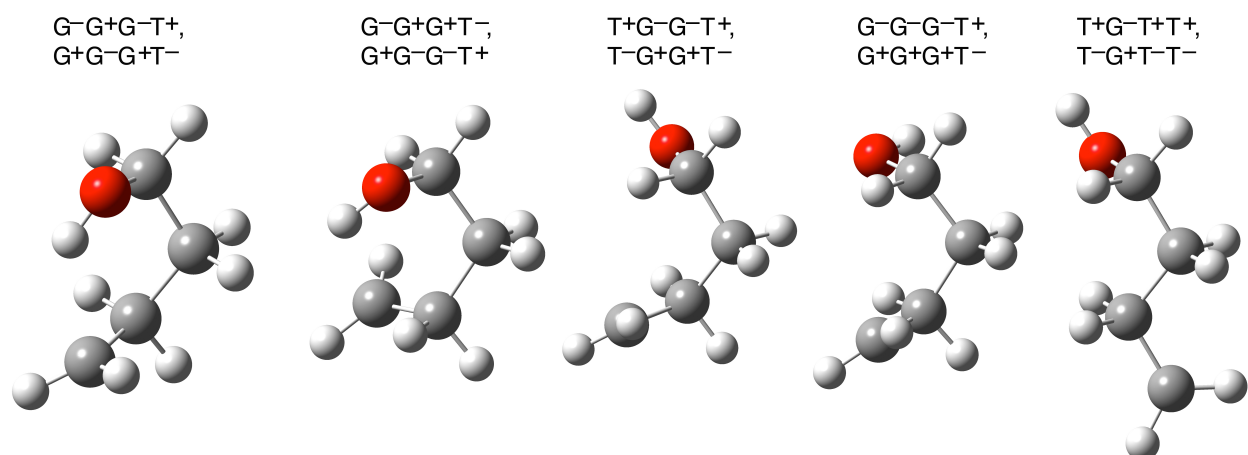
Fig. 2 Five lowest-energy conformations for the 4-hydroxy-1-butyl radical. Conformations are depicted here in the order of increasing zero-point exclusive M08-SO/MG3S energy.
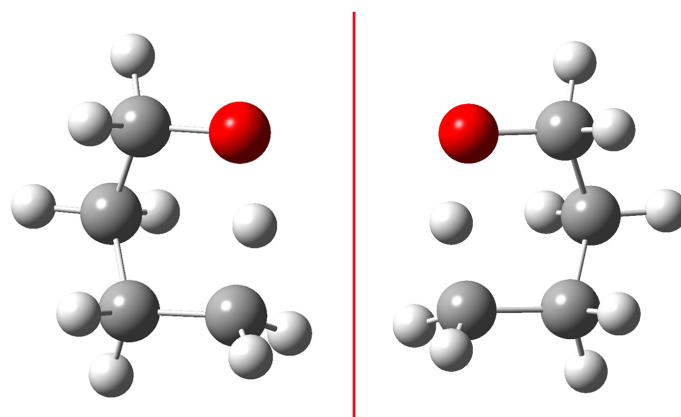
Fig. 3 Two distinguishable structures (TS1, TS2) of the transition state
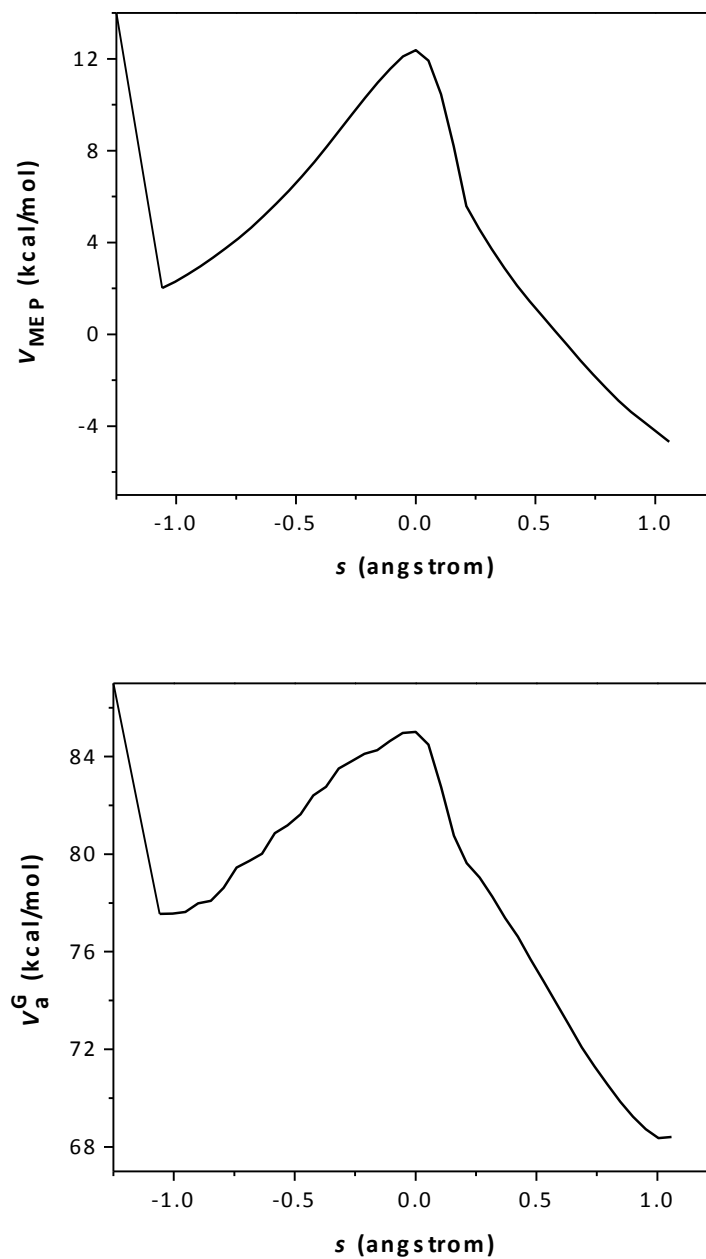
Fig. 4 Calculated potential energy along the minimum energy path (V_{MEP} V_{MEP}) and ground-state vibrationally adiabatic potential curve (V_a^G)V_a^G vs the reaction coordinate *s,* where the reaction coordinate is scaled to a reduced mass of 1 amu.
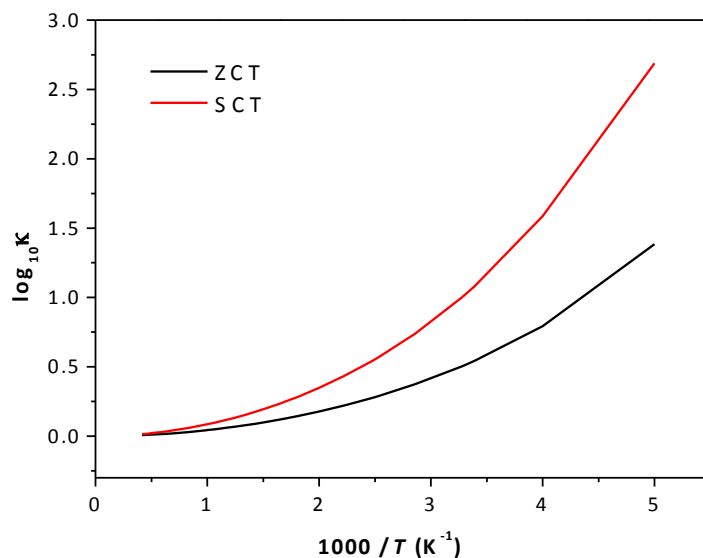
Fig. 5 Calculated common logarithm of the ZCT and SCT transmission coefficients κ vs reciprocal temperature (times a thousand)
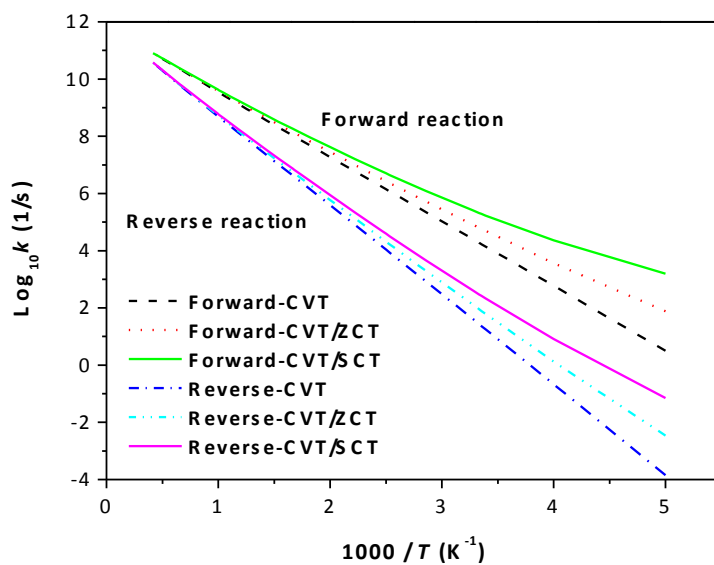
Fig. 6 The temperature dependence of k^{CVT} and $k^{CVT/MT}$ (MT can be ZCT or SCT) rate constants including tunneling for both forward and reverse reactions
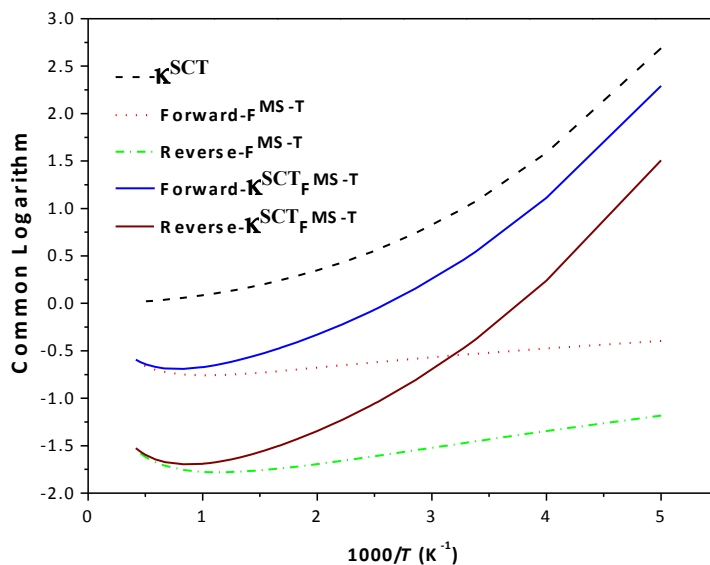
Fig. 7 Effect of κ^{SCT} and F^{MS-T} on final thermal rate constants of forward and reverse reactions as a function of temperature.
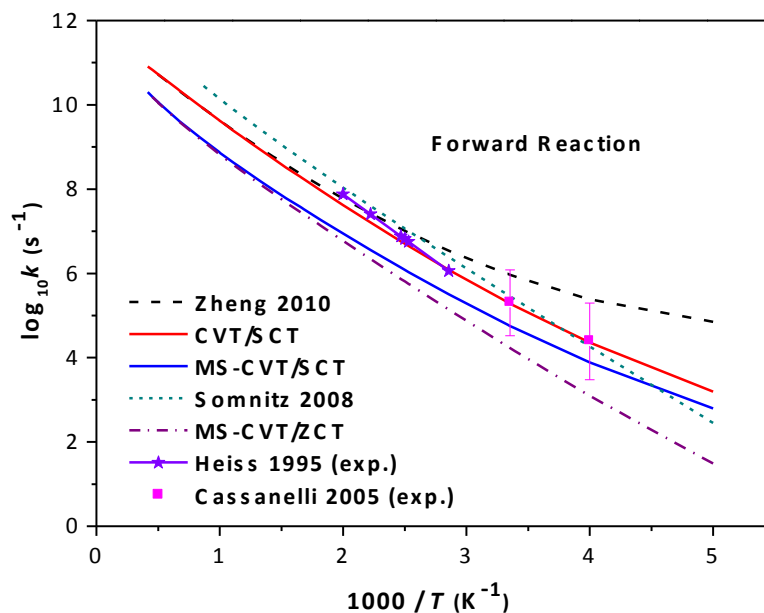
Fig. 8 The calculated $k^{CVT/SCT}$ and $k^{MS-CVT/MT}$ (MT can be ZCT or SCT) forward rate constants compared previous theoretical[4e,4f] and experimental[3b,3d] results.
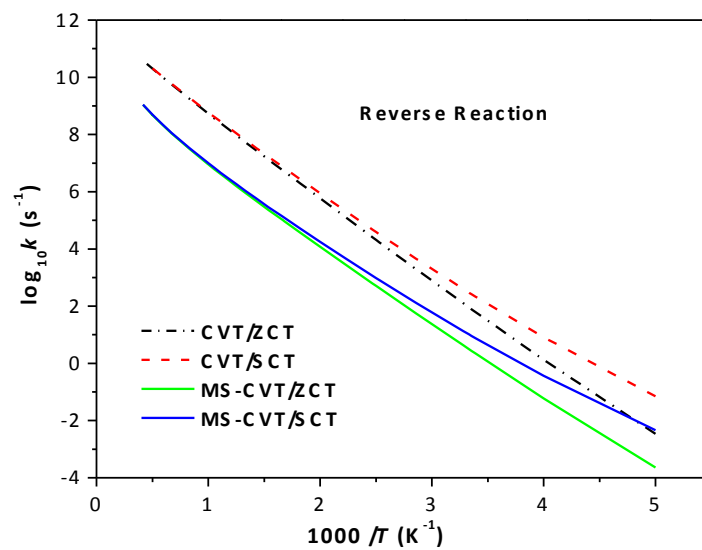
Fig. 9 The calculated $k^{\text{MS--CVT/MT}}$ (MT can be ZCT or SCT) reverse rate constants compared to corresponding $k^{\text{CVT/MT}}$ rate constant

Bibliography

M. J. Frisch, G. W. Trucks, H. B. Schlegel, G. E. Scuseria, M. A. Robb, J. R. Cheeseman, G. Scalmani, V. Barone, B. Mennucci, G. A. Petersson, H. Nakatsuji, M. Caricato, X. Li, H. P. Hratchian, A. F. Izmaylov, J. Bloino, G. Zheng, J. L. Sonnenberg, M. Hada, M. Ehara, K. Toyota, R. Fukuda, J. Hasegawa, M. Ishida, T. Nakajima, Y. Honda, O. Kitao, H. Nakai, T. Vreven, Jr., J. A. Montgomery, J. E. Peralta, F. Ogliaro, M. Bearpark, J. J. Heyd, E. Brothers, K. N. Kudin, V. N. Staroverov, R. Kobayashi, J. Normand, K. Raghavachari, A. Rendell, J. C. Burant, S. S. Iyengar, J. Tomasi, M. Cossi, N. Rega, N. J. Millam, M. Klene, J. E. Knox, J. B. Cross, V. Bakken, C. Adamo, J. Jaramillo, R. Gomperts, R. E. Stratmann, O. Yazyev, A. J. Austin, R. Cammi, C. Pomelli, J. W. Ochterski, R. L. Martin, K. Morokuma, V. G. Zakrzewski, G. A. Voth, P. Salvador, J. J. Dannenberg, S. Dapprich, A. D. Daniels, Ö. Farkas, J. B. Foresman, J. V. Ortiz, J. Cioslowski, and D. J. Fox, *Gaussian 09*, Revision A.02, Gaussian, Inc., Wallingford CT, 2009

H. Werner, P. J. Knowles, M. Scheutz, R. Lindh, P. Celani, T. Korona, G. Rauhut, F. R. Manby, R. D. Amos, A. Bernhardsson, A. Berning, D. L. Cooper, M. J. O. Deegan, A. J. Dobbyn, F. H. C. Ecker, A. Hertzer, W. Lloyd, S. J. McNicholas, W. Meyer, M. E. Mura, A. Nicklass, P. Palmieri, R. Pitzer, U. Schumann, H. Stoll, A. J. Stone, R. Torroni, T. Thorsteinsson, 1997, *MOLPRO 2006.1*; University College Consultants Ltd.: Cardiff, Wales, UK, 2006

H.-J. Werner, P. J. Knowles, F. R. Manby, M. Schütz, P. Celani, G. Knizia, T. Korona, R. Lindh, A. Mitrushenkov, G. Rauhut, T. B. Adler, R. D. Amos, A. Bernhardsson, A. Berning, D. L. Cooper, M. J. O. Deegan, A. J. Dobbyn, F. Eckert, E. Goll, C. Hampel, A. Hesselmann, G. Hetzer, T. Hrenar, G. Jansen, C. Köppl, Y. Liu, A. W. Lloyd, R. A. Mata, A. J. May, S. J. McNicholas, W. Meyer, M. E. Mura, A. Nicklaß, P. Palmieri, K. Pflüger, R. Pitzer, M. Reiher, T. Shiozaki, H. Stoll, A. J. Stone, R. Tarroni, T. Thorsteinsson, M. Wang, and A. Wolf, *Molpro* computer program, version 2010.1, University of Birmingham, Birmingham, 2010

Zhao, Y.; Truhlar, D. G. *MN-GFM: Minnesota Gaussian Functional Module–version 3.0*; University of Minnesota: Minneapolis, MN, 2007

Z. Zhao, R. Peverati, K. Yang, and D. G. Truhlar, *MN-GFM* version 5.2 computer program module, University of Minnesota, Minneapolis, 2011

J. Zheng, S. L. Mielke, K. L. Clarkson, and D. G. Truhlar, *MSTor* computer program, version 2011–2, University of Minnesota, Minneapolis, 2011

O. Tishchenko, M. Higashi, T. V. Albu, J. C. Corchado, Y. Kim, J. Villà, J. Xing, H. Lin, D. G. Truhlar, MCSI, version 2010, University of Minnesota, Minneapolis, 2010

T. V. Albu, O. Tishchenko, J. C. Corchado, Y. Kim, J. Villà, J. Xing, H. Lin, M. Higashi, D. G. Truhlar, MC-TINKERATE, version 2010, University of Minnesota, Minneapolis, 2010

J. Zheng, S. Zhang, B. J. Lynch, J. C. Corchado, Y. –Y. Chuang, P. L. Fast, W. –P. Hu, Y. –P. Liu, G. C. Lynch, K. A. Nguyen, et al. POLYRATE-version 2010-A, University of Minnesota, Minneapolis, 2010

E. Papajak, H.R. Leverentz, J. Zheng, and D.G. Truhlar, J. Chem. Theory Comput. 5, 1197 (2009). E. Papajak, H.R. Leverentz, J. Zheng, and D.G. Truhlar, J. Chem. Theory Comput. 5, 3330 (2009).

E. Papajak and D.G. Truhlar, J. Chem. Theory Comput. 6, 597 (2010)

E. Papajak and D.G. Truhlar, J. Chem. Theory Comput. 7, 10 (2011)

E. Papajak, J. Zheng, X. Xu, H.R. Leverentz, and D.G. Truhlar, J. Chem. Theory Comput. 7, 3027 (2011)

E. Papajak and D.G. Truhlar, accepted for publication in J. Chem. Phys. on July 10, 2012.

J. Zheng, T. Yu, E. Papajak, I.M. Alecu, S.L. Mielke, and D.G. Truhlar, Phys. Chem. Chem. Phys. 13, 10885 (2011).

P. Seal, E. Papajak, T. Yu, and D.G. Truhlar, J. Chem. Phys. 136, 034306 (2012).

E. Papajak, P. Seal, and D.G. Truhlar, accepted for publication in J. Chem. Phys. July 26, 2012

P. Seal, E. Papajak, and D.G. Truhlar, J. Phys. Chem. Lett. 3, 264 (2012)

X. Xu, E. Papajak, J. Zheng, and D.G. Truhlar, Phys. Chem. Chem. Phys. 14, 4204 (2012)

E. R. Davidson and D. Feller, Chem. Rev. 86, 681 (1986)

T. H. Dunning, J. Chem. Phys. 90, 1007 (1989)

R. A. Kendall, T. H. Dunning, and R. J. Harrision, J. Chem. Phys. 96, 6796 (1992)

D. E. Woon, and T. H. Dunning, J. Chem. Phys. 98, 1358 (1993)

D. E. Woon, and T. H. Dunning, J. Chem. Phys. 100, 2975 (1994)

T. H. Dunning Jr., K. A. Peterson, and A. K. Wilson, J. Chem. Phys. 114, 9244 (2001)

T. Clark, J. Chandresekhar, and P. v. R. Schleyer, J. Comput. Chem. 4, 294 (1983)

M. J. Frisch, J. A. Pople, and J. S. Binkley, J. Chem. Phys. 80, 3265 (1984)

S. F. Boys, and F. Bernardi, Mol. Phys. 19, 553 (1970)

D. W. Schwenke and D. G. Truhlar, J. Chem. Phys. 82, 2418 (1985)

S. Simon, M. Duran, and J. J. Dannenberg, J. Chem. Phys. 105, 11024 (1996) Errata: 86, 3760 (1987)

P. Valiron and I. Mayer, Chem. Phys. Lett. 275, 46 (1997)

B. J. Lynch, Y. Zhao, and D. G. Truhlar, J. Phys. Chem. A 107, 1384 (2003)

B. J. Lynch and D. G. Truhlar, J. Phys. Chem. A 107, 3898 (2003)

B. J. Lynch and D. G. Truhlar, J. Phys. Chem. A 107, 8996 (2004) Erratum: J. Phys. Chem. A 108, 1460 (2004)

J. Zheng, Y. Zhao, and D. G. Truhlar, J. Chem. Theory Comput. 3, 569 (2007)

B. J. Lynch, Y. Zhao, and D. G. Truhlar, J. Phys. Chem. A 109, 1643 (2005)

Y. Zhao and D. G. Truhlar, J. Phys. Chem. A 109, 5656 (2005)

Y. Zhao, N. E. Schultz, and D. G. Truhlar, J. Chem. Theory Comput. 2, 364 (2006)

Y. Zhao and D. G. Truhlar, Theor. Chem. Acc. 120, 215 (2008)

W. Kohn, A. D. Becke, and R. G. Parr, J. Phys. Chem. 100, 12974 (1996)

K. Raghavachari and J. B. Anderson, J. Phys. Chem. 100, 12960 (1996)

P. J. Stephens, F. J. Devlin, C. F. Chabalowski, and M. J. Frisch, J. Phys. Chem. 98, 11623 (1994)

Y. Zhao and D. G. Truhlar, J. Chem. Phys. 125, 194101 (2006)

Y. Zhao and D. G. Truhlar, J. Phys. Chem. A 110, 13126 (2006)

C. C. Roothaan, J. Rev. Mod. Phys. 23, 69 (1951)

C. Møller and M. S. Plesset, Phys. Rev. 46, 618 (1934)

G. D. Purvis and R. J. Bartlett, J. Chem. Phys. 76, 1910 (1982)

K. Raghavachari, G. W. Trucks, J. A. Pople, and M. Head-Gordon, Chem. Phys. Lett. 157, 479 (1989)

R. D. Bardo and K. Ruedenberg, J. Chem. Phys. 59, 5956 (1973)

A. K. Wilson, T. van Mourik, and T. H. Dunning Jr., Theochem. 388, 339 (1997)

M. O. Sinnokrot and C. D. Sherill, J. Phys. Chem. A 107, 8377 (2003)

R. Hwang, S. B. Muh, and J. S. Lee, Mol. Phys. 101, 1429 (2003)

A. M. Elsohly and G. S. Tschumpter, Int. J. Quantum Chem. 109, 91 (2009)

A. Halkier, H. Koch, P. Jorgensen, O. Christiansen, I. M. B. Nielsen, and T. Helgaker, Theor. Chem. Acc. 97, 150 (1997)

B. P. Prascher, B. R. Wilson, and A. K. Wilson, J. Chem. Phys. 127, 124110 (2007)

B. Mintz, S. Friskell, A. Shah, and A. K. Wilson, Int. J. Quantum Chem. 107, 3077 (2007)

J. C. Rienstra-Kiracofe, G. S. Tsuchumper, H. F. Schaefer III, S. Nanadi, and G. B. Ellison, Chem. Rev. 102, 1231 (2002)

F. Jensen, J. Chem. Phys. 117, 9234 (2002)

T. Clark, J. Chandrasekhar, G. W. Spitznagel, and P. v. R. Schleyer, J. Comp. Chem. 4, 294 (1983)

R. A. Kendall, T. H. Jr. Dunning, and R. J. Harrison, J. Chem. Phys. 96, 6796 (1992)

E. Papajak, H. R. Leverentz, J. Zheng, and D. G. Truhlar, J. Chem. Theory Comput. 5, 1197 (2009) Erratum and addendum: E. Papajak, H. R. Leverentz, J. Zheng, and D. G. Truhlar, J. Chem. Theory Comput. 5, 3330 (2009)

C. Lee, W. Yang, and R. G. Parr, Phys Rev. B 37, 785 (1988)

A. D. Becke, Phys. Rev. A 38, 3098 (1988)

A. D. Becke, J. Chem. Phys. 98, 5848 (1993)

P. J. Stephens, F. J. Devlin, C. F. Chabalowski, and M. J. Frisch, J. Phys. Chem. 98, 11623 (1994)

Y. Zhao and D. G. Truhlar, Theor. Chem. Acc. 120, 215 (2008), Y. Zhao and D. G. Truhlar, Acc. Chem. Res. 41, 157 (2008)

C. Møller and M. S. Plesset, Phys. Rev. 46, 618 (1934)

B. J. Lynch, Y. Zhao, and D. G. Truhlar, J. Phys. Chem. A 107, 1384 (2003)

B. J. Lynch, and D. G. Truhlar, J. Phys. Chem. A 107, 3898 (2003)

J. A. Pople, M. Head-Gordon, and K. Raghavachari, J. Chem. Phys. 87, 5968 (1987)

J. Zheng, Y. Zhao, and D. G. Truhlar, J. Chem. Theory Comput. 3, 569 (2007)

J. Zheng, Y. Zhao, and D. G. Truhlar, J. Chem. Theory Comput. 5, 808 (2009)

Y. Zhao and D. G. Truhlar, J. Chem. Theory Comput. 1, 415 (2005)

B. J. Lynch, Y. Zhao, and D. G. Truhlar, J. Phys. Chem. A 107, 1384 (2003)

B. J. Lynch and D. G. Truhlar, J. Phys. Chem. A 107, 3898 (2003)

B. J. Lynch and D. G. Truhlar, J. Phys. Chem. A 107, 8996 (2004) Erratum: J. Phys. Chem. A 108, 1460 (2004)

B. J. Lynch, Y. Zhao, and D. G. Truhlar, J. Phys. Chem. A 109, 1643 (2005)

A. A. Jarecki and E. R. Davidson, Chem.Phys. Lett. 300, 44 (1999)

J. M. Galbraith and H. F. Schaefer III, J. Chem. Phys. 105, 862 (1996)

L. Horny, N. D. K. Petraco, and H. F. Schaefer III, J. Am. Chem. Soc. 124, 14716 (2002)

B. J. Lynch, Y. Zhao, and D. G. Truhlar, ACS Symp. Ser. 958, 153 (2007)

F. Jensen, J. Chem. Phys. 116, 7372. F. Jensen, J. Chem. Phys. 117, 9234 (2002)

B. P. Prascher and A. K. Wilson, Mol. Phys. 105, 2899 (2007)

A. C. Schneider and J. W. Andzelm, J. Comp. Chem. 18, 775 (1997)

M. D. Halls and H. B. Schlegela, J. Chem. Phys. 109, 10587 (1998)

J. Florian and B. G. Johnson, J. Phys. Chem. 99, 5899 (1995)

C. W. Bauschlicher and H. Partridge Jr., Chem.Phys. Lett 240, 533 (1995)

W. J. Hehre, R. F. Stewart, and J. A. Pople, J. Chem. Phys. 51, 2657 (1969)

E. R. Davidson and D. Feller, Chem. Rev. 86, 681 (1986)

T. Clark, J. Chandresekhar, and P. v. R. Schleyer, J. Comput. Chem. 4, 294 (1983)

M. J. Frisch, J. A. Pople, and J. S. Binkley, J. S. J. Chem. Phys. 80, 3265 (1984)

D. E. Woon and T. H. Dunning Jr., J. Chem. Phys. 100, 2975 (1994)

D. E. Woon and T. H. Dunning Jr., J. Chem. Phys. 98, 1358 (1993)

J. Koput and K. A. Peterson, J. Phys. Chem. A, 106, 9595 (2002)

N. B. Balabanov and K. A. Peterson, J. Chem. Phys., 123, 064107 (2005)

A. K. Wilson, D. E. Woon, K. A. Peterson, and T. H. Dunning Jr., J. Chem. Phys. 110, 7667 (1999)

T. H. Dunning Jr., K. A. Peterson, and A. K. Wilson, J. Chem. Phys. 114, 9244 (2001)

T. H. Dunning Jr., J. Chem. Phys. 90, 1007 (1989)

R. A. Kendall, T. H. Dunning Jr., and R. J. Harrison, J. Chem. Phys. 96, 6796 (1992)

F. Jensen, J. Chem. Phys. 117, 9234 (2002)

J. E. Del Bene and I. Shavitt, J. Mol. Struct. Theochem 307, 27 (1994)

B. J. Lynch and D. G. Truhlar, In *Electron Correlation Methodology*; A. K. Wilson, K. A. Peterson, Eds.; ACS Symposium Series 958; American Chemical Society: Washington, DC, 2007.

E. Papajak, H. R. Leverentz, J. Zheng, and D. G. Truhlar, J. Chem. Theory Comput. 5, 1197 (2009); erratum: E. Papajak, H. R. Leverentz, J. Zheng, and D. G. Truhlar, J. Chem. Theory Comput. 5, 3330 (2009)

E. Papajak and D. G. Truhlar, J. Chem. Theor. Comput. 6, 597 (2010)

C. Møller and M. S. Plesset, Phys. Rev. 46, 618 (1934)

G. A. Petersson and M. Braunstein, J. Chem. Phys 83, 5129 (1985)

A. L. L. East and W. D. Allen, J. Chem. Phys. 99, 4638 (1993)

P. Hobza and J. Sponer, J. Am. Chem. Soc. 124, 11802 (2002)

P. Jurecka, J. Sponer, J. Cerny, and P. Hobza, Phys. Chem. Chem. Phys., 8, 1985 (2006)

M. S. Schuurmann, S. R. Muir, W. D. Allen, and H. F. Schaefer, J. Chem. Phys. 120, 11586 (2004)

I. Soteras, M. Orozco, and F. J. Luque, J. Comput. Aided Mol. Des 24, 281 (2010)

N. J. DeYonker, T. R. Cundari, and A. K. Wilson, J. Chem. Phys. 124, 114104 (2006)

Y. Zhao; D. G. Truhlar, and J. Phys. Chem. A 110, 10478 (2006)

K. Raghavachari, G. W. Trucks, J. A. Pople, and M. Head-Gordon, Chem. Phys. Lett. 157, 479 (1989)

P. L. Fast, J. C. Corchado, M. L. Sanchez, and D. G. Truhlar, J. Phys. Chem. A 103, 5129 (1999)

K. A. Peterson and T. H. Dunning, J. Phys. Chem. 99, 3898 (1995)

D. Schwenke, J. Chem. Phys. 122, 014107 (2005)

W. Kutzelnigg, Theor Chim Acta 68, 445 (1985)

W. Kutzelnigg and W. Klopper, J. Chem. Phys. 94, 1985 (1991)

W. Klopper and W. Kutzelnigg, W. Chem. Phys. Lett. 134, 17 (1987)

W. Klopper and C. C. M. Samson, J. Chem. Phys. 116, 6397 (2002)

F. R. Manby, J. Chem. Phys. 119, 4607 (2003)

S. Ten-no and F. R. Manby, J. Chem. Phys. 119, 5358 (2003)

S. Ten-no, J. Chem. Phys. 121, 117 (2004)

E. F. Valeev, Chem. Phys. Lett. 395, 190 (2004)

E. F. Valeev and C. L. Jansen, Chem. Phys. Lett. 121, 1214 (2004)

S. Ten-no, Chem. Phys. Lett. 121, 117 (2004)

H. -J. Werner, T. B. Adler, and F. R. Manby, J. Chem. Phys. 126, 164102 (2007)

T. D. Crawford, C. D. Sherrill, E. F. Valeev, J. T. Fermann, R. A. King, M. L. Leininger, S. T. Brown, C. L. Janssen, E. T. Seidl, J. P. Kenny, and W. D. Allen, J. Comp. Chem. 28, 1610 (2007)

G. Knizia and H. -J. Werner, J. Chem. Phys. 128, 154103 (2008)

O. Marchetti and H. -J. Werner, J. Phys. Chem. A 113, 11580 (2009)

F. A. Bischoff, S. Wolfsegger, D. P. Tew, and W. Klopper, Mol. Phys. 107, 963 (2009)

H. -J. Werner, G. Knizia, T. B. Adler, and O. Marchetti, Z. Phys. Chem. 224, 493 (2010)

J. R. Lane, and H. G Kjaergaard, J. Chem. Phys. 131, 034307 (2009)

K. A. Peterson, T. B. Adler, and H. -J. Werner, J. Chem Phys. 128, 084102 (2008)

J. Zheng, Y. Zhao, and D. G. Truhlar, J. Chem. Theory Comput. 3, 569 (2007)

J. Zheng, Y. Zhao, and D. G. Truhlar, J. Chem. Theory Comput. 5, 808 (2009)

Y. Zhao and D. G. Truhlar, J. Chem. Theory Comput. 1, 415 (2005)

B. J. Lynch, Y. Zhao, and D. G. Truhlar, J. Phys. Chem. A 107, 1384 (2003)

B. J. Lynch and D. G. Truhlar, J. Phys. Chem. A 107, 3898 (2003)

B. J. Lynch and D. G. Truhlar, J. Phys. Chem. A 107, 8996 (2004)

F. Weigend, Phys. Chem. Chem. Phys. 4, 4285 (2002)

C. Hättig, Phys. Chem. Chem. Phys. 7, 59 (2005)

F. Weigend, A. Kohn and C. Hattig, J. Chem. Phys. 116, 3175 (2002)

S. F. Boys and F. Bernardi, Mol. Phys. 19, 553 (1970)

J. R. Alvarez-Idaboy and A. Galano, Theor. Chem. Acc. 126, 75 (2010)

B. Skwara, W. Bartkowiak, and D. L. Da Silva, Theor. Chem. Acc. 122, 127 (2009)

R. A. King, W. D. Allen, B. Ma, and H. F. Schaefer III, Faraday Discuss. 110, 23 (1998)

B. Mintz, K. P. Lennox, and A. K. Wilson, J. Chem. Phys. 121, 5629 (2004)

R. Jurgens-Lutovsky and J. Almlof, J. Chem. Phys. Lett. 178, 431 (1991)

K. Wolinski and P. Pulay, J. Chem. Phys. 118, 9497 (2003)

T. Clark, J. Chandresekhar, G. W. Spitznagel, R. v. R. Schleyer, J. Comp. Chem. 4, 264 (1983)

E. R. Davidson and D. Feller, Chem. Rev. 86, 681 (1986)

E. Papajak, E.; H. R. Leverentz, J. Zheng, and D. G. Truhlar, J. Chem. Theory Comput. 5, 1197 (2009); 5, 3330 (2009)

E. Papajak and D. G. Truhlar, J. Chem. Theory Comput. 6, 597 (2010)

J. Zheng, X. Xu, and D. G. Truhlar, Theor. Chem. Acc. 128, 295 (2011)

E. Papajak and D. G. Truhlar, J. Chem. Theory Comput. 7, 10 (2011)

P. J. Stephens, F. J. Devlin, J. R. Cheeseman, and M. J. Frisch, J. Phys. Chem. A 105, 5356 (2001)

A. Baranowska, K. Z. Laczkowski, and A. J. Sadlej, J. Comput. Chem. 31, 1176 (2010)

J. R. Cheeseman, M. J. Frisch, F. J. Devlin, and P. J. Stephens, J. Phys. Chem. A 104, 1039 (2000)

R. A. Kendall, T. H. Dunning Jr., and R. J. Harrison, J. Chem. Phys. 96, 6769 (1992)

M. J. Frisch, J. A. Pople, and J. S. Binkley, J. Chem. Phys. 80, 3265 (1984)

P. L. Fast, M. L. Sanchez, and D. G. Truhlar, Chem. Phys. Lett. 306, 407 (1999)

L. A. Curtiss, K. Raghavachari, C. Redfern, V. Rassolov, and J. A. Pople, J. Chem. Phys. 109, 7764 (1998)

F. Weigend and R. Ahlrichs, Phys. Chem. Chem. Phys. 7, 3297 (2005)

J. Zheng and D. G. Truhlar, J. Phys. Chem. A 113, 11919 (2009)

J. Zheng and D. G. Truhlar, Phys. Chem. Chem. Phys. 12, 7782 (2010)

K. Yang, J. Zheng, Y. Zhao, and D. G. Truhlar, J. Chem. Phys. 132, 164117 (2010)

M. M. Meyer and S. R. Kass, J. Org. Chem. 75, 4274 (2010)

L. Hermosilla, S. Catak, V. Van Speybroeck, M. Waroquier, J. Vandenbergh, F. Motmans, P. Adriaensens, L. Lutsen, T. Cleij, and D. Vanderzande, Macromolecules 43, 7424 (2010)

B. J. Lynch, Y. Zhao, and D. G. Truhlar, J. Phys. Chem. A 107, 1384 (2003)

G. A. Petersson and M. Braunstein, J. Chem. Phys. 83, 5129 (1985)

A. L. L. East and W. D. Allen J. Chem. Phys. 99, 4638 (1993)

M. B. Sullivan, M. A. Iron, P. C. Redfern, J. M. L. Martin, L. A. Curtiss, and L. Radom, J. Phys. Chem. A 107, 5617 (2003)

S. Ten-no, Chem. Phys. Lett. 398, 56 (2004)

H. -J. Werner, T. B. Adler, and F. R. Manby, J. Chem. Phys. 126, 164102 (2007)

H. -J. Werner and W. Meyer, Mol. Phys. 31, 855 (1976)

H. -J. Werner and W. Meyer, Phys. Rev. A 13, 13 (1976)

M. A. Morrison and P. J. Hay, J. Phys. B 10, 647 (1977)

R. A. Eades, D. G. Truhlar, and D. A. Dixon, Phys. Rev. A 20, 867 (1979)

C. H. Douglass, Jr. D. A. Weil, R. A. Eades, D. G. Truhlar, D. A. Dixon, In *Chemical applications of Atomic and Molecular Electrostatic Potentials*; P. Politzer, D. G. Truhlar, Eds.; Plenum: New York, 1981; p. 173.

C. L. Darling and H. B. Schlegel, J. Phys. Chem. 98, 5855 (1994)

K. A. Peterson and T. H. Dunning Jr. J. Mol. Struct. Theochem 400, 93 (1997)

A. M. Cybulski, J. Chem. Phys. 111, 10520 (1999)

L. N. Oliveira, O. A. V. Amaral, M. A. Castro, and T. L. Fonseca, Chem. Phys. 289, 221 (2003)

P. M. Arruda, A. C. Neto, and F. E. Jorge, Int. J. Quantum Chem 109, 1189 (2009)

G. G. Camiletti, A. Canal Neto, F. E. Jorge, and S. F. Machado, J. Mol. Struct. Theochem 910, 122 (2009)

K. Raghavachari, G. W. Trucks, J. A. Pople, and M. Head-Gordon, Chem. Phys. Lett. 157, 479 (1989)

Z. Benkova, A. J. Sadlej, R. E. Oakes, and S. E. Bell, J. Comput. Chem. 26, 145 (2005).

A. Baranowska and A. J. Sadlej, J. Comput. Chem. 31, 552 (2010).

M. D. Halls and H. B. Schlegel, J. Chem. Phys. 111, 8819 (1999).

G. Zuber and W. Hug, J. Phys. Chem. 108, 2108 (2004).

K. Raghavachari, G. W. Trucks, J. A. Pople, and M. Head-Gordon, Chem. Phys. Lett. 157, 479 (1989)

W. Kutzelnigg, Theor Chim Acta 68, 445 (1985)

W. Klopper and W. Kutzelnigg, Chem. Phys. Lett. 134, 17 (1987)

W. Kutzelnigg and W. Klopper, J. Chem. Phys. 1991, 94, (1985)

W. Klopper and C. C. M. Samson, J. Chem. Phys. 116, 6397 (2002)

F. R. Manby, J. Chem. Phys. 119, 4607 (2003)

S. Ten-no and F. R. Manby, J. Chem. Phys. 119, 5358 (2003)

S. Ten-no, Chem. Phys. Lett. 398, 56 (2004)

W. Klopper J. Chem. Phys. 120, 10890 (2004)

S. Ten-no, J. Chem. Phys. 121, 117 (2004)

A. J. May and F. R. Manby, J. Chem. Phys. 121, 4479 (2004)

E. F. Valeev, Chem. Phys. Lett. 395, 190 (2004)

E. F. Valeev and C. L. Jansen, Chem. Phys. Lett. 121, 1214 (2004)

D. P. Tew and W. Klopper, J. Chem. Phys. 123, 074101 (2005)

E. F. Valeev, Chem. Phys. Lett. 418, 333 (2006)

F. R. Manby, H.-J. Werner, T. B. Adler, and A. J. May, J. Chem. Phys. 124, 094103 (2006)

H. -J. Werner, T. B. Adler, and F. R. Manby, J. Chem. Phys. 126, 164102 (2007)

J. Noga, S. Kedžuch, and J. Šimunek, J. Chem. Phys. 127, 034106 (2007)

T. B. Adler, G. Knizia, and H. -J. Werner, J. Chem. Phys. 127, 221106 (2007)

G. Knizia, T. B. Adler, and H. –J. Werner, J. Chem. Phys. 130, 054104 (2009)

T. D. Crawford, C. D. Sherrill, E. F. Valeev, J. T. Fermann, R. A. King, M. L. Leininger, S. T. Brown, C. L. Janssen, E. T. Seidl, J. P. Kenny, and W. D. Allen, J. Comp. Chem. 28, 1610 (2007)

H. Fliegl, W. Klopper, and C. Hättig, J. Chem. Phys. 122, 084107 (2005)

H. Fliegl, C. Hättig, W. Klopper, Int. J. Quantum Chem. 106, 2306 (2006)

D. P. Tew and W. Klopper, J. Phys. Chem. A, 111, 11242 (2007)

S. Kedžuch, M. Milko, and J. Noga, Int. J. Quantum Chem. 105, 929 (2005)

J. Noga, P. Valiron, and W. Klopper, J. Chem. Phys. 115, 2022 (2001)

C. Møller and M. S. Plesset, Phys. Rev. 46, 618 (1934)

P. Hobza and J. Sponer, J. Am. Chem. Soc. 124, 11802 (2002)

P. Jurecka, J. Sponer, J. Cerny, and P. Hobza, Phys. Chem. Chem. Phys. 8, 1985 (2006)

G. A. Petersson and M. Braunstein, J. Chem. Phys. 83, 5129 (1985)

A. L. L. East and W. D. Allen, J. Chem. Phys. 99, 4638 (1993)

L. A. Curtiss, K. Raghavachari, G. W. Trucks, and J. A. Pople, J. Chem. Phys. 94, 7221 (1991)

[33] L. A. Curtiss, K. Raghavachari, P. C. Redfern, V. Rassolov, and J. A. Pople, J. Chem. Phys. 109, 7764 (1998)

L. A. Curtiss, P. C. Redfern, K. Raghavachari, and J. A. Pople, J. Chem. Phys. 114, 108 (2001)

L. A. Curtiss and K. Raghavachari, ACS Symp. Ser 677, 176 (1998)

A. L. L. East and W. D. Allen, J. Chem. Phys. 99, 4638 (1993)

A. G. Császár, W. D. Allen, and H. F. Schaefer, J. Chem. Phys. 108, 9751 (1998)

P. L. Fast, J. C. Corchado, M. L. Sanchez, and D. G. Truhlar, J. Phys. Chem. A 103, 5129 (1999)

B. J. Lynch and D. G. Truhlar, J. Phys. Chem. A 107, 3898 (2003)

T.-H. Li, H.-R. Chen, and W. -P. Hu Chem. Phys. Lett. 412, 430 (2005)

F. B. Brown and D. G. Truhlar, Chem. Phys. Lett. 117, 307 (1985)

M. S. Gordon and D. G. Truhlar, J. Amer. Chem. Soc. 108, 5412 (1986)

M. S. Schuurman, S. R. Muir, W. D. Allen, and H. F. Schaefer J. Chem. Phys. 120, 11586 (2004)

R. A. King, W. D. Allen, B. Ma, and H. F. Schaefer III, Faraday Discuss. 110, 23 (1998)

M. R. Nyden and G. A. Petersson, J. Chem. Phys. 75, 1843 (1981)

G. A. Petersson, ACS Symp. Ser. 677, 237 (1998)

B. J. Lynch and D. G. Truhlar, J. Phys. Chem A 107, 3898 (2003)

D. E. Woon and T. H. Dunning Jr., J. Chem. Phys. 100, 2975 (1994)

D. E. Woon and T. H. Dunning Jr., J. Chem. Phys. 98, 1358 (1993)

J. Koput and K. A. Peterson, J. Phys. Chem. A 106, 9595 (2002)

N. B. Balabanov and K. A. Peterson, J. Chem. Phys. 2005, 123, 064107

A. K. Wilson, D. E. Woon, K. A. Peterson, and T. H. Dunning Jr., J. Chem. Phys. 110, 7667 (1999)

T. H. Dunning Jr., K. A. Peterson, and A. K. Wilson, J. Chem. Phys. 114, 9244 (2001)

T. H. Dunning Jr., J. Chem. Phys. 90, 1007 (1989)

R. A. Kendall, T. H. Dunning, Jr. R. J. Harrison, J. Chem. Phys. 96, 6796 (1992)

E. Papajak, H. R. Leverentz, J. Zheng, and D. G. Truhlar, J. Chem. Theory Comput. 5, 1197 (2009); 5, 3330 (2009)

E. Papajak and D. G. Truhlar, J. Chem. Theory Comput. 6, 597 (2010)

J. Zheng, X. Xu, and D. G. Truhlar, Theor. Chem. Acc. 128, 295 (2011)

E. Papajak and D. G. Truhlar, J. Chem. Theory Comput. 7, 10 (2011)

J. R. Cheeseman and M. J. Frisch, J. Chem. Theory Comput. 7, 3323 (2011)

E. Papajak, J. Zheng, X. Xu, H. R. Leverentz, and D. G. Truhlar, J. Chem. Theory Comput. 7, 3027 (2011)

J. M. L. Martin, A. Sundermann, P. L. Fast, and D. G. Truhlar, J. Chem. Phys. 113, 1348 (2000)

K. A. Peterson and T. H. Dunning Jr., 2002 J. Chem. Phys. 117, 10548 (2002)

A. Karton, E. Rabinovitch, J. M. L. Martin, and B. Ruscic, J. Chem. Phys. 125, 144108 (2006)

J. Zheng, Y. Zhao, and D. G. Truhlar, J. Chem. Theory Comput. 5, 808 (2009)

J. Alecu and D. G. Truhlar, J. Phys. Chem. A 115, 2811 (2011)

Y. Zhao, N. González-García, and D. G. Truhlar, J. Phys. Chem. A 109, 2012 (2005)

B. J. Lynch, Y. Zhao, and D. G. Truhlar, J. Phys. Chem. A 107, 1384 (2003)

B. J. Lynch, Y. Zhao, and D. G. Truhlar, J. Phys. Chem. A 109, 1643 (2005)

P. J. Knowles, J. S. Andrews, R. D. Amos, N. C. Handy, and J. A. Pople, Chem. Phys. Lett. 186, 130 (1991)

A. Karton, A. Tarnopolsky, J.-, F. Lamere, G. C. Schatz, and J. M. L. Martin, J. Phys. Chem. A 112, 12868 (2008)

S. Hirata, P.-D. Fan, A. A. Auer, M. Nooijen, and P. Piecuch, J. Chem. Phys. 121, 12197 (2004)

K. A. Peterson, D. Feller, and D. A. Dixon, Theor. Chem. Acc. 131, 1079 (2012)

R. P. Feynman and A. R. Hibbs, Quantum Mechanics and Path Integrals; McGraw-Hill, New York, 1965

R. P. Feynman, Statistical Mechanics; Benjamin, Reading, MA, 1972

V. A. Lynch, S. L. Mielke, and D. G. Truhlar, J. Chem. Phys., 121, 5148 (2004)

V. A. Lynch, S. L. Mielke, and D. G. Truhlar, J. Phys. Chem. A, 109, 10092 (2005); 110, 5965(E) (2005)

S. Chempath, C. Predescu, and A. T. Bell, J. Chem. Phys., 124, 234101 (2006)

D. R. Herschbach, J. Chem. Phys. 31, 91 (1959)

D. G. Truhlar, J. Comput. Chem. 12, 266 (1991)

J. Gang, M. J. Pilling and S. H. Robertson, J. Chem. Soc. Faraday Trans. 92, 3509 (1996)

A. L. L. East and L. Radom, J. Chem. Phys. 106, 6655 (1997)

R. B. McClurg, R. C. Flagan, and W. A. Goddard III, J. Chem. Phys., 106, 6675 (1999); 111, 7165(E) (1999)

W. Witschel and C. Hartwigsen, Chem. Phys. Lett. 273, 304 (1997)

P. Y. Ayala and H. B. Schlegel, J. Chem. Phys. 108, 2314 (1998)

Y.-Y. Chuang and D. G. Truhlar, J. Chem. Phys. 112, 1221 (2000); 121, 7036(E) (2004); 124, 179903(E) (2006)

B. A. Ellingson, V. A. Lynch, S. L. Mielke and D. G. Truhlar, J. Chem. Phys., 125, 084305 (2006)

A. C. P. Bitencourt, M. Ragni, G. S. Maciel, V. Aquilanti, and F. V. Prudente, J. Chem. Phys. 129, 154316 (2008)

S. Sharma, S. Raman, and W. H. Green, J. Phys. Chem. A, 114, 5689 (2010)

D. Gruzman, A. Karton, and J. M. L. Martin, J. Phys. Chem. A, 113, 11974 (2009)

T. H. Lay, L. N. Krasnoperov, C. A. Venanzi, J. W. Bozzelli, and N. V. Shokhirev, J. Phys. Chem. 100, 8240 (1996)

T. Yamada, T. H. Lay, and J. W. Bozzelli, J. Phys. Chem. A, 102, 7286 (1998)

T. Yamada, J. W. Bozzelli, and R. J. Berry, J. Phys. Chem. A, 103, 5602 (1999)

K. S. Pitzer and W. D. Gwinn, J. Chem. Phys. 10, 428 (1942)

B. M. Wong and W. H. Green, Mol. Phys. 103, 1027 (2005)

T. F. Miller III, and D. C. Clary, J. Chem. Phys. 116, 8262 (2002)

V. Van Speybroeck, D. V. Neck, and M. Waroquier, J. Phys. Chem. A, 106, 8945 (2002)

P. Vansteenkiste, D. Van Neck, V. Van Speybroeck, and M. Waroquier, J. Chem. Phys. 124, 044314 (2006)

D. A. McQuarrie, Statistical Mechanics Ed.; Harper & Row, New York, 1973

T. F. Miller, III and D. C. Clary, Mol. Phys. 103, 1573 (2005)

M. Tafipolsky and R. Schmid, J. Comput. Chem. 26, 1579 (2005)

Y. K. Sturdy and D. C. Clary, Phys. Chem. Chem. Phys. 9, 2397 (2007)

S. W. Benson, Thermochemical Kinetics, 2nd; Wiley-Interscience, New York, 1976

H. E. O'Neal and S. W. Benson, Int. J. Chem. Kinet., 1969, 1, 221 (1969)

H. E. O'Neal and S. W. Benson, in Free Radicals, ed. J. H. Koshi, Wiley, New York, 1973, pp. 275

N. Cohen, J. Phys. Chem., 1992, 96, 9052 (1992)

T. H. Lay, J. W. Bozzelli, A. M. Dean, and E. R. Ritter, J. Phys. Chem. 99, 14514 (1995)

K. K. Irikura, in Computational Thermochemistry, ed. K. K. Irikura and D. J. Frurip, ACS Symposium Series Vol. 677, 1998, pp. 402

V. Van Speybroeck, R. Ganib, and R. J. Meier, Chem. Soc. Rev. 39, 1764 (2010)

K. S. Pitzer, J. Chem. Phys. 8, 711 (1940)

W. J. Taylor, J. Chem. Phys. 16, 257 (1948)

P. J. Flory and R. L. Jernigan, J. Chem. Phys., 1965, 42, 3509 (1965)

R. A. Scott and H. A. Scheraga, J. Chem. Phys. 44, 3054 (1966)

R. Janoschek and J. Kalcher, Anorg. Allg. Chem. 628, 2724 (2002)

G. L. Dirichlet, J. Reine Angew. Math., 40, 209 (1850)

G. Voronoi, J. Reine Angew. Math., 133, 97 (1907)

F. Aurenhammer, ACM Computing Surveys 23, 345 (1991)

G. Katzer and A. F. Sax, J. Comput. Chem. 26, 1438 (2005)

K. S. Pitzer, J. Chem. Phys. 14, 239 (1946)

J. E. Kilpatrick and K. S. Pitzer, J. Chem. Phys. 17, 1064 (1949)

T. Miyazawa and K. Fukushima, J. Mol. Spectrosc. 15, 308 (1965)

H. Bonadeo, E. D'Alessio, and E. Silberman, J. Mol. Spectrosc., 22, 402 (1967)

G. Keresztury, A.-Y. Wang, and J. R. Durig, Spectrochimica Acta A 48, 199 (1992)

G. Tasi, F. Mizukami, I. Palinko, J. Csontos, W. Gyorffy, P. Nair, K. Maeda, M. Toba, S.-i. Niwa, Y. Kiyozumi, and I. Kiricsi, J. Phys. Chem. A 102, 7698 (1998)

D. Bond, J. Phys. Chem. A 112, 1656 (2008)

P. Pulay, Mol. Phys. 17, 197 (1969)

G. Fogarasi and P. Pulay, Molecular Vibrational Spectra and Structure, Ed.; Elsevier, Amsterdam, 1985

C. F. Jackels, Z. Gu, and D. G. Truhlar, J. Chem. Phys. 102, 3188 (1995)

K. A. Nguyen, C. F. Jackels, and D. G. Truhlar, J. Chem. Phys. 104, 6491 (1996)

Y.-Y. Chuang and D. G. Truhlar, J. Chem. Phys. 107, 83 (1997)

E. B. Wilson, Jr., J. C. Decius, and P. C. Cross, Molecular Vibrations, Ed.; McGraw-Hill, New York, 1955

C.-L. Huang, C.-L. Liu, C.-K. Ni, and J. T. Hougen, J. Mol. Spectrosc. 233, 122 (2005)

V. Hanninen and L. Halonen, J. Chem. Phys. 126, 064309 (2007)

G. Katzer and A. F. Sax, Chem. Phys. Lett. 368, 473 (2003)

K. L. Clarkson, K. Mehlhorn, and R. Seidel, Lect. Notes Comput. Sci. 577, 463 (1992)

Y. Zhao and D. G. Truhlar, Theor. Chem. Acc. 120, 215 (2008)

B. J. Lynch, P. L. Fast, M. Harris, and D. G. Truhlar, J. Phys. Chem. A 104, 4811 (2000)

R. Krishnan, J. S. Binkley, R. Seeger, and J. A. Pople, J. Chem. Phys. 72, 650 (1980)

T. Clark, J. Chandrasekhar, G. W. Spitznagel, and P. v. R. Schleyer, J. Comput. Chem. 4, 294 (1983)

I. M. Alecu, J. Zheng, Y. Zhao, and D. G. Truhlar, J. Chem. Theory Comput. 6, 2872 (2010)

S. W. Benson, F. R. Cruickshank, D. M. Golden, G. R. Haugen, H. E. O'Neal, A. S. Rodgers, R. Shaw, and R. Walsh, Chem. Rev. 69, 279 (1969)

J. Koput, S. Carter and N. C. Handy, J. Phys. Chem. A 102, 6325 (1998)

K. Ohno, H. Yoshida, H. Watanabe, T. Fujita and H. Matsuura, J. Phys. Chem. 98, 6924 (1994)

J. Moc, J. M. Simmie, and H. J. Curran, J. Mol. Struct. 928, 149 (2009)

L. V. Gurvich, I. V. Veyts, and C. B. Alcock, Thermodynamic Properties of Individual Substances, 4th, Ed.; Hemisphere Pub. Co., New York, 1989

J. F. Counsell, J. L. Hales, and J. F. Martin, Trans. Faraday Soc. 61, 1869 (1965)

E. Hirota, J. Chem. Phys. 28, 839 (1958)

R. M. Lees, J. Chem. Phys. 59, 2690 (1973)

R. Meyer, J. Mol. Spectrosc. 76, 266 (1979)

G. A. Guirgis, J. B. A. Barton, and J. R. Durig, J. Chem. Phys. 79, 5918 (1983)

J. A. Kunc, Mol. Phys. 101, 413 (2003)

C. Y. Lin, E. I. Izgorodina, and M. L. Coote, J. Phys. Chem. A 112, 1956 (2008)

C. –W. Zhou, J. M. Simmie, and H. J. Curran, Combustion and Flame 158, 726 (2011)

S. S. Vasu, D. F. Davidson, R. K. Hanson, and D. M. Golden, Chem. Phys. Lett. 497, 26 (2010)

M. D. Hurley, T. J. Wallington, L. Laursen, M. S. Javadi, O. J. Nielsen, T. Yamanaka, and M. Kawasaki, J. Phys. Chem. A 113, 7011 (2009)

D. H. Semmes, A. R. Ravishankara, C. A. Gump-Perkins, and P. H. Wine, Int. J. Chem. Kinet. 17, 303 (1985)

J. A. Kerr and D. W. Sheppard, Environ. Sci. Technol. 15, 960 (1981)

G. S. Parks, J. Am. Chem. Soc. 47, 338 (1925)

J. Tjebbes, Acta Chem. Scand. 14, 180 (1960)

E. Strömsöe, H. G. Rönne, and A. L. Lydersen, J. Chem. Eng. Data 15, 286 (1970)

S. W. Benson, *Thermochemical Kinetics*, 2nd ed. (Wiley-Interscience, New York, 1976)

J. Zheng, T. Yu, E. Papajak, I. M. Alecu, S. L. Mielke, and D. G. Truhlar, Phys. Chem. Chem. Phys. 13, 10885 (2011)

T. Yu, J. Zheng and D. G. Truhlar, Chem. Sci. 2, 2199 (2011)

J. Zheng, T. Yu, and D. G. Truhlar, Phys. Chem. Chem. Phys. 13, 19318 (2011)

T. F. Miller III and D. C. Clary, Phys. Chem. Chem. Phys. 6, 2563 (2004). T. F. Miller III and D. C. Clary, Mol. Phys. 103, 1573 (2005)

P. Vansteenkiste, V. Van Speybroeck, E. Pauwels, and M. Waroquier, Chem. Phys. 314, 109 (2005). K. Van Cauter, V. Van Speybroeck, P. Vansteeenkiste, M.-F. Reyniers, and M. Waroquier, ChemPhysChem 7, 131 (2006)

I. M. Alecu, J. Zheng, Y. Zhao, and D. G. Truhlar, J. Chem. Theor. Comput. 6, 2872 (2010)

Y. Zhao and D. G. Truhlar, Theor. Chem. Acc. 120, 215 (2008)

Y. Zhao and D. G. Truhlar, J. Chem. Theory Comput. 4, 1849 (2008)

R. Krishnan, J. S. Binkley, R. Seeger, and J. A. Pople, J. Chem. Phys. 72, 650 (1980)

T. Clark, J. Chandrasekhar, G. W. Spitznagel, and P. v. R. Schleyer, J. Comp. Chem. 4, 294 (1983)

M. J. Frisch, J. A. Pople, and J. S. Binkley, J. Chem. Phys. 80, 3265 (1984)

B. J. Lynch, Y. Zhao, and D. G. Truhlar, J. Phys. Chem. A 107, 1384 (2003)

E. Papajak and D. G. Truhlar, J. Chem. Theor. Comput. 6, 597 (2010)

E. Papajak and D. G. Truhlar, J. Chem. Theor. Comput. 7, 10 (2011)

T. B. Adler, G. Knizia, and H. –J. Werner, J. Chem. Phys. 127, 221106 (2007)

G. Knizia, T. B. Adler, and H. –J. Werner, J. Chem. Phys. 130, 054104 (2009)

F. R. Manby, J. Chem. Phys. 119, 4607 (2003)

Basic terminology of stereochemistry, (IUPAC Recommendations 1996), 68, 2193 (PAC, 1996)

K. Ohno, H. Yoshida, H. Watanabe, T. Fujita, and H. Matsuura, J. Phys. Chem. 98, 6924 (1994)

J. Moc, J. M. Simme, and H. J. Curran, J. Mol. Struct. 928, 149 (2009)

T. Yu, J. Zheng, and D. G. Truhlar, Phys. Chem. Chem. Phys. 13, 19318, (2011)

TRC Data Series: M. Frenkel, G. J. Kabo, K. N. Marsh, G. N. Roganov, and R. C. Wilhoit, *Thermodynamics of Organic Compounds in the Gas State*, Vol. II, (CRC Press, Boca Raton, FL, 1994)

CRC Handbook of Chemistry and Physics, 91st ed. (CRC press, Boca Raton, 2011)

API Tables: *Selected Values of Properties of Hydrocarbons and Related Compounds*, American Petroleum Institute Research Project 44, Carnegie Press (Carnegie Institute of Technology, Pittsburgh, 1953)

J. Zheng, T. Yu, E. Papajak, I. M. Alecu, S. L. Mielke, and D. G. Truhlar, Phys. Chem. Chem. Phys. 13, 10885 (2011)

J. Zheng, T. Yu, and D. G. Truhlar, Phys. Chem. Chem. Phys. 13, 19318 (2011)

T. Yu, J. Zheng, and D. G. Truhlar, Phys. Chem. Chem. Phys. 14, 482 (2011)

J. Zheng and D. G. Truhlar, Faraday Discuss. 157, (2012)

P. Seal, E. Papajak, T. Yu, and D. G. Truhlar, J. Chem. Phys. 136, 034306 (2012)

P. Seal, E. Papajak, J. Zheng, and D. G. Truhlar, J. Phys. Chem. Lett. 3, 264 (2012)

T. Yu, J. Zheng, and D. G. Truhlar, Chem. Sci., 2, 2199 (2011)

T. Yu, J. Zheng, and D. G. Truhlar, J. Phys. Chem. A 116, 297 (2012)

X. Xu, E. Papajak, J. Zheng, and D. G. Truhlar, Phys. Chem. Chem. Phys. 14, 4204 (2012)

J. Platt, J. Chem. Phys. 15, 419 (1947)

J. Platt, J. Phys. Chem. 56, 328 (1952)

J. Greenshields and F. Rossini, J. Phys. Chem. 62, 271 (1958)

G. Somayajulu and B. Zwolinski, J. Trans. Faraday Soc. 62, 2327 (1966)

T. -P. Thinh, J. -L. Duran, and R. Ramalho, Ind. Eng. Process Des. Dev. 10, 576 (1971)

T. –P. Thinh and T. Trong, Can. J. Chem. 54, 344 (1976)

R. Joshi, J. Macromol. Sci.-Chem. A4, 1819 (1970)

S. W. Benson, *Thermochemical Kinetics*, 2nd ed. (Wiley-Interscience, New York, 1976)

N. Cohen, S. Benson, Chem. Rev. 93, 2419 (1993)

N. Cohen, J. Phys. Chem. Ref. Data 25, 1411 (1996)

T. H. Lay and J. W. Bozzelli, J. Phys. Chem. A 101, 9505 (1997)

N. Sebbar, J. W. Bozzelli, H. Bockhorn, J. Phys. Chem. A 108, 8353-8366 (2004)

H. O'Neal, S. Benson, In Free Radicals; J. K. Kochi, Ed.; Wiley: New York, 1973; pp 275

T. Ni, R. Caldwell, L. Melton, J. Am. Chem. Soc. 111, 457 (1989)

N. Cohen, J. Phys. Chem. 96, 9052 (1992)

M. K. Sabbe, F. De Vieeschower, M.-F. Reyniers, M. Waroquier, and G. B. Marin, J. Phys. Chem. A 112, 12235 (2008)

V. V. Turovtsev, Y. D. Orlov, Y. A. Lebedev, Russ. J. Phys. Chem. A 83 245 (2009)

I. Marsi, B. Viskolcz, L. Seres, J. Phys. Chem. A 104, 4497 (2000)

S. S. Khan, X. Yu, J. R. Wade, D. Malmgren, and L. J. Broadbelt J. Phys. Chem. 113, 5176 (2009)

M. K. Sabbe, M. Saeys, M.-F. Reyniers, and G. B. Marin J. Phys. Chem. A 109, 7466 (2005)

J. M. Hudzik, J. W. Bozzelli, J. Phys. Chem. A 114, 7984 (2010)

Y. Zhao, N. E. Schultz, and D. G. Truhlar, J. Chem. Theory Comput. 4, 1849 (2008)

B. J. Lynch, Y. Zhao, and D. G. Truhlar, J. Phys. Chem. A 107, 1384 (2003)

T. H. Jr. Dunning, J. Chem. Phys. 90, 1007 (1989)

R. A. Kendall, T. H. Jr. Dunning, and R. J. Harrison, J. Chem. Phys. 96, 6796 (1992)

E. Papajak, H. R. Leverentz, J. Zheng, and D. G. Truhlar, J. Chem. Theory Comput. 5, 1197 (2009); 5, 3330 (2009)

E. Papajak and D. G. Truhlar, J. Chem. Theory Comput. 6, 597 (2010)

R. Krishnan, J. S. Binkley, R. Seeger, and J. A. Pople, J. Chem. Phys. 72, 650 (1980)

T. Clark, J. Chandrasekhar, G. W. Spitznagel, and P. v. R. Schleyer, J. Comp. Chem. 4, 294 (1983)

M. J. Frisch, J. A. Pople, and J. S. Binkley, J. Chem. Phys. 80, 3265 (1984).

I. M. Alecu, J. Zheng, Y. Zhao, and D. G. Truhlar, J. Chem. Theory Comput. 6, 2872 (2010)

G. Knizia, T. B. Adler, and H.-J. Werner, J. Chem. Phys. 130, 054104 (2009)

E. Papajak and D. G. Truhlar, J. Chem. Theory Comput. 7, 10 (2011)

W. Kutzelnigg Theor. Chim. Acta 68, 445 (1985)

W. Kutzelnigg and W. Klopper, J. Chem. Phys., 94, 1985, (1991)

W. Klopper and W. Kutzelnigg, Chem. Phys. Lett. 134, 17 (1987)

W. Klopper, C. C. M. J. Samson, Chem. Phys. 116, 6397 (2002)

F. R. Manby, J. Chem. Phys. 119, 4607 (2003)

S. Ten-no and F. R. Manby, J. Chem. Phys. 119, 5358 (2003)

S. J. Ten-no, Chem. Phys. 121, 117 (2004)

E. F. Valeev, Chem. Phys. Lett. 395, 190 (2004)

E. F. Valeev and C. L. Jansen, Chem. Phys. Lett. 121, 1214 (2004)

S. Ten-no, Chem. Phys. Lett. 121, 117 (2004)

H. –J. Werner, T. B. Adler, and F. R. Manby, J. Chem. Phys. 126, 164102 (2007)

T. D. Crawford, C. D. Sherrill, E. F. Valeev, J. T. Fermann, R. A. King, M. L. Leininger, S. T. Brown, C. L. Janssen, E. T. Seidl, J. P. Kenny, and W. D. J. Allen, J. Comp. Chem. 28, 1610 (2007)

J. Zheng, S. L. Mielke, K. L. Clarkson, and D. G. Truhlar, Computer Phys. Commun. 183, 1803, 2012

G. P. Moss, Pure Appl. Chem. 68, 2193 (1996)

J. Zheng, T. Yu, E. Papajak, I. M. Alecu, S. L. Mielke, and D. G. Truhlar, Phys. Chem. Chem. Phys. 13, 10885 (2011)

J. Zheng, T. Yu, and D. G. Truhlar, Phys. Chem. Chem. Phys. 13, 19318 (2011)

T. Yu, J. Zheng, and D. G. Truhlar, Phys. Chem. Chem. Phys., 14, 482 (2011)

J. Zheng and D. G. Truhlar, Faraday Discuss. 157 (2012)

P. Seal, E. Papajak, T. Yu, and D. G. Truhlar, J. Chem. Phys. 136, 034306 (2012)

P. Seal, E. Papajak, J. Zheng, and D. G. Truhlar, J. Phys. Chem. Lett. 3, 264 (2012)

T. Yu, J. Zheng, and D. G. Truhlar, Chem. Sci. 2, 2199 (2011)

T. Yu, J. Zheng, and D. G. Truhlar, J. Phys. Chem. A 116, 297 (2012)

X. Xu, E. Papajak, J. Zheng, and D. G. Truhlar, Phys. Chem. Chem. Phys. 14, 4204 (2012)

J. Platt, J. Chem. Phys. 15, 419 (1947)

J. Platt, J. Phys. Chem. 56, 328 (1952)

J. Greenshields and F. Rossini, J. Phys. Chem. 62, 271 (1958)

G. Somayajulu and B. Zwolinski, J. Trans. Faraday Soc. 62, 2327 (1966)

T. -P. Thinh, J. -L. Duran, and R. Ramalho, Ind. Eng. Process Des. Dev. 10, 576 (1971)

T. –P. Thinh and T. Trong, Can. J. Chem. 54, 344 (1976)

R. Joshi, J. Macromol. Sci.-Chem. A4, 1819 (1970)

S. W. Benson, *Thermochemical Kinetics*, 2nd ed. (Wiley-Interscience, New York, 1976)

N. Cohen, S. Benson, Chem. Rev. 93, 2419 (1993)

N. Cohen, J. Phys. Chem. Ref. Data 25, 1411 (1996)

T. H. Lay and J. W. Bozzelli, J. Phys. Chem. A 101, 9505 (1997)

N. Sebbar, J. W. Bozzelli, H. Bockhorn, J. Phys. Chem. A 108, 8353-8366 (2004)

H. O'Neal, S. Benson, In Free Radicals; J. K. Kochi, Ed.; Wiley: New York, 1973; pp 275.

T. Ni, R. Caldwell, L. Melton, J. Am. Chem. Soc. 111, 457 (1989)

N. Cohen, J. Phys. Chem. 96, 9052 (1992)

M. K. Sabbe, F. De Vieeschower, M.-F. Reyniers, M. Waroquier, and G. B. Marin, J. Phys. Chem. A 112, 12235 (2008)

V. V. Turovtsev, Y. D. Orlov, Y. A. Lebedev, Russ. J. Phys. Chem. A 83 245 (2009)

I. Marsi, B. Viskolcz, L. Seres, J. Phys. Chem. A 104, 4497 (2000)

S. S. Khan, X. Yu, J. R. Wade, D. Malmgren, and L. J. Broadbelt J. Phys. Chem. 113, 5176 (2009)

M. K. Sabbe, M. Saeys, M.-F. Reyniers, and G. B. Marin J. Phys. Chem. A 109, 7466 (2005)

J. M. Hudzik, J. W. Bozzelli, J. Phys. Chem. A 114, 7984 (2010)

Y. Zhao, N. E. Schultz, and D. G. Truhlar, J. Chem. Theory Comput. 4, 1849 (2008)

B. J. Lynch, Y. Zhao, and D. G. Truhlar, J. Phys. Chem. A 107, 1384 (2003)

T. H. Jr. Dunning, J. Chem. Phys. 90, 1007 (1989)

R. A. Kendall, T. H. Jr. Dunning, R. J. Harrison, J. Chem. Phys. 96, 6796 (1992)

E. Papajak, H. R. Leverentz, J. Zheng, and D. G. Truhlar, J. Chem. Theory Comput. 5, 1197 (2009); 5, 3330 (2009)

E. Papajak and D. G. Truhlar, J. Chem. Theory Comput. 6, 597 (2010)

R. Krishnan, J. S. Binkley, R. Seeger, and J. A. Pople, J. Chem. Phys. 72, 650 (1980)

T. Clark, J. Chandrasekhar, G. W. Spitznagel, and P. v. R. Schleyer, J. Comp. Chem. 4, 294 (1983)

M. J. Frisch, J. A. Pople, and J. S. Binkley, J. Chem. Phys. 80, 3265 (1984)

I. M. Alecu, J. Zheng, Y. Zhao, and D. G. Truhlar, J. Chem. Theory Comput. 6, 2872 (2010)

G. Knizia, T. B. Adler, and H.-J. Werner, J. Chem. Phys. 130, 054104 (2009)

E. Papajak and D. G. Truhlar, J. Chem. Theory Comput. 7, 10 (2011)

W. Kutzelnigg Theor. Chim. Acta 68, 445 (1985)

W. Kutzelnigg, W. Klopper, J. Chem. Phys., 94, 1985, (1991)

W. Klopper, W. Kutzelnigg, Chem. Phys. Lett. 134, 17 (1987)

W. Klopper, C. C. M. J. Samson, Chem. Phys. 116, 6397 (2002)

F. R. Manby, J. Chem. Phys. 119, 4607 (2003)

S. Ten-no, F. R. Manby, J. Chem. Phys. 119, 5358 (2003)

S. J. Ten-no, Chem. Phys. 121, 117 (2004)

E. F. Valeev, Chem. Phys. Lett. 395, 190 (2004)

E. F. Valeev and C. L. Jansen, Chem. Phys. Lett. 121, 1214 (2004)

S. Ten-no, Chem. Phys. Lett. 121, 117 (2004)

H. –J. Werner, T. B. Adler, and F. R. Manby, J. Chem. Phys. 126, 164102 (2007)

T. D. Crawford, C. D. Sherrill, E. F. Valeev, J. T. Fermann, R. A. King, M. L. Leininger, S. T. Brown, C. L. Janssen, E. T. Seidl, J. P. Kenny, and W. D. J. Allen, J. Comp. Chem. 28, 1610 (2007)

J. Zheng, S. L. Mielke, K. L. Clarkson, and D. G. Truhlar, Computer Phys. Commun. 183, 1803, 2012.

G. P. Moss, Pure Appl. Chem. 68, 2193 (1996)

C. –W. Zhou, J. M. Simmie, and H. J. Curran, Combust. Flame 158, 726 (2011)

D. M. A. Karwat, S. W. Wagnon, P. D. Teini, P. D., M. S. Wooldridge, J. Phys. Chem. A 115, 4909 (2011)

S. S. Vasu, D. F. Davidson, R. K. Hanson, D. M. Golden, Chem. Phys. Lett. 497, 26 (2010)

J. Moc, J. M. Simmie, J. Phys. Chem. A 114, 5558 (2010)

G. Black, J. M. Simmie, *J. Comput. Chem.* 31, 1236 (2010)

J. Moc, J. M. Simmie, and H. J. Curran, J. Mol. Struct. 928, 149 (2009)

T. Wallner, S. A. Miers, S. McConnell, *Proc. Spring Tech. Conf.*; ASME Internal Combustion Engine Division: Chicago, USA, 2008.

M. Z. Jacobson, Environ. Sci. Technol. 41, 4150 (2007)

J. Fargione, J. Hill, D. Tilman, S. Polasky, P. Hawthorne, Science 319, 1235 (2008)

M. Golombok, S. Tierney, Ind. Eng. Chem. Res. 36, 5023 (1997)

C. K. Westbrook, Proc. Combust. Inst. 28, 1563 (2000)

M. E. Wright, B. G. Harvey, R. L. Quintana, Energy Fuels 22, 3299 (2008)

B. G. Harvey, R. L. Quintana, Energy Environ. Sci. 3, 352 (2010)

T. Yu, J. Zheng, D. G. Truhlar, Chem. Sci. 2, 2199 (2011)

B. C. Garrett, D. G. Truhlar, J. Chem. Phys. 70, 1593 (1979)

D. G. Truhlar, B. C. Garrett, Acc. Chem. Res. 13, 440 (1980)

D. G. Truhlar, A. D. Isaacson, B. C. Garrett, *Theory of Chemical Reaction Dynamics*; Baer, M., Ed.; CRC Press: Boca Raton, FL, 1985; Vol. 4, pp 65–137 (1985)

C. F. Jackels, Z. Gu, D. G. Truhlar, J. Chem. Phys. 102, 3188 (1995)

A. Fernandez-Ramos, B. A. Ellingson, B. C. Garrett, D. G. Truhlar, Variational Transition State Theory with Multidimensional Tunneling. In *Reviews in Computational Chemistry*; Lipkowitz, K. B., Cundari, T. R., Eds.; Wiley-VCH: Hoboken, NJ, 2007; Vol. 23, pp 125–232

Y. –P. Liu, G. C. Lynch, T. N. Truong, D.–H. Lu, D. G. Truhlar, J. Am. Chem. Soc. 115, 2408 (1993)

I. M. Alecu, J. Zheng, Y. Zhao, D. G. Truhlar, J. Chem. Theor. Comput. 6, 2872 (2010)

Y. Zhao, D. G. Truhlar, J. Chem. Theory Comput. 4, 1849 (2008)

B. J. Lynch, Y. Zhao, D. G. Truhlar, J. Phys. Chem. A 107, 1384 (2003)

P. Seal, E. Papajak, T. Yu, and D. G. Truhlar, J. Chem. Phys. 136, 034306 (2012)

J. Zheng, T. Yu, E. Papajak, I. M. Alecu, S. L. Mielke, D. G. Truhlar, Phys. Chem. Chem. Phys. 13, 10885 (2011)

Y. Zhao, D. G. Truhlar, Theor. Chem. Acc. 120, 215 (2008)

R. Krishnan, J. S. Binkley, R. Seeger, J. A. Pople, J. Chem. Phys. 72, 650 (1980)

T. Clark, J. Chandrasekhar, G. W. Spitznagel, P. v. R. Schleyer, J. Comp. Chem. 4, 294 (1983)

M. J. Frisch, J. A. Pople, J. S. Binkley, J. Chem. Phys. 80, 3265 (1984)

J. Zheng, X. Xu, D. G. Truhlar, Theor. Chem. Acc. 128, 295 (2011)

E. Papajak, D. G. Truhlar, J. Chem. Theor. Comput. 6, 597 (2010)

E. Papajak, D. G. Truhlar, J. Chem. Theor. Comput. 7, 10 (2011)

X. Xu, I. M. Alecu, D. G. Truhlar, J. Chem. Theory Comput. 7, 1667 (2011)

T. B. Adler, G. Knizia, H. –J. Werner, J. Chem. Phys. 127, 221106 (2007)

G. Knizia, T. B. Adler, H. –J. Werner, J. Chem. Phys. 130, 054104 (2009)

F. R. Manby, J. Chem. Phys. 119, 4607 (2003)

Y. Kim, J. C. Corchado, J. Villa, J. Xing, and D. G. Truhlar, J. Chem. Phys. 112, 2718 (2000)

T. V. Albu, J. C. Corchado, and D. G. Truhlar, J. Phys. Chem. A 105, 8465 (2001)

H. Lin, Y. Zhao, O. Tishchenko, and D. G. Truhlar, J. Chem. Theory Comput. 2, 1237 (2006)

O. Tischenko and D. G. Truhlar, J. Phys. Chem. A 110, 13530 (2006)

O. Tischenko and D. G. Truhlar, J. Chem. Theory Comput. 5, 1454 (2009)

B. C. Garrett and D. G. Truhlar, J. Phys. Chem. **95**, 10374 (1991)

J. Zheng and D. G. Truhlar, Phys. Chem. Chem. Phys. **12**, 7782 (2010)